Comparison of metamorphic evolution and tectonic position of metasediments of the Austevoll islands with rocks from the Samnanger Complex (Major Bergen Arc, Norwegian Caledonides)

Øystein Hordvik

Master of Science Thesis

Department of Earth Science
University of Bergen

August 2015

Acknowledgments

First I would like to thank my supervisor Jiri Konopásek for excellent feedback. He has been very helpful, in particular during the final phase of writing the thesis, responding to my e-mails day and night.
I would also like to thank my co-supervisor Rolf Birger Pedersen for sharing his knowledge on the regional geology around Bergen, and for an insightful boat trip through the Bergen Arc System.

A substantial amount of time of the thesis has been spent in various laboratories, and the lab technicians have provided invaluable guidance and assitance. A thank you is in order to Tereza Konopásek for teaching me step-by-step how to separate minerals. A thank you to Irina Maria Dumitru for showing me the procedure on how to create glass tablets for XRF analysis, subsequently I thank Ole Tumyr for analysing the tablets. Muriel Erambert spent many days in the microprobe lab in UiO guiding me, and programing and calibrating the microprobe for the different samples, for that I am grateful. I would also like to thank Egil Erichsen for preparing the SEM and guiding me during my many visits to the lab.

A final thank you to my fellow students at UiB for making the last five years fun experience.

Oslo, 31 july 2015

Øystein Hordvik

Øystein Hordvik

Abstract

Metasedimentary rocks represent a substantial component of the Bergen Arcs System and they are mostly confined to the Minor and Major Bergen Arcs. The arcs represents imbricate structures composed of island arc lithologies, prism sediments and gneissic continental substrate thrust, one upon another during the Caledonian Orogeny.
In the westernmost Austevoll, surrounded by the massive Sunnhordland Batholith, islands consisting of metasediments occurs. Due to their location, their tectonic position is somewhat enigmatic with respect to the nearby nappes and they have only been vaguely correlated with the metasediments of the Major Bergen Arc.

In order to gain insight in the metamorphic evolution and the tectonic position of the metasediment in Austevoll, a petrological study on garnet-bearing mica-schists from the island of Møkster has been carried out, complemented by thermodynamic modelling in order to constrain the pressure and temperature conditions at which the prograde assemblage of the rock formed. The same methods have been utilized on garnet-bearing micaschists collected from the Samnanger Complex of the Major Bergen Arc to compare them.

The petrological study suggests that the metasediments all share common textures with respect to prograde metamorphism. The metasediments from Møkster experienced the highest metamorphic grade resulting in a mineral assemblage, containing staurolite, while the metasediments from the Samnanger Complex only contain garnet-bearing assemblages at the metamorphic peak. The PT conditions for the prograde assemblages could be constrained via thermodynamic modelling to 605-635 ^{O}C and 7.5-8.2 kbar for the metasediment from Møkster, and to 480-565 ^{O}C and 4.7-6.6 kbar for the metasediment from the Samnanger Complex. Corresponding depths were calculated to 30-31 km and 24-25 km, respectively. By calculating a geothermal gradient based on the above estimations, a common geotherm of 20-24 ^{O}C/km was found for the metasediments which is considered a «normal» geothermal gradient, associated with burrial of sediment along an active margin.

From their similar textures and metamorphism along a common thermal gradient it is inferred that the metasediments on Møkster and in the Samnanger Complex may have been part of the same tectonic unit during prograde metamorphism. Thus, the tectonic position of the metasediments on Møkster may have been similar to that of the metasediments of the Samnanger Complex in the Major Bergen Arc.

Contents

1 INTRODUCTION

Metasediments represent a common rock-type within the Scandinavian Caledonides. Along the coast of SW Norway, the metasediments represent continental margin and prism sediments, which were mineralogically and texturally modified during continent/continent or continent/island arc collisions in the course of the Caledonian Orogeny (Færseth et al., 1977; Ingdahl, 1985; Rykkelid, 1987). The collision involved the burial and deformation of the passive margin of Baltica with its sedimentary cover sediments and occasional intrusion of magmatic rocks (Jansen and Andresen, 1987).

The gradual burial of a rock is followed by an increase in the temperature and/or pressure to which the rock is subjected. The temperature in the rock may further be modified by intrusions of igneous rock (Volmer, 2009; Winter, 2014). Rocks with a specific composition will, when chemically equilibrated at certain pressure and temperature intervals, accommodate distinctive mineral assemblages (Winter, 2014). When moving away from this pressure and temperature interval (usually during subsequent exhumation), the rocks may re-equilibrate, and as a result the assemblage may be modified. Rocks following a path towards an increasing grade of metamorphism, will typically modify their assemblage by replacing hydrous mineral phases with non-hydrous phases, and the fluid will be lost to the surroundings. Because of this, the reverse or retrograde reaction will commonly not occur, unless there is additional fluids present, and even in the presence of fluid the chemical equilibrium reaction is slower due to the lower temperature (Vernon, 2004). Thus, the prograde (progressive) assemblage is often somewhat preserved. During growth, porphyroblasts may overgrow and preserve older or contemporaneous minerals and textures. As such, a polymetamorphosed rock may contain mineral phases of several assemblages, as well as information about the tectonic environment to which the assemblages were subject. With the use of facies and facies series, a metamorphic evolution can be interpreted based on the mineralogy of the different assemblages (Winter, 2014). The petrological study of rocks is therefore an extremely important tool in unravelling the metamorphic history and the methods for interpreting microstructures, as well as past and present stable assemblages (including possible pitfalls) have been studied extensively (e.g. Spry, 1969; Thompson and Rubie, 1985; Vernon, 2004; Vernon et al., 2008; Barker, 2013; Winter, 2014).

Furthermore, with the use of SEM (Scanning Electron Microscope) and electron microprobe, important micro-inclusions can be detected. Micro-inclusions of minerals, which are suitable for radiometric dating may be preserved in prograde or retrograde minerals. If undissolved, the radiometric clock may provide the timing of the metamorphic event. With the use of electron microprobe, mineral compositions can be analyzed, which can be used to identify chemical differences between similar minerals occupying different textural positions, or compositional zonations across minerals, implying the way of change in the assemblage.

Whole-rock chemical data acquired from a sample, can be used to calculate P-T pseudosections with the aid of computer programs, such as Perple_X (Connolly, 2005; 2009). Such thermodynamic software enables forward modelling of mineral phase relationships and phase compositions for various P-T conditions, from which we can gain insight into the metamorphic history of a rock (Murphy, 2010). When the calculated stability fields of various mineral assemblages are used in conjunction with compositional isopleths calculated for multi-component minerals, such as garnet, the P-T conditions can be constrained providing more detailed insight in the metamorphic history of the rock.

By using a combination of these methods, various information can be extracted from a single rock as long as it contains suitable mineral assemblages.

Aim

The work in this thesis was done in the Upper Allochthon unit of the Norwegian Caledonides, and metasedimentary rocks situated in western Norway south of Bergen was the target of the study.
Three samples were collected from the Melkevik Formation (OS-2) and metasediment on Osøyro (BGA2-1, BGA2-2), belonging to the Samnanger Complex (Tab.2.1, Fig. 2.6, 2.7) of the Major Bergen Arc in Os. A third sample was collected from the westernmost island in Austevoll (Tab.2.1, Fig. 2.4, 2.5), Møkster (MOK), the tectonic position of which is somewhat enigmatic.

By considering the principles and using the methods mentioned above, the goal of this project is to study the metamorphic evolution of the garnet-bearing mica schists on Møkster, in order to provide data for interpretation of their tectonic position. The same will be done for samples of metasediments collected from the Samnanger Complex in the Major Bergen Arc. The results will then be compared in order to gain insight in similarities or differences in their metamorphic evolution and tectonic position.

2 REGIONAL GEOLOGY

2.1 GENERAL: SCANDINAVIAN CALEDONIDES

The Caledonides consists of a multitude of north-south trending outboard terrains thrust upon one another during the closing of the Iapetus Ocean, and the subsequent continental collision between Baltica and Laurentia. The thrust sheets comprises rock complexes of different origins and a wide range of metamorphic grades that developed via a series of tectonic events in the early Palaeozoic (Roberts, 2003). During the Silurian to early Devonian, gradual, oblique convergence of the Laurentian and Baltic continents ultimately lead to a collision where the margin of Baltica was thrust underneath Laurentia to the west. This subduction event lead to the compression and subsequent stacking of the shelfs and continental rise successions of Baltica, as well as exotic oceanic and island arc terranes indigenous to the Iapetus Ocean, onto the crystalline rocks of the Precambrian baltic shield (Rey et al., 1997; Roberts, 2003; Corfu et al., 2007). A later nappe complex composed of sediments derived from the peri-Laurentian margin, was stacked on top of the ophiolite/island arcs (Roberts, 2003). During the subduction, the westernmost part of the Baltic margin was subject to ultra high pressure (UHP), which lead to the formation of the partially eclogitized gneiss, known as the Western Gneiss Complex (WGC). As a result of the telescoping of the various rocks and sediments caused by the Caledonian events, a distinctive tectonostratigraphy can be recognized, consisting of Lower, Middle, Upper and Uppermost Allochthons, involving nappe translations of up to several 100 kilometers (Roberts, 2003). Subadjacent to these Allochthons are the Autochthon and Parautochthon. The Autochthon and Parautochthon consist of the basement of the Fennoscandian shield and sedimentary cover of late Proterozoic (Neoproterozoic) – early Palaeozoic age (Andersen and Andresen, 1994; Roberts, 2003; Corfu et al., 2007). The Lower Allocthon consists mainly of sedimentary sequences of Proterozoic to Palaeozoic ages, in the upper part, slices of Fennoscandian crystalline rock is involved in the thrust sheets (Andersen and Andresen, 1994). The Middle Allochton consists of slices of Precambrian rocks and psammites, cut by mafic intrusive rocks, and locally overlain by Vendian to lower Palaeozoic metasediments (Andersen and Andresen, 1994; Corfu et al., 2007). The Upper Allocthon consists of early Palaeozoic outboard terranes, composed of ophiolite, immature to mature island arc complexes, and volcanic sediments (Andersen and

Andresen, 1994; Corfu et al., 2007). The Uppermost Allochton consists of a mixture of gneissic, sedimentary and Palaeozoic rocks (Corfu et al., 2007). The Lower to Middle Allochthon represents shelf and continental rise successions of the Baltoscandian margin of Baltica (Roberts, 2003), while the Upper Allocthon represents Oceanic type lithologies. The Uppermost Allocthon represents the peri-Laurentian marginal sediments (Roberts, 2007; Roberts et al., 2014).

2.2 SOUTHWESTERN NORWAY

Three of the four allochtons occur in SW norway, the lower, middle and upper allochtons respectively (Fig. 2.1). The Upper Allochton is typically located in westernmost part of SW Norway, represented by coastal islands and the outer parts of the mainland (Gee et al., 1985; Roberts, 2003; Corfu et al., 2014; Roberts et al., 2014). The Middle Allocthon is the most abundant allocthon in SW Nortway (Corfu et al., 2014). The most extensive mass is mainly located to the east of the Upper Allochton and it stretches far inland in a NE direction (Gee et al., 1985; Corfu et al., 2014). Smaller nappes of this allocthon occupies parts of the coastal mainland to the west and in islands to the south-west. The lower allochton typically underlies or are located adjacent to the Middle Allocthon (Gee et al., 1985; Corfu et al., 2014; Roberts et al., 2014).

2.3 OVERVIEW OF THE REGIONAL GEOLOGY IN BERGEN AND SUNNHORDLAND

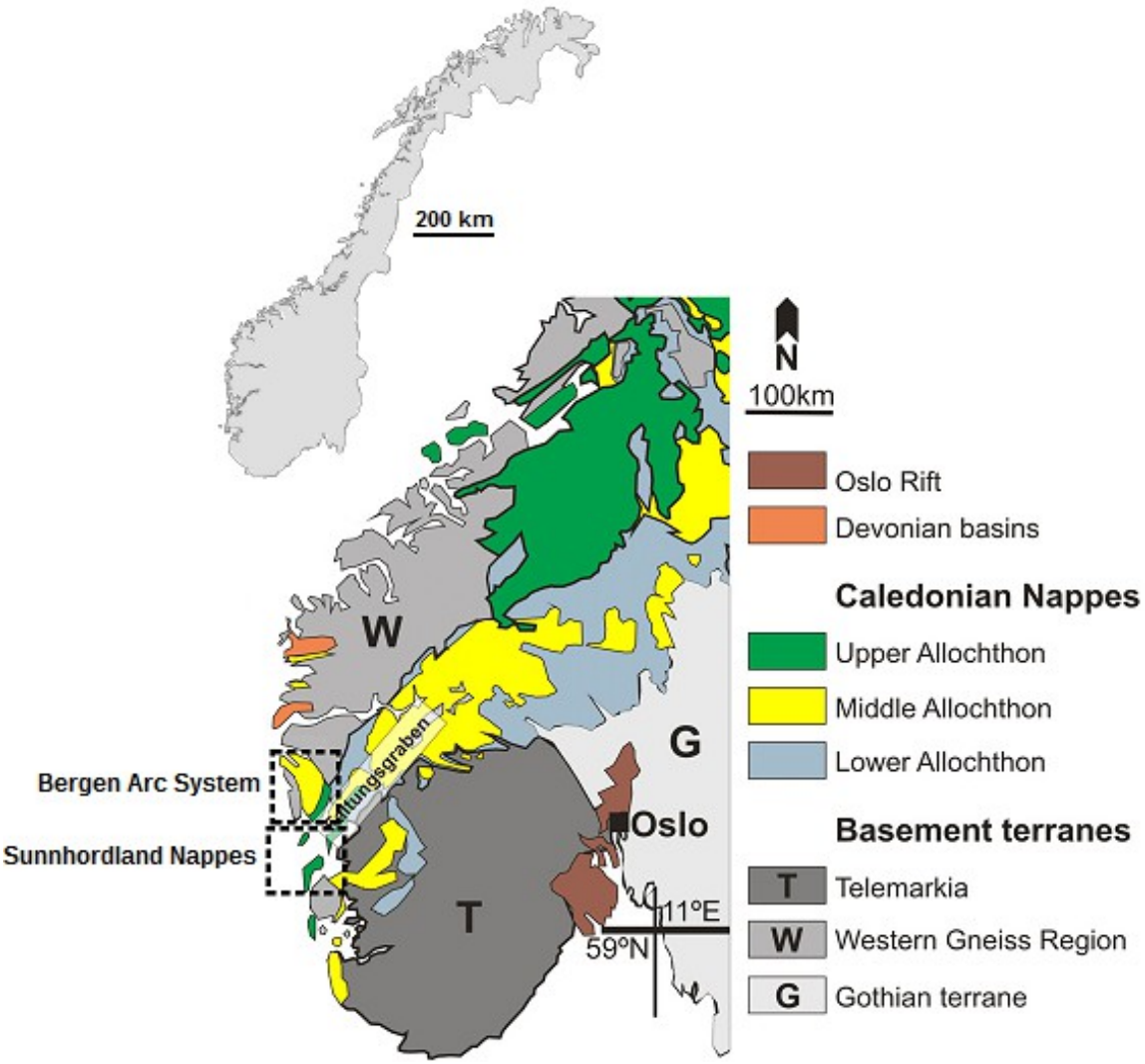

Fig. 2.1: Simplified tectonostratigraphic map displaying the major units of the Scandian Caledonides in SW Norway (from Corfu et al., 2014). The marked areas are described below.

2.3.1 THE BERGEN ARC SYSTEM

The Bergen Arc System (Fig. 2.2) comprises a series of arcuate nappe units with different lithologies and tectonometamorphic histories (Sturt and Ingdahl, 1978), they are regarded as Caledonian thrust sheets that occupy a major depression in the Baltic Basement (Færseth et al., 2011). Their succcession from west to east is as follows: Øygården Gneiss Complex, the Minor Bergen Arc, the Ulrikken Gneiss Complex, the Lindås Nappe, and the Major Bergen Arc. The arc system is bounded to the west by the North Sea, to the north-east by the Western Gneiss Region and to the south-east by the Bergsdalen Nappes. The Øygården Gneiss Complex (ØGC) is considered to be Parautochtonous Basement cover, and it consists of reworked Precambrian migmatites and granites, where the migmatitic structures has been overprinted by a strong shear deformation caused by the overriding nappes (Larsen et al., 2003). Eastwardly bounded by and succeeding the ØGC is the Minor Bergen Arc (MiBa), it consists of mica schists, tectonically melanged with ophiolite/island arc rocks which contains metasediments and Precambrian gneiss. The gneiss is considered Parautochtonous and derived from the ØGC (Boundy et al., 1997). The other rocks are considered Upper Allocthonous (Khun et al., 2000). Tightly hugging the MiBa to the east, appears the Upper Allocthonous (Khun et al., 2000) Ulrikken Gneiss Complex (UGC), composed of Caledonian banded gneisses, reworked migmaticic gneisses and a lesser deformed migmatite complex. Inbetween the UGC, a psammitic rock complex, the Rundemannen Formation occurs (Fossen, 1988). Creeping around the UGC is the Lindås Nappe, which is inferred to be Middle Allocthonous, the nappe comprises granulite facies anorthosite (Boundy et al., 2002), and to a lesser extent veins of charnockite and granite (Khun et al., 2002; Roffeis et al., 2013). On Holsnøy (NW Lindås), sheared eclogite facies rocks can be found. The two facies are of different ages, where the elcogite is attributed to the Scandian subduction (Boundy et al., 2002), and the granulite is considered to be an older continental type rock. The Lindås Nappe is therefore interpreted as one of many far travelling nappes (Boundy et al., 2002).
Bounded by the Lindås Nappe, the Western Gneiss Region and the Bergsdalen Nappes is the Major Bergen Arc (MaBa). It bears many similarities to the Minor Bergen Arc and consists of a dismembered ophiolite/island arc complex termed the Gullfjell Ophiolite Complex (GOC), unconformably overlain by metaconglomerates and metasediments (Ulven and Os Group). To the east, older metasediments together with gneisses and intrusives (the Samnanger Complex)

constitute the arc. GOC plus cover, and the metasediments including the youngest gneisses belongs to the Upper Allocthon, while the older gneisses (Haukenes Gneiss) belongs to the Parautochton (Sturt et al., 1978; Roberts et al., 2014).

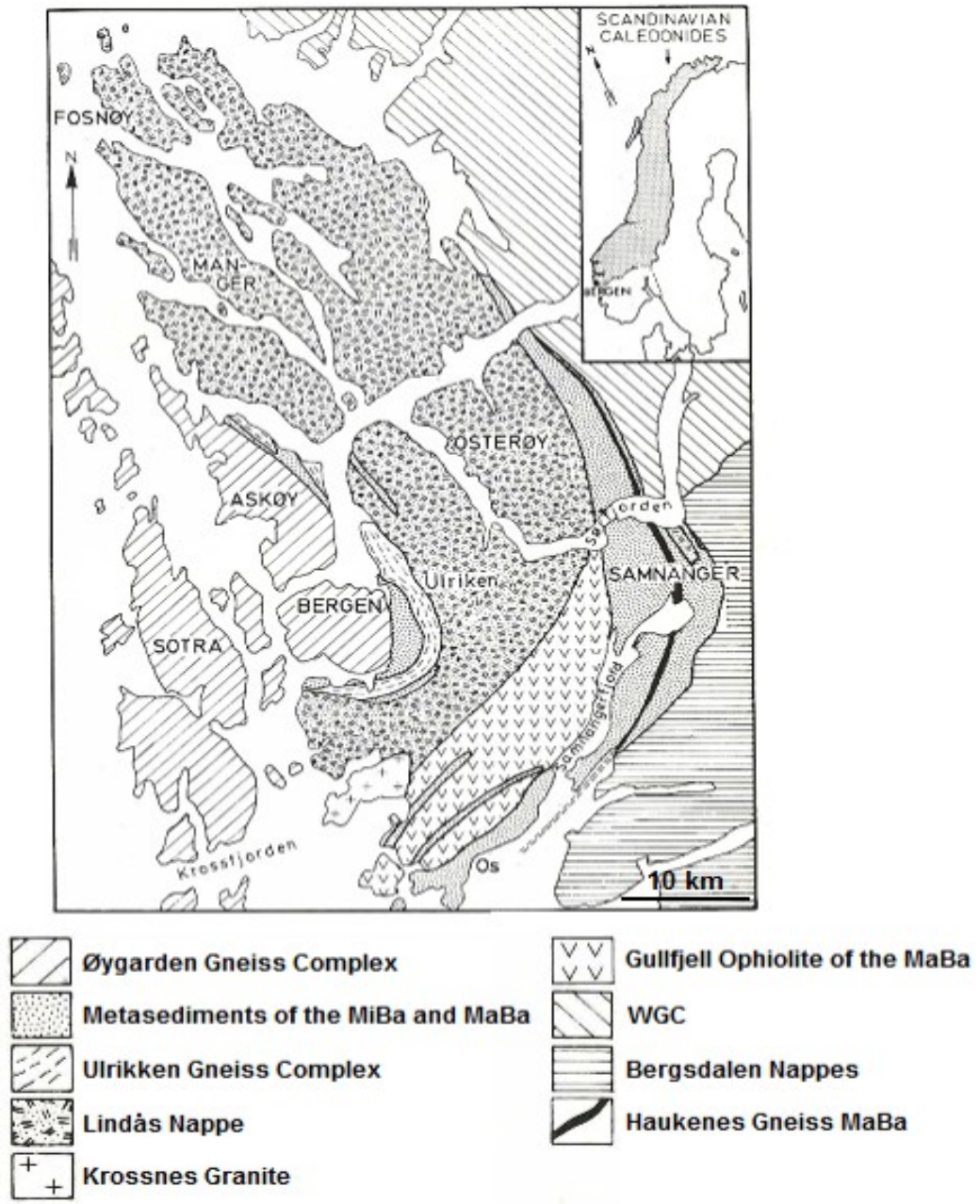

Fig. 2.2. Simplified geological map of the Bergen Arc System showing the five main nappes and their succession from west to east (slightly modified version of Færseth et al., 1977).

2.3.2 THE SUNNHORDLAND NAPPES

The Sunnhordland region (Fig. 2.3) consists of two nappe complexes separated by two faults/shear zones, Hardangerfjorden Shear Zone (HFSZ)/Faltungsgraben, a northeast-southwest striking fault system, which runs close and parallel to Hardangerfjorden (Andersen and Andresen, 1994), and the Sunnhordland Fault, which is divided into two segments, one NW-SE striking segment that runs between Korsfjorden and Hovlandsnuten (NE Tysnesøy), and one NE-SW striking segment, continuing from NE Tysnesøy and can be traced to the sea south of Bømlo (Andresen and Jansen, 1987; Rykkelid, 1987; Andersen and Andresen, 1994). The nappe stacks on the hanging wall side of each of the respective NE-SW trending faults are considered to occupy a higher tectonostratigraphic level than the nappe stacks on the footwall side. On the east side of the HFSZ (foot wall, in the Hardanger region), from the lowest to the highest tectonostratigraphic level, the nappe complex is composed of basement rocks plus Autochton and a Parautochthonous cover, Lower Allcothonous phyllites overlain by the far-travelling crystalline rocks, Hardanger-Ryfylke (lower) Jotun-Halsnøy Nappes, which are considered to be Middle Allochthonous (Andersen and Andresen, 1994; Roffeis et al., 2013; Roberts et al., 2014). The nappe complex located to the west of the HFSZ and bounded by the Sunnhordland fault to the NW comprises basement, succeeded by a thin layer of antennuated Middle Allochthonous rocks, which in turn is unconformably overlain by Upper Allochtonous rocks. The rocks of the Upper Allochthon consists of ophiolite and island-arc lithologies, including arc-related metavolcanites. Collectively these rocks are termed the Ølve-Varaldsøy Complex. Unconformably overlying them are groups of mostly marine metasediments with basal clastic materials derived from the underlying substrate (Andersen and Andresen, 1994; Brekke et al., 1984).This is particulary conspicuous in the Mundheim group, located on northern Varaldsøy. A continentally derived metasediment formation (the Grånut Formation), trapped in a syncline, unconformably overlays the ophiolites SW on Varaldsøy (Andersen and Andresen, 1994). The formation resembles the metasediment synclines found in the Major Bergen Arc (Andersen and Andresen, 1994). To the west of the Sunnhordland Fault, on the hanging wall side, a similar nappe complex can be identified. It consists, at it's base, of the Lykling Ophiolite, which was intruded by plagiogranites. Unconformably overlaying them is the island-arc rocks of the Geitung Unit (Brekke et al., 1984; Dunning and Pedersen, 1997; Andersen and Andresen, 1994) and

succeeding the Lykkling-Geitung units is the arc-related volcanics of the Siggjo-Katnakken extrusives (Brekke et al., 1984; Dunning and Pedersen, 1997). Resting on the correlatives of the Lykling Ophiolite and the Siggjo-Katnakken complexes are the Vikafjord and Dyvikvågen groups. The Vikafjord Group (Bømlo) consists of shallow and deep marine sediments, on top of which rests a thick pile of subarial mafic lavas (Brekke et al., 1984; Andersen and Andresen, 1994). The Dyvikvågen Group (Stord) comprises marbles overlain by submarine basic volcanics, which in turn is overlain by the Utslettefjell Granitic Conglomerates (Færseth and Steel, 1978; Andersen and Andresen, 1994).

The highest tectonostratigraphic unit in the Bergen-Sunnhordland region, the island of Tysnes, is mainly composed of gabbroic and granitic intrusives, however, it also consists of basaltic metavolcanites, conglomerates, island arc and ophiolithe lithologies. Most of the Tysnes Nappe is located in the hanging wall of the Sunnhordland Fault, however, the metavolcanites located in the southwestern part of eastern Tysnesøy are considered to be the laterally equivalent of the Mundheim Group. The intrusives are part of the Sunnhordland Batholith (Andresen and Jansen, 1987; Andersen and Andresen, 1994).

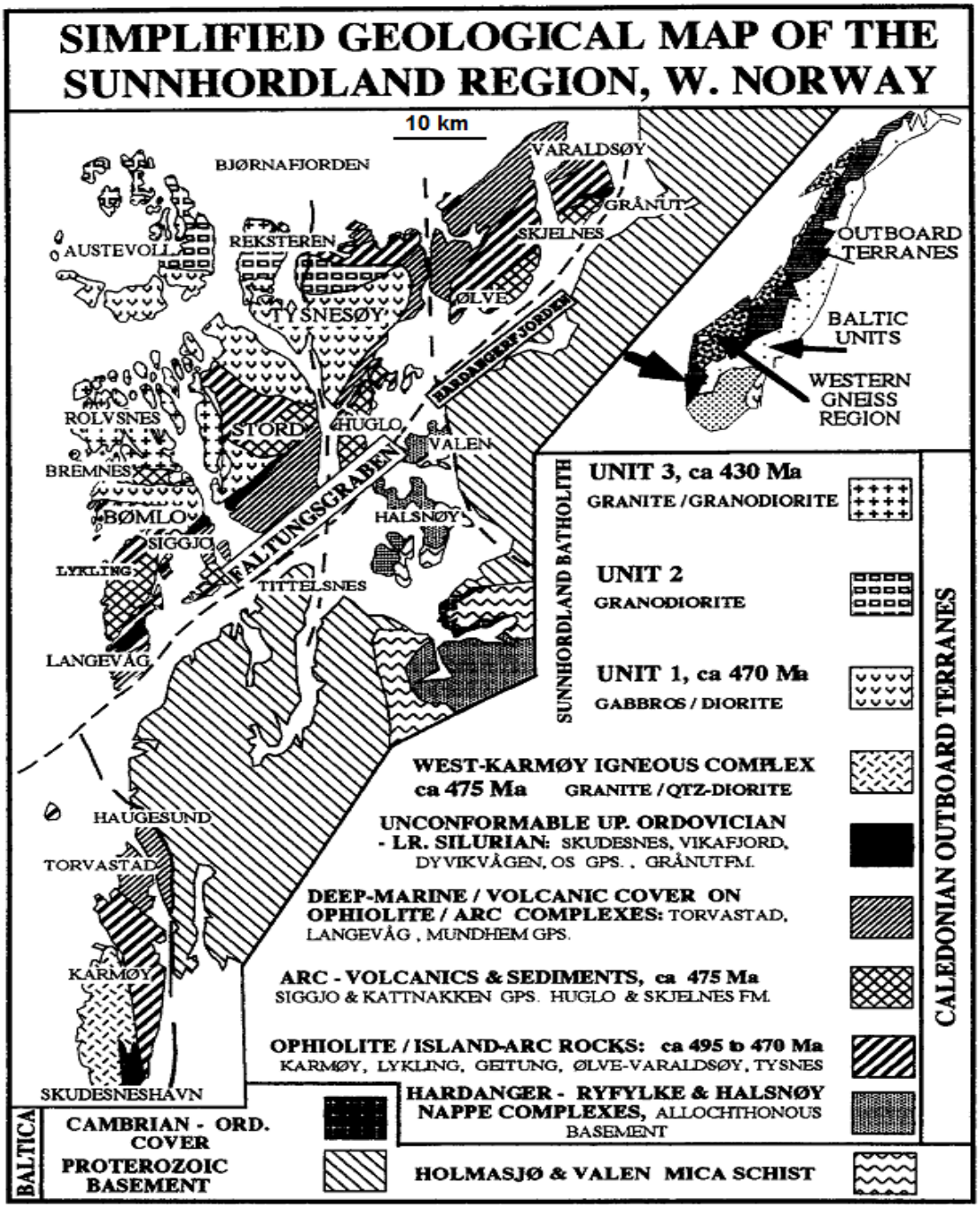

Fig. 2.3: Simplified geological map of the Sunnhordland region. showing the distribution of the tectonostratigraphc units, including the extensive Sunnhordland Batholith (Andersen and Andresen, 1994).

2.3.3 SUNNHORDLAND BATHOLITH

The Sunnhordland Batholith (Fig. 2.3) is a large igneous body which covers an area of over 1000km^2 between the Bergen Arc System and the Sunnhordland Nappes. It is composed of three units. Unit 1 comprises gabbros and metadiorites, unit 2 consists of plutonic granodioritic rocks and unit 3 of plutonic granodiorites and monzogranites (Andresen and Jansen, 1987). The units are dated to between 430-470Ma (Andersen et al, 1994) where the gabbroic unit is the oldest (465-470Ma), and the granitic units are the youngest (430-450Ma). The batholith consitutes a major part of Stord and Bømlo, and the major part of the Rolvsnes, Tysnes, and Austevoll islands. The batholith crosscut dykes in the Lykling-Geitung and Siggjo-Katnakken complexes and is assumed to post-date these units, while it is inferred to be contemporaneous with the metasediments on Bømlo and in the Austevoll area in which it intrudes and partially envelopes (Andresen and Jansen, 1987; Rykkelid, 1987). Furthermore, a satellite pluton of the batholith (the Krossnes Granite, Fig. 2.2) intrudes the Gullfjell Ophiolites and cuts the folliation of the adjacent older metasediments in the Major Bergen Arc (Fossen and Ingdahl, 1988).

2.4 POST CALEDONIAN EXTENSION

In the early Devonian, the Scandian convergence ceased and the orogen experienced a reversal in kinematics (Fossen and Dunlapp, 2006). This extensional period of the Scandian phase, which spanned several phases during the Devonian, can be identified in the SW Norway, where the direction of crustal shortening typically trends NW-SE in the Bergen area, and NE-SW in the Sunnhordland region and in the Jotun Nappe (Fossen, 1998). This extension resulted in further deformation of the already deformed nappes, overprinting or even obliterating previous structures. Futhermore, this deformation may be subdivided into Mode 1 and Mode 2 (Fossen, 1998; Fossen and Dunlapp, 2006), which correlates to reverse and oblique nappe movement, respectively. Most of the Bergen Arc System show indications of Mode 1 type shear, but parts of the MaBa are likely Mode 2 (Fossen, 1998; Fossen and Ingdahl, 1998; Færseth et al., 2011). The same is true for the WGR. The decollement under and part of the Hardanger-Ryfylke Nappes, plus ophiolite/island arc lithologies of Sunnhordland are subject to Mode 1 extension. Mode 1 is thought to represent nappe movements, i.e. nappes sliding back. While Mode 2 represents the extensional movement that may have continued after the backsliding stopped (Fossen, 1998). Thus parts of the nappe stacks in SW Norway may have continued to move by extension while other parts of the nappes were close to stationary. This, together with the assumed movement of 20 km, attributed to post-caledonian extension (Fossen, 1998) explains the complicated tectonostratigraphy found in the Bergen-Sunnhordland region.

2.5 AREAS OF GEOLOGICAL INTEREST

This chapter is an overview of the geology from which four metasedimentary rock samples were collected as well as of the units and formations that are related to them. Underneath is a list (Tab.2.1) of the samples, their locations, lithologies and coordinates. A simplified geological map illustrates their locations with respect to eachother (Fig. 2.4).

Tab. 2.1: List of samples.

Sample	Locality	Lithology	Coordinates
BGA2-1	Os	Garner-bearing quartz-mica schist	N 60.19823° E 005.51146°
BGA2-2	Os	Albite-mica schist	N 60.19823° E 005.51146°
OS-2	Melkevik	Chlorite-garnet-mica schist	N 60.135465º E 005.435445º
MOK	Møkster	Garnet-mica schist	N 60.06847° E 005.08196°

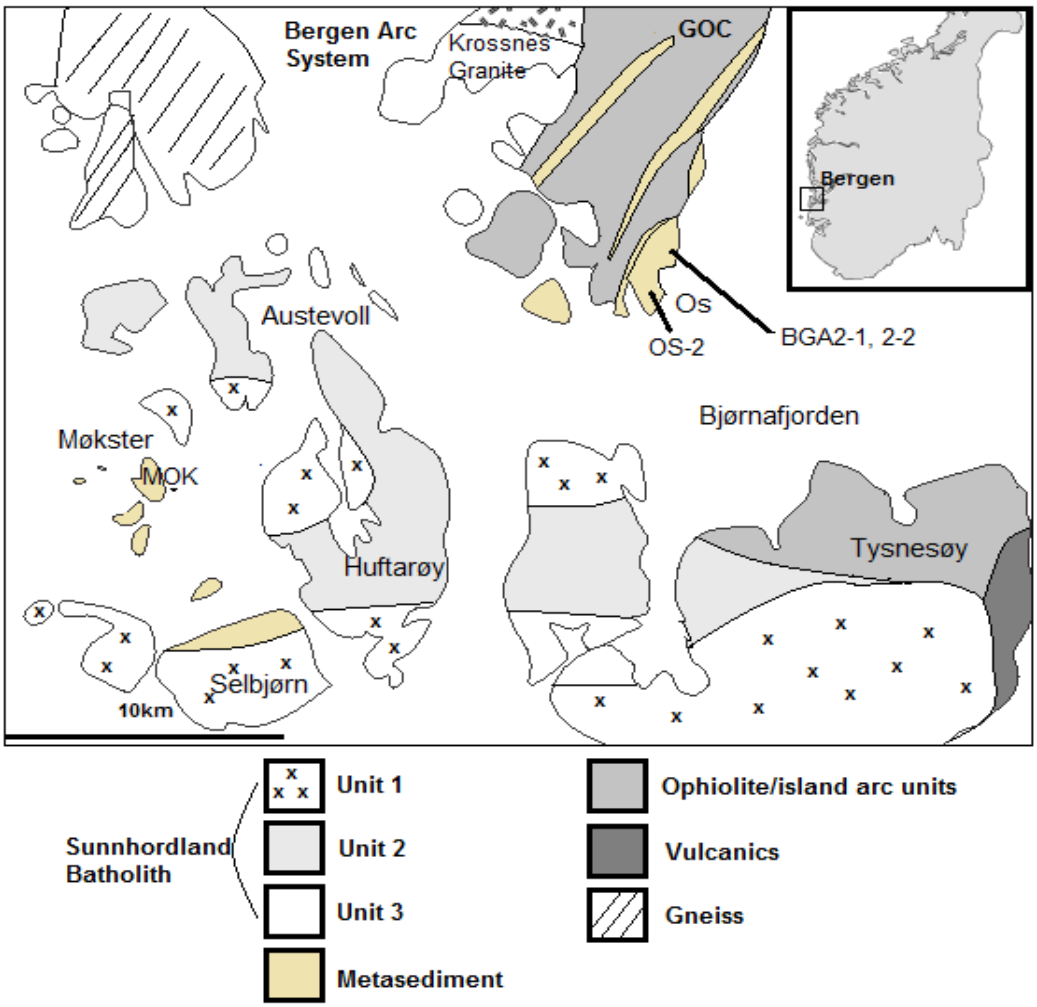

Fig. 2.4: A highly simplified geological map of the northern Sunnhordland-Bergen region, drawn to illustrate the MOK, OS-2, BGA2-1, 2-2 sample locations with respect to eachother. The metasediment in the Bergen Arc System is part of a nappe stack sequence, while the metasediment in Austevoll is surrounded by the Sunnhordland Batholith and has a somewhat enigmatic tectonic position in comparison. The map is a modified version of Andersen and Jansen (1987).

2.5.1 METASEDIMENTS IN THE SUNNHORDLAND BATHOLITH

Bremnes

The metasediments is located in an enclave within the batholith on northern Bømlo, it comprises migmatic arkoses, mica schists, quartzites and meta-limestones. Where the batholith comes into contact with the metasediments, the rocks show overprinting structures related to high-grade metamorphism. Garnet-sillimanite and coriderite-sillimanite are the mineral assemblages here (Andresen and Jansen, 1987; Rykkelid, 1987).

Møkster

Of similar exposure and composition are the metasediments of Austevoll (Andresen and Jansen, 1987), and of special interest are the metasediments on Møkster (Fig. 2.4, Fig 2.5). Møkster comprises layers of migmatized psammites and pelites, quartzites, marbles and banded calc-silicates (Rykkelid, 1987). This order of sequence was inferred by Rykkelid (1987) to be a result of imbrication caused by a tectonic event. The metasediments are intruded by the gabbroic unit of the Sunnhordland Batholith, represented by layered dykes of gabbro and cumulatives (Rykkelid, 1987). The intrusions caused a relatively high degree of melting in the adjacent sediments, which is conspicuous in the psammites and pelites which may contain up to 50% neosome (Rykkelid, 1987). These migmatized sediments hosts vaguely defined zones of gneisses and mica schists, as a result of a tectonically related deformation of the melt (Rykkelid, 1987). The mica schists are commonly garnet-rich muscovite schists with varying amounts of biotite, plagioclase, staurolite, chlorite, chloritoid, silimanite, kyanite, epidote, tourmaline, apatite and sulfides. The garnet is typically rimmed by chlorite (Rykkelid, 1987). The overlying layer of quartzite consists of strongly tectonized lenses that can be observed as thinner lenses emplaced in the migmatite. The boundaries between the two layers are vague. In a sharp contact, a layer of marble succeeds the quartzite (Rykkelid, 1987). The marble consists of a calcitic and a dolomitic component, both of which have been brecciated and deformed in some locations (Rykkelid, 1987). A calc-silicate layer gradually transitions from the marbles. It consist of alternating bands of marble and calc-silicate, the calc-silicate comprises microcline, actinolite, muscovite and chlorite (Rykkelid,

1987). The muscovite, chlorite and chloritoid components found in the sequence was inferred as retrograde minerals by Rykkelid (1987), while the garnet, staurolite, actinolite etc. represents the prograde assemblage of the rocks. The sequence is correlated with the metasediments on Lundøy and is assumed to be the stratigraphic successor of the arkoses and pelites found there (Rykkelid, 1987). The pelites on Lundøy is underlain by greywackes succeeding a basal conglomerate which comprises clasts derived from the underlying Selbjørn Ophiolite (Rykkelid, 1987). This unconformable metasediment sequence on ophiolite was correlated with similar sequences, such as the Holdhus Group (inferred to be of Upper Ordovician-Sillurian age by Færseth et al., 2011) in the Major Bergen Arc by Rykkelid (1987). Later research on similar complexes with a peri-Laurentian affinity makes this less likely (Pedersen, 2015).

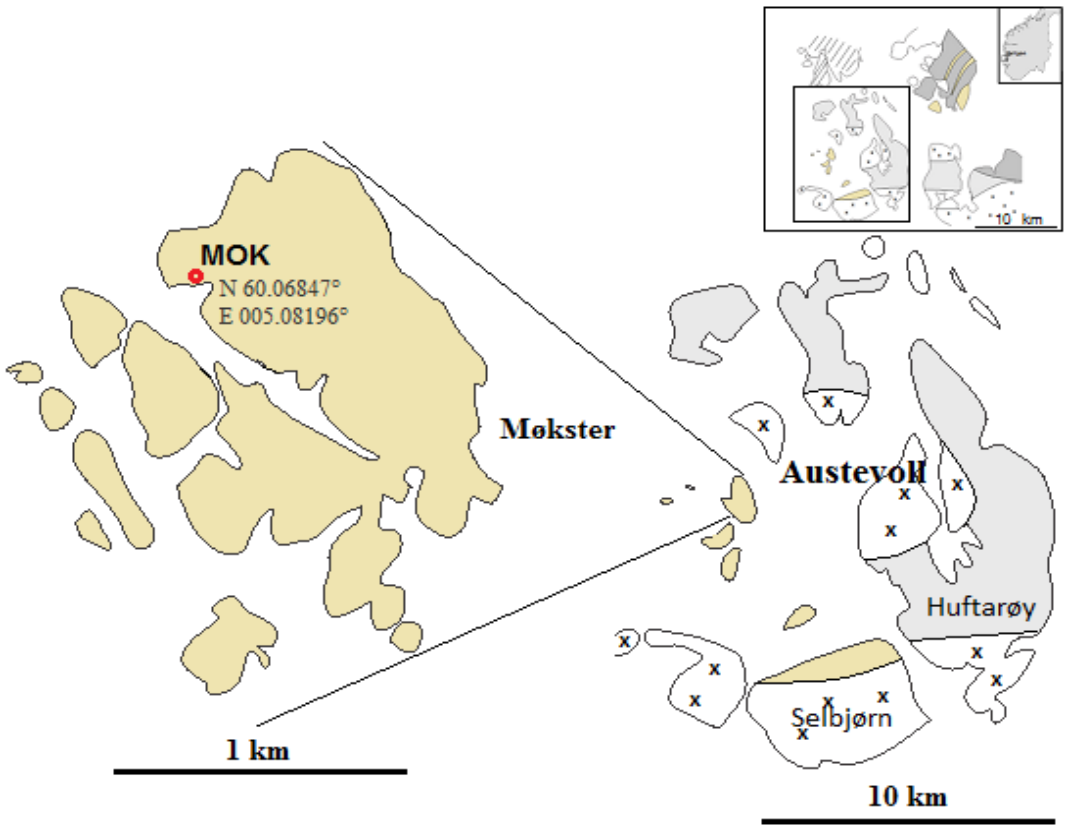

Fig. 2.5: A zoomed figure of the Austevoll area on map (Fig. 2.4) to show the location of MOK on Møkster (red dot).

2.5.2 THE MAJOR BERGEN ARC

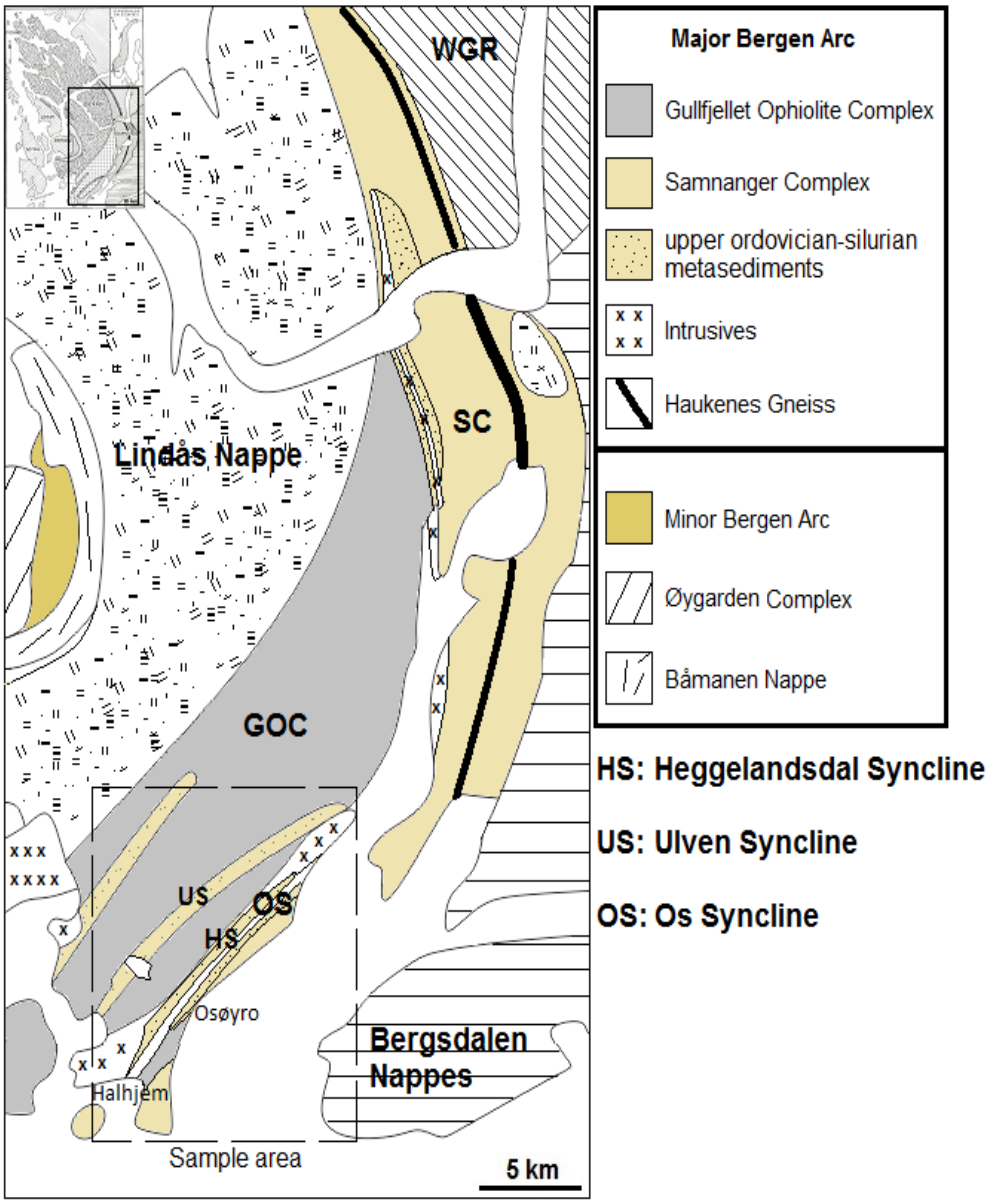

Fig. 2.6: Simplified geological map of the Major Bergen Arc, modified map of Færseth et al. (1977). The stipled square is the area where the samples were collected from.

The Major Bergen Arc (Fig. 2.6) is roughly composed of the Gullfjell Ophiolite Complex (GOC), the Samnanger Complex (SC) and the OS/Holdhus Groups. The two complexes are the most extensive by far. The Samnanger Complex occupies most of the northern and eastern part of the arc, while the GOC occupies much of the central-western to south-western part. The OS Group and its correlatives occurs, squeezed/pinched between or within the Samnanger Complex and the GOC in the central NW of the arc and in the Os area (Færseth et al., 1977; Ingdahl, 1989; Færseth et al., 2011). Tectonostratigraphically, the oldest part of the Samnanger Complex occupies the lowermost section, while the subsequent parts are on the same level as the Gullfjell Ophiolite Complex. Following a break, the OS/Holdhus Group overly the aforementioned units.

The Gullfjell Ophiolite Complex

The Gullfjell Ophiolite Complex (Fig. 2.6) comprises sheeted dykes, greenstones, gabbros and arc-related granitoid intrusives. The gabbros have been dated to 489 ± 3 Ma (Dunning and Pedersen, 1988) while the granitoid intrusions has been dated to 482 ± 3 Ma (Dunning and Pedersen, 1988). Both pre-date the Scandian orogen by some 40 Ma, and their zircon provenance lack the Timanide signature permeating the Baltic rocks (Pedersen, 2015). Because of this, many authors suggest a Peri-Laurentian origin for the GOC (Dunning and Pedersen, 1988; Roberts, 2007; Roberts et al., 2014). The Gullfjell Ophiolite Complex is in contact with strongly deformed pelitic and psammitic rocks which have be intruded by the granitoids. These metasediments may represent the original cap rock to the ophiolite (Færseth et al., 2011).

The Samnanger Complex

The Samnanger Complex (Fig. 2.6) is a highly deformed rock complex with a complicated tectonostratigraphy composed extensively of metasedimentary slices. The metasediment comprises mica schists as the major constitutent, with moderate amounts of quartz schist, conglomerates and tectonic melanges (Færseth et al., 1977; Ingdahl, 1985). In the eastern part

of the complex, a major amphibolite unit occurs in a sharp contact with the metasediment, together with the extensive Precambrian gneisses which comprises the Haukness Gneiss and the anorthosite gneisses farther east. The complex is also riddled with intrusives, from ultramafic lenses to quartz-dioritic dykes. The ultramafic lenses are interpreted as rocks thrust up from the bottom of the GOC and into the sediments (Færseth et al., 1977 ; Færseth et al., 2011). As such, in the words of Færseth et al. (2011), «the Samnanger Complex resembles a large scale imbricate structure involving ophiolites, continental prism sediments and their gneissic substrate». Færseth et al. (1977) inferred that the metasediments of the Samnanger Complex (SC) in the Samnanger-Osterøy area were subject to an early Caledonian (Ordovician) phase of deformation/foliation accompanied by metamorphism at upper greenschist to lower amphibolite facies conditions. The heat required was pressumably generated by the numerous granitoid intrusions which riddles the complex, and there are textures implying contact metamorphism between the intrusives and the metasediment supporting this (Færseth et al., 1977). Most of the granitoids in the complex was affected by the early Caledonian/Prescandian Deformation (Færseth et al., 1977), however, some quartz-diorites appears to cut the foliation in the metasediment as well as cutting other granitoids. Thus, the Samnanger Complex contains granitoids of several generations (Færseth et al., 1977). During the Scandian shear deformation phase, the rocks of the Samnanger Complex were subject to metamorphism in the lower to upper greenschist facies conditions according to Færseth et al. (1977), which for the metasediments in the Samnanger Complex is regarded as a retrograde metamorphic event (Færseth et al., 1977; Færseth et al., 2011).

Metasediments

The mica schist is by far the most extensive rock of the Samnanger Complex and makes up a major part of both the western and eastern Samnanger Complex. Generally the composition can be summarized to quartz-ablite-muscovite-biotite-chlorite, with accessories of garnet, graphite, actinolite epidote, apatite and pyrite (Færseth et al., 1977). The garnet is typically affected by strong deformation and has been replaced by chlorite to various extents due to retrogression (Færseth et al., 1977). Other metasediments, interlayered with the mica schists includes conglomerates and quartz schists. A prominent quartz schist with alternating layers of mica-rich and quartzite-rich compositions occurs mostly to the west of the Precambrian gneisses. Only the albite-mica schist can be mapped as a unit in the Samnanger-Osterøy area

(Færseth et al., 1977). However, in the southern Os area, Ingdahl (1985) mapped 5 formations and melanges (Fig. 2.7) described below.

The Ådnavik Formation

The Ådnavik Formation consists of a strongly deformed banded mixture comprising mica schist, phyllites, chert, garnet mica schist, calcareous schist and meta-sandstones (Ingdahl, 1985).To the west of the Ådnavik formation is the Bjørnen Melange. The melange comprises fragmented blocks of psammite, marble, chert, conglomerate, metagabbro, amphibolite and trondhjemite found in a pervasively deformed mica schist matrix (Ingdahl, 1985). The matrix consists of alternating quartz- and mica-rich bands which locally contains garnets or amphibole. The melange contains blocks both from the overlying Bjørnatrynet Formation and from other, exotic lithologies (Ingdahl, 1985).

Bounded by the Bjørnen Melange to the east and by the Melkevik Formation to the west, The Bjørnatrynet Formation unconformably overlies the aforementioned units. It consists of phyllite, sandstone and conglomerate members interpreted as deltaic sediments by Ingdahl (1985).The sequence is dominated by the conglomerate member, with subordinate sandstone and thin phyllitic members (Ingdahl, 1985).

The Melkevik Formation occurs in a zone between the Skarholmen Melange and the Bjørnetrynet Formation. It is essentially a mica schist which comprises garnet-albite-mica-quartz schist with minor greenschist bands and serpentinite bodies scattered within (Ingdahl, 1985).

The Skarholmen Melange occurs to the west of the Melkevik Formation in a sharp tectonic contact. Westward, the melange transitions into the rocks which constitutes the cap rock to the Gullfjell Ophiolite (Ingdahl, 1985). The melange comprises blocks of garnet-albite-mica-quartz schist, chert, psammite, vein quartz, greenstone, trondhjemite, mica schist, amphibole-rich sediments and marble, all located in a phyllite and mica schist matrix (Ingdahl, 1985). The melange represents a deep marine environment covered by pyroclastics and intruded by trondhjemite. During the Scandian deformation the sequence was brittely deformed, mixing the different rocks, thus creating a tectonic melange (Ingdahl, 1985).

Ingdahl (1985) recognized a pre-Scandian deformation/foliation in the rocks of all of the formations and melanges with the exception of the Bjørnatrynet Formation, which resembles the rocks of the OS and Ulven Group (Pedersen, 2015).

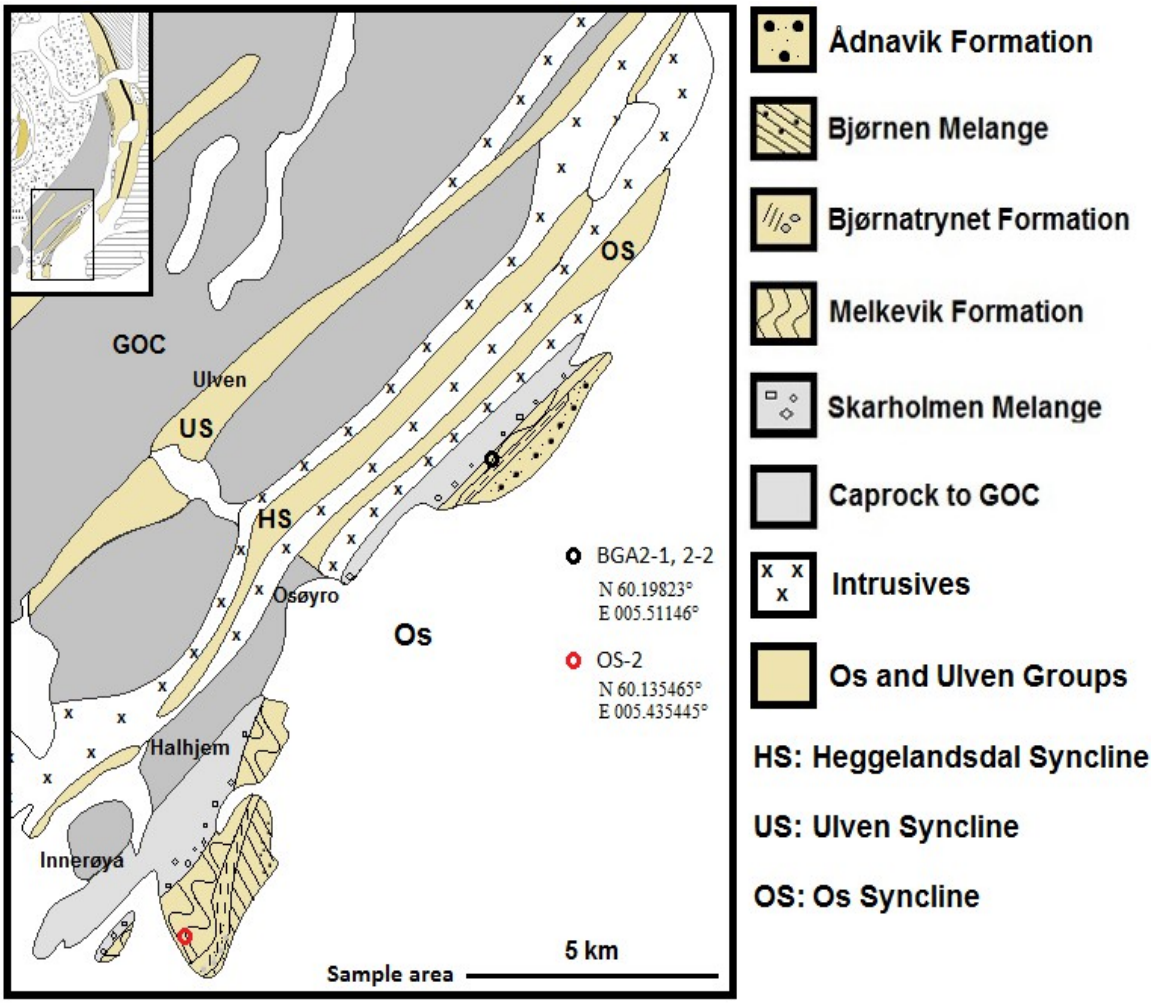

Fig. 2.7: Simplified geological map over the southernmost part of the Samnanger Complex adapted from and Færseth et al. (2011).

THE OS GROUP

The OS Group (Ingdahl, 1989) (Fig. 2.6, 2.7) comprises Upper Ordovician-Silurian metasediments which were folded and squeezed between the rocks of the Gullfjell Ophiolite Complex and the Samnanger Complex during the Scandian deformation event (Færseth et al., 2011). It is composed of two metasedimentary groups, The Holdhus Group and the Ulven Group.

The Holdhus Group

The Holdhus Group occurs within the Samnanger area and on Os. It can be divided into three formations, Heggelandsdal Formation, Valla Formation, and the Moberg Conglomerate (Færseth et al., 1977; Ingdahl, 1989).

The Moberg Conglomerate can be traced from the Os area in the south through the Samnanger area to Osterøy in the north. It represents an alluvial fan, made up of coarse, polymict conglomerate with minor lenses of sandstone (Færseth et al., 1977; Ingdahl, 1989). The coarse conglomerate contains a mixture of igneous and metamorphic clasts set in a matrix composed of medium-grained lithic to feldspathic greywacke. The volcanic clasts includes greenstones derived from the adjacant exposed Gullfjell Ophiolite. The conglomerate is also intruded by granitoids (i.e. quartz-diorites) which may both cut or appear parallel with the foliation (Ingdahl, 1985) Conformably overlying the Moberg Conglomerate is the Valla Formation. It consists of marble and fossiliferous limestones (Ashgillian age) overlain by phyllite/mica schist (Llanodverian age). Despite it's conformable relationship to the Moberg Formation, tectonized contacts occurs at several localties, and in Samnanger, marble appears, interfingered with the conglomerate (Færseth et al., 1977; Ingdahl, 1989).
The Heggelandsdal Formation occurs within the Heggelandsal Syncline (Fig. 2.7), and it represents the uppermost part of the Holdus Group. The formation consists of a sandstone sequence with minor amounts of conglomerate and mica schist. Locally the formation contains basal conglomerate in sharp contact with the underlying limestone or greywacke of the Valla Formation. The conglomerate is similar to the underlying Moberg Conglomerate (Færseth et al., 1977; Ingdahl, 1989).

The Ulven Group

Occuring in a syncline between ophiolitic rocks south in the GOC (US in Fig. 2.7), the Ulven Group comprise two metasedimentary units, the Vaktdal, and the Skarfjell Formation.
The group occupies a 12 km long 850 m wide (maximum) area in the GOC (Ingdahl, 1989; Færseth et al., 2011).

The Vaktal Formation is stratigraphically the lower of the two and is in tectonic contact with the ophiolite, leaving no clear boundary between them. The formation consists chiefly of Llanodvery graptolitic phyllite with thin quartzite stringers, interbedded with frequent incursons if quartzite veins. The upper part of the formation consists of a gradually coarsening uppwards quartzite. The top of the formation is abruptly truncated by the overlying Skarfjell Formation (Færseth et al., 2011; Ingdahl., 1989).
The Skarfjell Formation consists of alternating layers of conglomerate and sandstone, where the conglomerates constitute the base layer of the formation. Generally, the conglomerate fines uppwards and in a sharp contact, it is succeeded by much a thicker layer of sandstone (Ingdahl, 1989; Færseth et al., 2011). Following this, several alternating beds of conglomerates and sandstones occurs. The conglomerates consists of well-rounded cobbles of quartzite, sandstone, phyllite, and serpentinite in a quartzitic matrix (Færseth et al., 1977; Ingdahl, 1989; Færseth et al., 2011). The sandstones preserves various erosional structures and it is composed mainly of medium grained quartzite (Færseth et al., 2011).

The Ulven Group is correlated with the Vaktdal Formation of the OS Group and above, based on their common Llandoverian phyllite and other lithological similarities. Both the OS and the Ulven Group have been affected by prograde metamorphism within greenschist facies conditions which Ingdahl (1989), Færseth et al. (1977, 2011) interpreted to be the result of the Scandian deformation event. Thus, the Ulven and OS Group constitutes the youngest metasediment in the Major Bergen Arc.

3 METHODS

SAMPLE COLLECTION

Four samples were collected for this study. First comes from Møkster island in Austevoll (sample MOK), two others are from Samnanger (BGA2-1 and 2-2) and one from the Melkevik Formation in the vicinity of the town of Os (OS-2). Reference to a Figure with sample locations.

Petrographic thin sections

A part of each rock sample was cut off with a diamond saw, put in individual plastic bags and labeled. The samples were then given to the thin section lab technician for preparation. All of the thin sections were polished so that they could have been analysed with electron microprobe.

MINERAL SEPARATION

Crushing and milling

The rock samples were cut into cobble-sized pieces with a diamond saw and crushed with a jaw crusher (Fig. 3.1 a) into the gravel size.

A fraction of the crushed samples was milled in an agate mill (Fig. 3.1 b) until no grains could be felt between the fingers. Each resulting powder was then taken to a mineral preparation lab and heated up to 1000 ^{O}C in an oven for between 2 and 3 hours in order to turn the various elements into oxides. The heating led to a general loss of volatiles and the amount of volatiles removed was determinted as loss on ignition (LOI), by weighting the difference in mass before and after heating.

Glass Tablet Preparation

0.96g of the oxidized rock powder was mixed together with 6.72g of dried flux (spectromelt A-10, lithium tetraborate, $Li_2B_4O_7$). The flux reduces the melting point and time necessary to melt the rock powder. The powder mix was transferred to a platinum crucible which was mounted above a gas torch in a fusion furnace (Claisse, model fluxy). A platinum collector plate was mounted above the crucible containing the sample. During the run time of the furnace, the sample was rotated at an angle continuously to evenly distribute the heat through the sample and to gradually pour the melt into the collector. After around 30 min. plus a cooling period, up to three glass disks was produced. The entire melting and cooling process is automated.

MAJOR ELEMENT ANALYSIS

Whole-rock major element concentrations were analyzed by standard X-ray fluorescence spectroscopy (XRF) procedures by a technician using a Phillips PW1404 in the XRF-laboratory at UiB. All the resulting analyses had total concentrations of main element oxides between 98.6 and 99.8%.

MINERAL ANALYSIS

The mineral compositions were determined in 6 polished thin sections representing 4 samples with a Cameca SX100 Electron microprobe at the Department of Geosciences of the Oslo University. The electron microprobe operated under 15 keV accelerating voltage and a beam current of 20 nA, with a 2 μm beam size. In two of the samples, the microprobe was set to automatically acquire analyses with the step of 8 μm across garnet grains , in order to detect compositional differences along a profile.

Tab 3.1: Overview of other methods.

Methods/Software	**Aim**
Optical microscopy	Identification of mineral assemblages, microstructures and mineral modes.
SEM	Detection of monazite micro inclusions, micro-textures, acquisition images.
Perple_X (Connolly, 2005; 2009)	Modelling of the PT conditions at which the determined mineral assemblages formed.
Gabbrosoft, mineral formula recalculation spread sheets.	Recalculation of the mineral formulas from the analysed mineral compositions.
Corel Draw/Ghostscript	Draw/redraw postscript files (Perple_X output language).

Fig. 3.1. **a)** Jaw crusher located in the basement in UiB.

b) Agate mill located in the basement in UiB.

4 RESULTS

4.1 WHOLE ROCK CHEMISTRY

The whole-rock analysis results are shown in the table below (Tab. 4.1).

Tab. 4.1: Whole rock chemistry from each respective sample.

WT%				
SiO2	71,98	55,19	40,41	55,30
TiO2	0,69	1,15	1,59	1,11
Al2O3	9,00	18,72	29,70	20,50
Fe2O3	8,99	8,80	17,00	11,66
MnO	1,46	0,16	0,24	0,25
MgO	2,81	4,58	2,52	3,03
CaO	1,10	1,40	0,92	1,26
Na2O	1,03	2,54	1,06	0,75
K2O	3,14	6,59	5,19	4,76
P2O5	0,07	0,27	0,05	0,11
Total	100,27	99,40	98,68	98,73
LOI	1,4	1,9	3,05	3,4

4.2 SAMPLE DESCRIPTIONS

Thin sections of the four samples collected in the field were investigated under the microscope and analysed with electron microprobe. The thin sections from the Møkster samples are termed MOK(1-5), thin sections from the sample collected from the Os area are termed BGA2-1, BGA2-2 and OS-2. Each sample is described on a textural and compositional basis and the text is complemented with Figures illustrating mineralogical evolution and differences. All of the mineral abbreviations used in this chapter is after Whitney (2010).

4.2.1 MOK Garnet-mica-schist

The sample is composed of a matrix with large garnet porphyroblasts (Fig.4.1). The matrix generally consist of chlorite (10-15%), white mica (75-80%), quartz and feldspars (4-5%), ilmenite (1-4%), chloritoid (0,5-1%), and small amounts of staurolite. The porphyroblasts are represented by large crystals of highly fractured garnet (15-25% of the total thin section area), containing inclusions of white mica, biotite, ilmenite, quartz, staurolite, chlorite and micro inclusions of monazite. The cracks (and some fractures) are filled by matrix minerals, though chlorite is the main constituent (60%) together with white mica (35-40%). The rest is quartz (0-4%), chloritoid, and ilmenite. Chlorite is much more abundant in the garnet cracks than in the matrix.

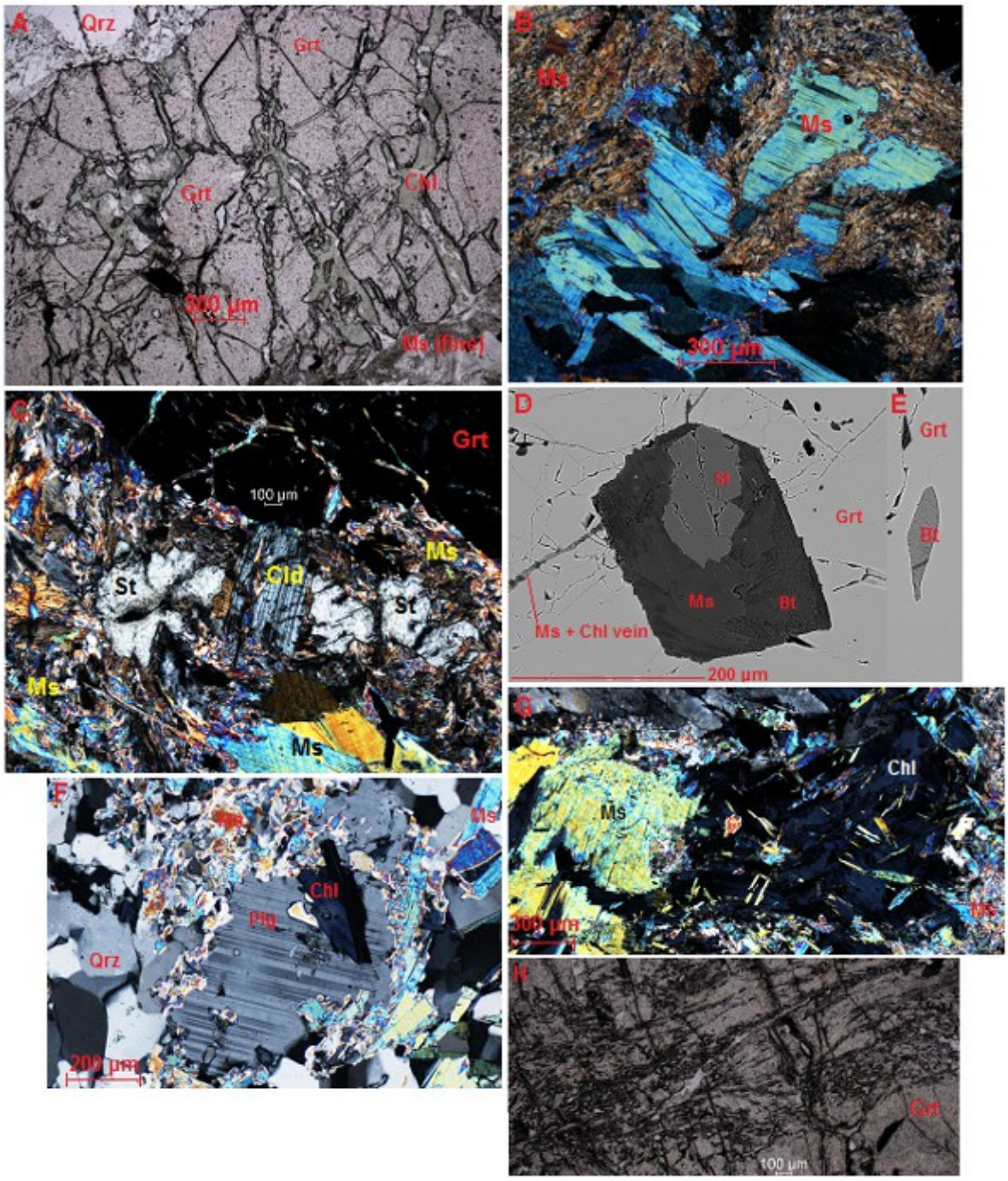

Fig. 4.1:

A) A highly cracked garnet partly consumed by chlorite. **B)** Coarse grained muscovite crystals recrystallized into fine muscovite in the matrix. **C)** Strongly corroded staurolite surrounded by fine-grained white mica. Staurolite is close to a well developed, nearly euhedral chloritoid, all located in the matrix. The staurolite is apparantly being consumed while the chloritoid is growing. **D)** Staurolite-muscovite-biotite pseudomorph enveloped in garnet and penetrated by a crack filled with fine-grained muscovite + chlorite. The staurolite inclusion is an indication of it's concurrent stability with the garnet. **E)** Tiny biotite inclusion inside garnet, completely shielded from the matrix, where the

biotite is absent. **F)** Sericitized feldspar in the matrix, interlocked with quartz. **G)** Chlorite intergrown with coarse muscovite and surrounded by both coarse- and fine-grained muscovite in the matrix. Chlorite accumulations may possibly represent altered biotite crystals. **H)** A slightly curved inclusion trail in garnet porphyroblast. Equal trails cannot be found in the matrix which is chaotic, and any previous foliation has been erased.

Tab. 4.2: Representative electron microbe analyses in wt%. recalculated to structural formulas with indicated numbers of oxygen. The formulas were recalculated by using excel sheets listed in table. 3.1. in the methods chapter.

MOK													
	Garnet							Matrix					
Sample:													
	Bt	Chl	Grt	Grt	Grt	Ms	St	Chl	Cld	Pl	Ms	Ms	St
	2 / 1 .	4 / 1 .	3 / 1 .	1	50	26 / 1 .	27 / 1	20 / 1 .	40 / 1 .	25 / 1	36 / 1 .	32 / 1 .	49 / 1 .
				rim	core								
SiO2	35,09	23,01	36,77	37,77	37,05	46,29	27,43	23,76	24,47	61,63	46,19	45,44	27,20
TiO2	1,83	0,26	0,08		0,02	0,88	0,71	0,13	0,01		0,21	0,14	0,78
Al2O3	18,37	23,09	20,57	21,20	21,07	35,87	53,99	21,55	40,29	24,28	37,01	41,64	53,68
Fe2O3													
FeO	21,81	32,25	37,58	36,10	36,70	1,89	9,38	32,19	24,34	0,06	1,05	0,36	10,23
MnO		0,07	0,18	0,06	0,44	0,04	0,04	0,12	0,05		0,00	0,01	0,03
MgO	8,41	8,78	2,36	3,40	2,76	0,63	0,68	9,37	2,06		0,41	0,04	0,87
CaO	0,03	0,07	2,23	1,70	1,93	0,02		0,06	0,03	5,38		1,03	
Na2O	0,29	0,07	0,01			1,36	0,19	0,03	0,00	8,87	1,26	5,81	0,14
K2O	9,39	0,04	0,02			8,97		0,06	0,01	0,07	9,59	2,09	0,01
ZnO							5,05						4,35
Total	95,22	87,64	99,80	100,20	99,97			87,27	91,27	100,28	95,72	96,56	92,94
No.O	22,00	28,00	12,00	12,00	12,00	22,00	48,00	28,00	12,00	8,00	22,00	22,00	48,00
Si	5,53	5,05	2,99	3,00	3,00	6,10	4,01	5,24	2,04	2,73	6,08	5,77	3,99
Ti	0,22	0,04	0,01		0,01	0,09	0,08	0,02	0,00	0,00	0,02	0,01	0,09
Al	3,41	5,98	1,97	2,00	2,00	5,57	9,30	5,60	3,97	1,27	5,75	6,23	9,28
Fe2O3			0,03										
FeO	2,87	5,92	2,52	2,42	2,48	0,21	1,15	5,94	1,70	0,00	0,12	0,04	1,25
Mn	0,00	0,01	0,01		0,02	0,00	0,00	0,02	0,00		0,00	0,00	0,00
Mg	1,97	2,87	0,29	0,41	0,33	0,12	0,15	3,08	0,26		0,08	0,01	0,19
Ca	0,00	0,02	0,19	0,15	0,17	0,00	0,00	0,01	0,00	0,26	0,32	0,14	0,00
ZnO							0,55						0,47
Na	0,09	0,03				0,35	0,05	0,01	0,00	0,76	1,61	1,43	0,04
K	1,89	0,01				1,51	0,00	0,02	0,00	0,00		0,34	
Sum	16,0	19,9	8,0	8,0	8,0	13,9	15,3	20,0	8,0	5,0	14,0	14,0	15,3
X_{Mg}	0,41	0,33	0,10	0,14	0,11		0,11	0,34	0,13				0,13
Almandine			84,00	81,00	82,00								
Grossular			6,00	5,00	5,50								
Pyrope			9,50	14,00	11,00			An		25			
Spessartine			0,50		1,50			Ab		75			

Mineral assemblages

Two distinct assemblages M1 and M2, that have been identified in all five thin sections of the MOK sample. Summarized in Tab. 4.3.

Tab. 4.3:
Mineral assemblages corresponding to M1-M2 metamorphic phases.

Metamorphic phase	M1	M2
Bt	——— -	
Chl	...?	———
Cld		———
Fsp	- - ———	
Grt	———	
Ilm	———	———
Ms(coarse)	———	-
Ms(fine)		———
Qrz	———	———
St	- ———	
Mnz	———	
Pg		———

M1 assemblage

The M1 assemblage is represented by mineral phases enclosed within the garnet porphyroblast and comprises Bt, Grt, Ilm, Qrz, St,white mica (coarse) and plagioclase. With the exception of Qrz and Ilm, all of these minerals appear to be unstable in or absent in the matrix. This is shown and commented on in Fig. 4.1.

Mineral compositions for M1:

Biotite

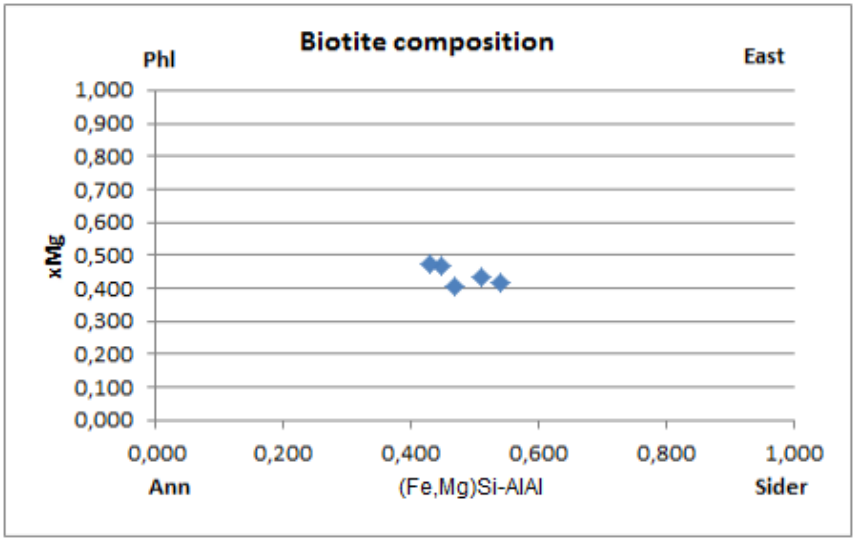

Fig. 4.2: Biotite endmember content in mol%

The composition of biotite is described here as a solid solution among four endmembers: annite- $KFe_3AlSi_3O_{10}(OH,F)_2$, phlogopite-$KMg_3AlSi_3O_{10}(OH,F)_{10}$, siderophyllite-$KFe_2Al(Al_2Si_2)O_{10}(OH,F)_2$ and eastonite-$KMg_2Al(Al_2Si_2)O_{10}(OH,F)_2$ (Deer et al. 1989). The same solid solution endmembers will be used for any subsequent descriptions. The biotite has X_{Mg} = 0.407-0.473, and the end member molar proportions are: 27-32% Ann, 23-33% Sid, 19-27% Phl, 19-23% East (Fig. 4.2). There are no discernable differences between biotite composition and it's position in the garnet.

Garnet

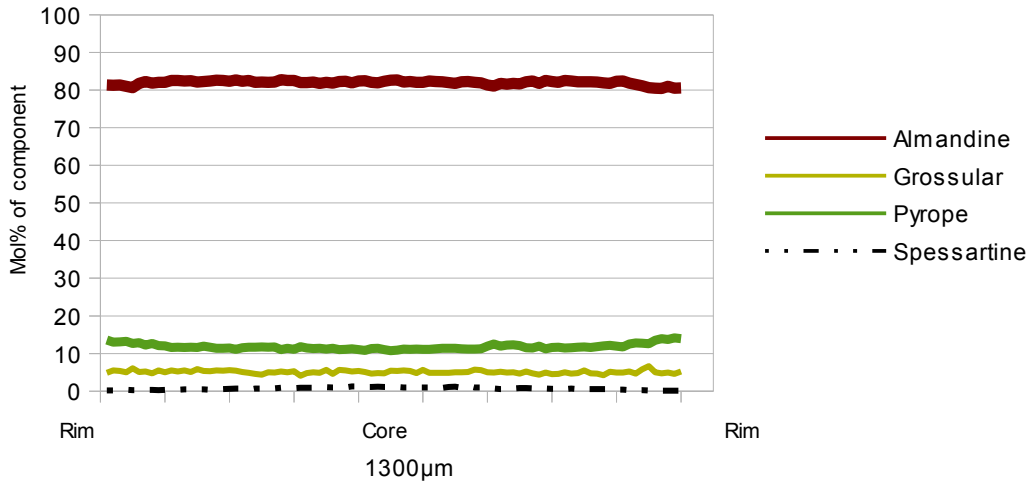

Fig. 4.3: Compositional profile across the garnet from the MOK sample.

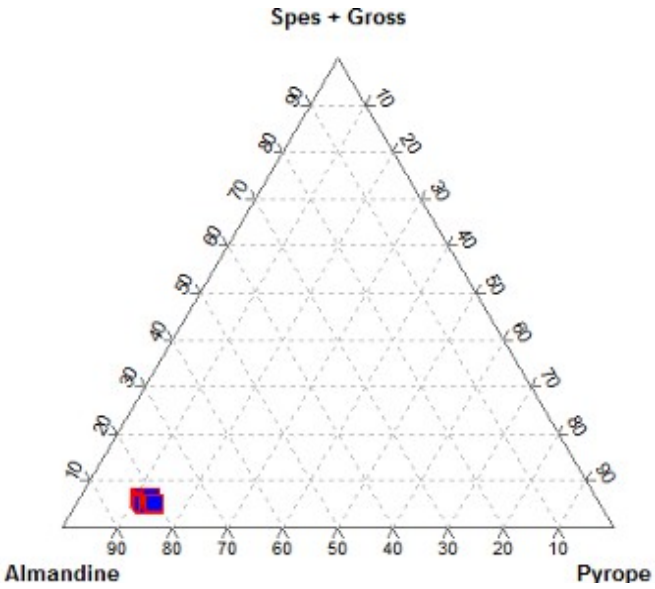

Fig. 4.4: Ternary diagram of mol% content with respect to Alm, Py, Sps and Grs endmembers.

The ternary diagram (Fig. 4.4) and measured compositional profile (Fig. 4.3) show that there is nearly no evolution in chemical composition of the garnet. The analyses all collect in a cluster with $Alm_{83->81}$, Grs_{5-6}, $Py_{11->14}$, Sps_{0-1} Almandine content decreases slightly towards the rim, while the pyrope content increases. Grossular and Spessartine contents remains almost constant.

Feldspar

The feldspars are composed of 22-31% anorthite i.e. they are classified as oligoclase to andesine.

Coarse muscovite

The coarse muscovite consists of Ms 79% , Cel 1-5%, Pg 10-19% and 4-6% Bt endmembers. The composition of the coarse muscovite is illustrated in a the ternary diagram, Fig. 4.6, together with the composition of fine-grained muscovite.

Staurolite

The chemical composition is relatively homogenous, with X_{Mg} = 0.87-0.88 and the staurolite included in garnet has the same composition as that in the matrix. However, zinc oxide (ZnO) makes up about 5 wt% of the staurolite.

M2 assemblage

The M2 assemblage is present in the matrix and is represented by chlorite, chloritoid and fine grained white mica. These are the matrix or retrograde minerals that are inferred to be stable in the matrix, some of them may also consume minerals of the M1 assemblage.

Mineral compositions for M2:

Chloritoid

The X_{Mg} of chloritoid varies from 0.13 to 0.14. This makes the Fe-bearing endmember the most prominent constituent. The Si content is almost constant at 2.00-2.05 a.p.f.u and so is the Al content (3.88-3.95 a.p.f.u).

Chlorite

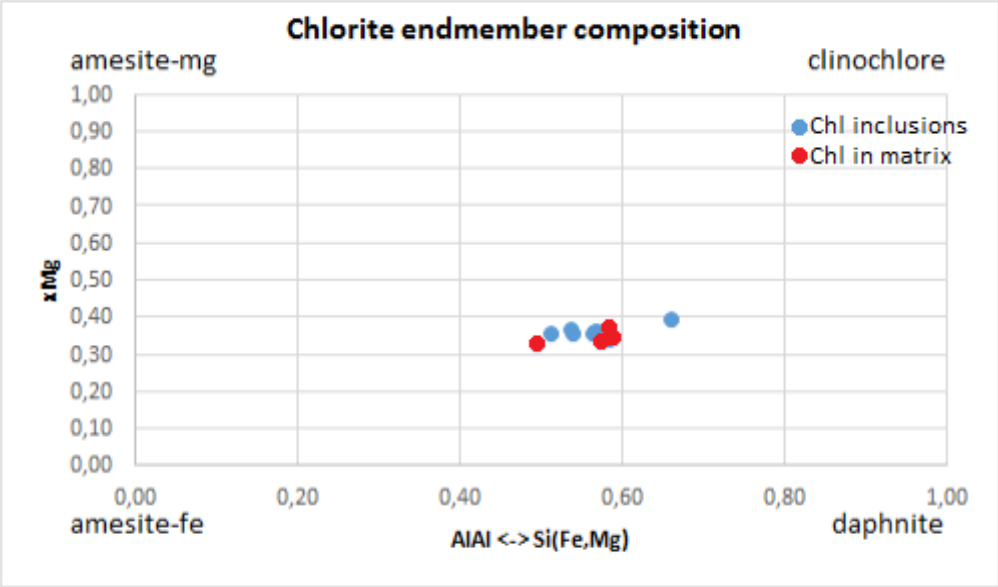

Fig. 4.5: Chlorite endmember content in mol%.

The chlorite has X_{Mg} values of 0.33-0.39, and Al and Si concentrations of 5.33-5.90 and 5.50-

5.30 a.p.f.u., respectively. Fig 4.5 shows the molar content with respect to the endmembers choosen to be in accord with the solution model (Holland and Powell, 1998) used in the modeling software: clinochlore ($Mg_5Al_2Si_3O_{10}(OH)_8$), daphnite($Fe_5Al_2Si_3O_{10}(OH)_8$), Mg-amesite ($Mg_4Al_4Si_2O_{10}(OH)_8$) and Fe-amesite ($Fe_4Al_4Si_2O_{10}(OH)_8$). The endmembers based on Holland and Powell 1998 was used in the description of all of the samples. There are no discernable differences between chlorites in different textural positions.

Fine-grained white mica

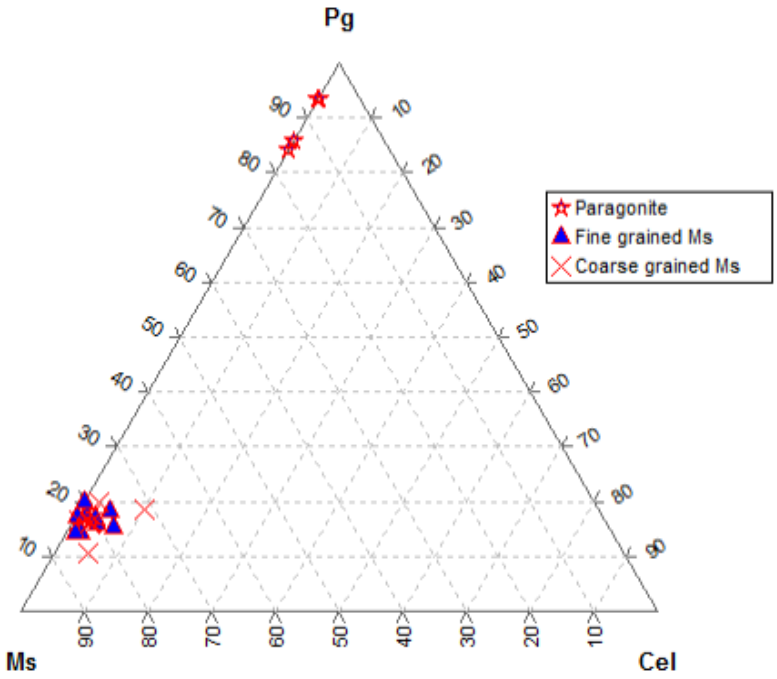

Fig. 4.6: Ternary diagram of the mol% content of the white micas in the MOK sample with respect to Ms, Cel, Pg endmembers.

Fine-grained white mica in the matrix is represented mostly by muscovite (composition in molar%: Ms 74-81%, Cel 0-7%, Pg 14-17% and Bt 2-5%), though there is also a paragonitic white mica present (composition in molar%: Ms 6-15%, Cel 0%, Pg 81-89%, and Bt 3-4%). In the ternary diagram (Fig. 4.6), the fine-grained muscovite and the coarse variety collect in approximately the same field. This is slightly misleading, because there generally is a compositional difference between the coarse and fine muscovites with respect to Fe^{2+} and

Mg^{2+} contents with 0.18-0.23 a.p.f.u Fe^{2+} and 0.15-0.20 a.p.f.u of Mg^{2+}, and 0.11-0.18 a.p.f.u Fe^{2+} and 0.08-0.10 a.p.f.u Mg^{2+} for the coarse and fine muscovite respectively.

4.2.2 OS-2 Chlorite-garnet-mica schist

This sample is composed of a matrix with large garnet porphyroblasts. The matrix comprises chlorite (ca. 30%), muscovite (ca. 40%) and quartz (ca. 25%), with accessory amounts of epidote, apatite, titanite, opaque minerals and negliglibe amounts of tourmaline, albite and carbonate. The garnet porphyroblasts contain inclusions of epidote, quartz, titanite and ilmenite, some of which may form trails. The garnet is often highly consumed by chlorite, which often forms pseudomorphs. The matrix does not show a strong foliation and is strongly folded. This is particulary visible for muscovite, but it can be clearly seen with accessory minerals as well. The chlorite may both be folded or occur as interlocked clusters of a less deformed character. Quartz occurs as arcuate pockets bounded by muscovite and/or chlorite, or it may occur between garnet and muscovite, apparently less deformed.

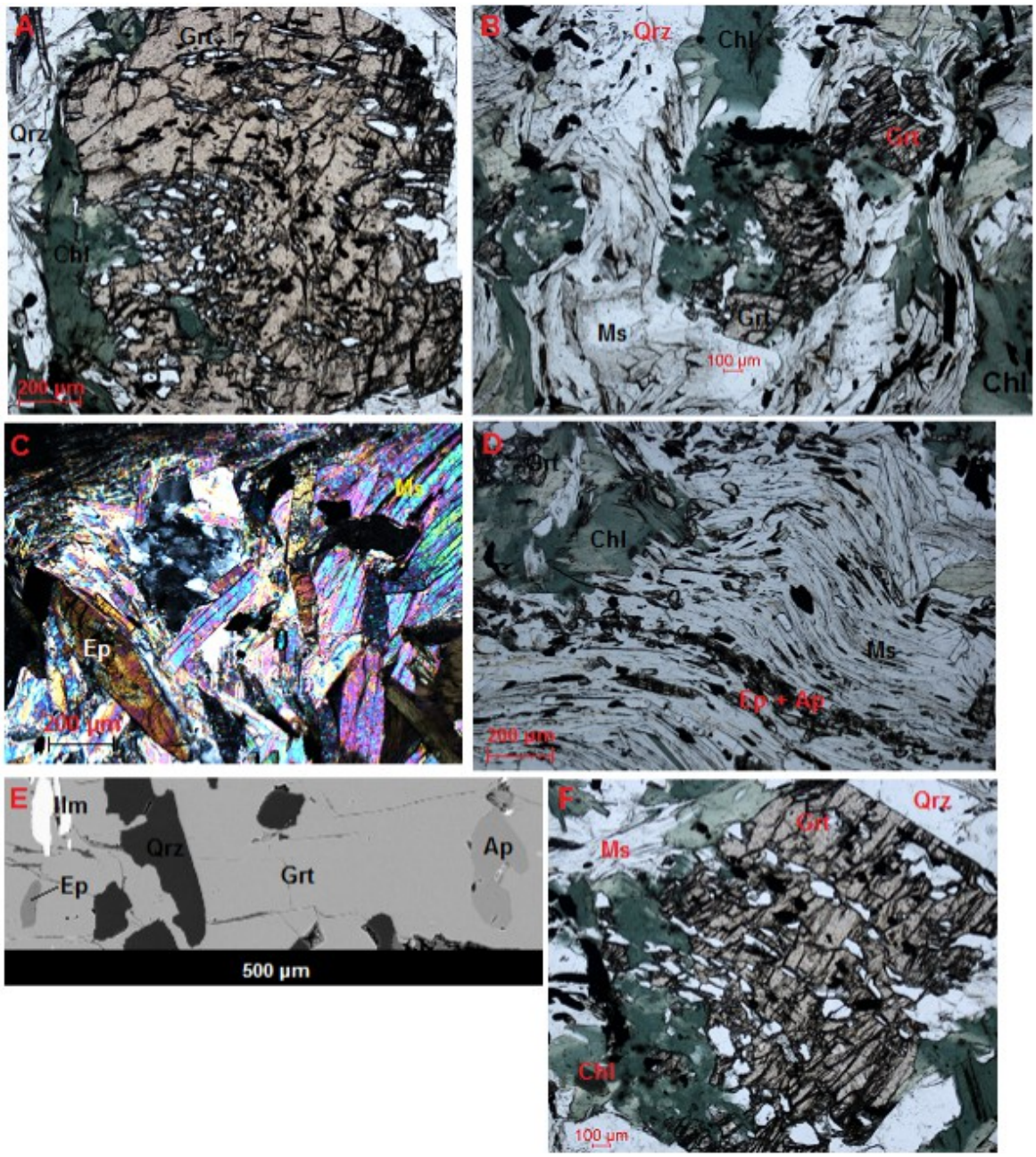

Fig. 4.7: A) A garnet containing slightly curved inclusion trails of ilmenite and quartz. The garnet is also consumed by chlorite to a lesser degree. **B)** In the middle, a garnet consumed extensively by chlorite. Note how the chlorite mirrors and complements the garnet-half in structure, forming a near euhedral shape between the two of them, i.e. it is a pseudomorph, most likely due to alteration of the garnet. On the far left and right side of the picture, the chlorite in the matrix is both elongated and folded. **C)** Accessory epidote in muscovite, oriented obliquely with respect to the muscovite in which it resides. However, the matrix is chaotic and there is no general foliation direction observed. **D)** A section of folded matrix minerals, the accessories here tightly follow the muscovite foliation. **E)** A backscattered electron image showing the various inclusions found in garnet. Qrz, Ep and Ilm are located close to the outer core. **F)** Garnet with straight/slightly curved inclusion trails. A and F indicates that garnet has overgrown an external folation different to what is now observed in the matrix.

Tab. 4.4: Representative electron microbe analyses in wt%. recalculated to structural formulas with indicated numbers of oxygen.

OS-2							
		Garnet				Matrix	
Sample:	Ep	Ab	Grt	Grt	Chl	Ep	Ms
	1 / 1 .	25 / 1	78	1	20 / 1	17 / 1 .	26 / 1
			core	rim			
SiO2	37,82	69,51	36,83	37,31	24,62	37,45	47,17
TiO2	0,07	0,01	0,20	0,10	0,04	0,09	0,38
Al2O3	22,91	19,77	20,40	21,00	21,36	23,67	32,41
Fe2O3	15,21					13,68	
FeO		0,02	27,50	32,65	26,21		3,77
MnO	0,65		7,04	1,86	0,36	0,36	0,02
MgO	0,00	0,00	1,14	2,10	13,92	0,01	1,54
CaO	22,77	0,07	0,07	4,95	0,05	22,67	
Na2O	0,04	11,78			0,01		1,07
K2O	0,02	0,04			0,02		9,61
Total	99,48	101,20			86,57	97,93	95,96
No.O	12,50	8,00	12,00	12,00	28,00	12,50	22,00
Si	2,98	3,00	3,00	3,00	5,29	2,98	6,30
Ti	0,00	0,00			0,01	0,01	0,04
Al	2,13	1,01	1,94	1,99	5,41	2,22	5,10
Fe3	0,90	0,00				0,82	
Fe2		0,00	1,84	2,20	4,71		0,42
Mn	0,04	0,00	0,48	0,13	0,07	0,02	0,00
Mg	0,00	0,00	0,14	0,24	4,46	0,00	0,31
Ca	1,92		0,58	0,43	0,01	1,93	0,00
Na	0,01	0,99			0,01		0,28
K	0,00	0,00			0,01		1,64
Sum	8,00	5,00	7,98	7,99	19,98	7,99	14,07
X_{Mg}			0,04	0,07	0,486448		
Almandine			61	73			
Andradite			2	2			
Grossular			16	14			
Pyrope			4	7			
Spessartine			17	4			

Mineral assemblages

Two mineral assemblages, M1 and M2 can be inferred based on textural observations (Tab. 4.5).

Tab. 4.5:
Mineral assemblages corresponding to M1-M2 metamorphic phases.

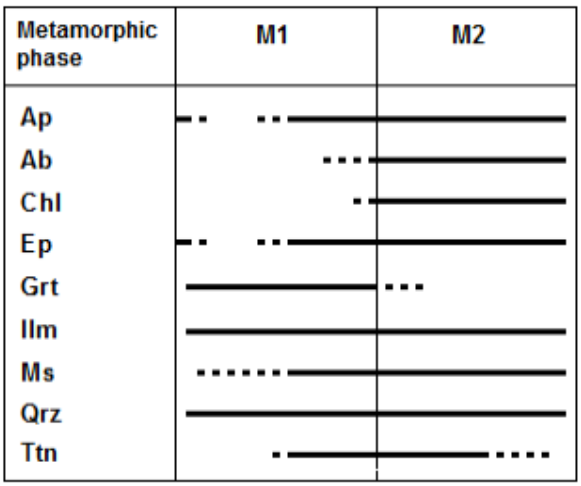

M1 assemblage

M1 is defined by the garnet and the minerals which constitutes it's inclusion trails. M1 is represented by: Grt, Ilm and Qrz. The mineral phases: Ms, Ap, Ep and Ttn overlaps M2 as they occur as inclusions in garnet, but are much more abundant in the matrix and quite visibly folded. Textural positions are shown in Fig. 4.7.

Mineral compositions for M1:

Garnet

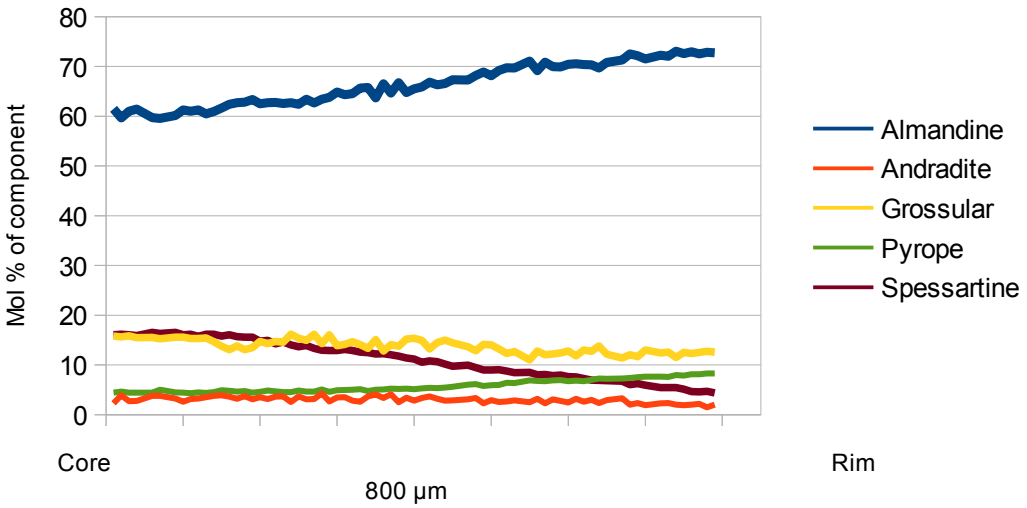

Fig. 4.8: Compositional profile of garnet from core to rim.

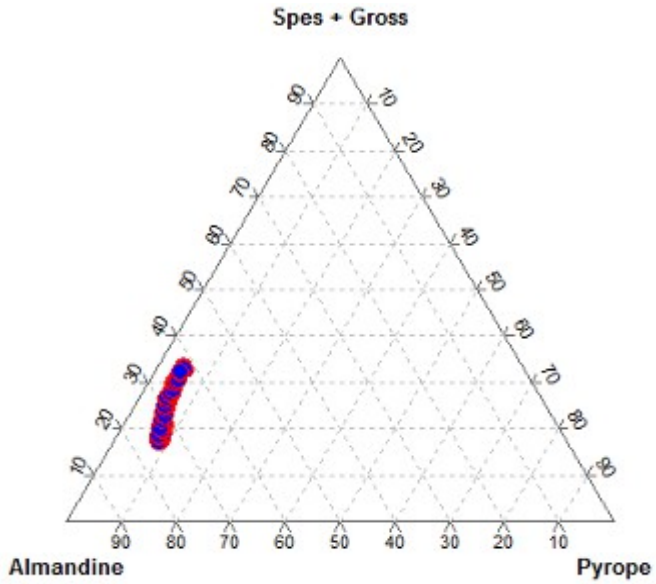

Fig. 4.9: Ternary diagram of the Alm, Grs, Py, Sps garnet endmember mol% content.

A compositional profile from core to rim in a garnet (Fig. 4.8) and a ternary diagram (Fig. 4.9) show a significant chemical zoning, with $Alm_{62->76}$, $Andr_{4->2}$, $Grs_{17->11}$, $Py_{5->8}$, $Sps_{17->4}$. Andr is relatively stable and experiences the least change, while Alm and Sps changes strongly.

M2 assemblage

M2 is defined by the matrix minerals that do not occur in garnet as inclusions or those that may be alteration products (pseudomorphs), M2 is represented by Ab, Chl, Ms, Ilm, Qrz, Ep, Ap and Ttn.

Mineral compositions for M2:

Chlorite

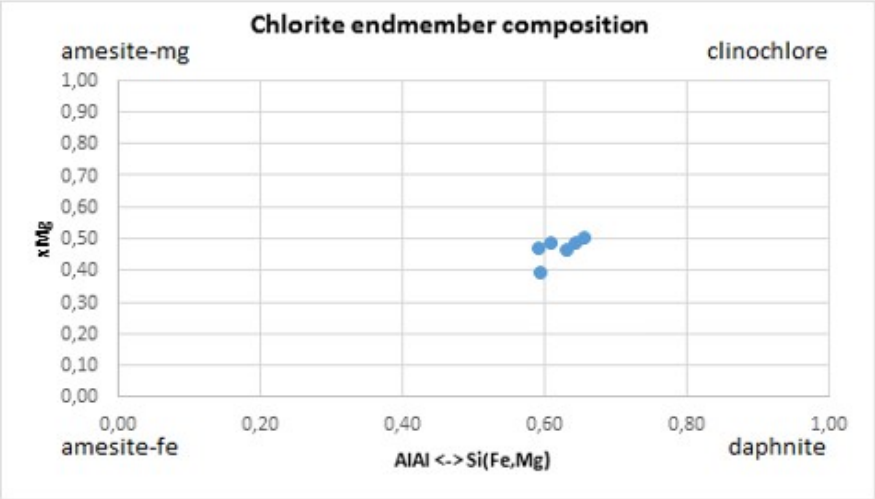

Fig. 4.10: Chlorite endmember content in mol%.

The X_{Mg} for the chlorite is 0.47-0.50, the Si and Al contents are 5.20-5.40 and 5.40-5.50 a.p.f.u respectively. The clinochlore, daphnite, Mg-and Fe-amesite endmembers are presented in molar % content in Fig. 4.10. The analyses were taken from the matrix or from pseudomorphs. There are no discernable differences between them.

Epidote

The Fe^{3+} content of epidote is 0.64-0.93 a.p.f.u., and the Ca content is 1.9-1.97 a.p.f.u. The epidote inclusions appear to have a higher content and a wider range of Fe^{3+} (0.67-0.93 a.p.f.u) than the epidote in the matrix (0.64-0.82 a.p.f.u). The Al content varies slightly with 2.13-2.35 a.p.f.u.

Muscovite

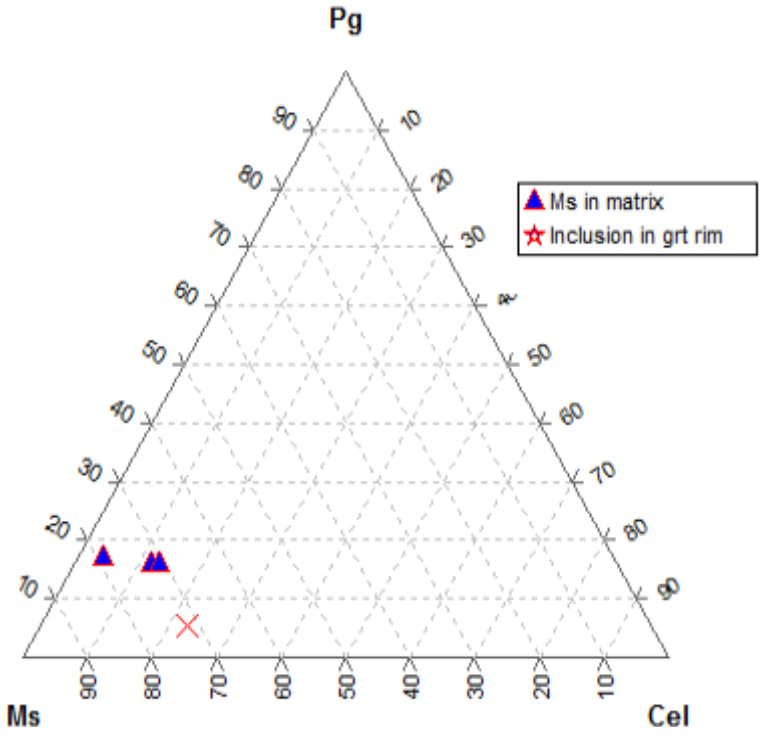

Fig. 4.11: Ternary diagram of the mol% content with respect to Ms-Cel-Pg endmembers.

The muscovite composition is represented by Ms-Cel-Pg-Bt endmembers: 65-73% Ms, 4-21% Cel, 5-15% Pg, and 8-9.75% Bt. The molar content of the endmembers is plotted in a ternary diagram (Fig. 4.11) which shows that, of the 5 analyses most (3) muscovites collect in point. The Cel-rich and Pg-poor outlier is included in the very edge of a garnet. All other analyses were taken from muscovite in the matrix and they do not occupy a textural position different to that of the other crystals .

Feldspar

Feldspar in this sample consists of 97-99 molar % of albite component and is thus classified as albite.

4.2.3 BGA2-1 Garnet-bearing quartz schist

Sample BGA2-1 is banded rock characterized by alternating quartz-rich and mica-rich layers. The quartz-rich layers are by far the most abundant and will henceforth be refered to as the matrix.

The matrix consists of quartz (80%) interlocked with biotite (11%) and muscovite (8%), with accessory amounts of amphibole and chlorite. The matrix has an apparent general foliation. At various locations in the matrix, crystals of anhedral/irregular garnet occur. The garnet contains numerous large quartz inclusions ultimately making the garnet poikilitic in appearance.

Within a spacing of every 0.5-4mm in the matrix, horizontal bands composed either solely of biotite or of both micas (biotite and muscovite) plus quartz, ilmenite, and accessory amounts of epidote, apatite and feldspar occur. Most of these minerals follow a general foliation and many of them are folded. Inside these bands, nearly euhedral garnet, seemingly wrapped around by the mica appears. The garnet contains inclusions of quartz, ilmenite and, to lesser extent, apatite. These minerals may occur as straight inclusion trails, orientated obliquely with respect to the general foliation and folding in the sample.

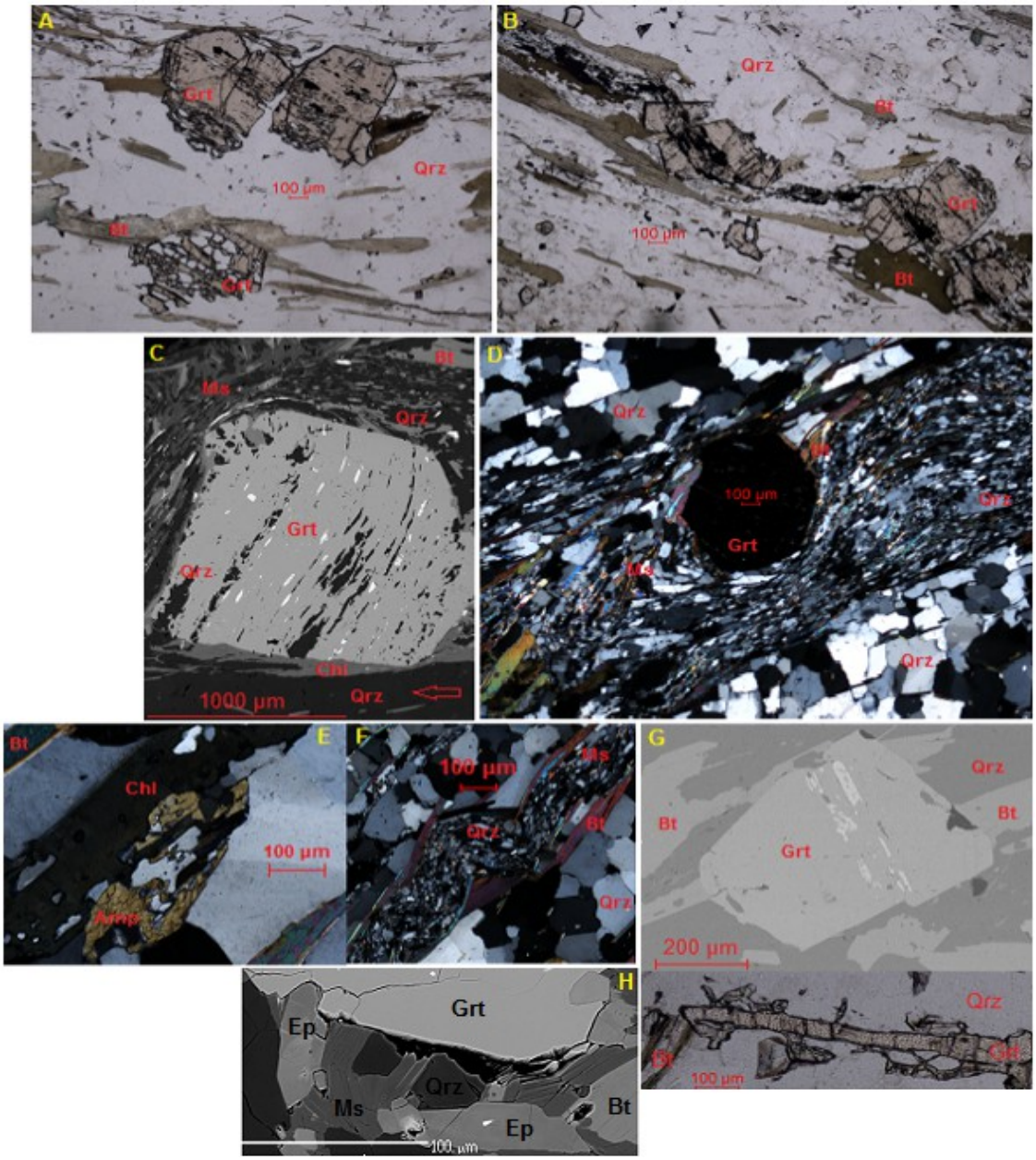

Fig. 4.12:

A)and **B)** Garnets with straight inclusion trails orientated at a slight angle with respect to the foliation. Note the poikilitic appearance of the garnet in the lower part of A which is located in the matrix. **C)** and **G)** (upper part) **1.** Garnet with inclusion trails orientated at high angles with respect to the foliation, suggesting their growth prior to the formation of the external foliation. Note that these garnets are almost entirely surrounded by mica. **2.** In the lower part of C, chlorite rims the garnet, seemingly replacing it. **D) 1.** A garnet wrapped around by mica and quartz. **2.** This Figure also shows a clear difference in the crystal size of quartz in the matrix and inside the quartz-dominated bands. **E**) Chlorite intergrown with or replacing amphibole. **F)** Folded band qrz+ms. **G)** (lower part). Another garnet with an irregular shape, crystallized in the matrix. **H)** Back-scattered electron image of the typical mineral assemblage found in the matrix inside bands.

Tab. 4.6:

Representative electron microbe analyses in wt%. recalculated to structural formulas with indicated numbers of oxygen.

BGA2-1											
Sample:	Amp 9 / 1 .	Amp 13 / 1 .	Bt 46 / 1 .	Bt 64 / 1 .	Chl 15 / 1 .	Ep 36 / 1	Ab 67 / 1 .	Grt 1 Core	Grt 61 Rim	Ms 39 / 1 .	Ms 58 / 1 .
SiO2	43,76	41,80	35,72	36,56	25,65	37,78	69,74	36,72	36,60	46,43	49,06
TiO2	0,21	0,26	2,21	1,16	0,07	0,06	0,01	0,21	0,18	0,38	0,36
Al2O3	10,78	13,73	16,37	16,78	19,99	25,07	20,01	19,61	20,08	31,77	28,56
Fe2O3						10,66					
FeO	24,08	20,86	21,41	20,78	26,30		0,00	16,24	20,05	3,96	3,67
MnO	0,82	0,38	0,24	0,19	0,46	0,19	0,02	19,75	15,60		
MgO	6,96	6,71	8,95	9,92	14,03		0,01	0,61	0,62	0,05	0,06
CaO	7,63	10,46	0,06	0,08	0,03	23,20	0,00	6,59	7,21	1,80	2,44
Na2O	2,06	2,05	9,75	9,74	0,02	0,02	12,06			0,39	0,64
K2O	0,46	0,67			0,16	0,02	0,04			10,20	9,94
Total	96,77	96,91	94,73	95,21	86,55	96,97	101,86	99,88	100,49	94,98	94,75
No.O	23,00	23,00	22,00	22,00	28,00	12,50	8,00	12,00	12,00	22,00	22,00
Si	6,48	6,32	5,67	5,72	5,52	3,01	2,99	2,99	2,96	6,28	6,63
Ti	0,02	0,03	0,26	0,14	0,01	0,00	0,00	0,01	0,01	0,04	0,04
Al	1,88	2,45	3,07	3,09	5,07	2,35	1,01	1,89	1,92	5,07	4,55
Fe3	2,02	0,73				0,64		0,09	0,09		
Fe2	0,96	1,91	2,84	2,72	4,73		0,00	1,01	1,27	0,45	0,41
Mn	0,10	0,05	0,03	0,03	0,08	0,01	0,00	1,36	1,07	0,01	0,01
Mg	1,53	1,51	2,12	2,31	4,50	0,00	0,00	0,07	0,08	0,36	0,49
Ca	1,21	1,69	0,00	0,00	0,01	1,98	0,00	0,58	0,63	0,00	0,00
Na	0,59	0,60	0,02	0,02	0,01	0,00	1,00			0,10	0,17
K	0,09	0,13	1,98	1,94	0,04	0,00	0,00			1,76	1,71
Sum	14,89	15,43	16,00	15,97	19,97	8,00	5,01	8,01	8,03	14,07	14,00
X_{Mg}	0,61	0,44	0,43	0,46	0,49			0,02	0,03		
Almandine								32	40		
Andradite								5	5		
Grossular								15	17		
Pyrope								2	3		
Spessartine								46	36		

Mineral assemblages

Two assemblages, M1 and M2 could be inferred based on textural observations (Tab. 4.7).

Tab. 4.7:

Mineral assemblages corresponding to M1 and M2 metamorphic phases.

Metamorphic phase	M1	M2
Amp	- - -	———
Ap	- - - ———	——— - - -
Ab	- - -	———
Bt	- - - - - - - - -	———
Chl	- - -	———
Ep	- - -	———
Grt	———	- - -
Ilm	———	———
Ms	- - - - - - - - -	———
Qrz	———	———

M1 assemblage

The M1 assemblage is represented by the garnet and the inclusion minerals forming its internal foliation. M1 comprises: Ap, Grt, Ilm, and Qrz. The micas may also have been stable during M1 as suggested in table. 4.7, however, the stability is assigned to the M2 metamorphic phase. The textural positions are shown in Fig. 4.12.

Mineral compositions for M1:

Garnet

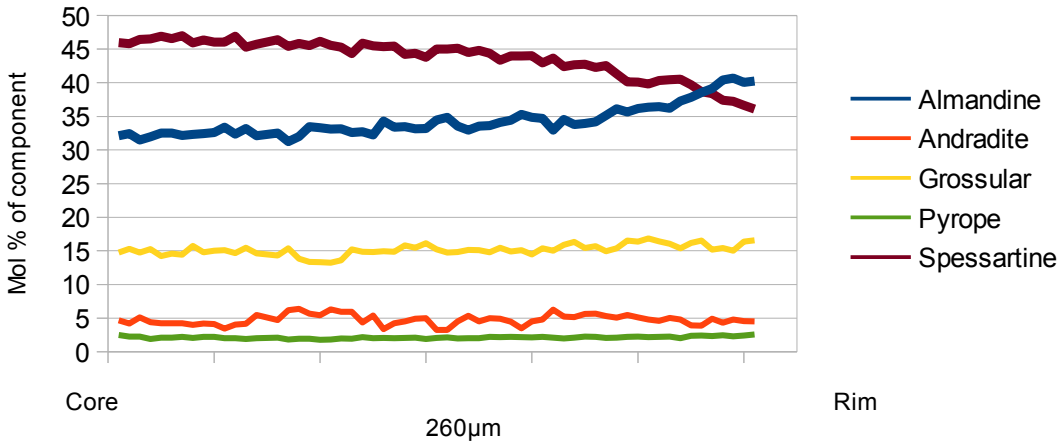

Fig. 4.13: Compositional profile of garnet in the sample, BGA2-1- from core-to-rim.

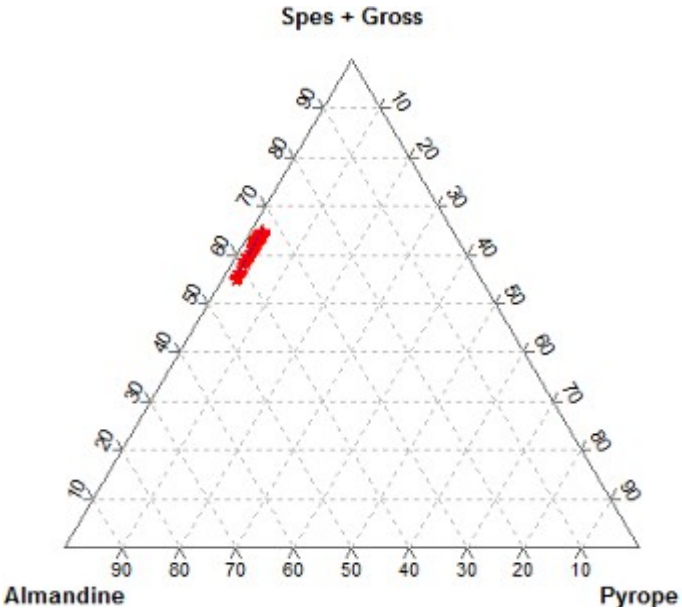

Fig. 4.14: Ternary diagram of the Alm-Grs-Py-Sps garnet endmember content mol%.

The ternary (Fig. 4.14) diagram and measured compositional half-profile (Fig. 4.13) show that there is significant chemical evolution in the garnet with: Alm53->67, Grs18->14, Sps47- >38. The Py (2-3) and Adr (3-6) content remains relatively constant, however.

M2 assemblage

The M2 mineral assemblage is represented by the minerals which form the main foliation of the sample or may show indications of consuming older minerals. M2 comprises: Amp, Chl, Ms Bt, Ep, Qrz and Ilm.

Mineral compositions for M2:

Amphibole

There are two types of amphibole in the sample; sub-calcic hornblende and hornblende (Tab. 4.6). The most conspicuous compositional differences between them are given by: Ca 1.2-1.3, Fe^{3+} 2.0-1.7 content (a.p.f.u) for the sub-calcic hornblende and Ca = 1.7-1.8, Fe^{3+} = 0.73-0.68 a.p.f.u for the hornblende. However, these two amphiboles are typically located next to eachother and too rare to be assigned to any particular textural position.

Biotite

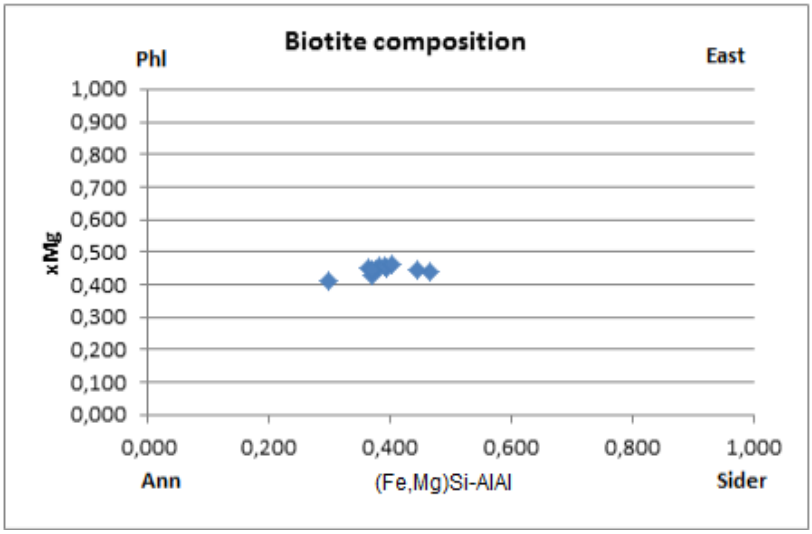

Fig. 4.15: Biotite endmember content in mol%.

The composition of biotite is described here as a solid solution among four endmembers. The

biotite has X_{Mg}(X_{Mg}=Mg/Mg+Fe) of 0.41-0.46, and endmember molar proportions of 30-41.5% Ann, 17.6-26% Sid, 23.5-29% Phl and 12.2-20.5% East. The only discernable differences between the biotite found in the bands and biotite found in the matrix is a predisposition towards Ti in the biotite in mica-rich bands (0.19-0.26, vs 0.14 a.p.f.u). One particular biotite in the biotite band, squeezed between two subhedral/anhedral garnets (Fig. 4.12. a), shows a significant increase in Mn relative to other biotites, with 0.09 compared to 0.03-0.04 a.p.f.u. Fig. 4.4 illustrates the range of biotite composition. The far left outlier in Fig. 4.15 is the Mn rich biotite.

Epidote

The composition of epidotes is constant with Al = 2.3, Fe^{3+} = 0.70 and a Ca = 1.95 a.p.f.u.

Feldspar

All of the analysed feldspars show Ab molar proportions of 99% or above. They are classified as pure albite.

Chlorite

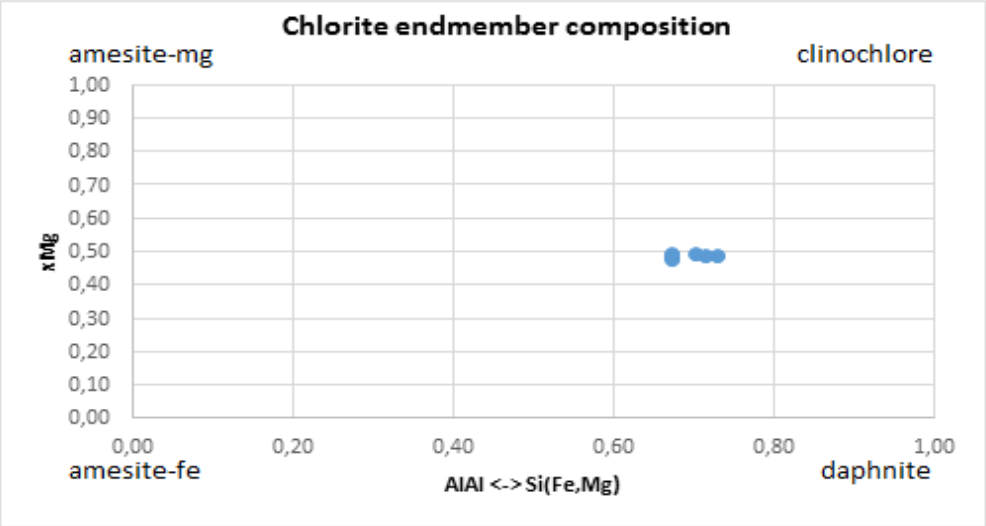

Fig. 4.16: Chlorite endmember content in mol%.

The chlorite X_{Mg}($X=_{Mg}/(Mg+Fe)$) values are: 0.48-0.50, where 0.48 is somewhat of an outlier. Most analyses have X_{Mg} = 0.49-0.50 which is a modest change. The Al and Si content is 5.10-5.50 and 5.30-5.50 a.p.f.u., respectively. Fig. 4.16 shows the clinochlore, daphnite, Mg-and Fe-amesite endmembers are presented in molar % content in. The chlorite analyses were taken from chlorite interlocked with amphibole and/or biotite or on a garnet rim. All of the analyses from different textural positions plot within the same range of molar content of the endmembers.

Muscovite

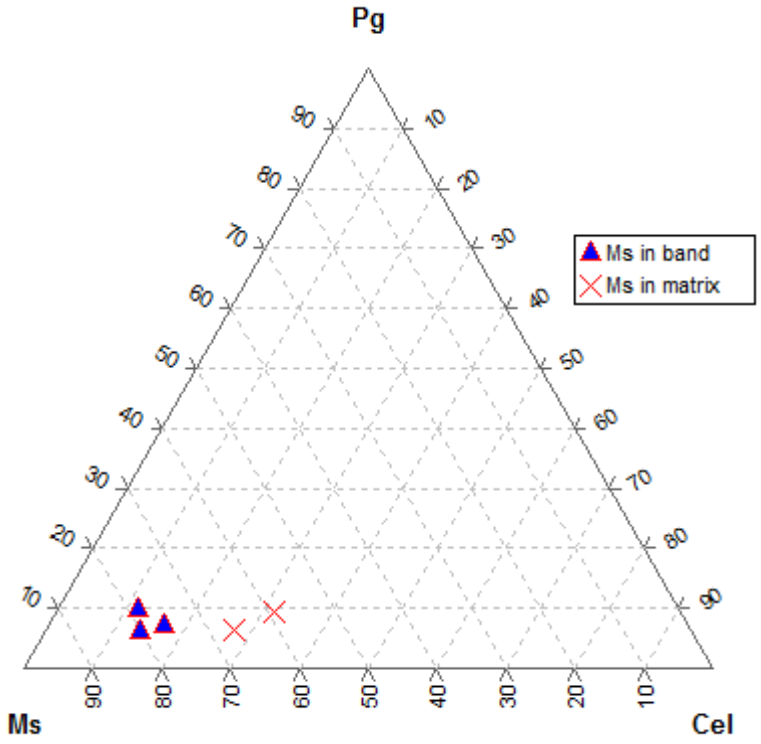

Fig. 4.17: Ternary diagram of the mol% content of Ms-Cel-Pg endmembers in anlaysed white micas.

The muscovite is represented by the Muscovite (Ms) — Celadonite (Cel) — Paragonite (Pg) — Biotite (Bt) endmembers by molar percent : 69-72% Ms, 10-15% Cel, 5-9% Pg and 10-11% Bt for the muscovite located in the mica-rich bands and: 55-60% Ms, 25-30% Cel, 6-9% Pg, and 6-10% Bt for muscovite located in the matrix. As illustrated in the ternary diagram (Fig. 4.17) , they appear to be different, however, this is only particulary true for the Mg content which is 0.31-0.36 a.p.f.u for the muscovite in the band and 0.49-0.56 a.p.f.u for the muscovite the matrix, the Fe content is 0.42-046 a.p.f.u. for both textural positions, but the diagram shows a clear difference in the celadonite content.

4.2.4 BGA2-2 Albite mica schist

The sample, BGA2-2 is composed of folded bands of white mica alternating with feldspar and muscovite-rich layers and biotite layers. Epidote, opaques minerals and apatite are the essential accessories. Chlorite is locally intergrown with biotite, and quartz occurs as single pockets between folds. The sample is not uniformly folded, but rather has varying degrees of curvature, where the curvature increases towards a central S-fold. All of the minerals are elongated within the general foliation, however, the accessories appears to be cutting the foliation, and may even overgrow other minerals in a number of locations.

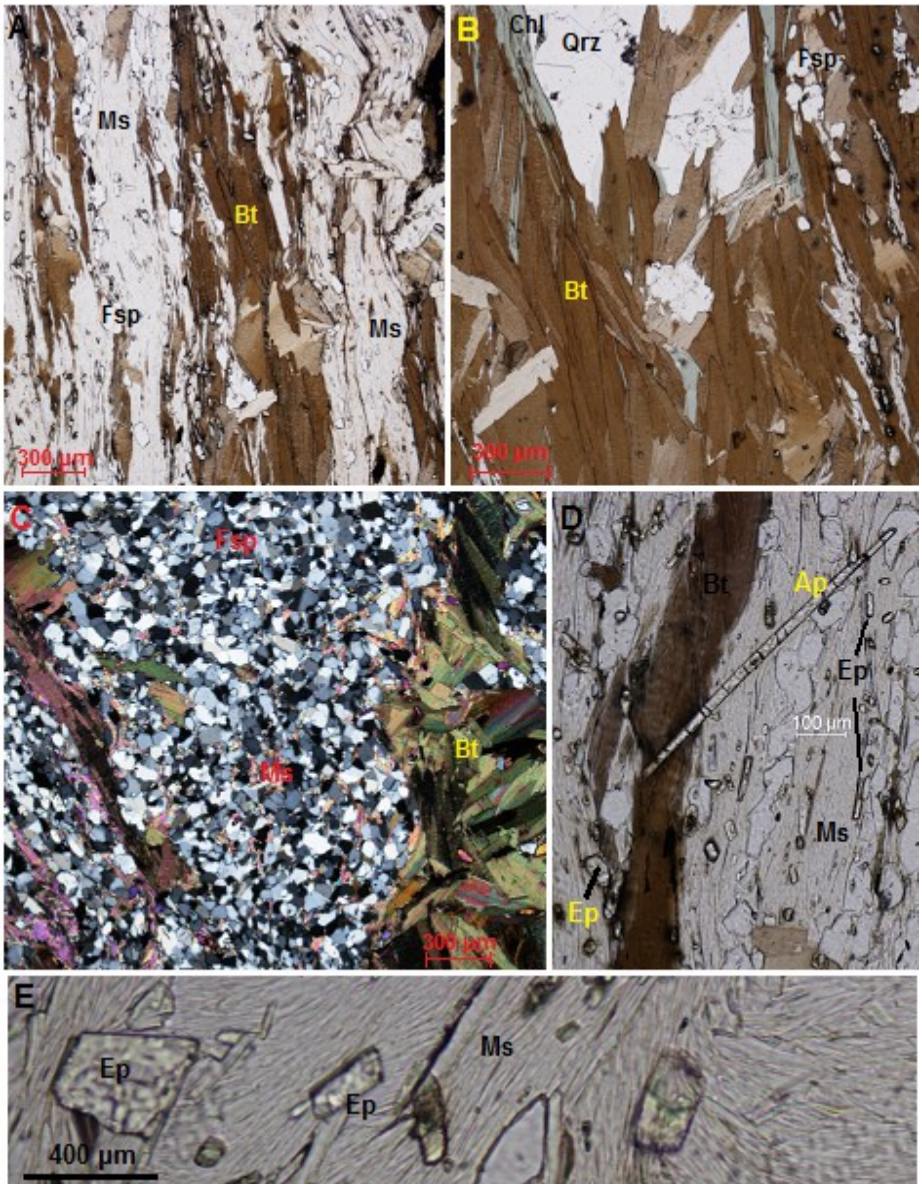

Fig. 4.18:
A) The typical matrix assemblage composed of alternating feldspar-rich muscovite and biotite layers, they all follow a general foliation and are interlocked or intergrown with eachother.
B) Chlorite growing along biotite cleavage, possibly as an alteration product from biotite due to retrogression. Next to it is a localized aggregate of quartz.
C) How the matrix looks in the S-fold. Feldspar appears more abundant, but this is, in part, because muscovite is masked by it's much smaller grain size and the general discontinuity of it's bands here. -> -> **D)** Apatite and epidote accessories in the micas. One conspicious apatite cuts the foliation and appears to grow on top of the micas, which typically means late crystallization **E)** Tiny crystals of epidote which may have overgrown muscovite as the crystals acts like “windows” through which textures similar to those found in the matrix can be seen.

Tab. 4.8: Representative electron microbe analyses in wt%. recalculated to structural formulas with indicated numbers of oxygen.

BGA2-2						
Sample:	Bt	Chl	Ep	Pl	Ms	Ms
	55 / 1 .	1 / 1 .	78/1.	48 / 1 .	66 / 1 .	70 / 1 .
SiO2	36,95	25,85	37,96	67,40	47,80	46,19
TiO2	1,84	0,07	0,14	0,01	0,42	0,61
Al2O3	16,56	21,22	25,44	20,18	30,08	30,01
Fe2O3			10,26			
FeO	17,79	21,76		0,13	3,16	4,60
MnO	0,23	0,41	0,37		0,03	0,03
MgO	11,92	17,64	0,01	0,01	2,54	2,76
CaO			22,95	1,18		0,01
Na2O	0,10	0,00	0,02	11,34	0,35	0,23
K2O	9,60	0,02	0,02	0,08	10,34	10,10
Total	95,00	86,95	97,17	100,33	94,70	94,54
No.O	22,00	28,00	12,50	8,00	22,00	22,00
Si	5,70	5,39	3,01	2,94	6,46	6,31
Ti	0,21	0,01	0,01	0,00	0,04	0,06
Al	3,01	5,22	2,38	1,04	4,79	4,83
Fe3	0,00		0,61			
Fe2	2,30	3,80		0,00	0,36	0,53
Mn	0,03	0,07	0,02	0,00	0,00	0,00
Mg	2,74	5,49	0,00	0,00	0,51	0,56
Ca	0,00		1,95	0,06	0,00	0,00
Na	0,03	0,00	0,00	0,96	0,09	0,06
K	1,89	0,00	0,00	0,00	1,78	1,76
Sum	15,92	19,99	7,99	5,00	14,04	14,12
X_{Mg}	0,54	0,59				
An				6,00		
Ab				94,00		

Mineral assemblages

Two mineral assemblages, M1 and M2, were inferred (Tab. 4.9). However, several mineral phases could not be constrained to one particular metamorphic phase based on textural observations alone.

Tab. 4.9:
Mineral assemblages corresponding to M1 and M2 metamorphic phases.

Metamorphic phase	M1	M2
Ap	- - -	———
Ab	———	- - -
Bt	———	- - - - - -
Chl	- - -	———
Ep	- - - -	———
Ilm	———	———
Ms	———	- - - - - -
Qrz	———	———

M1 assemblage

M1 is defined by Bt, Fsp, Ilm, Ms, and Qrz ± Ep. The phases which are clearly affected by the folding. Epidote is in textural positions ssuggesting its presence in both M1 and M2. It did likely crystallize in both metamorphic phases. In the description it is placed in the M2 section because the overgrowth textures are apparantly more abundant. In Fig. 4.18 the textural positions of the minerals are shown.

Mineral compositions for M1:

Biotite

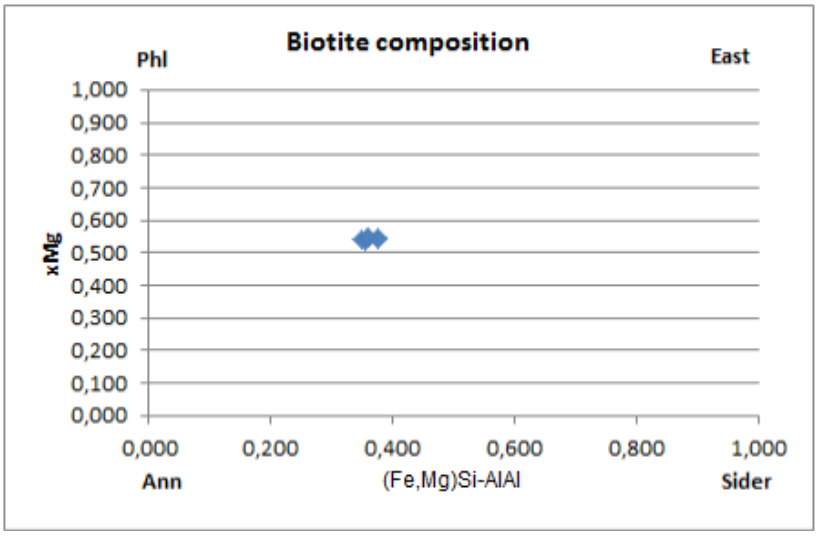

Fig. 4.19: Biotite endmember content in mol%.

Biotite were analysed in various places throughout the sample. The X_{Mg} is 0.54-0.55 and the biotite composition in molar percent of the endmembers is: 28-29% Ann, 16-17% Sid, 34-35% Phl and 19-20% East. Their composition remains relatively constant (Fig. 4.19).

Feldspar

Feldspars are mainly albitic with 94.1-98.2% Ab, and 1.5-5.4% An. They are thus classified as albite.

Muscovite

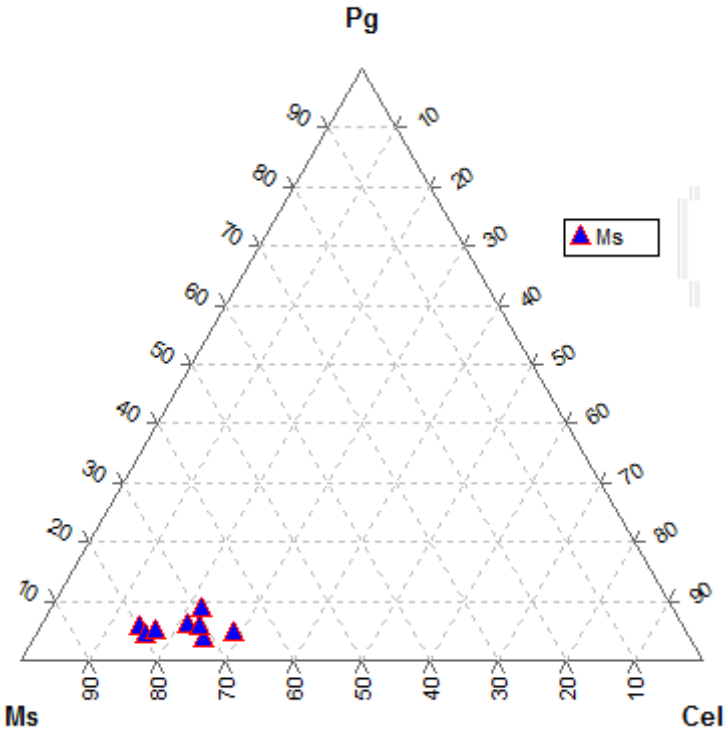

Fig. 4.20: Ternary diagram of the mol% content with respect to Ms-Cel-Pg endmembers.

The muscovite molar content with respect to the Ms-Cel-Pg-Bt endmembers is: 60-71% Ms, 13-26% Cel, 3-8% Pg, and 7-15% Bt. The variation in composition could not be assigned to its textural position or to the presence of any surrounding minerals. Fig. 4.20 illustrates the composition.

M2 assemblage

M2 is defined by minerals which can be seen cutting the foliation and folding, minerals which show overgrowth textures, or those that may be alteration products, M2 is represented by Chl, Ep and Ap (Fig. 4.18 B, D, E).

Mineral compositions for M2:

Chlorite

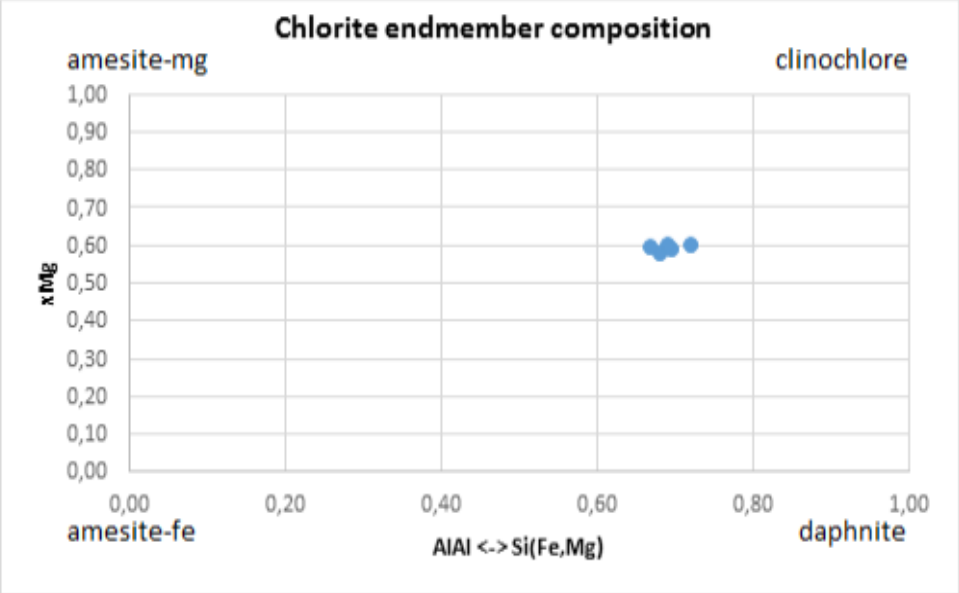

Fig. 4.21: Chlorite endmember content in mol%.

The X_{Mg} values are 0.59 to 0.6 and the Si and Al contents are 5.4-5.5 and 5.1-5.2 a.p.f.u respectively. The molar composition of chlorite is shown as the proportion of the clinochore-daphnite, Mg-and Fe amesite endmembers. Fig. 4.21 illustrates the composition.

Epidote

Epidote shows Fe^{3+} content of 0.61-0.64 a.p.f.u, Ca of 1.9-2.0 a.p.f.u. and Al = 2.3-2.4. a.p.f.u.

4.3 MONAZITE

Introduction

Monazite ($(Ce,La)PO_4$) is a light rare earth element (LREE) bearing phosphate mineral commonly occuring as accessory phase in metapelites. It contains high concentrations of U (up to 1 wt%) and Th (up to 20 wt%) while it contains a low initial concentration of Pb (Wing et al., 2003). Furthermore, the closure temperature for U/Pb diffusion is around $725^{O}C$ for monazite, which makes the loss of Pb via diffusion extremely slow, given that the mineral is unaltered (Lanzirotti et al., 1996). This makes monazite suitable for U/Pb and U-Th-Pb dating (Isotope ratio and TIMS or microprobe age determination, respectively). Monazite may form at metamorphic conditions between greenschist and granulite facies conditions depending on the bulk composition of the rocks (Wing et al., 2003; Lanzirotti et al., 1996). However, the mineral is most commonly associated with amphibolite facies metamorphism. The formation of monazite requires that LREE, P and U and Th are available for nucleation and subsequent crystallization. Prograde breakdown of the LREE mineral, allanite, which often is associated with monazite, readily yields the aformentioned elements. Conversely, the retrograde breakdown of monazite will yield the same elements for the formation of allanite (Wing et al., 2003). The concentrations of the LREE, P and U and Th in common minerals of metapelitic rocks (i.e. garnet, biotite, chlorite, feldspars) may also be enough to form monazite, given, of course, that the elements are made available (Wing et al., 2003). Monazite will typically dissolve during retrogression, and the introduction of hydrothermal fluids will further promote it's decomposition. This is especially true for fluids containing Ca^{2+} (often derived from carbonates or plagioclase), where the Ca^{2+} will readily exchange with the LREEs to form a mantle of apatite ($Ca_5(PO_4)$) surrounding the monazite (Lanzirotti et al., 1996). Following this reaction corrona may be another mantle of thin allanite which in turn is suceeded by a thicker mantle of epidote, presumably in solid-solution (Finger et al., 1998).
These associative textures together with the mineral's robustness and geochronologial properties makes monazite an important mineral for infering the timing of metamorphic events, particulary for prograde events.

4.3.1 MOK

Monazite occurs both in the garnet and in the matrix, however, their texture and associated minerals differ. This is highlighted in the brief description of the monazite in it's respective textural positions given bellow, including pictures to illustrate this.

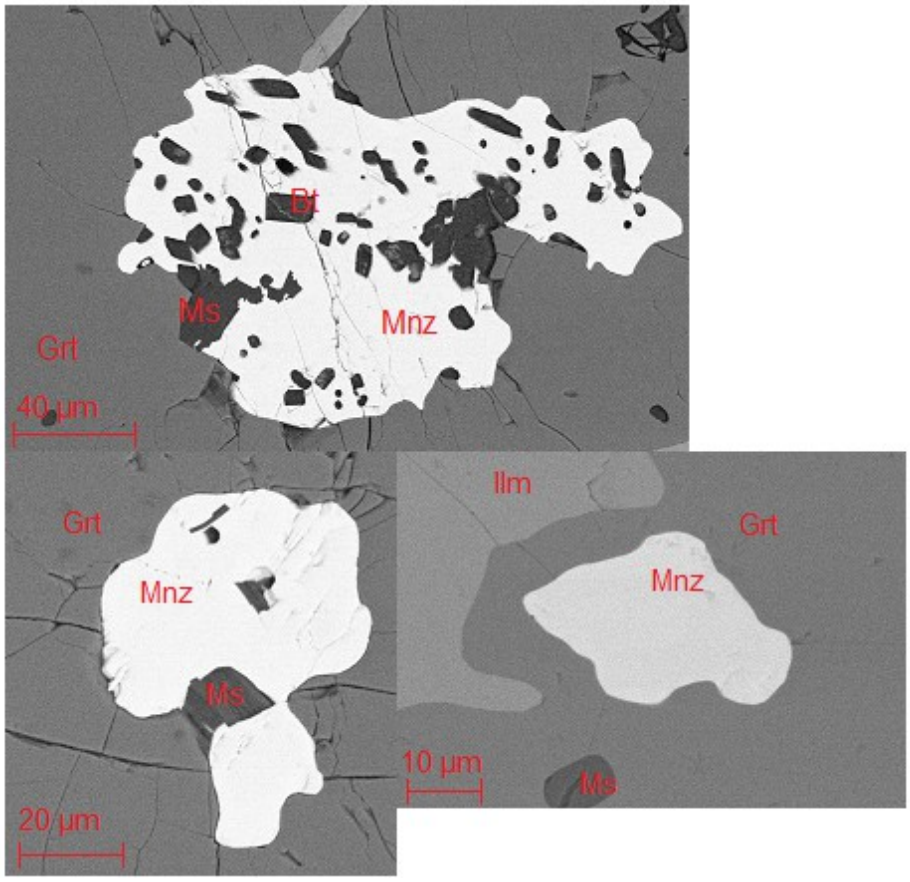

Fig. 4.22: Monazite inclusions in garnet.

In Garnet monazites occurs as relatively big crystals (some 120+ microns wide), they have sharp boundaries (Fig. 4.22) with the surrounding envelope which commonly is garnet, but often garnet plus micas, opaques and quartz, some of which may be micro-inclusions of accessories in the monazite (Fig. 4.22). A few monazites are fractured, and the fractures will typically also run through the envelope. In any case there will always be fractures in the garnet within the vicinity of the fractured monazite inclusions.

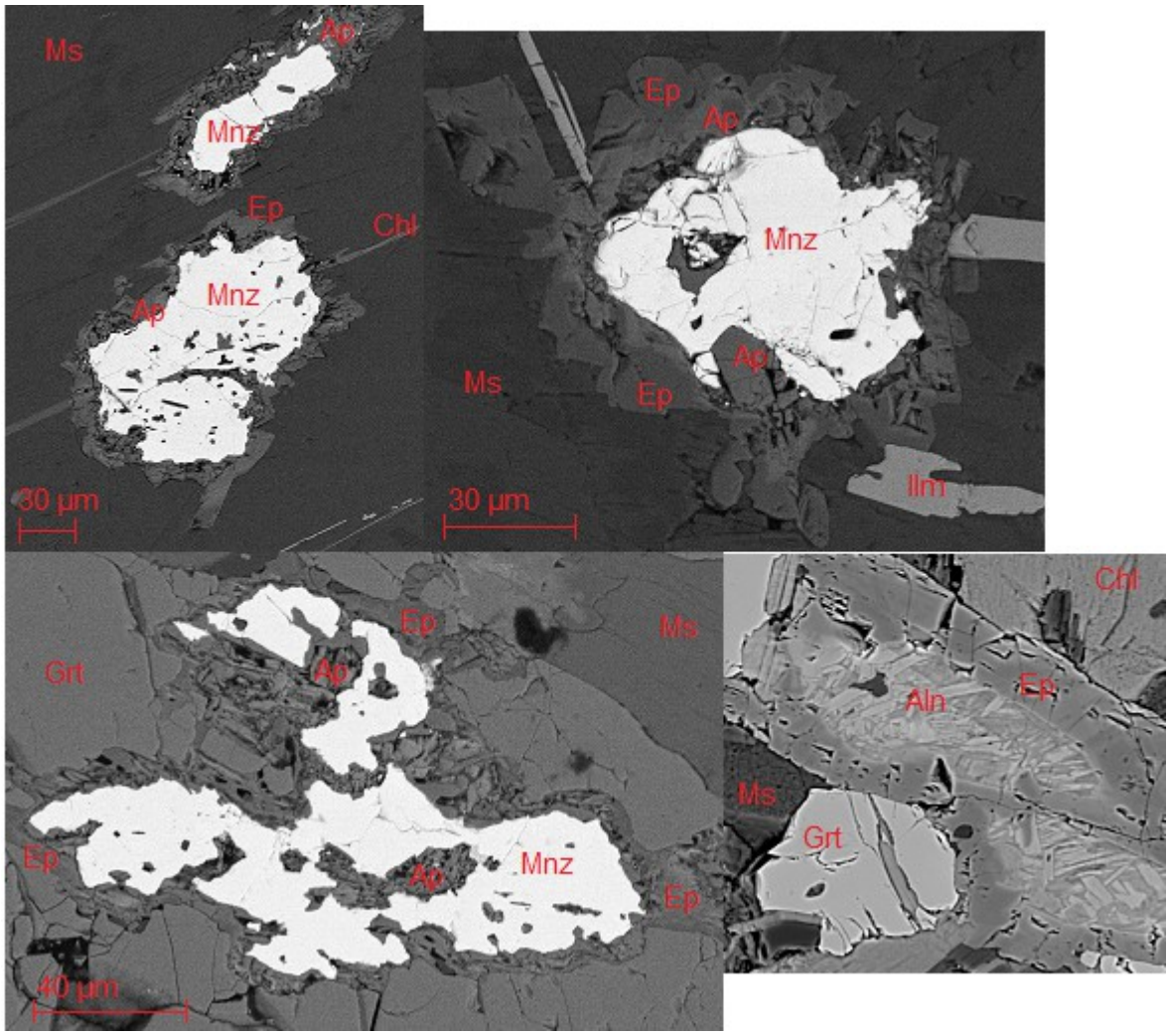

Fig. 4.23: Monazite in the matrix.

In the matrix, or in open cracks in the garnet, the monazite is usually smaller(40-60 microns wide), and always surrounded by a rim composed mostly of apatite and/or epidote (Fig. 4.23). This type of microstructure is completely absent from monazite enclosed by garnet.

5 METAMORPHIC EVOLUTION

5.1 Introduction and background

Three of the samples (BGA 2-1, MOK, OS-2) were chosen for modelling purposes. The samples all contain garnet, which due to its multi-component nature represents one of the best mineral phases for the geothermobarometry purposes. Additionally, the samples may contain Bt, Chl, Cld or St, all suitable for geothermometry due to mostly temperature dependent exchange between Mg^{2+} and Fe^{2+} cations (Indares, 1985; Karabinos, 1985; Moazzen, 2004). The thermodynamic modelling software Perple_X (Connolly, 2005; 2009) has been utilized to estimate the pressures and temperatures at which the assemblages of the samples formed. The calculations were performed with an internally consistent thermodynamic data set for mineral endmembers (Holland and Powell, 1998; 2004), and solution models were used to model the evolution of mineral compositions as close to the observed values as possible. Other tools within the Perple_X such as Werami and Pstable were utilized to plot the various compositional values extracted from the thermodynamic calculations onto the phase diagram. The chemistry of the minerals is plotted as compositional isopleths within the calculated P-T sections with the assumption that the isopleths for minerals in equilibrium cross in a small P-T range within the stability field of the observed mineral assemblage. The area where the compositional isopleths cross then represents the best estimate of the metamorphic conditions. All of the mineral abbreviations used in this chapter is after Whitney (2010).

5.1.1 General assumption

The metasedimentary rocks of the Major Bergen arc have been affected by several periods of metamorphism. Two major prograde metamorphic events have been recognized (Færseth et al., 1977; Færseth, 2011), one of which may be related to an Ordovician continent-island arc subduction, and the other to the subduction of the Baltic margin under Laurentia, followed by the Scandian mountain building event. The older, possibly Ordovician metamorphic event has a low-amphibolite facies signature according to Færseth et al. (1977) and Færseth (2011), while the Scandian metamorphism carries a middle- to upper greenschist metamorphic facies signature according to Færseth et al. (1977) and Ingdahl (1985). The rocks of the Samnanger

complex may have either of the signatures while the Os and Ulven group apparently experienced only the upper-medium greenschist facies metamorphism. After the event(s) of prograde metamorphism the rocks have been subject to retrograde metamorphism in the lower greenschist facies, presumably resulting from a combination of fluid influx, exhumation/uplift and decompression.

In the Møkster-Selbjorn area, the metasediments have undergone burial followed by high grade (Rykkelid, 1987) contact metamorphism from gabbroic intrusions (470 Ma) followed by further burial and subsequent medium grade metamorphism (Rykkelid, 1987) and succeeded by a pervasive retrogression characterized by greenschist facies assemblages.

The metamorphic trajectory is assumed to be clockwise (Fig. 5.1), i.e. representing a normal prograde-retrograde scenario: Fluid rich sediments were buried during subduction/collision. Following the geotherm, the temperature and pressure gradually increased and re-equilibrated the clastic components of the sediments into low grade and further into medium grade metamorphic minerals. Later decompression and cooling during exhumation lowered the P-T conditions, and the addition of fluids allowed for retrogression of some of the metamorphic minerals into the lower grade mineral assemblages. Depending on the measure of re-equilibration during retrogression the rocks may contain meta-stable porphyroblasts with relict inclusions not found in the surrounding matrix, effectively preserving evidence for two or more assemblages indicating the prograde-retrograde trajectory.

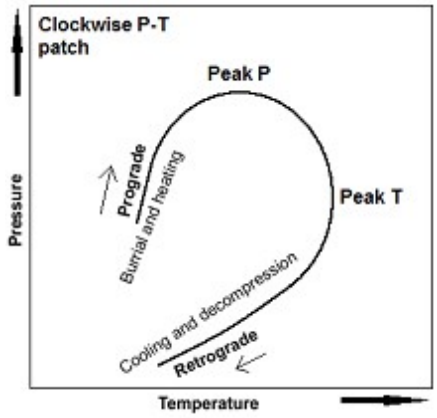

Fig. 5.1: Clockwise P-T-t path.

5.2 MOK

The mineral assemblages are represented by M1: Grt-Bt-St-Fsp-Ilm-Qrz-Ms (coarse), and M2: Chl-Cld-Ilm-Qrz-Ms (fine)-Pg. P-T sections was calculated at 450-650 °C and 6-10 kbar, in the system Na2O,MgO, Al2O3,SiO2, K2O, CaO, TiO2, MnO, FeO with H_2O saturation. The chemical composition of the system has been taken from the whole rock analysis and

recalculated into molar percentage (table. 5.1). The solution models used are biotite (Tajcmanova et al., 2009), chlorite (Holland and Powell, 1998), chloritoid (Holland and Powell, 2000), feldspar (Fuhrman et al., 1988) garnet (Holland and Powell, 1998), ilmenite (White et al., 2000), muscovite (Holland and Powell, 1998) and staurolite (Holland and Powell, 1998).

Tab. 5.1:

Components	Na_2O	MgO	Al_2O_3	SiO_2	K_2O	CaO	TiO_2	MnO	FeO
Mol%	1.27	4.63	21.53	49.76	4.08	1.171	1.47	0.25	15.77

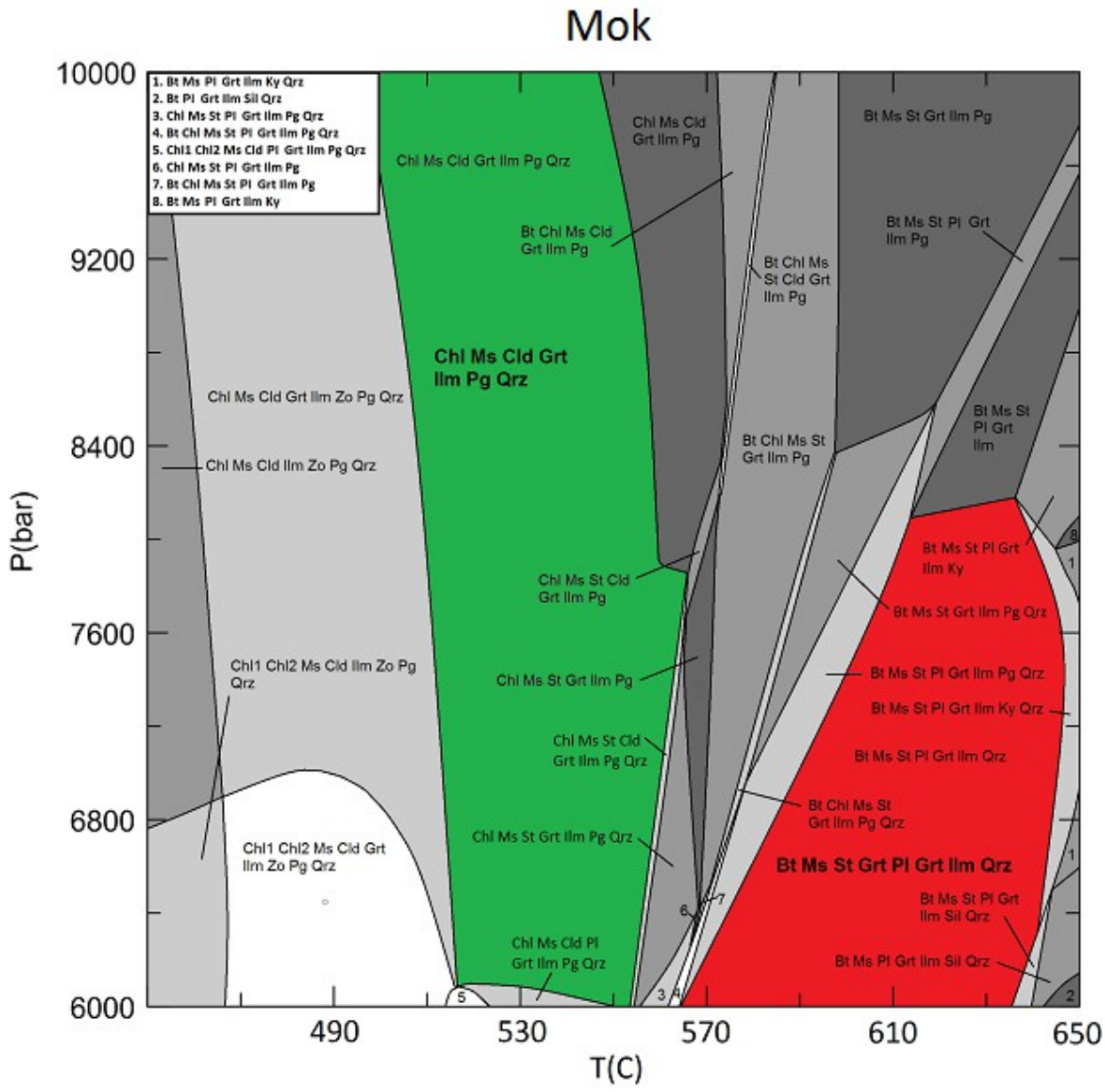

Fig. 5.2: The P-T section calculated for the whole-rock chemistry of the MOK sample with H2O in excess. The stability field marked in red is the assemblage corresponding to M1 and the field marked green corresponds to M2. The stability field is large so in order to better constrain the PT conditions of equilibration, the evolution of the mineral compositions was modelled as isopleths. The Chl1 and Chl2 phases is amesite and clinochlore (Holland and Powell, 1998), respectively.

Modelling of M1

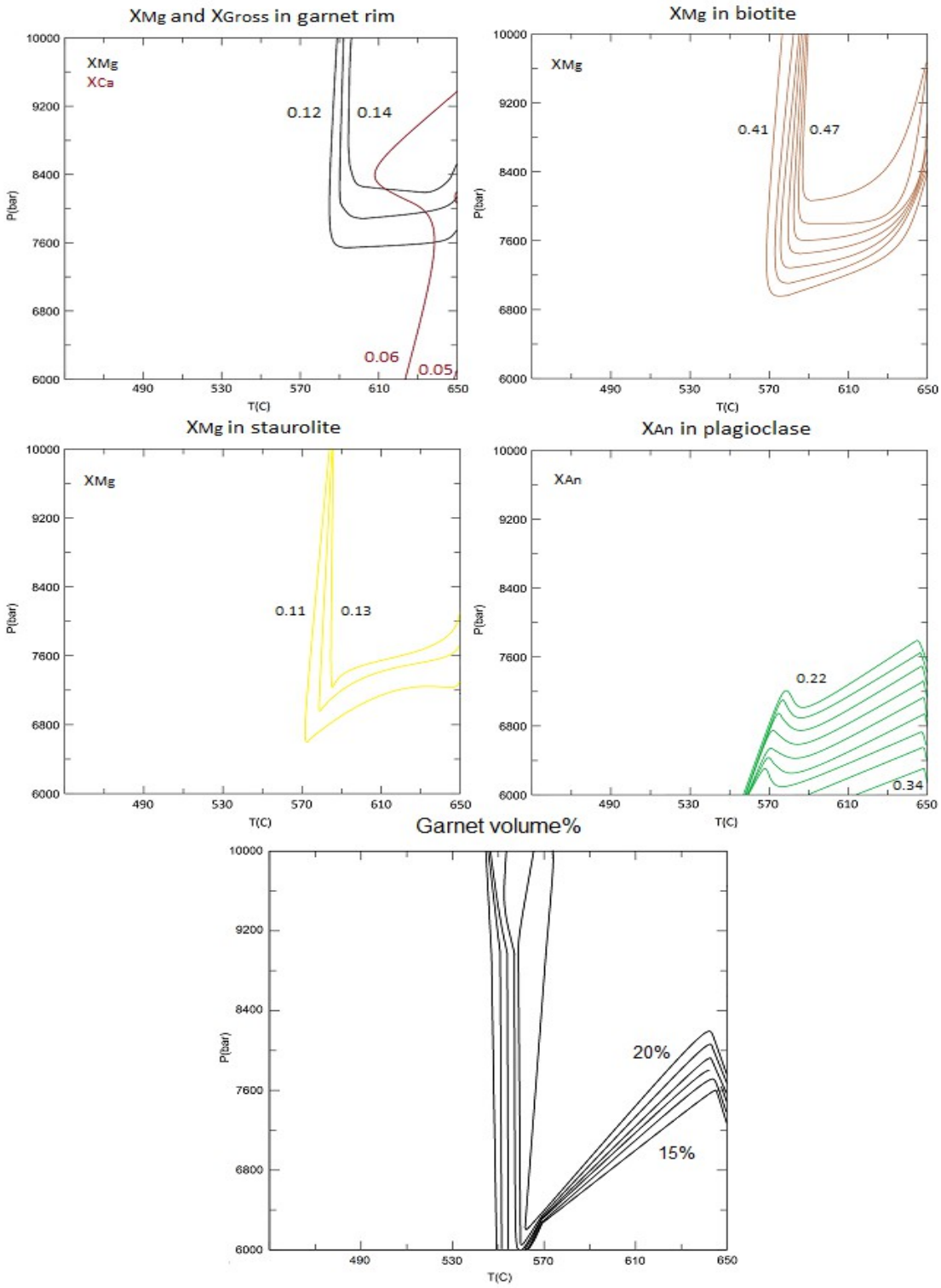

Fig. 5.3: The various isopleths as derived from the calculated PT section plotted for ranges of mineral compositions observed in the MOK sample. The steps are 0.01 for compositional isopleths and 1% for volume isopleths.

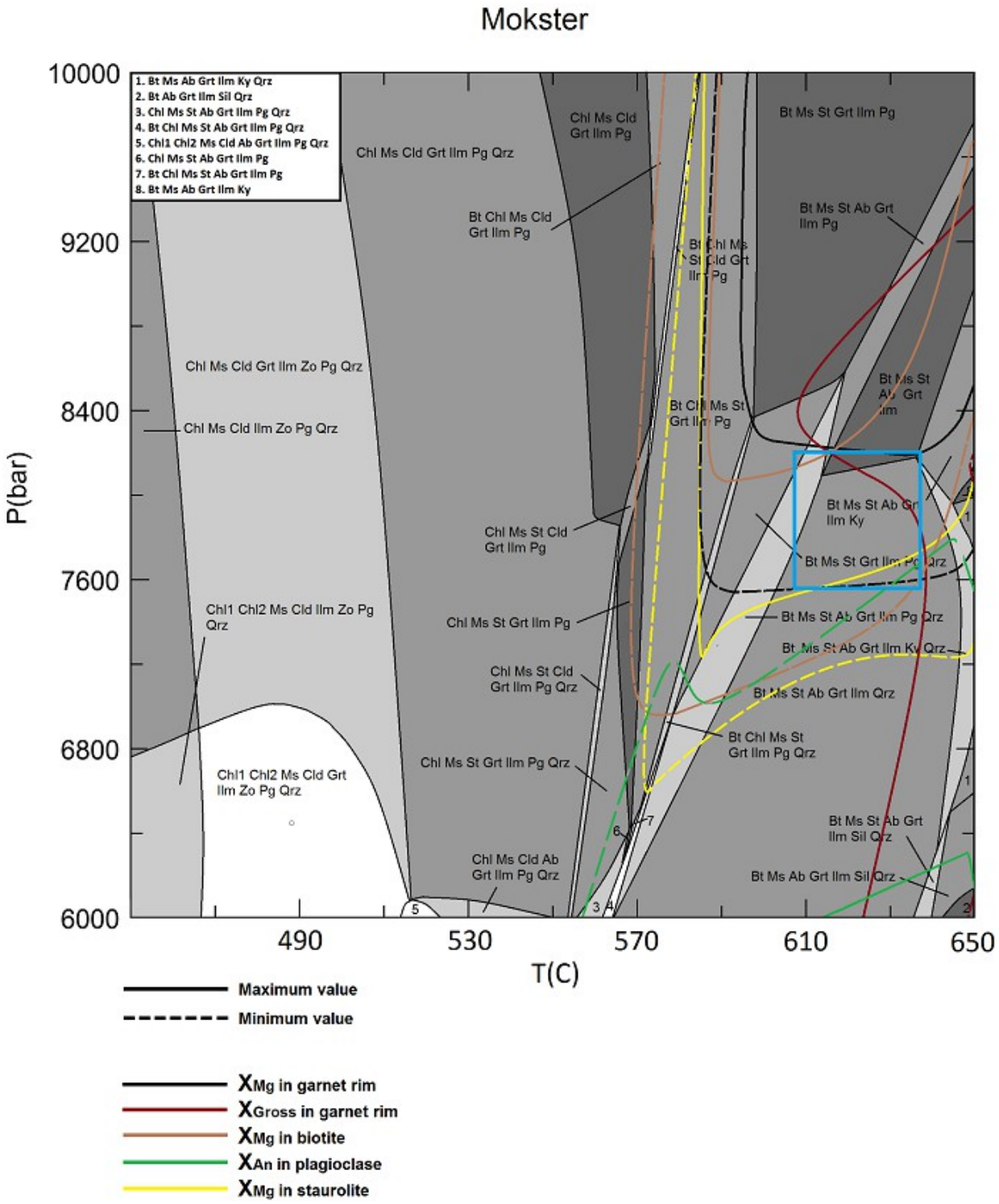

Fig. 5.4: Compositional isopleths of the M1 minerals plotted on the P-T diagram. The blue square is the P-T interval in which most of the compositional isopleths cross and it represents the best estimate for the P-T conditions of the M1 assemblage.

Modelling of M2

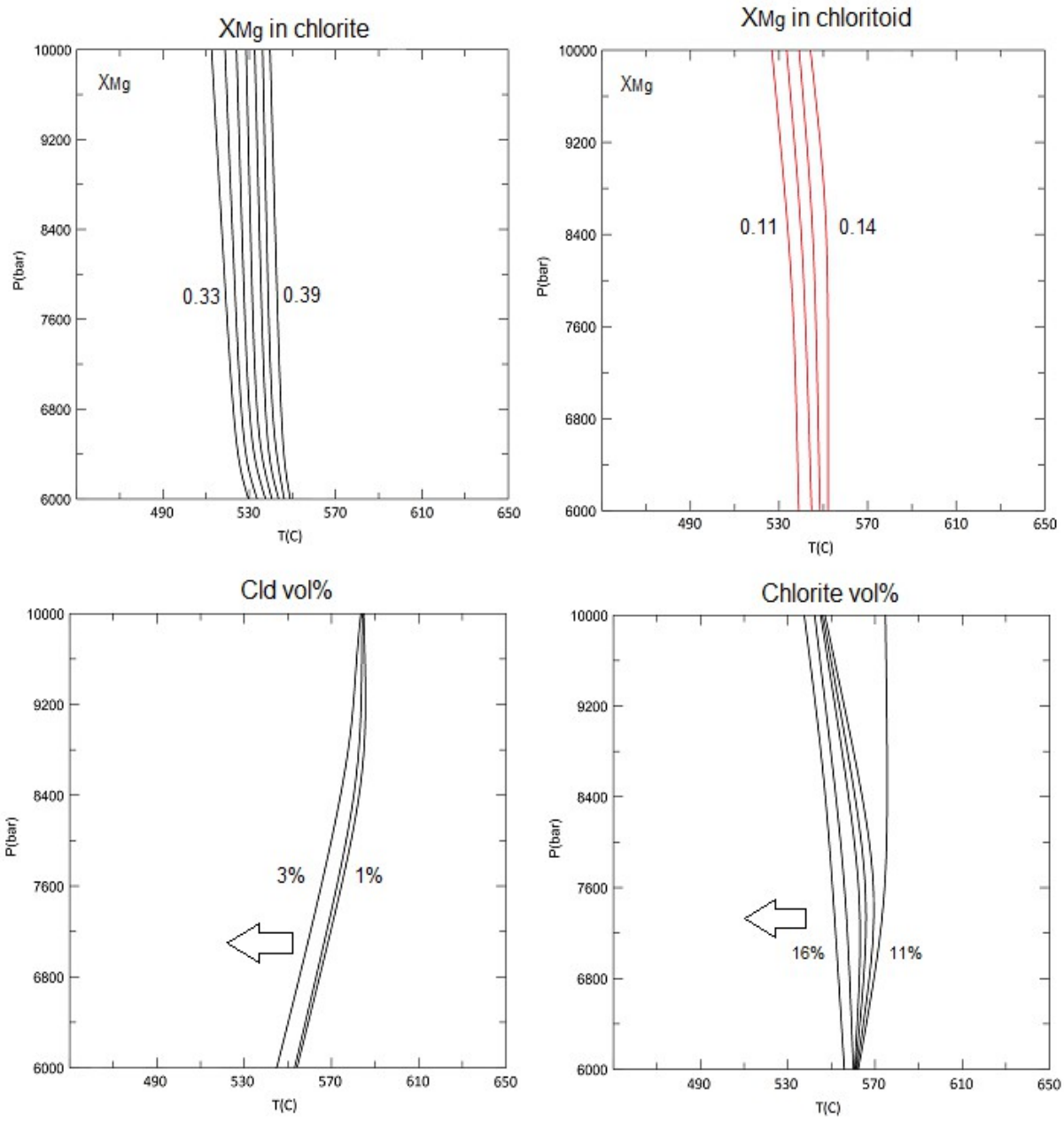

Fig. 5.5: Chl and Cld isopleths. The arrows show growth direction of phases, the vol% is based on the amounts of the corresponding minerals approximately observed in the MOK sample. Steps are 0.01 for compositional isopleths and 1% for vol% isopleths.

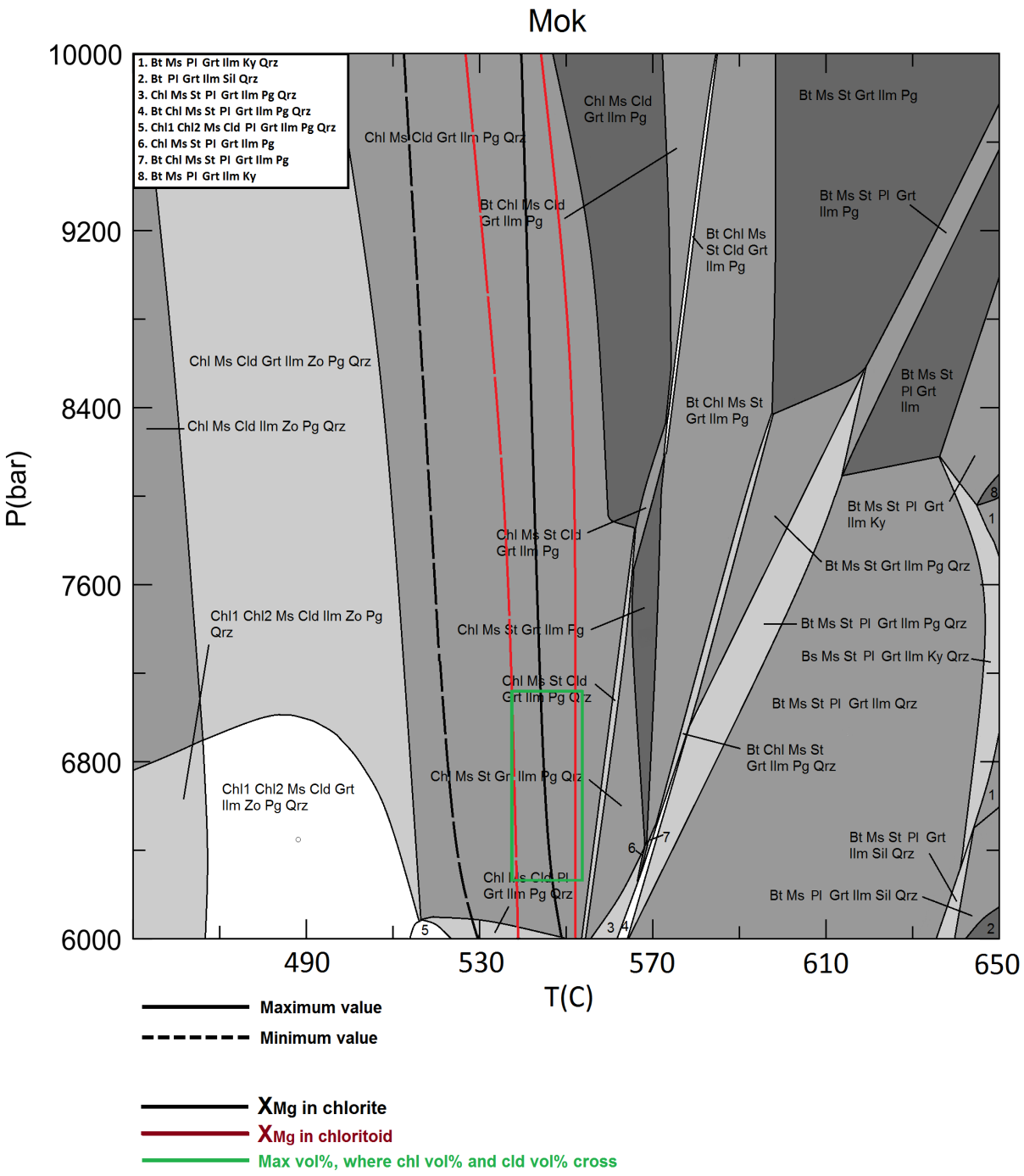

Fig. 5.6: Isopleths for X_{Mg} in Chl and Cld. The green box is the field in which Chl and Cld both attain the (highest) volumes best representing the actual observations from the sample. However, in case of the M2 assemblage the pressure is poorly quantified.

Result

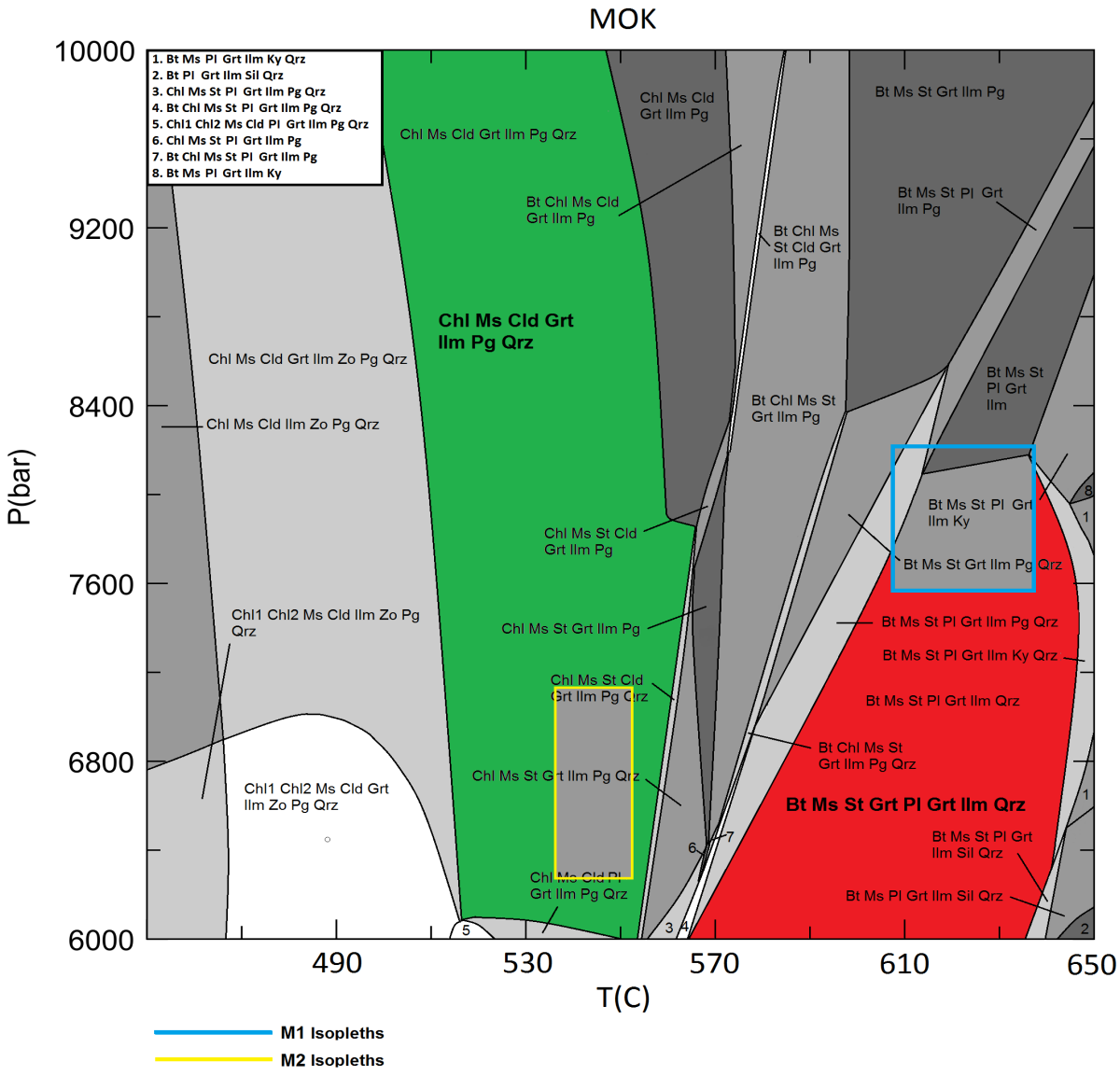

Fig. 5.7: The P-T diagram with the P-T conditions for M1 and M2 superimposed.

Comment on the results (Fig. 5.7).

The stability field of the M1 assemblage can be found between temperatures of 565-640 ^{O}C and pressures of 6-8.1 kbar. The compositional isopleths of the various minerals (X_{Mg}, X_{Gross}, X_{An} etc.) further constrain the P-T conditions to 605-635 ^{O}C and 7.5-8.2 kbar. The stability field covering the M2 assemblage can be found between temperatures of 500-565 ^{O}C and pressures of >6 kbar. The compositional isopleths (X_{Mg}) of chlorite and chloritoid further constrain the T conditions to 535-555 ^{O}C, whereas the pressure cannot be estimated.

5.3 OS-2

The mineral assemblages, M1 and M2, are represented by: M1 - Grt, Ilm, Qrz, Ep and Ms, M2 - Ab, Chl, Ep, Ms, Ilm, Qrz. The P-T section (Fig. X) was calculated at 250-650°C and 2-8 kbar in a system of Na_2O,MgO, Al_2O_3,SiO_2, K_2O, CaO, TiO_2, MnO, FeO, Fe_2O_3, with H_2O saturation. The system composition was taken from the whole rock analysis of the sample and recalculated as mol percent (Tab. 5.2). The solution models used were: biotite (Tajcmanova et al., 2009), chlorite (Holland and Powell, 1998), epidote (Holland and Powell, 1998), feldspar (Fuhrman et al., 1988), garnet (Holland and Powell, 1998), ilmenite (White et al., 2000) and muscovite (Holland and Powell, 1998) . The solution models for staurolite (Holland and Powell, 1998) and chloritoid (Holland and Powell, 2000) were also used, however, these phases were eliminated as unstable during the initial calculation phase in Perple_X.
Garnet solution model of Holland and Powell (1998) was preferred over the model involving Fe^{3+} (White et al., 2000), because the garnet composition calculated with both models does not show any andradite component and the model of Holland and Powell (1998) appears to be the more stable one.

Tab. 5.2: Whole-rock composition of the sample OS-2.

Component	Na_2O	MgO	Al_2O_3	SiO_2	K_2O	CaO	TiO_2	MnO	FeO*	Fe_2O_3*
Mol%	0.85	5.26	14.05	64.30	3.50	1.48	0.97	0.24	8.45	0.88

* The FeO/Fe_2O_3 ratio was chosen arbitrarily based on the fact that its value does not influence the garnet composition (see explanation below).

Estimation of the FeO/Fe_2O_3 ratio in the whole rock analysis

Chemical composition of garnet in the sample OS-2 shows no andradite component and all Fe_2O_3 is thus stored in epidote and ilmenite. In order to estimate how the amount of Fe_2O_3 influences the stability of garnet, a T-X section was calculated for an amount of Fe_2O_3

component increasing from 0 to 5mol% and contoured for the grossular and spessartine component, as well as for the X_{Mg} value. Initial calculations have shown, that for low amounts of Fe_2O_3 in the system composition, the crossing of the isopleths shows approximately the same P-T values regardless the Fe_2O_3 content. Based on this, the pressure for the calculation of the T-X section was selected as 5.6 kbar according to these initial calculations. The resulting T-X section is shown in Fig. 5.8 and confirms, that the garnet composition is nearly independent of the Fe_2O_3 content, but strongly depends on temperature. Based on the calculation, an arbitrary value of 0.88 mol% of Fe_2O_3 was chosen for the system composition

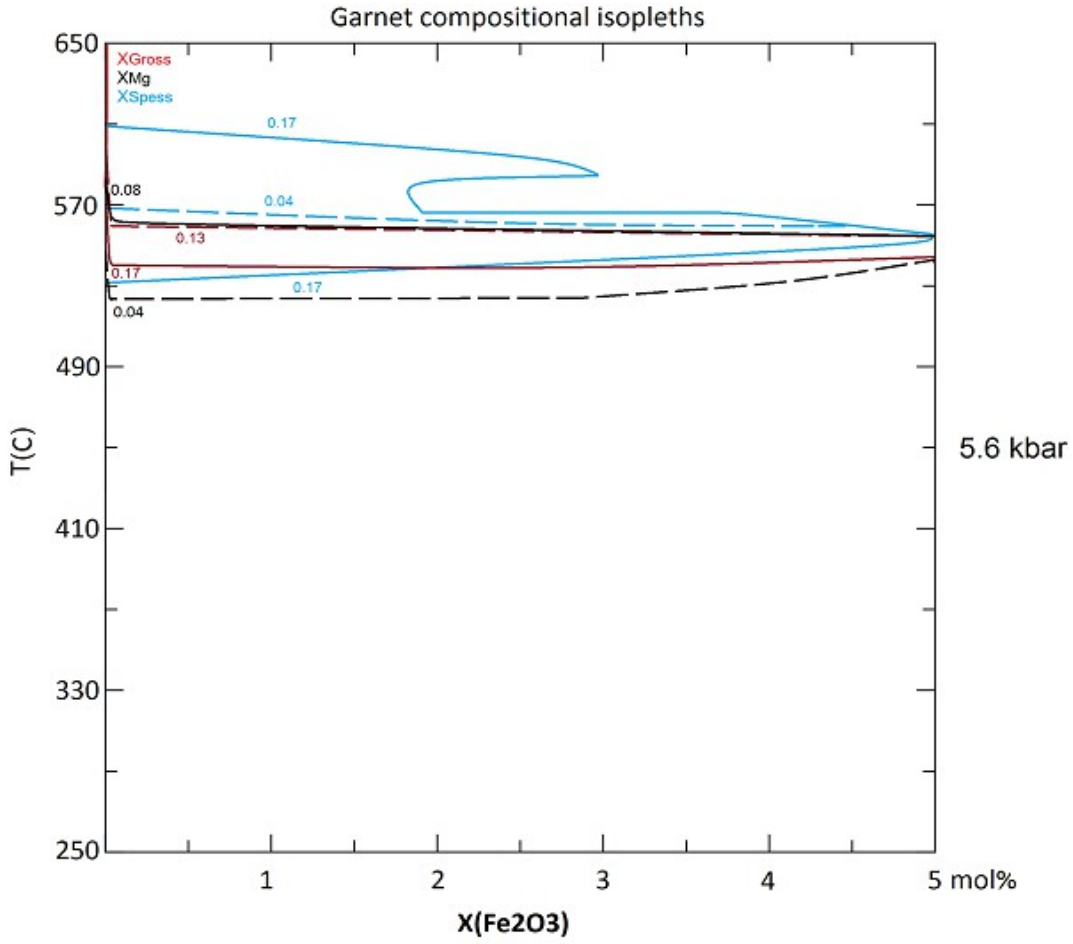

Fig. 5.8: Garnet isopleths plotted in a T-X(Fe_2O_3) diagram. The isopleths are nearly unaffected by the amount of Fe_2O_3.

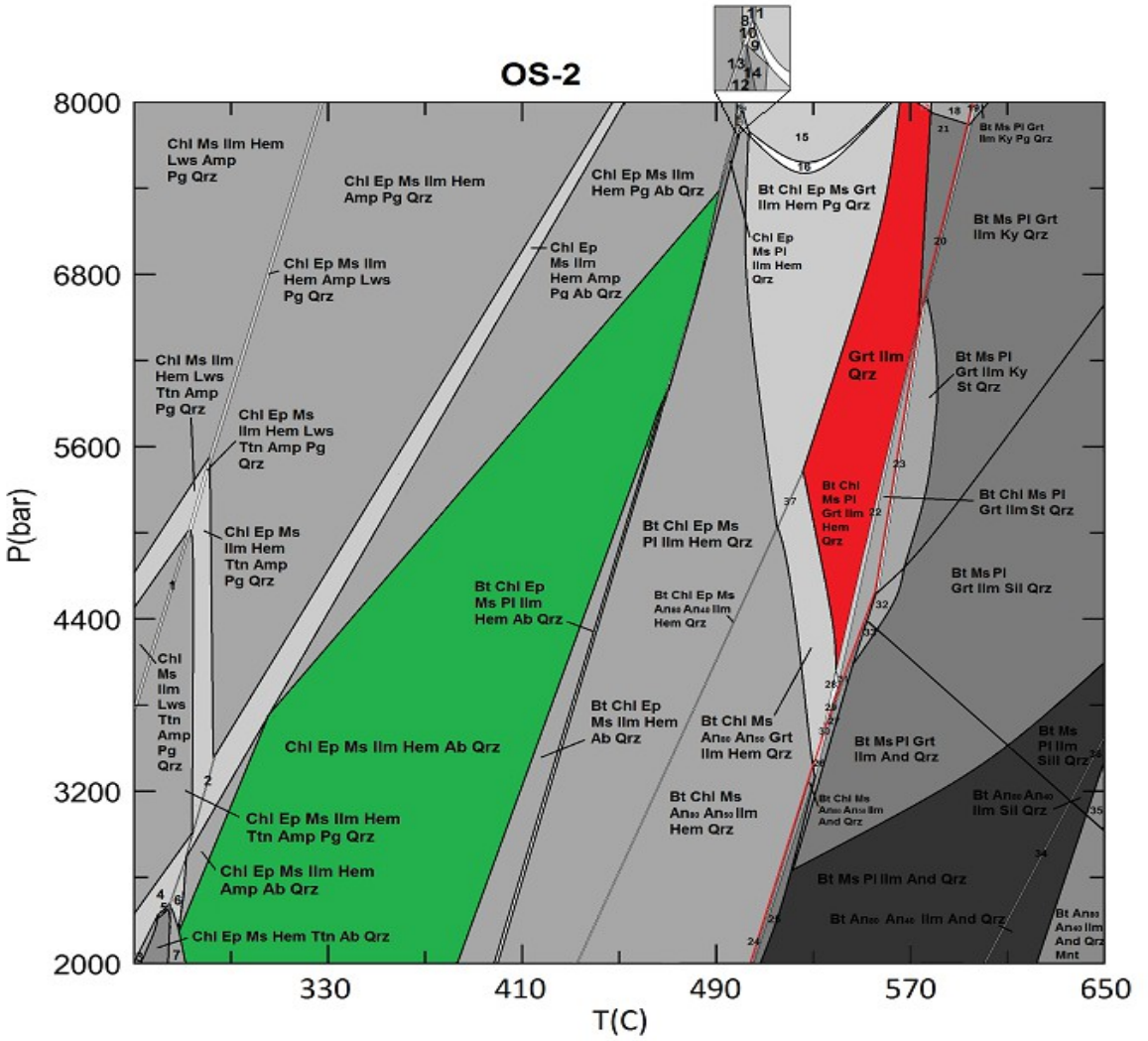

1. Chl Ep Ms Ilm Lws Ttn Amp Pg Qrz
2. Chl Ep Ms Ilm Hem Ttn Amp Pg Ab Qrz
3. Chl Ep Ms Ilm Ttn Amp Ab Qrz
4. Chl Ep Ms Ilm Ttn Amp Pg Ab Qrz
5. Chl Ep Ms Ilm Ttn Pg Ab Qrz
6. Chl Ep Ms Ilm Hem Ttn Amp Ab Qrz
7. Chl Ep Ms Ilm Hem Ttn Ab Qrz
8. Bt Chl Ep Ms Ilm Hem Pg Ab Qrz
9. Bt Chl Ep Ms Pl Ilm Hem Pg Qrz
10. Bt Chl Ep Ms Pl Ilm Hem Pg Ab Qrz
11. Bt Chl Ep Ms Ilm Hem Pg Qrz
12. Chl Ep Ms Pl Ilm Hem Pg Qrz
13. Chl Ep Ms Pl Ilm Hem Pg Ab Qrz
14. Chl Ep Ms Pl Ilm Hem Qrz
15. Bt Chl Ep Ms Grt Ilm Hem Pg Qrz
16. Bt Chl Ep Ms Pl Grt Ilm Hem Pg Qrz
17. Bt Chl Ms Pl Grt Ilm Hem Pg Qrz
18. Bt Chl Ms Pl Grt Ilm Pg Qrz
19. Bt Chl Ms Pl Grt Ilm Ky Pg Qrz
20. Bt Chl Ms Pl Grt Ilm Ky Qrz
21. Bt Chl Ms Pl Grt Ilm Qrz
22. Bt Chl Ms Pl Grt Ilm Hem Fo Qrz
23. Bt Chl Ms Pl Grt Ilm Ky Fo Qrz
24. Bt Chl Ms An_{80} An_{40} Ilm Hem And Qrz
25. Bt Chl Ms Pl Ilm And Qrz
26. Bt Ms Pl Grt Ilm And Qrz
27. Bt Chl Ms Pl Grt Ilm And Qrz
28. Bt Chl Ms An_{80} An_{40} Grt Ilm Hem Fo Qrz
29. Bt Chl Ms An_{80} An_{40} Grt Ilm Fo Qrz
30. Bt Chl Ms An_{80} An_{40} Grt Ilm Hem And Qrz
31. Bt Chl Ms Pl Grt Ilm And Fo Qrz
32. Bt Ms Pl Grt Ilm Sil Fo Qrz
33. Bt Ms Pl Grt Ilm And Fo Qrz
34. Bt Ms An_{80} An_{40} Ilm And Qrz
35. Bt An_{80} An_{40} Ilm Sil Qrz Mnt
36. Bt Ms An_{80} An_{40} Ilm Sil Qrz
37. Bt Chl Ep Ms An_{80} An_{40} Grt Ilm Hem Qrz

Al2SiO5 line

Fig. 5.9: The P-T section calculated for the whole-rock composition of the OS-2 sample.

The stability field marked in red is the assemblage corresponding to M1 and the field marked in green corresponds to M2. Both stability fields are large so in order to better constrain the PT conditions of the equilibration, the evolution of the mineral compositions was modelled as isopleths.

Modellling of M1

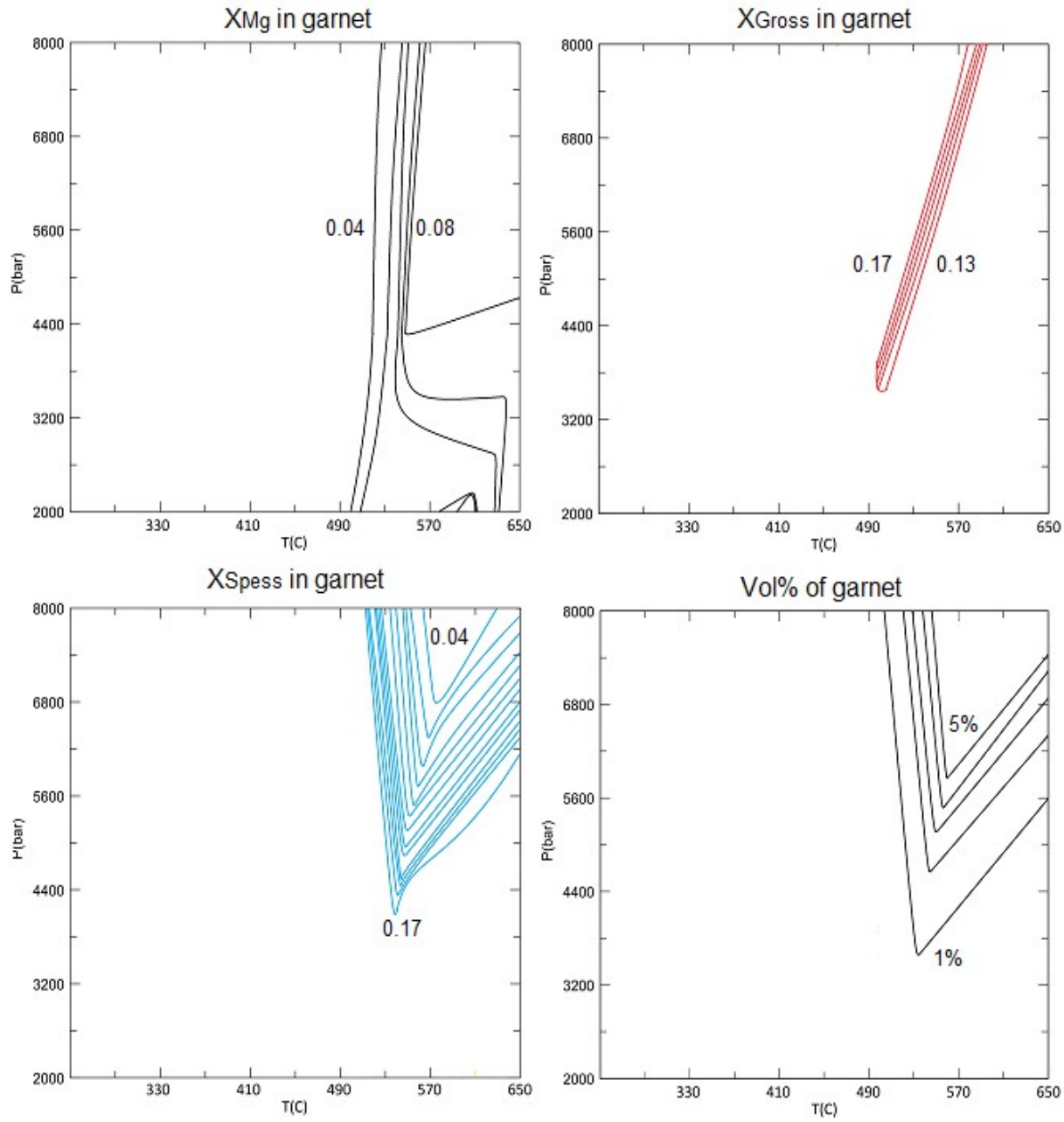

Fig. 5.10: Compositional isopleths of garnet, including vol%. The steps are 0.01 for the compositional isopleths and 1% for the vol% isopleth.

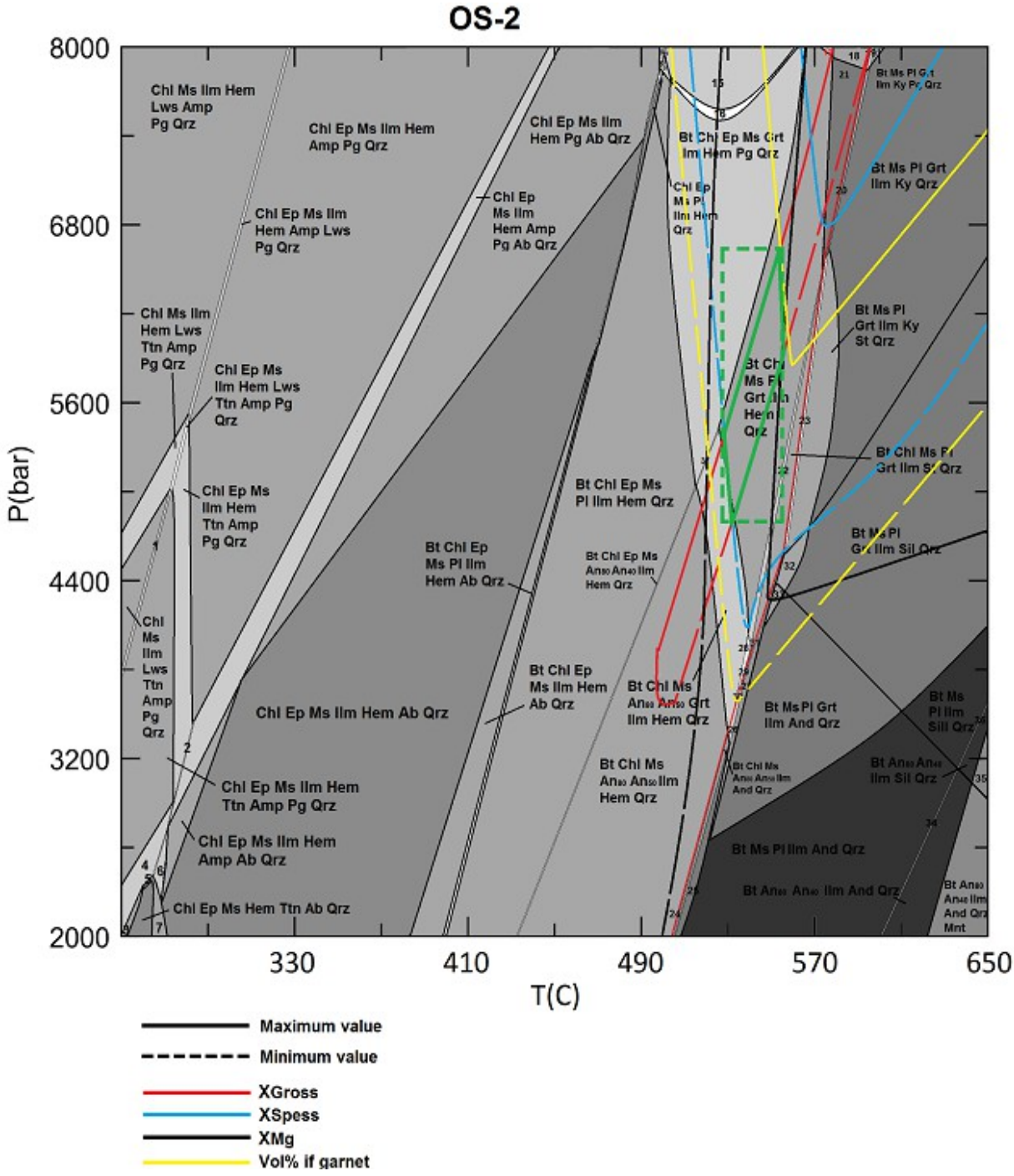

Fig. 5.11: Garnet compositional isopleths placed in the P-T diagram, including vol% isopleths. The green rectangle represents the P-T interval in which the isopleths cross and it is thus the best estimate for the P-T conditions of the M1 assemblage.

Modellling of M2

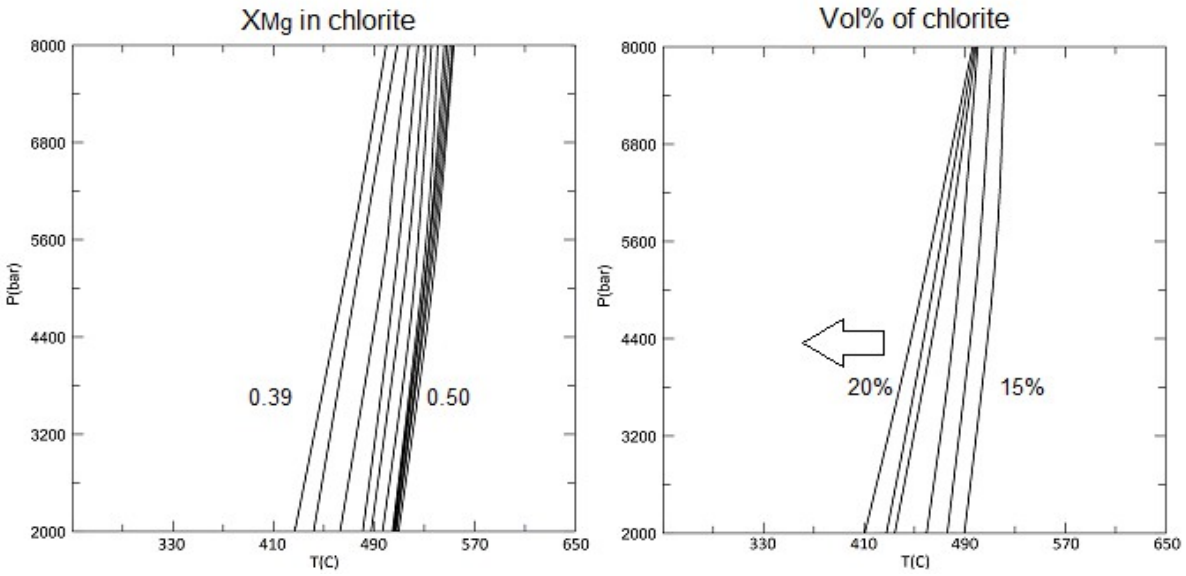

Fig. 5.12: Chl isopleths, including vol%. 0.01 steps and 1% steps for compositional and vol% isopleths, respectively.

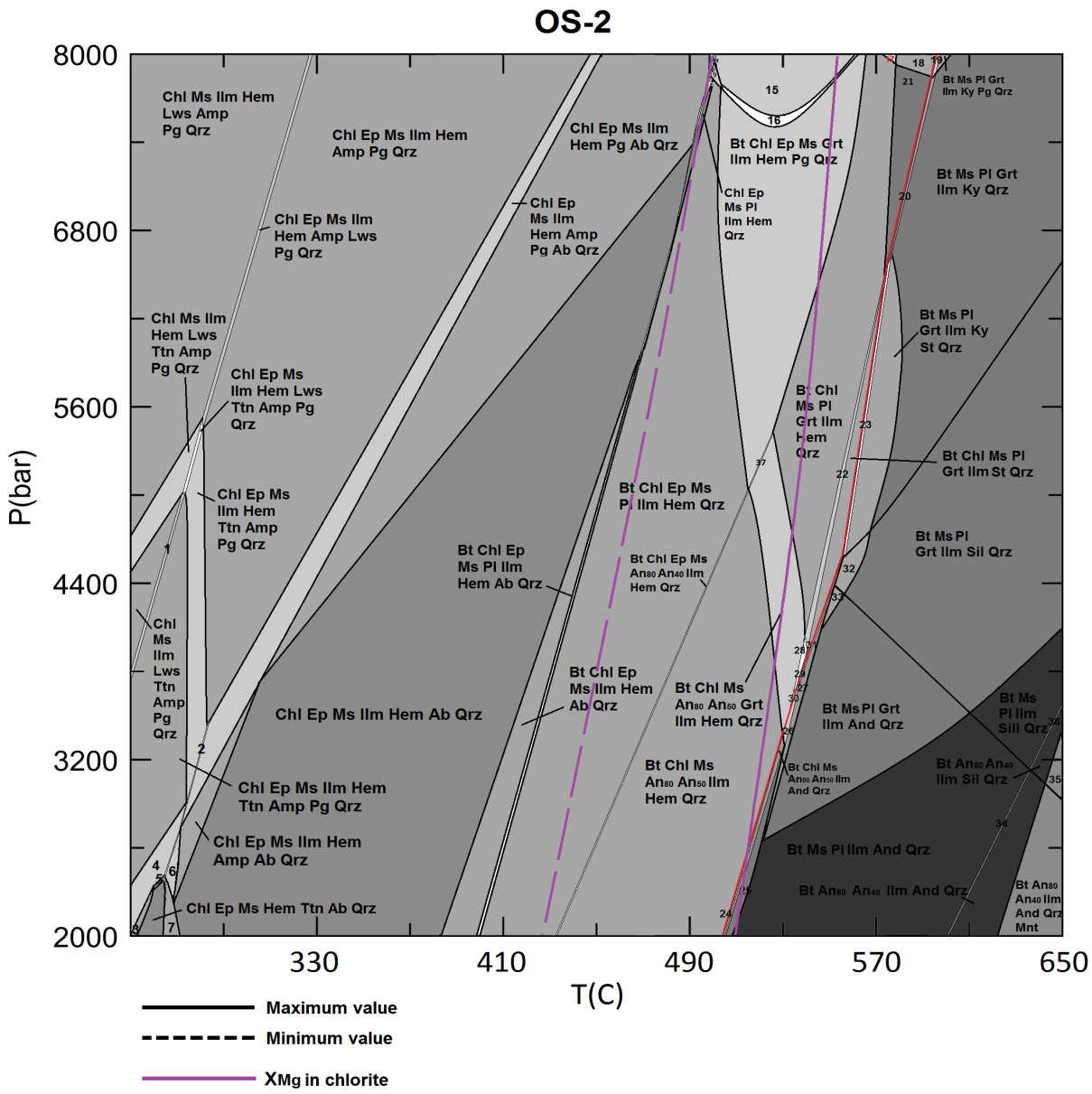

Fig. 5.13: Chlorite X_{Mg} isopleth plotted on the P-T diagram.

Result

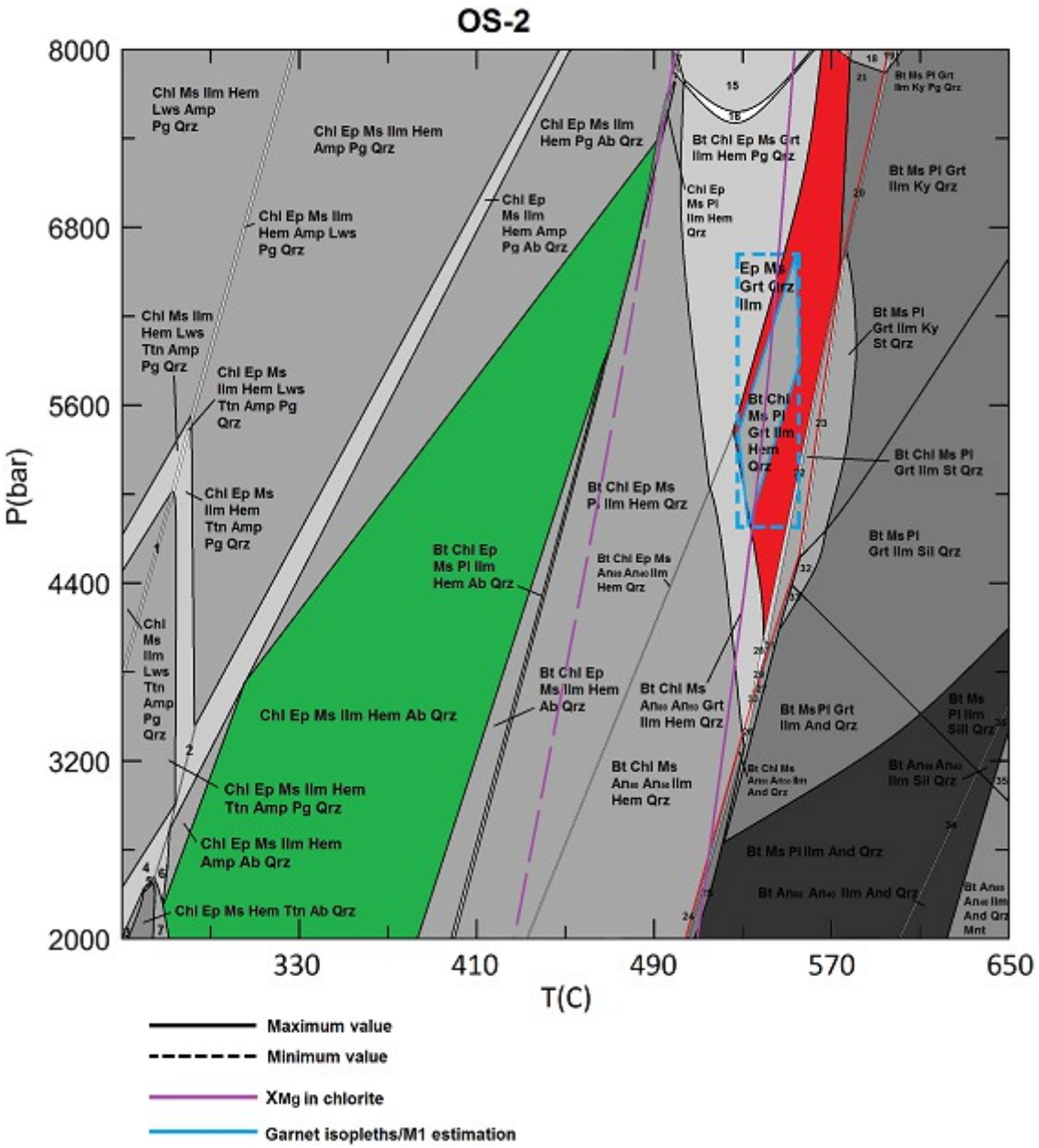

Fig. 5.14: The P-T diagram with the P-T conditions for M1 and M2 marked.

Comment on the results (Fig. 5.14).

The stability field best covering the M1 assemblage can be found between temperatures of 520-570 ^{O}C and pressures of 4.1-8 kbar. The compositional isopleths of garnet (X_{Mg}, X_{Gross} etc.) further constrain the PT conditions to 530-560 ^{O}C and 4.8-6.6 kbar. The stability field

covering the M2 assemblage can be found between temperatures of 290-450 ^{O}C and pressures of 2-7.4 kbar. The compositional isopleths (X_{Mg}) of chlorite do not fall within this stability field, however, the high P-T part of the X_{Mg} isopleth cross the garnet isopleths and so may help to constrain M1 with respect to temperature.

5.4 BGA 2-1

The mineral assemblages M1 and M2 are represented by: M1- Grt, Ilm, Qrz,± Ms, ± Bt, M2 - Ab, Amp, Bt, Ep, Chl, Ms, Ilm and Qrz. The P-T section was calculated at 400-600 ^{o}C and 2-8 kbar in the system of Na_2O,MgO, Al_2O_3,SiO_2, K_2O, CaO, TiO_2, MnO, FeO and Fe_2O_3 with H_2O saturation. The system composition used for the calculations corresponds to the molar percentage of the above components obtained by the whole rock analysis (Tab. 5.3). The solution models used were: biotite (Tajcmanova et al., 2009), chlorite (Holland and Powell, 1998), epidote (Holland and Powell, 1998), feldspar (Fuhrman et al., 1988), garnet (White et al., 2000), ilmenite (White et al., 2000) and muscovite (Holland and Powell, 1998). The solution models for staurolite (Holland and Powell, 1998) and chloritoid (Holland and Powell, 2000) were also used, however these phases were eliminated as unstable by Perple_X in the initial calculation phase. Note that no amp solution model was used, as the existing models are numerically unstable for the system composition used and they did not provide any consistent results. Garnet mixing model involving Fe^{3+} (White et al., 2000) was chosen because the garnet in this sample contains high percentage of andradite component.

Tab. 5.3: Wt% of components

Component	Na_2O	MgO	Al_2O_3	SiO_2	K_2O	CaO	TiO_2	MnO	FeO	Fe_2O_3*
Wt%	1.07	4.46	5.65	76.62	2.13	1.21	0.55	1.31	6.81	0.19

* FeO/Fe_2O_3 ratio cannot be determined from the XRF analysis and the method used for the estimate of this value is explained below.

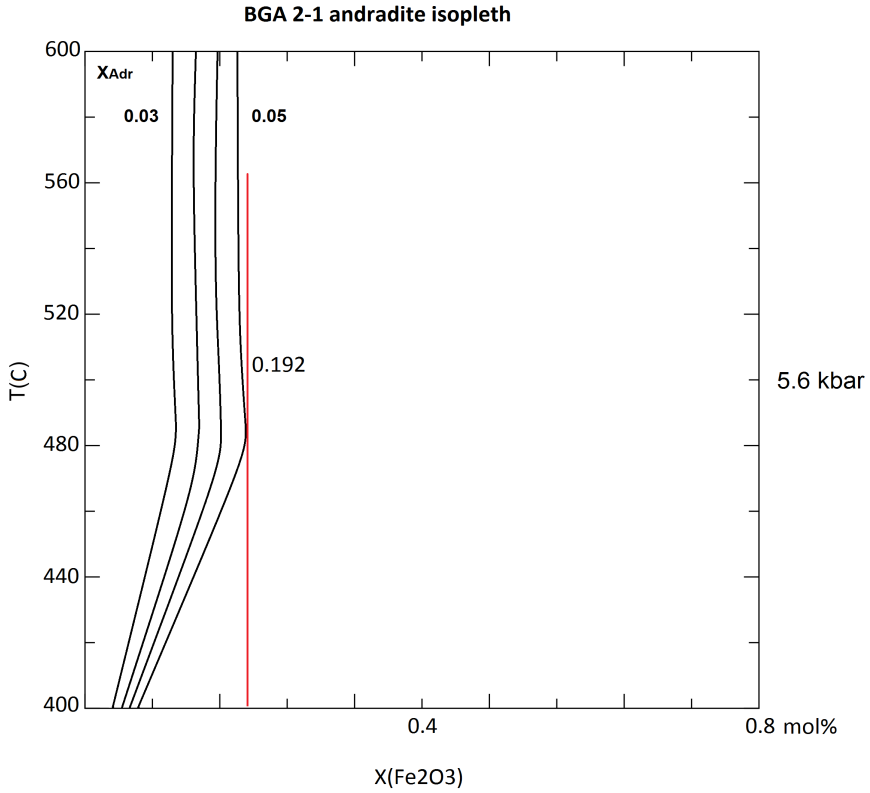

Fig. 5.15: T-X_{Fe2O3} diagram calculated for the system composition corresponding to the whole rock composition of the sample BGA2-1. The diagram presents only the isopleths for $X_{andradite}$ values observed in garnet of the sample BGA2-1. The calculation suggests the upper limit of ca. 0.192 mol% of Fe_2O_3 in the bulk of the sample.

Estimation of the FeO/Fe_2O_3 ratio in the whole rock analysis

The chemical composition of garnet in the sample, BGA 2-1 shows nearly constant content of 3-6% andradite component (Fig. 4.13 – profile through garnet in BGA2-1). In order to estimate which amount of Fe_2O_3 component in the system will ensure such composition of the garnet, a T-X section was calculated for an amount of Fe_2O_3 component increasing from 0 to 0.8 mol% and contoured for the andradite content. The pressure of 5.6 kbar was chosen for the calculation, as it is the pressure value estimated from the sample OS-2, which is in the field in close vicinity of the sample BGA2-1. The result of the calculation is shown in Fig. 5.15 and suggests that the andradite content of garnet is nearly independent of temperature, but strongly depends on Fe_2O_3 content of the rock. Based on the calculation, the vaule of 0.192 mol% of Fe_2O_3 was chosen for the system composition.

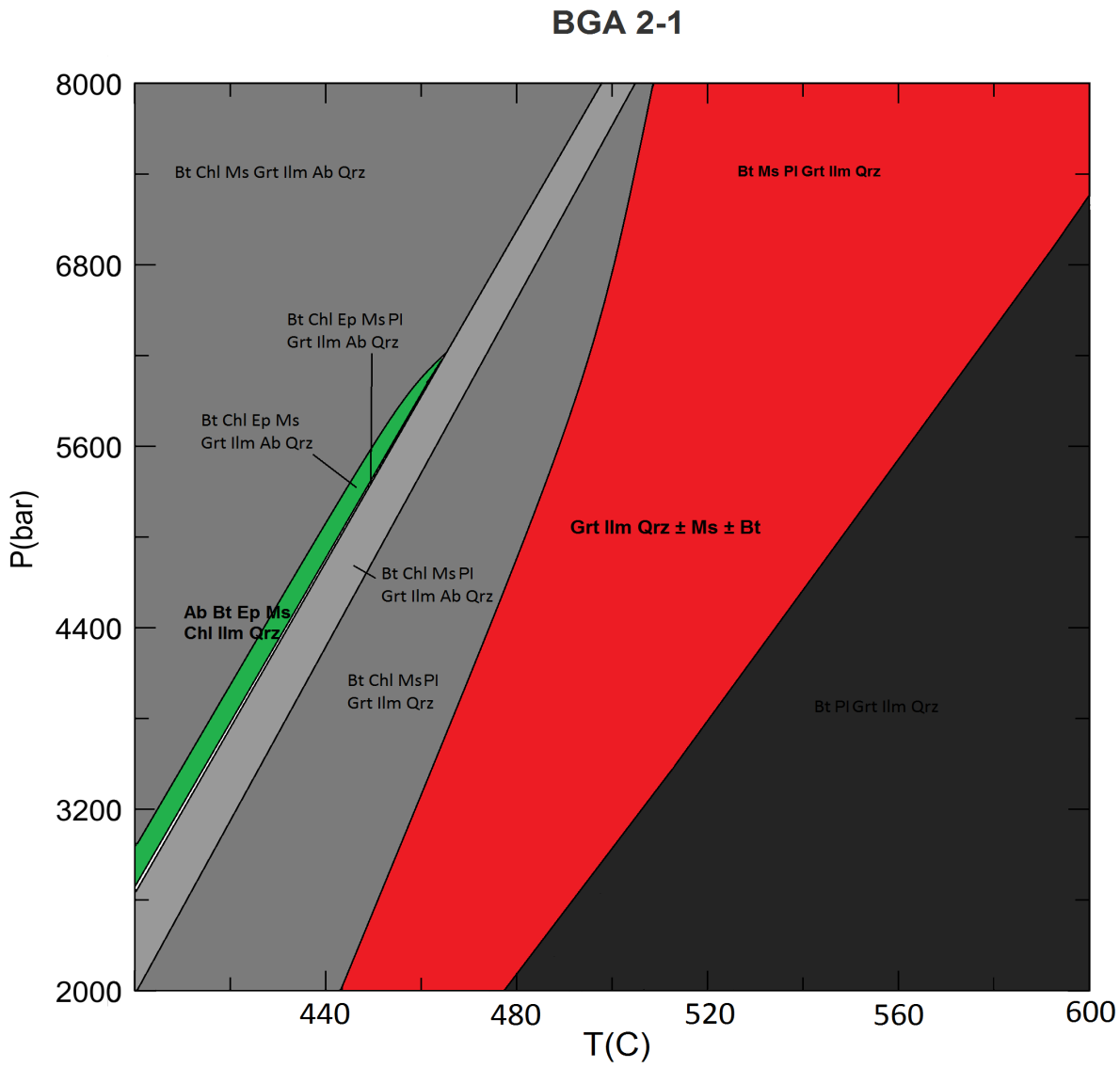

Fig. 5.16: The P-T section calculated from the whole-rock chemistry of the BGA 2-1 sample. The stability field marked in red is the assemblage corresponding to M1 and the field marked green corresponds to M2. The stability fields are large, so in order to better constrain the P-T conditions of equilibration, the evolution of the mineral compositions was modelled as isopleths.

Modelling of M1

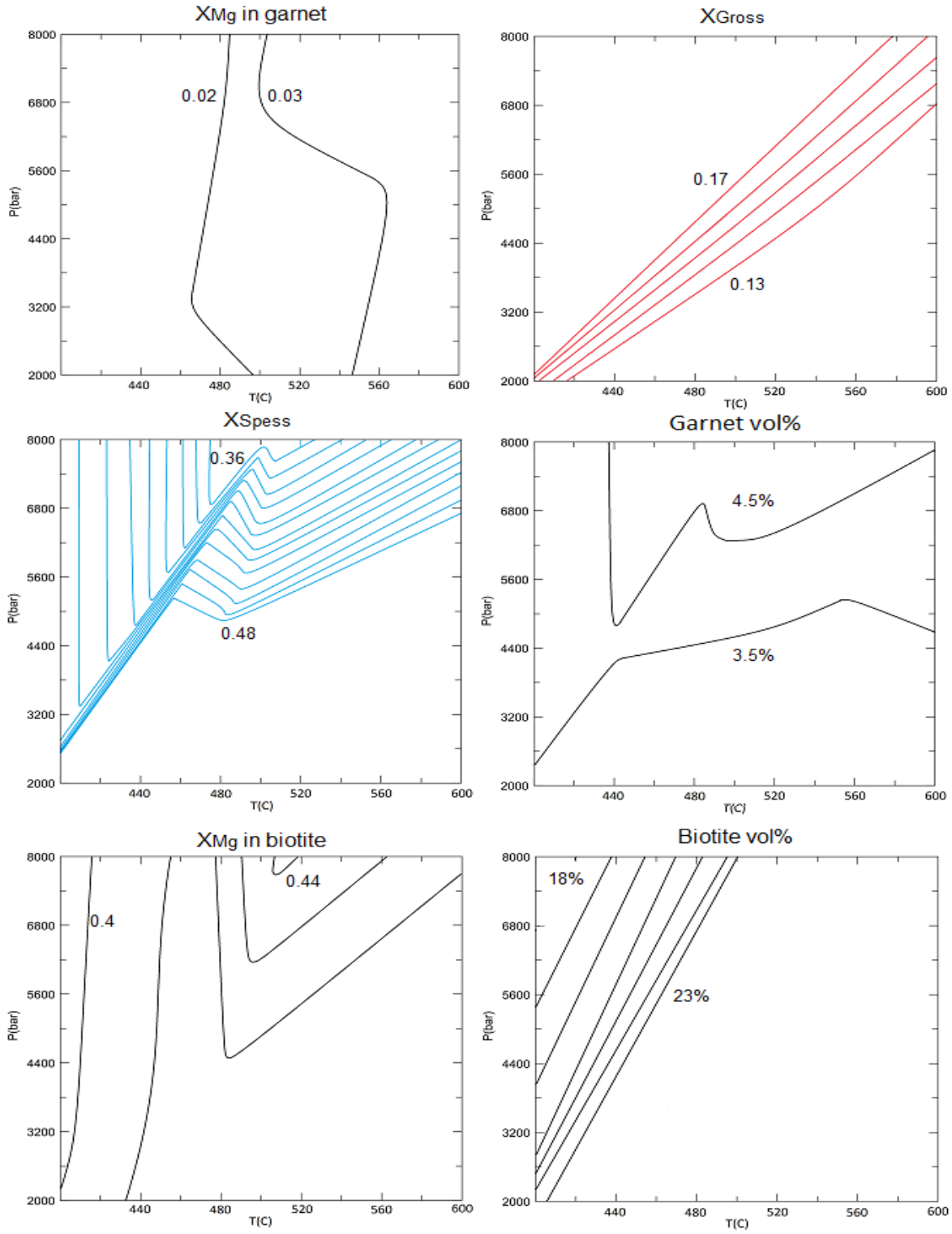

Fig. 5.17: Compositional isopleths for garnet and biotite, including isopleths for vol%. The steps are 0.01 for all the compositional isopleths and 1% for the vol% isopleths.

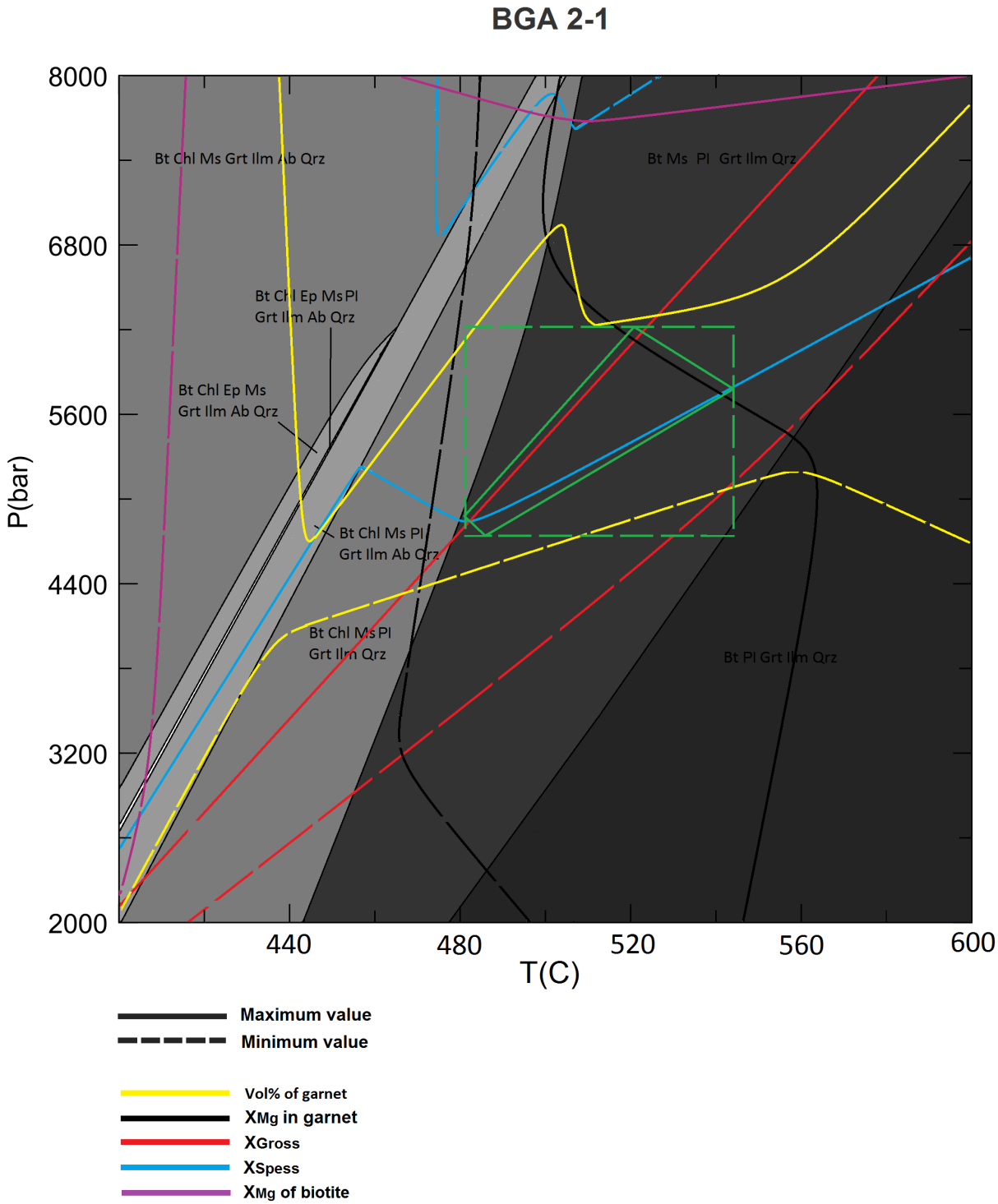

Fig. 5.18: Compositional isopleths of garnet. The green square represents the P-T interval in which the compositional isopleths cross and thus is the best estimate for the P-T conditions of the M1 mineral assemblage of the sample BGA2-1. Biotite covers everything and so does not constrain M1 further.

Modelling of M2

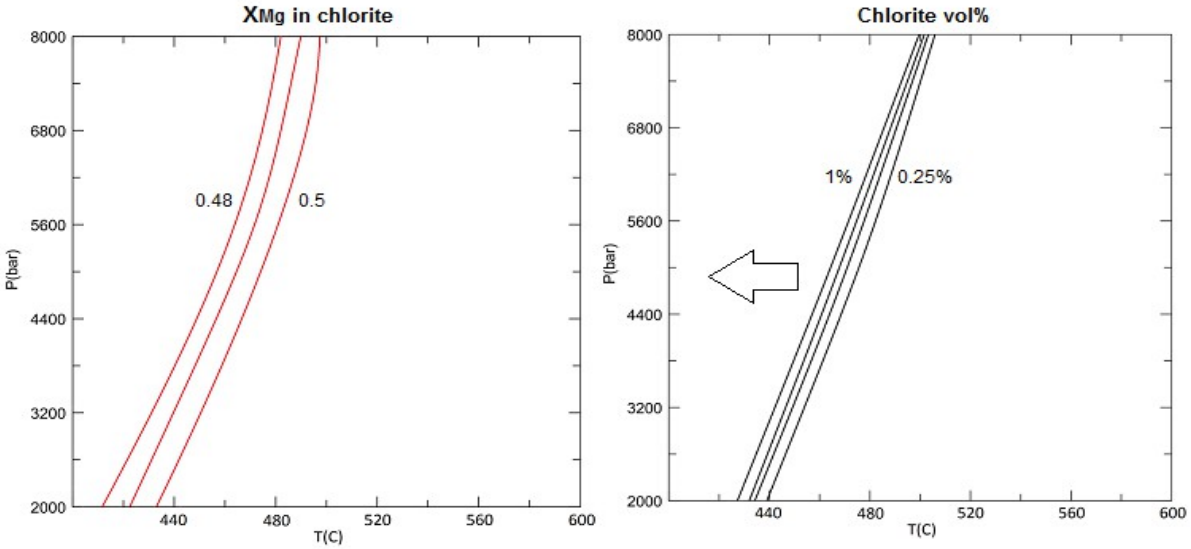

Fig. 5.19: Chl isopleths. The arrow shows growth direction of phases, the vol% is based on volume of chlorite approximately observed in the BGA 2-1 sample.

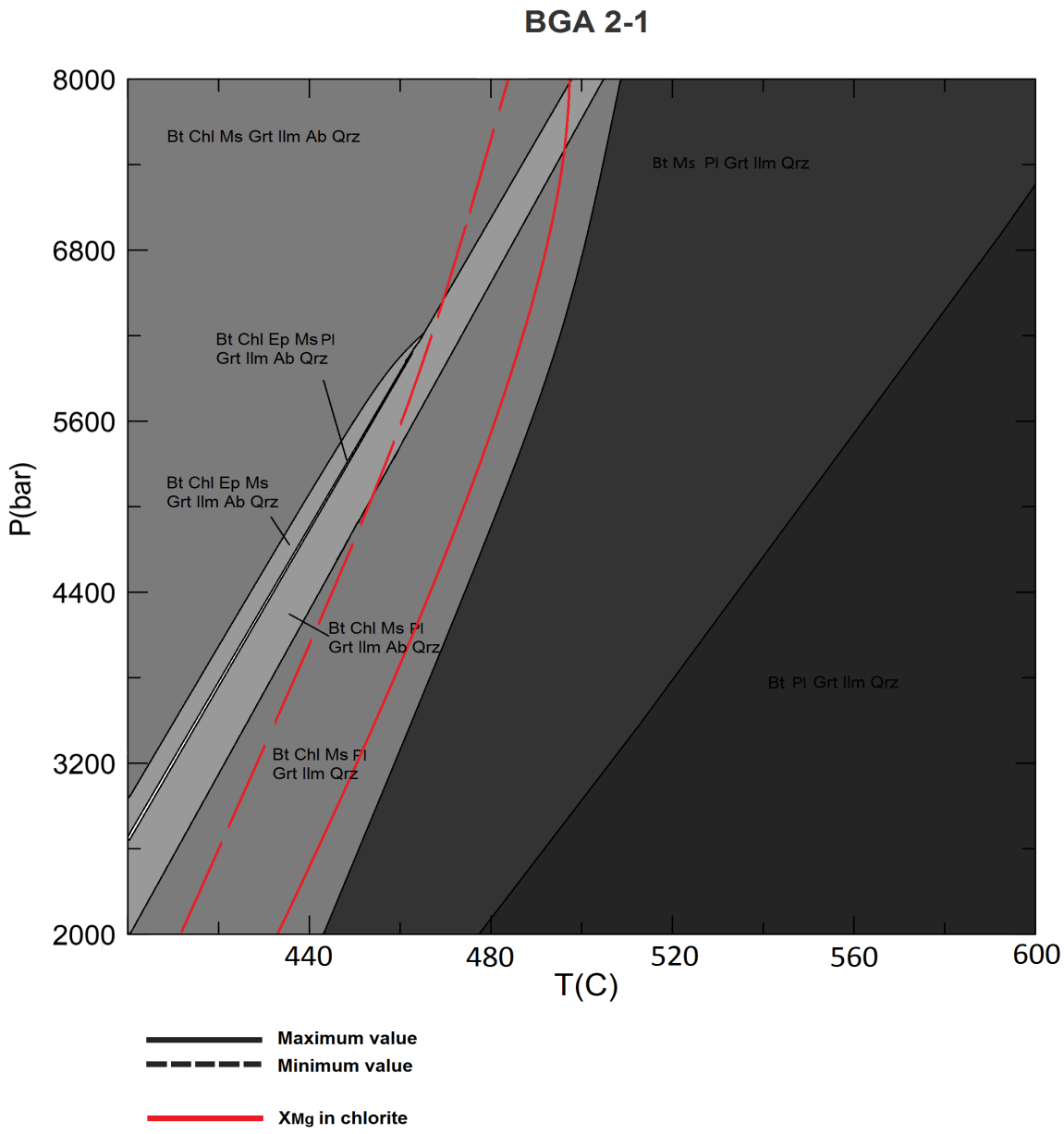

Fig. 5.20: Compositional isopleths of X_{Mg} in Chl plotted on the P-T diagram.

Result

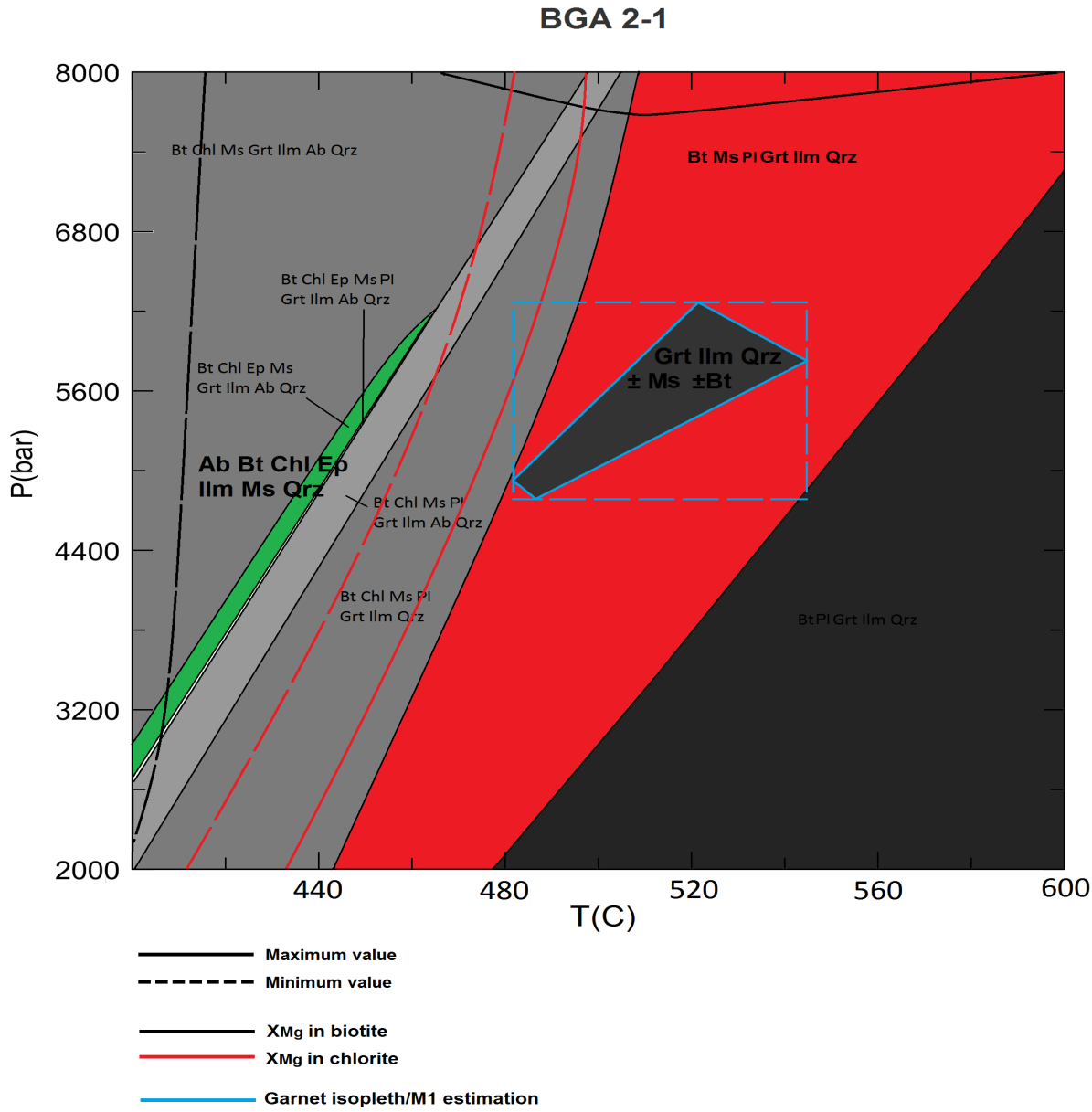

Fig. 5.21: The P-T diagram with the P-T conditions estimated from the garnet, chlorite and biotite isopleths superimposed.

Comment on the results (Fig. 5.21).

The stability field best covering the M1 assemblage can be found between temperatures of 445-600 ^{O}C and pressures of 2-8 kbar. The compositional isopleths of garnet (X_{Mg}, X_{Gross} etc.) further constrain the P-T conditions to 480-545 ^{O}C and 4.7-6.3 kbar. The stability field covering the M2 assemblage can be found between 400-465 ^{O}C and 2.7-6.2 kbar. The

compositional isopleths (X_{Mg}) of chlorite do not fall into this stability field and do not help constraining the P-T conditions for the assemblage. The compositional isopleths for biotite covers almost the entire diagram and so do not help constraining the P-T conditions either.

6 DISCUSSION

6.1 MOK

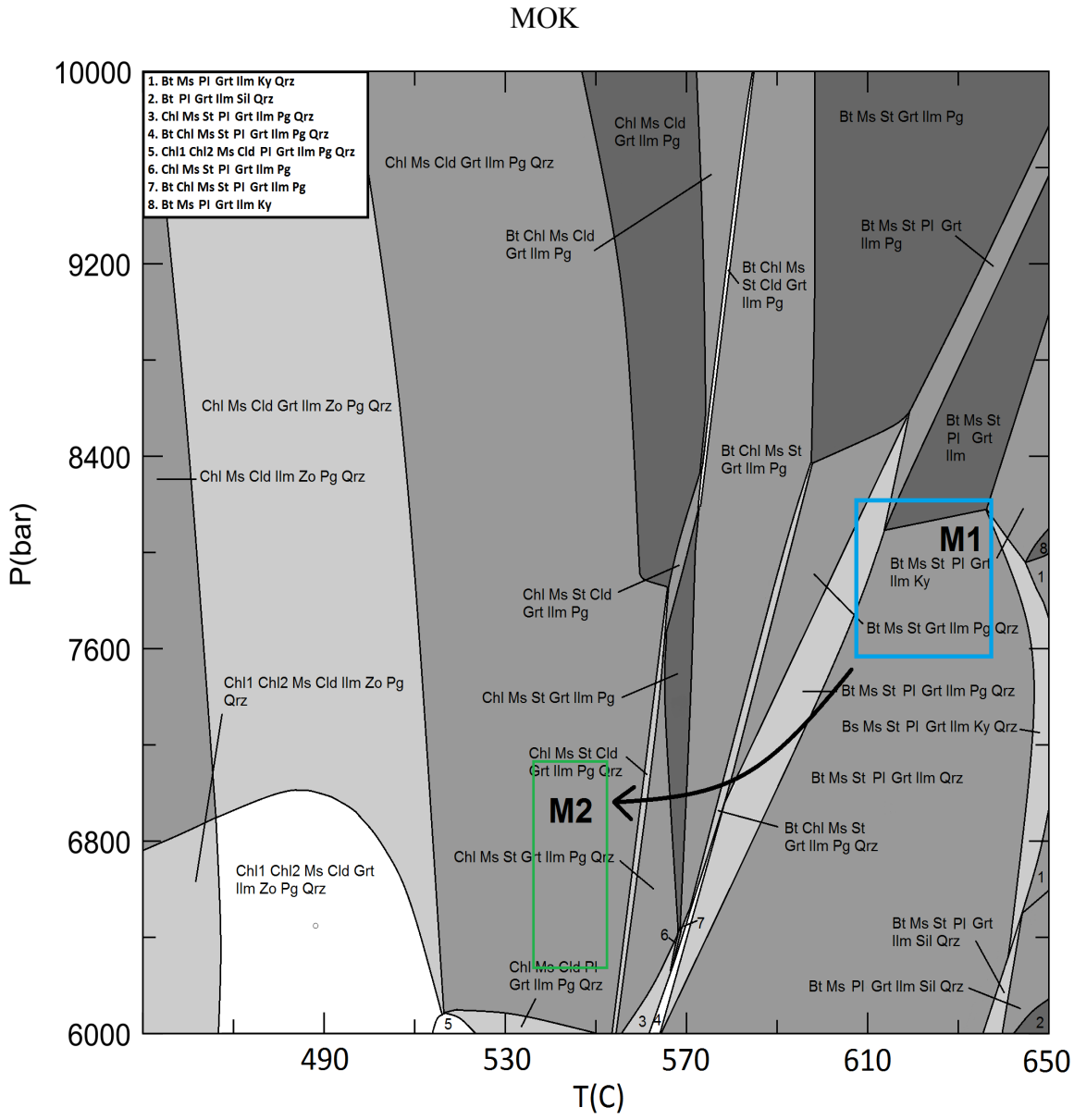

Fig. 6.1: P-T section for MOK with M1 and M2 superimposed. The arrow implies retrogression.

6.1.1 P-T diagram

In the P-T diagram (Fig. 6.1), the stability fields in which the M1 and M2 assemblages are located occur at two different P-T conditions. These conditions are further constrained by compositional isopleth plots. The modelled M1 assemblage lies within P-T conditions corresponding to the upper amphibolite facies, whereas M2 shows P-T conditions corresponding to the transition between the upper greenschist and the lower amphibolite facies. However, the metamorphic conditions for M2 assemblage are not well constrained as the X_{Mg} isopleths for chl and cld are mostly parallel in the calculated P-T section.

The stability field covering M1 is well constrained due to the number of minerals suitable for thermobarometry. The peak P-T conditions can be further constrained by considering stability fields of some other mineral phases as limits. The quartz-free stability field at higher pressures and the Al_2SiO_5-bearing stability fields at higher temperatures can be considered as such limits, as kyanite could not be observed in the sample and quartz is still present as a part of the M1 assemblage.
Paragonite was not observed in the garnet, and the lower T fields containing this mica may be considered such a limit. However, paragonite is difficult to distinguish from the other white micas in microscope, so there is some uncertainty here.

The conditions of retrogression and formation of the M2 assemblage were estimated based on the combination of the isopleths for X_{Mg} and vol% for both chl and cld. The isopleths fall in the large stability field corresponding to the M2 assemblage conditions and do somehow constrain the temperature of retrogression, whereas the pressure conditions could not be estimated.

6.1.2 Metamorphic evolution

Based on the observations, modelling and mineral chemistry, a metamorphic evolution of the MOK sample can be suggested.

Of the M1 assemblage, biotite may have been one of the first Fe-Mg minerals to nucleate, possibly at the expense of some earlier minerals (e.g. chlorite). A further increase in the PT conditions would have allowed for garnet to nucleate and grow, eventually overgrowing and enclosing the biotite. At the peak temperature conditions (605-635 ^{O}C), staurolite may have started to nucleate and grow together with the garnet rim in which it appears. Relics of strongly corroded staurolite crystals in the matrix suggest that staurolite was a part of the matrix mineral assemblage at the peak P-T conditions (Fig. 6.3 a). The plagioclase likely stabilized at the expense of the paragonite component of muscovite and of margarite, neither of which can be found in garnet. Compositional isopleths of X_{An} imply that plagioclase was rich in Ab at the peak P-T conditions, hence the phase belonging to the M1 assemblage.

After an apparent period of cooling and decompression without any fluid influx, a deformation event occurred at greenschist facies conditions with re-hydration of the sample. The combination of cooling and fluid influx probably led to a complete replacement of biotite in the matrix into chlorite, which is widespread in the sample (Fig.4.1 G). Staurolite and plagioclase experienced alteration as can be inferred from pseudomorphs (prism-shaped sericite aggregates), sericitized rims, close proximity to chloritoid etc. During the retrograde event, the garnet was fractured and infiltrated by fluids, which lead to its partial alteration into chlorite in the fractures (Fig. 4.1 A, Fig. 6.3 c). Partial consumption of plagioclase probably stabilized paragonite. The coarse muscovite in the matrix experienced partial recrystallization/re-equilibration into the fine-grained variety as evident by the texture and different chemistry (Figs. 4.1 B, and Fig. 4.6). The metamorphic evolution is summarized in Fig. 6.2 and 6.3.

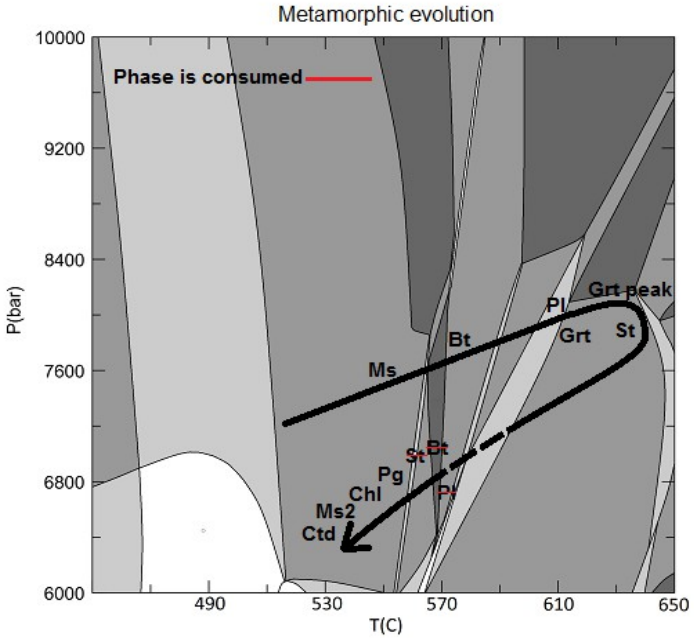

Fig. 6.2: Simplified illustration of the metamorphic evolution of the sample MOK. The stipled line implies a period of no change/metamorphism in the rock.

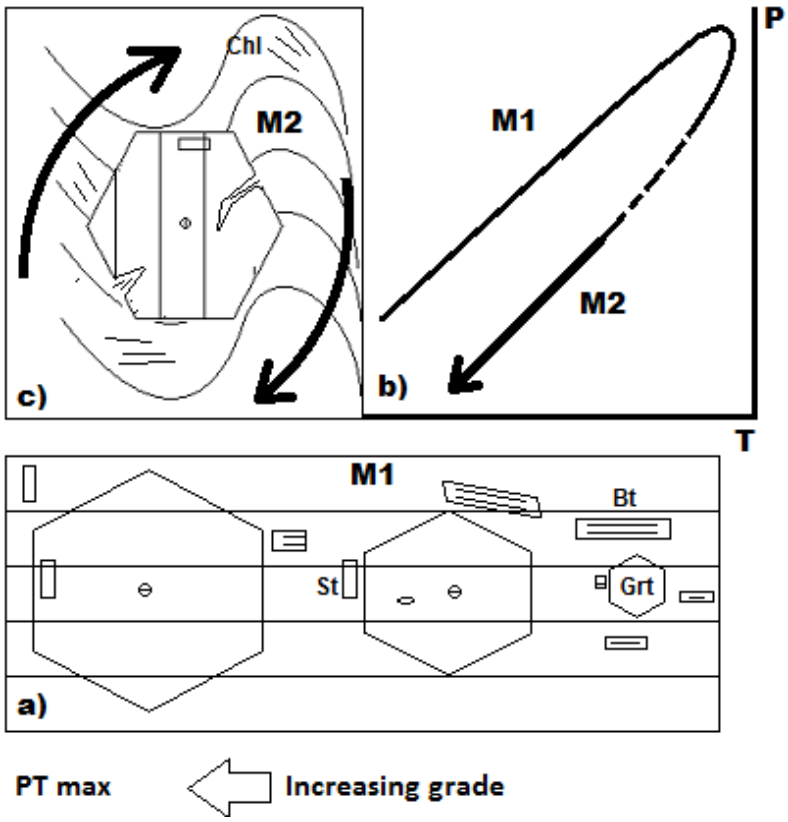

Fig. 6.3: a) Garnet nucleates in the biotite zone, garnet overgrows biotite. During peak metamorphism staurolite forms and is overgrown by garnet. Note that the foliation is straight **b)** PT-t path. **c)** Folding followed by retrogression, fracturing of garnet and the growth of chlorite in the fractures as well as in the matrix.

6.1.3 Depth and Temperature

By converting pressure into depth (h= P/ρg, P = GPa, ρ = 2650 g/m^3, g = 10 m/$s^{-2,}$), the depths of 29 to 31 km were calculated for the corresponding temperatures of 605-635 ^{O}C in M1. For the M2 conditions depths of 24-28 km were calculated, with temperatures of 535-555 ^{O}C. In a previous publication from the Møkster-Selbjørn area, Rykkelid (1987) published thermobarometric estimations of 630-750 ^{O}C, at depths of c. 24 km for an assemblage similar to M1 of the MOK sample, and PT conditions of 7 kbar (26 km) and 570 ^{O}C for a M2-equivalent assemblage. These PT conditions are similar to the PT conditions of the MOK, however, the samples of Rykkelid (1987) were taken from migmatites close to an intrusion consisting of gabbroic dykes. The metamorphic evolution has been attributed to contact metamorphism, which may explain somewhat elevated maximum temperatures when compared to MOK. The depths and metamorphic evolution appears to be opposite to the MOK sample, suggesting the highest grade of metamorphism occurring at shallower depths, while the subsequent retrogression taking place at increasing depth. Thus, although a part of the same island complex as Rykkelid's (1987) samples, the unit from which the MOK sample was collected may have been separated in time or space during the geological evolution. On the other hand, the tools used for the estimate of metamorphic conditions have been improved and upgraded, and thus older estimations could be somewhat erroneous. No clear link with respect to PT estimations can be drawn, though the intra-tectonic to syn-tectonic textures are pervasive in the MOK sample, as well as in the samples described by Rykkelid (1987).

6.1.4 Monazite, Age relation and implications for geochronology

In the sample, MOK, the monazite is clearly unstable in the current matrix assemblage as evident by the apatite and epidote reaction coronas surrounding it, and allthough allanite cannot be seen surrounding the monazite, there is evidence for allanite in solid solution with epidote elsewhere in the matrix. The corona microstructures are reminiscent of what was described by Finger et al., 1998, and given the sample's high concentration of chlorite and evidence for relict biotite as well as the recrystallizing white mica, the implications for hydrothermal alteration is strong. Furthermore, the sample contains partially dissolved plagioclase with an anorthite component of up to 31%, which may be a good source for Ca^{2+}. The monazites in the garnet is unaffected by any alteration, as it was seemingly shielded from the retrograde -hydrothermal event by the garnet. As inclusions, monazite has sharp boundaries with the garnet envelope and contains microinclusions of the very same minerals that occurs in garnet. All these observations indicate that monazite grew contemporaneously with garnet, which means that it can be used to acquire the timing of the prograde metamorphism and the garnet minimum age.

Monazites from another sample of the garnet micaschist from Møkster have been recently dated with the U-Pb method by using the secondary ion mass spectrometry (SIMS) of the NORDSIM facility in Stockholm (Konopásek, unpublished data). The dating provided a concordia age of 462 ± 5 Ma (95% confidence), which is interpreted as the age of the prograde metamorphism of the sample.

6.2 OS-2

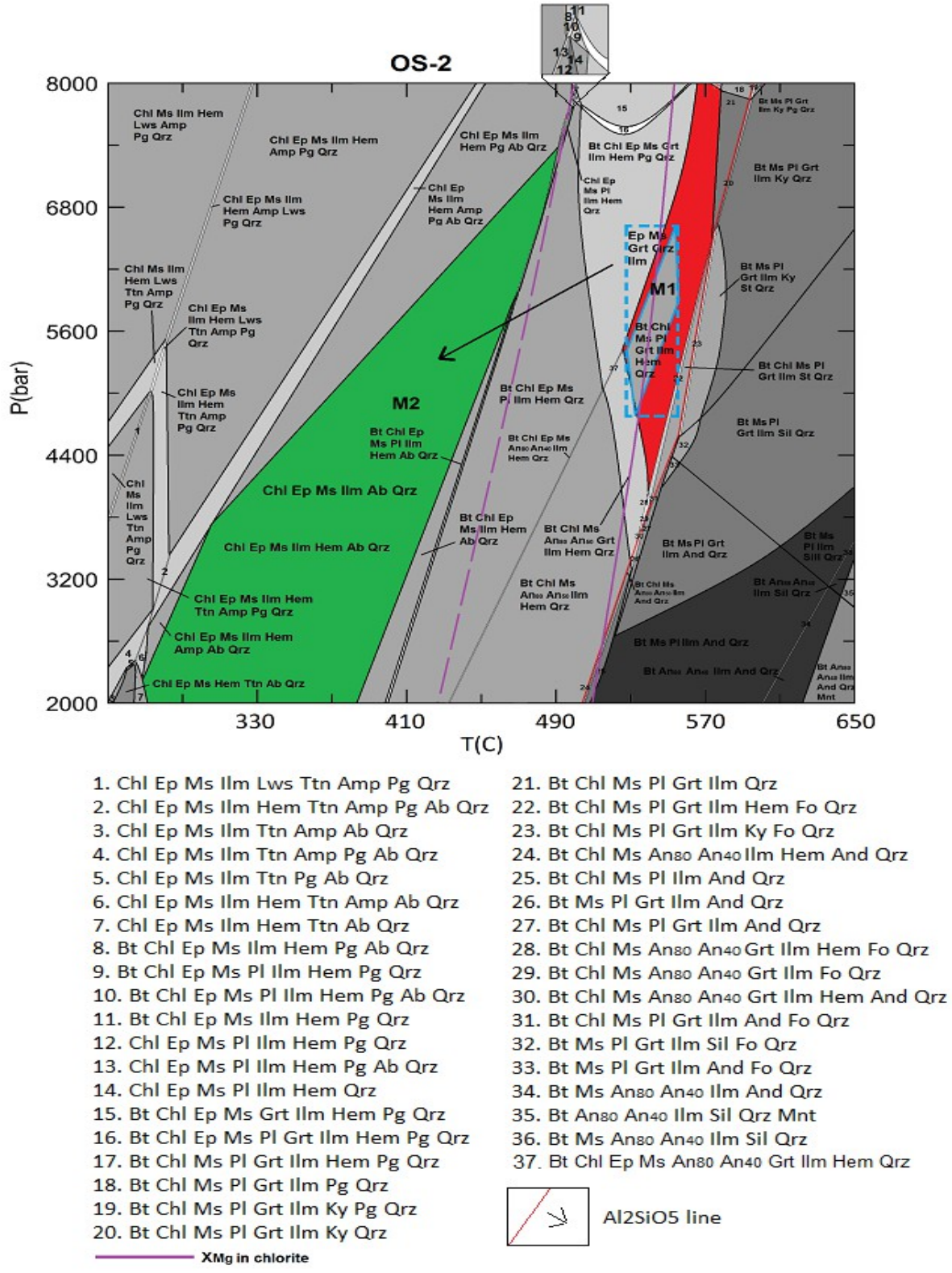

Fig. 6.4: P-T section for OS-2 with M1, M2 and chlorite compositional isopleths superinposed. The arrow indicates retrogression.

6.2.1 P-T section

The M1 mineral assemblage is represented by garnet, ilmenite, quartz and muscovite. The stability field marked in red (Fig. 6.4) best covers the assemblage, and with the use of the compositional isopleths for garnet, the P-T conditions for M1 is better constrained within this field. The maximum value of the chlorite compositional isopleth further constrains the assemblage to higher temperatures. This line represents the absolute maximum P-T conditions that chlorite can attain in the model, including the X_{Mg} values exceeding the values that was acquired through analysis. No chlorite has been observed in the garnet, so this provides a constraint for the lower temperature of the garnet maximum P-T conditions. However, there are inclusions of epidote in the garnet, which suggest that epidote was present during the garnet growth. Epidote is stable at lower temperatures in the field adjacent to the stability field marked in red, thus the garnet probably nucleated at these P-T conditions or shortly after, overgrowing and preserving epidote prior to attaining the maximum temperature.

The P-T section includes mineral phases such as staurolite and kyanite towards higher P-T, however, neither of these mineral phases occurs in the sample. Thus, the rock probably did not attain these temperatures, and the red field with the marked field for the crossing of the garnet isopleths (blue trapoezoid) best constrains the max P-T conditions of the OS-2 sample.

The stability field best representing the M2 (marked green) fits with the observed mineral assemblage, however, the compositional isopleths for chlorite do not fall into this stability field (Fig. 6.4). The reason may be an incomplete re-equilibration of the sample and inheritance of the X_{Mg} value of chlorite from the garnet. In the thin section, chlorite is consuming garnet to a large extent (Fig. 4.7 A, B and F) suggesting that garnet was past its stability field and that the retrogression occurred at low pressures and temperatures. Furthermore, chlorite may be folded, whereas garnet has straight inclusion trails. With this in mind, the P-T conditions for the M2 mineral assemblage cannot be accurately constrained. However, both the chlorite compositional isopleths and the position of the stability field of the M2 assemblage in the modeled P-T section suggest a decrease in temperature, i.e. retrogression, from the P-T conditions of the M1. Also, the M2 assemblage is bounded to the right (high T) by the stability fields containing phases such as biotite and plagioclase, which

do not occur in the matrix of the sample. Here, albite is the only feldspar found in the matrix. It is likely that plagioclase was present at maximum metamorphic conditions attained by the sample, but broke down during retrogression providing calcium for the new crystallization of epidote.

6.2.2 Metamorphic evolution

The conditions for M1 occurred prior to the second deformation phase as inferred from the straight inclusions trails/internal foliation of the garnet. Based on the garnet zoning, where X_{Spess} is highest in the core and decreases progressively towards the rim (Fig. 4.8), the nucleation most likely occurred at lower temperatures and subsequent growth was associated with increasing temperature, possibly achieving peak conditions close to the rim where the X_{Mg} ratio is highest (Winter, 2014). It is likely that epidote growth occurred prior to, or simultaneously with, the garnet nucleation and that the sample at some point crossed from the epidote stability field into the stability field in which epidote is no longer present. This is further substantiated by the occurrence of epidote inclusions close to the core in some garnets. Epidote does, however, also occur in garnet rims, which is possible at elevated pressures or lower temperatures in the P-T diagram with respect to the P-T conditions of the M1 assemblage (Fig. 6.4 and Fig. 6.6 a).
Muscovite can be found as inclusions in the garnet rim, which may represent the peak P-T conditions. It is assumed that muscovite was present prior to metamorphic peak, as it is also suggested by the P-T diagram. Muscovite may have surrounded garnet in the sample during its growth and provided a soft medium for the garnet to rotate in. This is suggested by the internal foliation that is orientated obliquely with respect to the foliation of the rock (Fig. 4.7 F)

After reaching peak metamorphic conditions, the rock may have experienced a decrease in pressure and temperature at the beginning of exhumation, but no retrogression due to the lack of free fluid phase in the rock. In an apparent period of deformation (Fig. 6.6 C) associated with influx of H_2O at lower greenschist facies conditions, the strong retrogression of garnet

into chlorite occurred, eventually resulting in the euhedral chlorite pseudomorphs (Fig. 4.7 B). The combination of deformation and H_2O influx led to re-crystallization of muscovite together with neo-crystallization of epidote and apatite, possibly forming at the expense of the anorthite component of plagioclase, leaving pure albite as the only remaining feldspar. The epidote and apatite is texturally different from what is found in the garnet (Fig. 4.7 C, E), with well developed, relatively large crystals compared to the small and typically round inclusions. Epidote found in the matrix also contains less Fe^{3+} than the inclusions on average. In addition its crystals clearly follow the matrix foliation, thus it can be assumed that they represent a second generation of epidotes and apatites in the sample. The folded chlorite shows the same textural features as muscovite (Fig. 4.7 B), though the X_{Mg} ratio is equal to that of the chlorite pseudomorphs. Given the sample's chemistry and modelled peak metamorphic conditions, there may have been opportunities for biotite to form at some point during the prograde path of the rock, all of which was replaced by chlorite during retrogression. The metamorphic evolution is illustrated in Fig. 6.5 and 6.6.

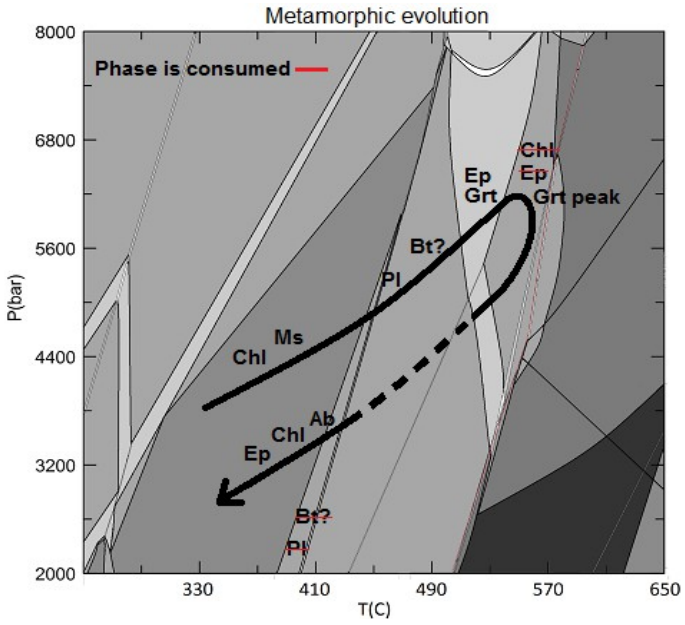

Fig. 6.5: Simplified illustration of the metamorphic evolution of the sample OS-2. The stipled line implies a period ofno change/metamorphism in the rock.

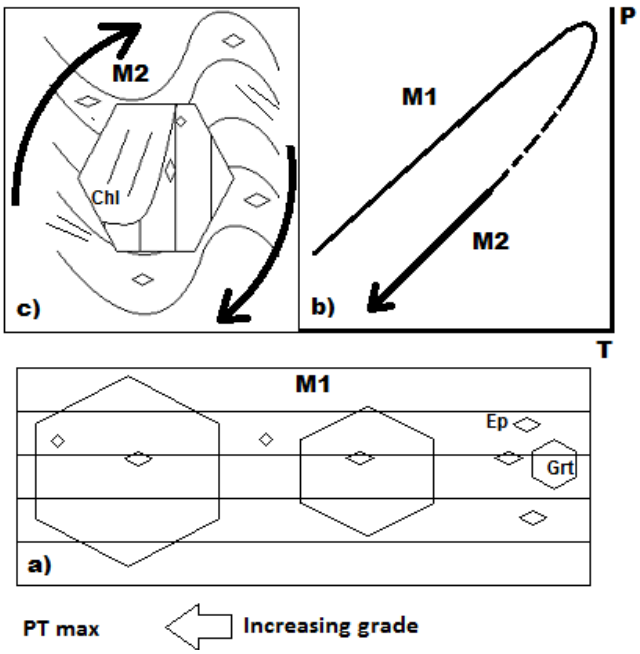

Fig. 6.6: **a)** Garnet growth followed by overgrowing of epidote. At top P, epidote stabilizes again, resulting in inclusions both in the core and in the rim. Note that the foliation is straight **b)** P-T-t path. **c)** Deformation ensues, garnet is rotated and dissolved, chlorite pseudomorphs form.

6.2.3 Burrial depth

Maximum burial depth for the M1 P-T conditions varies from 18-25 km at temperatures of 530-560 ^{O}C. M2 could not be constrained well enough to make a useful calculation for depth.

6.3 BGA2-1

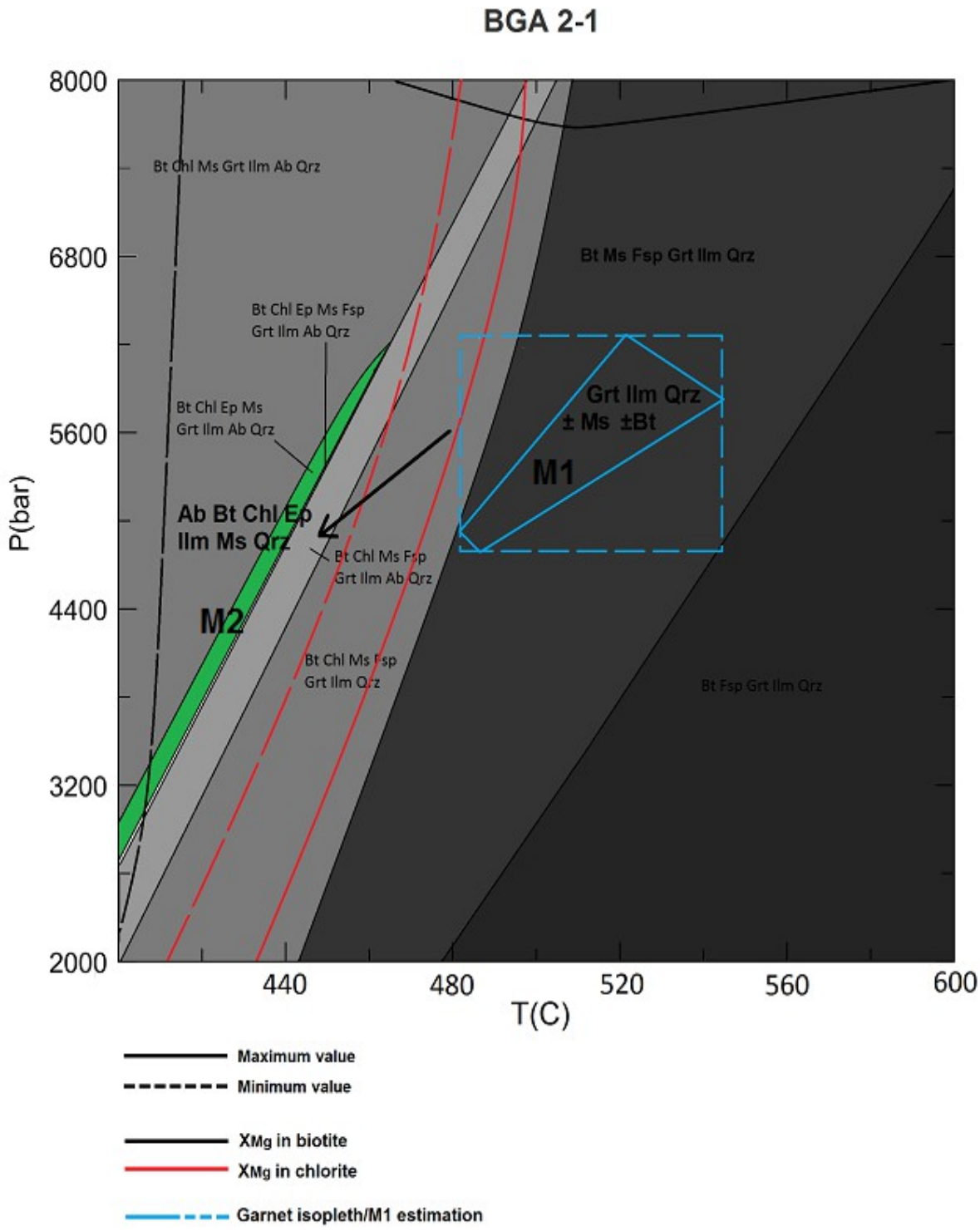

Fig. 6.7*:* P-T section for BGA2-1 with M1, M2 and chlorite compositional isopleths superimposed. The arrow indicates retrogression.

6.3.1 P-T section

There is a clear difference in P-T (Fig. 6.7) conditions between the modelled M1 and M2 conditions of the sample BGA2-1, in particular with respect to temperature. The M1 (garnet isopleth) conditions lie at the boundary of the upper greenschist and the lower amphibolite facies, while the stability field which covers the M2 (stability field marked green in Fig. 6.7) assemblage lies within the lower to middle greenschist facies conditions.

The modelled P-T conditions of the M1 mineral assemblage adequately cover all of the M1 mineral phases. The modelled composition of the garnet falls into the stability field of the mineral assemblage that does not involve chlorite or epidote. This suggests that both these phases grew during retrogression.

Although the P-T conditions of the M2 assemblage could not be accurately constrained, the position of its stability field in the modeled P-T section suggests that the M2 minerals have formed at lower metamorphic temperatures than the M1. The albite endmember of plagioclase is the only feldspar that occurs in the sample and it is also the only stable feldspar in the stability field of the M2 assemblage. At higher temperatures, plagioclase appear as a stable phases. At lower temperatures, epidote disappears, which constraints the lower temperature limit of the M2 assemblage. The isopleths for biotite cover the estimated P-T conditions for M2 with the lower limit of the X_{Mg} values observed in the sample. However, the chlorite X_{Mg} isopleths do not cross the M2 stability field at any P-T conditions (Fig. 6.7).

Chlorite growth is modelled towards lower temperatures (Fig. 5.19, 6.7), and the X_{Mg} ratio decreases in the same direction. Based on this, chlorite did most likely form as part of a retrograde event. The discrepancy in observed compositions suggests, that the chlorite has inherited its X_{Mg} from the prograde phases such as garnet or biotite, which it does appear to consume. Though given the small extent and apparently low intensity of retrogression (chlorite is considered an accessory mineral), this is not obvious. It can, however, be assumed that the chlorite is indeed a part of a retrograde mineral assemblage.

Biotite occurs in all of the stability fields (Fig. 6.7), though the X_{Mg} value increases towards higher P-T conditions. Moreover, modelling shows that biotite grows towards higher P-T. Regarding the biotite composition, only the lower limit of measured X_{Mg} values crosses M2 mineral assemblage. Some of the analysed X_{Mg} values exceeded the calculated values, which may suggest that the system composition does not adequately represent the M2 mineral assemblage. However, the modelled extent of most of the observed biotite compositions fits well with the assumption that the biotite was present during both M1 and M2 stages of the rock development.

Minerals such as ilmenite and quartz are present at any of the modelled conditions, which agrees with observations. Muscovite may have behaved similarly to biotite with regard to its occurrence.

6.3.2 Metamorphic evolution

Based on the modelling, observations in thin sections and mineral chemistry, a metamorphic evolution of the BGA2-1 sample could be construed. The M1 assemblage probably consisted of Apatite, Bt, Grt, Ilm, ± Ms ± Pl and Qrz. It occurred prior to the folding (based on the presence of internal folliation in garnet, Fig. 4.12 C) and biotite (± muscovite) was likely the first minerals of this assemblage to form. This is supported by their overall occurrence and growth direction/X_{Mg} increase in the model P-T diagram. It is further assumed that the micas could have provided the garnet with a soft medium to grow euhedral crystals (Fig. 4.12 D). In contrast, the poikiloblastic and anhedral garnets (Fig.4.12 A and G) in the rigid quartz matrix may have been restricted to grow along quartz boundaries. Furthermore, the only inclusions found in the garnet are ilmenite in contact with quartz and biotite (Fig. 4.12 A and B). The soft biotite + muscovite bands could have allowed for garnet to rotate during the subsequent deformation/folding period (Fig. 6.9). With increasing P-T conditions, the garnet probably nucleated, incorporating Mn^{2+} into spessartine-enriched core. Mn^{2+} rich garnet is typical for not only lower temperatures, but it is commonly associated with growth at the expense of chlorite (Masoudi et al., 2006; Barker, 2013). As such, an earlier chlorite phase may have been consumed by the growth of garnet, finally disappearing as the stability field in which M1

resides was crossed.

The pervasive chemical zonation from the core to the rim (Fig. 4.13) in the analysed garnet is indicative of continuous growth zoning and the absence of retrograde diffusion in the garnet (Masoudi et al., 2006; Barker, 2013; Winter, 2014). Moreover, the equilibration and subsequent diffusion of Mn^{2+} with the matrix may require temperatures at upper greenschist facies to proceed (Masoudi et al., 2006). Thus, the garnet growth presumably continued towards increasing P-T conditions and the element fractionation resulted in the observed chemical zonation (Fig. 4.13). After reaching peak conditions at lower amphibolite facies, a period of new deformation phase took place, which is documented by the presence of folded minerals. Based on the mineralogy and the modeling, this event may have occurred at lower to middle greenschist facies conditions with fluid in excess. The deformation was probably concentrated in the soft micaceous bands, which show textures such as microfolds and rotated garnet porphyroblasts indicating second deformation phase. The internal foliation of garnets inside mica-rich bands is orientated obliquely with respect to the foliation in the matrix, while the internal foliation of garnets located in the quartz-rich matrix is only gently oblique with respect to the general foliation (Fig. 4.12 A, C and G). Thus, the garnets surrounded by mica have rotated more (and maybe even several times) during the second deformation phase (Fig. 6.9), than the garnets in the quartz-rich matrix.

During the retrograde phase, biotite and garnet were partially dissolved and probably altered to chlorite. Some of the components likely also formed new ilmenite as well as epidote (from grossular). Muscovite apparently experienced deformation and probably neo/recrystallization. Modeling has suggested the stability of plagioclase in the rock during M1. During retrogression, the anorthite endmember was likely dissolved and the Ca^{2+} component used for the growth of epidote, leaving only pure albite as the remaining feldspar.
Amphibole probably appeared locally during retrogression as it is intergrown with chlorite and follows the general folliation. Quartz and ilmenite are assumed to occur at any of the metamorphic conditions. The metamorphic evolution is illustrated in fig. 6.8.

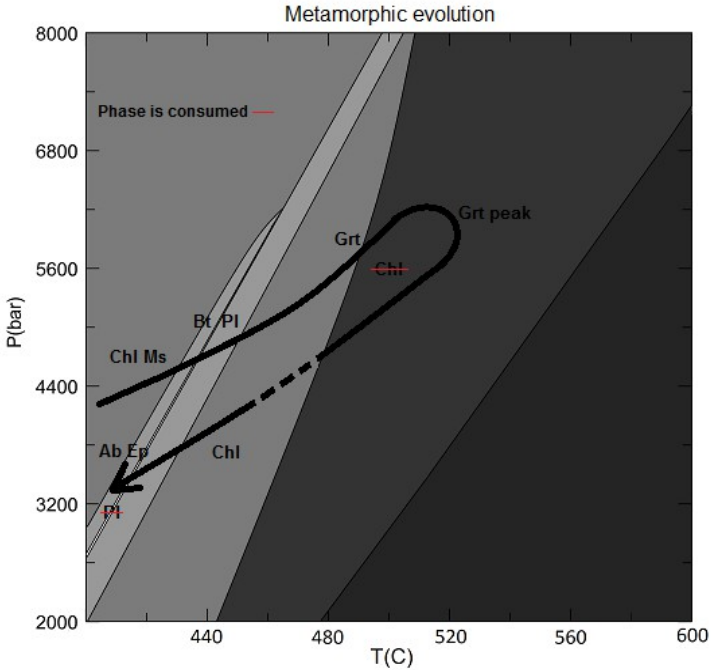

Fig. 6.8: Simplifed illustration of metamorphic evolution of the sample BGA2-1. The stippled line indicates a period of no or little change in the mineral assemblage.

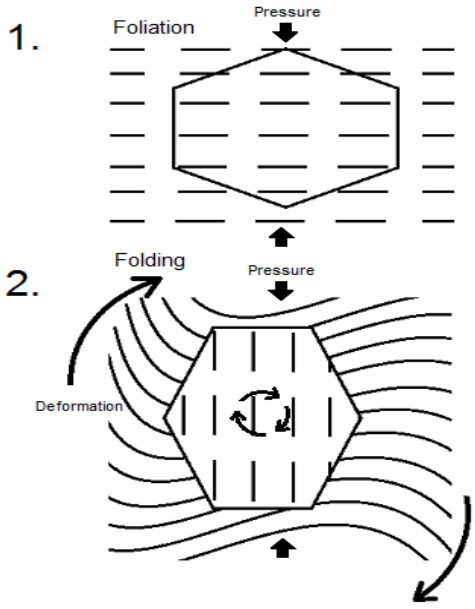

Fig. 6.9: 1) Garnet growing in mica in an intra-tectonicsetting. 2) A later deformation event folds the mica and garnet is rotated as a result.

6.3.3 Burrial depth

When converting pressure to depth, the sample achieved peak metamorphic conditions at depths of 18-24 km and temperatures of 480-545 ^{O}C.

6.4 BGA2-2

The stability conditions of the mineral assemblage found in this sample were not modelled, however, in the field the rock occurs as a layer in direct contact with BGA2-1 and both rocks show the same deformation fabric.

Both rocks are superficially similar, with folded bands of mica (biotite and muscovite), apatite, epidote, quartz and ilmenite. The dominating silicate, however, is albite. The metamorphic evolution based on textural observations alone seems to be: A period of deformation inferred by the folded micas, followed by a period of apatite and chlorite growth, which is documented by apatite growing across the foliation and chlorite occurring as pseudomorphs after biotite (Fig. 4.18 B and D). Epidote shows textures similar to apatite and may have continued to grow after deformation as well (Fig. 4.18 E).

It may be that the micas, and potentially also plagioclase, formed at higher P-T conditions than did the epidote and apatite in a period pre-dating the development of the dominant foliation. Following the deformation, the plagioclase broke down losing Ca^{2+} (An) which was used for the formation of epidote and apatite. Based on the proximity of the BGA2-1sample in the field it is likely to assume that the sample BGA2-2 experienced the same metamorphic and deformation history as BGA2-1.

6.5 A COMPARISON OF THE SAMPLES

The samples BGA 2-1, OS-2 and MOK show several similar features. All three of the samples contain garnets with internal foliations oriented obliquely with respect to the foliation in the matrix. The internal foliation is represented by straight to slightly curved inclusion trails. Furthermore, all of the samples have experienced deformation related to the appearance of retrograde mineral phases such as chlorite, chloritoid and/or epidote, although the retrogression is far more conspicuous in the MOK and OS-2 samples. This can be attributed, in part, to their much more micaceous composition, which probably allowed for a more widespread deformation and migration of fluid. The more rigid quartz-rich matrix of BGA 2-1 resisted this deformation such that the deformational stress was concentrated in the mica bands, where indeed most of the evidence for retrograde reactions occurs. The modelled metamorphic evolution for each of the samples also has a common feature, which is a relatively large drop in P-T conditions from M1 to M2. However, the estimated P-T conditions in which the assemblages of the studied samples formed are quite different. Based on mineralogy, chemistry and modelling, MOK has experienced the highest grade of metamorphism both with respect to temperature and depth (605-635 ^{O}C and 28-31 km depth). OS-2 has experienced temperatures and depths of 520-570 ^{O}C and 18-25 km. BGA2-1 has the lowest P-T conditions of all of the samples estimated at 480-545 ^{O}C and a depths of 18-24 km.

When comparing the spessartine content of garnet in the OS-2 and BGA 2-1 samples, both are strongly zoned with the spessartine component decreasing towards the rim. However, spessartine is much more abundant in the BGA2-1 than the in OS-2 garnets. A high Mn content is typically linked to garnet growth in upper greenschist facies conditions or with H2O saturation, the content may increase with decreasing temperature (Masoudi et al., 2006; Makrygina, 2011). As such, the much higher X_{Spess} in BGA2-1 may imply lower temperatures for the early growth of garnet than in the OS-2 sample. In any case, it is the composition of the protholith which is an important factor in controlling the presence of phases which may or may not stabilize during metamorphism. BGA 2-1 is in fact the most Mn-rich rock when looking at the whole rock chemistry (Tab. 4.1). The garnet in MOK contains almost no spessartine component and the garnet shows almost no zonation. This can be associated either with almost complete diffusional re-equilibration at high temperatures, or it can be attributed

to fast garnet growth without substantial fractionation of the elements. This feature is different from the strong zoning observed in the other two samples.

The P-T conditions for the retrograde assemblages of each of the samples is difficult to constrain. The modelled M2 for BGA2-1 and OS-2 appear to overlap and both may have occurred at lower greenschist facies conditions, while the M2 for MOK lies within the upper greenschist to lower amphibolite facies conditions. Moreover, the retrograde conditions of the MOK sample are comparative to the peak conditions for BGA2-1 and OS-2. To illustrate the differences (or similarities), the P-T conditions estimated for each of the studied samples are summarized in a P-T diagram presented in Fig. 6.10.

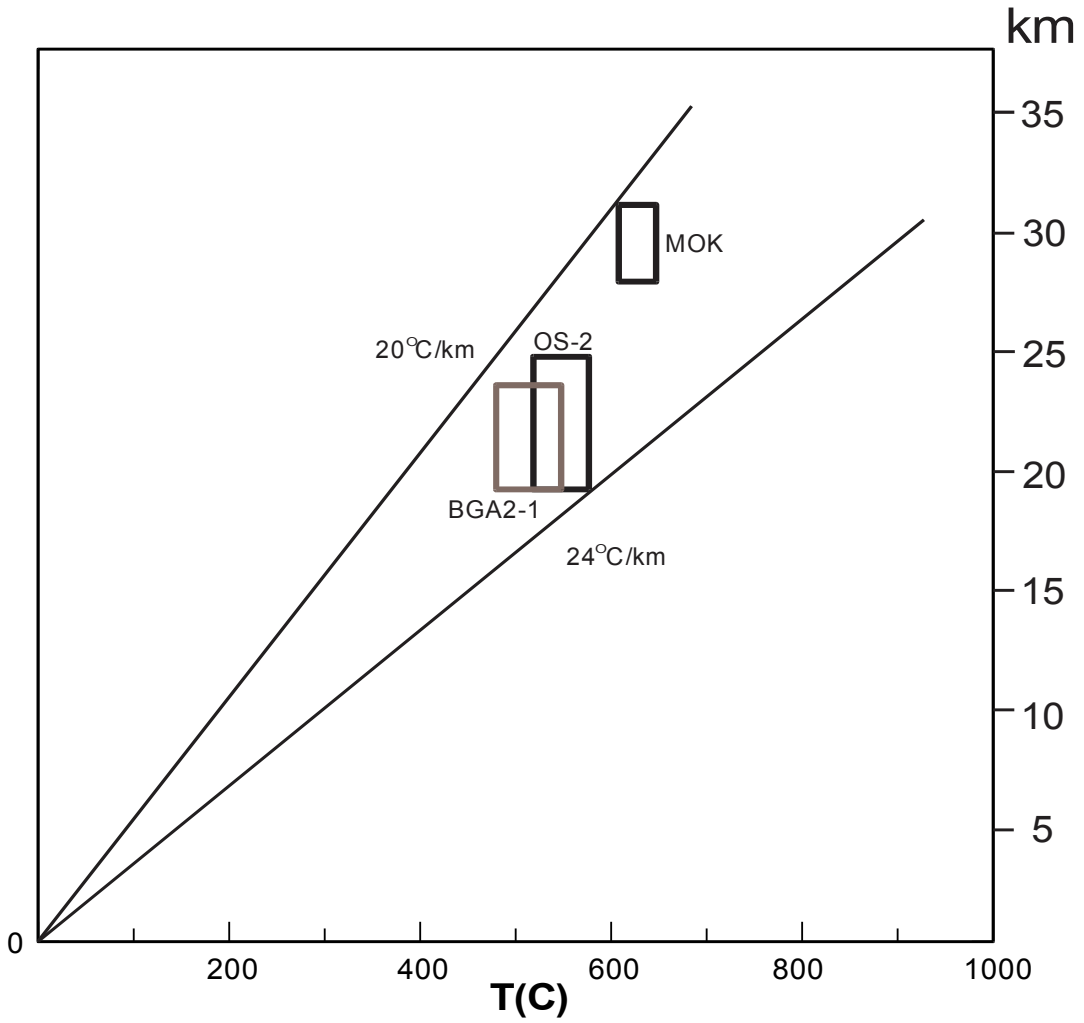

Fig. 6.10: A comparison of the P-T conditions for M1 mineral assemblages in BGA2-1, OS-2 and MOK samples. The interval of estimated P-T conditions suggests that the samples have probably experienced early prograde metamorphism along a common thermal gradient of ca. 20–24 ^{O}C/km.

The interval of inferred geothermal gradients for the studied samples presented in Fig. 6.10 shows values of 20–24 ^{O}C/km, which is considered a “normal” geothermal gradient for stable continental interiors (Nelson, 2004; Winter, 2014). A “normal” geotherm may be higher or lower, depending on the tectonic environment. Along the convergent plate margins compression occurs, where the rocks (e.g. prism sediments) may be pushed down along a normal geothermal gradient or along a slightly elevated geothermal gradient.

In the case of the samples, the internal foliation (straight elongate inclusions) of garnet indicates compression/shear throughout the prograde evolution of the minerals. Furthermore, the evolution of the mineral phases, based on inclusion-porphyroblast relationship and P-T constraints in the modells, appears to be roughly Chl >Bt>Grt>±St with increasing metamorphic grade. The sequence is similar to that of the classical Barrovian sequence for metapelites, which is associated with medium P/T metamorphism in orogenic belts (Vollmer and Walker, 2009) of Ordovician ages (Taconic and Grampian Orogenies). Based on the apparent similarities in texture, the analogous metamorphic evolution and the common geothermal gradient, there is reason to believe that the rocks were part of one coherent unit during the Caledonian orogenesis. A possible scenario explaining this is shown below in Fig. 6.11.

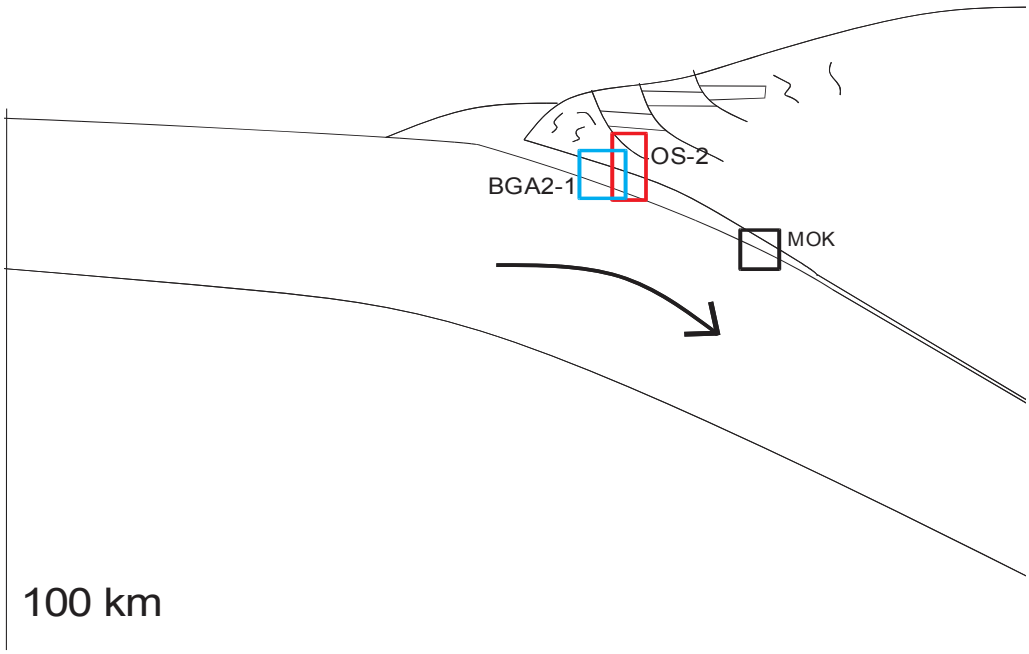

Fig. 6.11: The sample rocks and their respective tectonic position in a compressional tectonic environment.

The MOK sample reached peak P-T conditions at 462 ± 5 Ma according to monazite dating. The metamorphic ages of the other samples could not have been determined, because no monazite was found in the samples, the reason for which may have been the lower grade of metamorphism when compared to MOK. Apatite and epidote is conspicous in the OS-2 and BGA2-1 samples, both mineral phases which may stabilize at the expense of, or instead of monazite (Lanzirotti et al., 1996; Finger et al., 1998).
However, as inferred from petrology, all three studied samples probably come from one tectonic unit, which was according to the dating of the MOK sample active ca. 462 Ma ago, in the middle Ordovician period.

The burial of the sample rocks (Fig. 6.11) was followed by a deformational event involving fluid influx, cooling and probably exhumation. This pattern of burial followed by decompression, cooling and deformation is typical of collisional tectonics, where a sedimentary basin between two continental units is closing, eventually leading to a collision between them, followed by exhumation and deformation of the rocks that were buried along the active margin of a down-going plate.

7 CONCLUSION

The petrological study and thermodynamic modelling of the four metasediment samples revealed similarities which allowed for a conclusion to be made:

1. All of the samples have similar textures in the inferred M1 and M2 assemblages.
2. All of the samples show the same metamorphic trend with regards to P-T-t paths.
3. All of the M1 assemblages of the samples follow a geothermal gradient of 20-24^{O}C/km.
4. The observed textures of monazite crystals in the MOK sample show evolution compatible with the main mineral assemblage. Recent dating of monazite from the Møkster metasediments provided an age of c. 462 Ma. Consequently, this date also represents the timing of the stability of the peak mineral assemblage.

As such, the samples probably belong to one coherent tectonic unit that was active during the Ordovician period. The tectonic position of the Møkster metasediments may have been similar to that of the metasediments of the Samnager Complex in the Major Bergen Arc.

BIBLIOGRAPHY

Andersen, T. and A. Andresen (1994). "Stratigraphy, tectonostratigraphy and the accretion of outboard terranes in the Caledonides of Sunnhordland, W. Norway." Tectonophysics **231**(1): 71-84.

Andersen, T. B. (1998). "Extensional tectonics in the Caledonides of southern Norway, an overview." Tectonophysics **285**(3): 333-351.

Andersen, T. B., et al. (2012). "Evidence for hyperextension along the pre-Caledonian margin of Baltica." Journal of the Geological Society **169**(5): 601-612.

Andersen, T. B. and Ø. J. Jansen (1987). "The Sunnhordland Batholith, W. Norway: regional setting and internal structure, with emphasis on the granitoid plutons." Norsk geologisk tidsskrift **67**(3): 159-183.

Anderson, S. (2004). Metamorphic Facies & Metamorphism and Plate Tectonics. Retrieved July 30, 2015, from http://www.tulane.edu/~sanelson/eens211/metamorphic_facies.htm

Appleyard, E. (1987). "Metamorphic reactions-kinetics, textures and deformation." Earth-Science Reviews **24**(2): 152-153.

Barker, A. J. (2002). "Crack-fill porphyroblastesis." Journal of Metamorphic Geology **20**(2): 283-294.

Barker, A. J. (2013). Introduction to metamorphic textures and microstructures, Routledge.

Boundy, T., et al. (2002). "Discovery of eclogite facies carbonate rocks from the Lindås Nappe, Caledonides, Western Norway." Journal of Metamorphic Geology **20**(7): 649-667.

Boundy, T. M., et al. (1997). "Temporal and tectonic evolution of the granulite-eclogite association from the Bergen Arcs, western Norway." Lithos **39**(3): 159-178.

Brekke, H., et al. (1984). "Lower Palaeozoic convergent plate margin volcanism on Bømlo, SW Norway, and its bearing on the tectonic environments of the Norwegian Caledonides." Journal of the Geological Society **141**(6): 1015-1032.

Connolly, J. (2005). "Computation of phase equilibria by linear programming: a tool for geodynamic modeling and its application to subduction zone decarbonation." Earth and Planetary Science Letters **236**(1): 524-541.

Connolly, J. (2009). "The geodynamic equation of state: what and how." Geochemistry, Geophysics, Geosystems **10**(10).

Corfu, F., et al. (2014). "The Scandinavian Caledonides: main features, conceptual advances and critical questions." Geological Society, London, Special Publications **390**(1): 9-43.

Corfu, F., et al. (2014). New Perspectives on the Caledonides of Scandinavia and Related Areas, Geological Society of London.

Corfu, F., et al. (2007). "Peri-Gondwanan elements in the Caledonian nappes of Finnmark, northern Norway: implications for the paleogeographic framework of the Scandinavian Caledonides." American Journal of Science **307**(2): 434-458.

Corrie, S. L. and M. J. Kohn (2008). "Trace-element distributions in silicates during prograde metamorphic reactions: Implications for monazite formation." Journal of Metamorphic Geology **26**(4): 451-464.

Dunning, G. and R. Pedersen (1988). "U/Pb ages of ophiolites and arc-related plutons of the Norwegian Caledonides: implications for the development of Iapetus." Contributions to Mineralogy and Petrology **98**(1): 13-23.

Finger, F., et al. (1998). "Replacement of primary monazite by apatite-allanite-epidote coronas in an amphibolite facies granite gneiss from the eastern Alps." American Mineralogist **83**(3): 248-258.

Fossen, H. (1989). "Geology of the minor Bergen arc, west Norway." Bull Nor geol unders **416**: 47-62.

Fossen, H. (1992). "The role of extensional tectonics in the Caledonides of south Norway." Journal of structural geology **14**(8): 1033-1046.

FOSSEN, H. (1998). "Advances tn understanding the post-Caledonian structural evolution of the Bergen area, West Norway."

Fossen, H. and H. Austrheim (1988). "Age of the Krossnes granite, west Norway." Norges Geologiske Undersøkelse Bulletin **413**: 61-65.

Fossen, H. and W. J. Dunlap (2006). "Age constraints on the late Caledonian (Scandian) deformation in the Major Bergen Arc, SW Norway." Norsk geologisk tidsskrift **86**(1): 59.

Fossen, H. and S. Ingdahl (1988). "Tectonostratigraphic Position of the Rocks in the Western Extreme of the Major Bergen Arcs (Fanafjell Nappe)." Nor. Geol. Tidsskr **67**: 59-66.

Fuhrman, M. L. and D. H. Lindsley (1988). "Ternary-feldspar modeling and thermometry." American Mineralogist **73**(3-4): 201-215.

Færseth, R. and R. J. Steel (1978). "Silurian conglomerate sedimentation and tectonics within the Fennoscandian continental margin, Sunnhordland, western Norway." Norsk geologisk tidsskrift **58**: 145-159.

Færseth, R., et al. (1977). "Geology of the Lower Palaeozoic rocks in the Samnanger-Osterøy area, major Bergen arc, western Norway." Norges geologiske undersøkelse **234**: 19-58.

Færseth, R. B., et al. (2011). "Structural geology and sedimentology of Silurian metasediments in the Ulven area, Major Bergen Arc, SW Norway." Norwegian Journal of Geology/Norsk Geologisk Forening **91**.

Holland, T. and R. Powell (1998). "An internally consistent thermodynamic data set for phases of petrological interest." Journal of Metamorphic Geology **16**(3): 309-343.

Indares, A. and J. Martignole (1985). "Biotite-garnet geothermometry in granulite-facies rocks: evaluation of equilibrium criteria." Can. Mineral. **23**: 187-193.

Ingdahl, S. (1985). "Stratigraphy, structural geology and metamorphism in the Os area, Major Bergen Arc." Cand Real thesis, University of Bergen, Norway.

Ingdahl, S. (1989). "The Upper Ordovician-Lower Silurian rocks in the Os area, Major Bergen Arc, Western Norway." Norsk geologisk tidsskrift **69**(3): 163-175.

Karabinos, P. (1985). "Garnet and staurolite producing reactions in a chlorite-chloritoid schist." Contributions to Mineralogy and Petrology **90**(2-3): 262-275.

Kim, Y. and M. Cho (2008). "Two-stage growth of porphyroblastic biotite and garnet in the Barrovian metapelites of the Imjingang belt, central Korea." Journal of Metamorphic Geology **26**(3): 385-399.

Kruhl, J. H., et al. (2013). "Quartz grain boundaries as fluid pathways in metamorphic rocks." Journal of Geophysical Research: Solid Earth **118**(5): 1957-1967.

KUhn, A., et al. (2002). "The Caledonian tectono-metamorphic evolution of the Lindas Nappe: constraints from U-Pb, Sm-Nd and Rb-Sr ages of granitoid dykes." Norsk geologisk tidsskrift **82**(1): 45-58.

Lanzirotti, A. and G. N. Hanson (1996). "Geochronology and geochemistry of multiple generations of monazite from the Wepawaug Schist, Connecticut, USA: implications for monazite stability in metamorphic rocks." Contributions to Mineralogy and Petrology **125**(4): 332-340.

Larsen, O., et al. (2003). "Kinematics and timing of polyphase post-Caledonian deformation in the Bergen area, SW Norway." Norsk geologisk tidsskrift **83**(3): 149-166.

Lundmark, A. and F. Corfu (2007). "Age and origin of the Årdal dike complex, SW Norway: False isochrons, incomplete mixing, and the origin of Caledonian granites in basement nappes." Tectonics **26**(2).

Makrygina, V. and L. Suvorova (2011). "Spessartine in the greenschist facies: Crystallization conditions." Geochemistry International **49**(3): 299-308.

Makrygina, V. and L. Suvorova (2011). "Spessartine in the greenschist facies: Crystallization conditions." Geochemistry International **49**(3): 299-308.

Mineralogical Spreadsheet Download Page. (n.d.). Retrieved August 1, 2015, from http://www.gabbrosoft.org/spreadsheets.html

Masoudi, F., et al. (2006). "Garnet (Almandine-Spessartine) Growth Zoning and Its Application to Constrain Metamorphic History in Dehsalm Complex, Iran." Journal of Sciences, Islamic Republic of Iran **17**(3): 235-244.

Moazzen, M. (2004). "Chlorite–chloritoid–garnet equilibria and geothermometry in the Sanandaj–Sirjan metamorphic belt, southern Iran." Iran J Sci Technol **28**: 1-14.

Murphy, D. B. (2010). "Metamorphism and the PT History of Alpine Schist from the Newton Range, Southern Alps, New Zealand."

Pedersen, R.B. (2015) Bergensbuene, [Lecture to geologisk institutt UiB] GEOV345 : Regionalgeologisk feltkurs Vestlandet. Os. 25 Mai.

Rey, P., et al. (1997). "The Scandinavian Caledonides and their relationship to the Variscan belt." Geological Society, London, Special Publications **121**(1): 179-200.

Roberts, D. (2003). "The Scandinavian Caledonides: event chronology, palaeogeographic settings and likely modern analogues." Tectonophysics **365**(1): 283-299.

Roberts, D. and D. G. Gee (1985). "An introduction to the structure of the Scandinavian Caledonides." The Caledonide orogen–Scandinavia and related areas **1**: 55-68.

Roffeis, C., et al. (2013). "A Sveconorwegian terrane boundary in the Caledonian Hardanger–Ryfylke Nappe Complex: The lost link between Telemarkia and the Western Gneiss Region?" Precambrian Research **228**: 20-35.

Spry, A. (1969). Metamorphic textures, 352 p, Pergamon Press, Oxford.

Sturt, B. A. and A. Thon (1978). "Caledonides of southern Norway." Caledonian-Appalachian orogen of the North Atlantic region, IGCP project **27**: 39-47.

Tajčmanová, L., et al. (2009). "A thermodynamic model for titanium and ferric iron solution in biotite." Journal of Metamorphic Geology **27**(2): 153-165.

Vernon, R., et al. (2008). "False metamorphic events inferred from misinterpretation of microstructural evidence and P–T data." Journal of Metamorphic Geology **26**(4): 437-449.

Vernon, R. H. (2004). A practical guide to rock microstructure, Cambridge university press.

Vollmer, F. W. and J. Walker (2009). The classic Barrovian metamorphic sequence of Dutchess County and it's structural and stratigraphic context in the Taconic Orogeny. 81st annual meeting, field trip guidebook, New York State Geological Association.

White, R., et al. (2000). "The effect of TiO~ 2 and Fe~ 2O~ 3 on metapelitic assemblages at greenschist and amphibolite facies conditions: mineral equilibria calculations in the system K~ 2O-FeO-MgO-Al~ 2O~ 3-SiO~ 2-H~ 2O-TiO~ 2-Fe~ 2O~ 3." Journal of Metamorphic Geology **18**(5): 497-512.

Whitney, D. L. and B. W. Evans (2010). "Abbreviations for names of rock-forming minerals." American Mineralogist **95**(1): 185.

Wing, B. A., et al. (2003). "Prograde destruction and formation of monazite and allanite during contact and regional metamorphism of pelites: petrology and geochronology." Contributions to Mineralogy and Petrology **145**(2): 228-250.

Winter, J. D. (2014). Principles of igneous and metamorphic petrology, Pearson.

APPENDIX

MOK

Sample:	MOK II						
					matrix	matrix	matrix
Position	incl in Grt	incl in Grt	incl in Grt	incl in Grt			
Mineral	Bt	Bt	Bt	Bt	Chl	Chl	Chl
Sample nr	2 / 1 .	9 / 1 .	17 / 1 .	20 / 1 .	6 / 1 .	9 / 1 .	13 / 1 .
Wt%							
SiO2	35,09	35,28	34,43	33,84	23,44	23,62	23,42
TiO2	1,83	1,55	1,58	1,73	0,45	0,03	0,08
Al2O3	18,37	18,39	19,67	19,60	21,96	22,00	22,02
FeO	21,81	19,98	20,86	19,94	31,20	30,79	31,05
MnO		0,12	0,03	0,10	0,02	0,04	0,09
MgO	8,41	9,86	8,40	10,02	9,64	9,96	9,61
CaO	0,03	0,06	0,06				0,08
Na2O	0,29	0,19	0,25	0,34	0,01	0,01	0,05
K2O	9,39	9,20	9,45	8,38	0,02	0,01	0,06
Total	95,22	94,63	94,73	93,95	86,74	86,47	86,46
No.O	11,00	11,00	11,00	11,00	14,00	14,00	14,00
Si	5,53	5,51	5,43	5,27	5,17	5,21	5,19
Ti	0,22	0,18	0,19	0,20	0,08	0,00	0,01
Al	3,41	3,38	3,66	3,60	5,71	5,73	5,75
FeO	2,87	2,61	2,75	2,60	5,76	5,68	5,75
Mn	0,00	0,02	0,00	0,01	0,00	0,01	0,02
Mg	1,97	2,30	1,98	2,33	3,17	3,28	3,17
Ca	0,00	0,01	0,01	0,00	0,00	0,00	0,02
Na	0,09	0,06	0,08	0,10	0,00	0,00	0,02
K	1,89	1,83	1,90	1,66	0,01	0,00	0,02
Sum	15,98	15,90	15,99	15,77	19,90	19,92	19,95
X_{mg}	0,41	0,47	0,42	0,47	0,36	0,37	0,36

	MOK II						
matrix	matrix	matrix	matrix	matrix	matrix	matrix	matrix
Chl	**Chl**	**Chl**	**Chl**	**Chl**	**Chl**	**Chl**	**Chl**
20 / 1 .	**23 / 1 .**	**37 / 1 .**	**43 / 1 .**	**44 / 1 .**	**1 / 1 .**	**4 / 1 .**	**7 / 1 .**
23,76	23,91	23,93	23,25	24,27	22,91	23,01	24,48
0,13	0,06	0,03	0,26	0,08	0,15	0,26	0,04
21,55	21,55	22,50	22,18	20,51	21,98	23,09	22,98
32,19	31,38	31,54	31,22	30,39	32,00	32,25	30,85
0,12	0,11	0,05	0,05	0,04	0,06	0,07	0,03
9,37	9,80	9,64	9,99	11,02	9,14	8,78	8,45
0,06	0,04	0,02	0,01	0,05	0,02	0,07	0,02
0,03	0,01	0,02	0,02	0,01	0,20	0,07	0,01
0,06	0,02				0,12	0,04	0,42
87,27	86,88	87,73	86,98	86,39	86,58	87,64	87,29
14,00	14,00	14,00	14,00	14,00	14,00	14,00	14,00
5,24	5,27	5,21	5,12	5,35	5,11	5,05	5,34
0,02	0,01	0,01	0,04	0,01	0,03	0,04	0,01
5,60	5,60	5,78	5,76	5,33	5,77	5,98	5,91
5,94	5,78	5,75	5,75	5,61	5,96	5,92	5,63
0,02	0,02	0,01	0,01	0,01	0,01	0,01	0,01
3,08	3,22	3,13	3,28	3,62	3,04	2,87	2,75
0,01	0,01	0,00	0,00	0,01	0,00	0,02	0,00
0,01	0,01	0,00	0,00	0,03	0,09	0,03	0,00
0,02	0,00	0,01	0,01	0,00	0,03	0,01	0,12
19,95	19,92	19,90	19,96	19,98	20,04	19,94	19,76
0,34	0,36	0,35	0,36	0,39	0,34	0,33	0,33

Sample:		**MOK II**		**MOK II**
Position	**matrix**	**matrix**	**incl in Grt**	**matrix**
Mineral	**Cld**	**Cld**	**Cld**	**Fsp**
Sample nr	**35 / 1 .**	**40 / 1 .**	**11 / 1 .**	**25 / 1**
Wt%				
SiO2	24,41	24,47	24,43	61,63
TiO2	0,01	0,01		24,28
Al2O3	40,22	40,29	39,51	0,06
FeO	24,59	24,34	24,92	5,38
MnO	0,05	0,05	0,23	8,87
MgO	2,23	2,06	2,32	0,07
CaO	0,01	0,03		
Na2O	0,01	0,00		
K2O		0,01		
Total	91,52	91,27	91,41	100,28
No.O	12,00	12,00	12,00	8,00
Si	2,04	2,04	2,04	2,73
Ti	0,00	0,00	0,00	0,00
Al	3,95	3,97	3,88	1,27
FeO	1,71	1,70	1,74	0,00
Mn	0,00	0,00	0,02	
Mg	0,28	0,26	0,29	
Ca	0,00	0,00		0,26
Na	0,00	0,00		0,76
K	0,00	0,00		0,00
Sum	7,99	7,97	7,96	5,02
X_{mg}	0,14	0,13	0,14	
An				25,02
Ab				74,57
Or				0,41

Sample:										MOK II
Position	rim	inner rim	inner rim							
Mineral	Grt	Grt	Grt	Grt	Grt	Grt	Grt	Grt	Grt	Grt
Sample nr	2/1	4/1	5/1	7/1	10/1	12/1	15/1	17/1	19/1	24/1
Wt%										
SiO2	37,12	36,85	37,05	37,34	36,98	37,05	37,33	37,13	36,90	36,59
TiO2	0,02	0,00	0,04	0,04	0,02	0,02		0,33		0,01
Al2O3	20,91	20,66	20,94	20,96	20,75	21,12	20,72	21,14	20,93	20,86
FeO	36,98	36,50	37,05	37,42	36,96	36,86	36,38	36,17	36,43	35,77
MnO	0,03	0,11	0,15	0,16	0,15	0,16	0,20	0,33	2,31	2,87
MgO	3,39	3,09	3,02	3,05	2,93	2,83	3,02	2,87	2,14	2,72
CaO	1,77	2,12	2,10	1,85	1,86	1,83	1,81	1,76	1,48	1,50
Na2O	0,03	0,01	0,02		0,04	0,04	0,04		0,00	0,02
K2O	0,01	0,04			0,03	0,03	0,01	0,02		
Total	100,27	99,38	100,35	100,81	99,72	99,94	99,52	99,75	100,20	100,34
No.O	12,00	12,00	12,00	12,00	12,00	12,00	12,00	12,00	12,00	12,00
Si	2,98	2,99	2,98	2,99	2,99	2,99	3,02	2,99	2,99	2,96
Ti	0,00	0,00	0,00	0,00	0,00	0,00	0,00	0,02	0,00	0,00
Al	1,98	1,98	1,99	1,98	1,98	2,01	1,98	2,01	2,00	1,99
Fe2O3	0,03	0,03	0,03	0,03	0,02	0,00	0,00	0,00	0,01	0,04
FeO	2,46	2,45	2,47	2,48	2,48	2,49	2,46	2,46	2,46	2,38
Mn	0,00	0,01	0,01	0,01	0,01	0,01	0,01	0,02	0,16	0,20
Mg	0,41	0,37	0,36	0,36	0,35	0,34	0,36	0,34	0,26	0,33
Ca	0,15	0,18	0,18	0,16	0,16	0,16	0,16	0,15	0,13	0,13
Sum	8,01	8,01	8,01	8,01	8,01	8,00	7,99	7,99	8,00	8,03
X_{mg}	0,14	0,13	0,13	0,13	0,12	0,12	0,13	0,12	0,10	0,12
Almandine	81,23	81,09	81,46	82,16	82,45	82,95	81,99	82,60	81,74	77,87
Andradite	1,44	1,36	1,30	1,33	0,97	0,00	0,19	0,00	0,36	2,12
Grossular	3,64	4,62	4,55	4,06	4,37	5,29	5,05	4,95	3,78	2,29
Pyrope	13,61	12,50	12,14	12,17	11,82	11,38	12,25	11,55	8,65	11,09
Spessartin	0,07	0,26	0,33	0,36	0,35	0,37	0,47	0,76	5,31	6,65

	rim	rim	rim	rim							
Grt	Grt	Grt	Grt	Grt	Grt	Grt	Grt	Grt	Grt	Grt	Grt
28/1	29/1	30/1	38/1	41/1	3 / 1 .	6 / 1 .	8 / 1 .	10 / 1 .	12 / 1 .	18 / 1 .	21 / 1 .
37,34	37,01	36,77	37,56	36,99	36,77	36,58	36,68	36,95	36,32	36,71	36,68
	0,04	0,01		0,03	0,08	0,21	0,01	0,01		0,04	0,04
20,81	20,88	20,91	21,36	20,93	20,57	20,80	20,93	20,92	20,52	21,28	20,63
36,76	35,95	36,04	36,24	36,53	37,58	38,08	37,23	35,79	36,15	36,26	36,01
0,10	0,06	0,05	0,06	0,07	0,18	0,13	0,21	3,41	3,40	3,01	2,72
3,04	3,43	3,37	3,45	3,50	2,36	2,23	2,86	2,09	1,78	2,28	2,56
1,85	1,83	2,09	1,81	1,77	2,23	1,93	1,91	1,14	1,12	1,32	1,23
0,01	0,00	0,01	0,00	0,02	0,01	0,07		0,01	0,03	0,02	0,02
0,02	0,03	0,03	0,00	0,01	0,02	0,02	0,01	0,01	0,00	0,00	0,03
99,94	99,24	99,28	100,49	99,85	99,80	100,04	99,83	100,33	99,32	100,93	99,93
12,00	12,00	12,00	12,00	12,00	12,00	12,00	12,00	12,00	12,00	12,00	12,00
3,01	2,99	2,98	3,00	2,98	2,99	2,97	2,97	2,99	2,99	2,96	2,98
0,00	0,00	0,00	0,00	0,00	0,01	0,01	0,00	0,00	0,00	0,00	0,00
1,98	1,99	2,00	2,01	1,99	1,97	1,99	2,00	2,00	1,99	2,02	1,98
0,01	0,01	0,02	0,00	0,02	0,03	0,02	0,03	0,01	0,02	0,01	0,03
2,47	2,43	2,42	2,43	2,44	2,52	2,57	2,50	2,42	2,46	2,43	2,41
0,01	0,00	0,00	0,00	0,00	0,01	0,01	0,01	0,23	0,24	0,21	0,19
0,36	0,41	0,41	0,41	0,42	0,29	0,27	0,35	0,25	0,22	0,27	0,31
0,16	0,16	0,18	0,15	0,15	0,19	0,17	0,17	0,10	0,10	0,11	0,11
8,00	8,00	8,01	8,00	8,01	8,01	8,01	8,02	8,00	8,01	8,02	8,01
0,13	0,15	0,14	0,14	0,15	0,10	0,10	0,12	0,09	0,08	0,10	0,11
82,17	80,73	80,14	80,99	80,60	83,51	84,97	82,32	80,43	81,48	79,91	79,73
0,52	0,28	0,91	0,00	1,19	1,61	1,01	1,27	0,32	1,14	0,74	1,67
4,74	4,76	5,12	5,12	3,88	4,88	4,66	4,30	3,00	2,16	3,12	1,92
12,23	13,83	13,65	13,71	14,12	9,58	9,08	11,62	8,44	7,29	9,28	10,39
0,24	0,14	0,12	0,13	0,16	0,42	0,29	0,48	7,81	7,93	6,95	6,29

Sample: **MOK II**

Position	vein in Grt	vein in Grt	vein in Grt	vein in Grt	vein in Grt	vein in Grt	matrix	matrix coarse	matrix coarse	matrix coarse	incl in Grt	incl in Grt	incl in Grt
Mineral	Ms	Ms	Ms	Ms	Ms	Ms	Ms	Ms	Ms	Ms	Ms	Ms	Ms
Sample nr	3 / 1 .	11 / 1 .	14 / 1 .	21 / 1 .	25 / 1 .	27 / 1 .	36 / 1 .	42 / 1 .	45 / 1 .	47 / 1 .	19 / 1 .	22 / 1 .	23 / 1 .
Wt%													
SiO2	46,07	46,21	46,85	46,37	46,54	46,17	46,19	45,13	46,09	45,06	46,21	46,09	48,13
TiO2	0,15	0,10	0,20	0,26	0,27	0,21	0,21	0,67	0,65	0,71	0,22	0,81	0,20
Al2O3	36,94	37,21	37,02	37,23	36,07	37,31	37,01	35,22	35,69	35,41	35,48	35,74	35,68
FeO	1,38	1,62	1,15	1,37	1,34	1,03	1,05	1,74	1,65	1,71	2,06	1,59	1,63
MnO		0,02			0,01		0,00	0,01		0,01	0,06		0,02
MgO	0,47	0,52	0,41	0,51	0,48	0,46	0,41	0,67	0,70	0,71	0,83	0,74	1,02
CaO			0,02	0,01	0,01				0,00		0,03		0,01
Na2O	1,06	1,23	1,26	1,04	1,13	1,29	1,26	1,29	1,16	1,16	0,72	1,17	1,33
K2O	10,06	9,64	9,01	10,06	9,72	9,64	9,59	9,61	9,47	9,47	10,01	9,69	9,27
Total	96,13	96,56	95,91	96,85	95,56	96,11	95,72	94,34	95,42	94,24	95,63	95,83	97,29
No.O	11,00	11,00	11,00	11,00	11,00	11,00	11,00	11,00	11,00	11,00	11,00	11,00	11,00
Si	6,07	6,05	6,13	6,06	6,15	6,06	6,08	6,08	6,11	6,07	6,14	6,09	6,24
Ti	0,02	0,01	0,02	0,03	0,03	0,02	0,02	0,07	0,07	0,07	0,02	0,08	0,02
Al	5,74	5,75	5,71	5,74	5,62	5,77	5,75	5,59	5,58	5,62	5,55	5,57	5,45
FeO	0,15	0,18	0,13	0,15	0,15	0,11	0,12	0,20	0,18	0,19	0,23	0,18	0,18
Mn		0,00			0,00		0,00	0,00		0,00	0,01	0,00	0,00
Mg	0,09	0,10	0,08	0,10	0,09	0,09	0,08	0,14	0,14	0,14	0,16	0,14	0,20
Ca			0,00	0,00	0,00	0,00					0,00	0,00	0,00
Na	0,27	0,31	0,32	0,26	0,29	0,33	0,32	0,34	0,30	0,30	0,19	0,30	0,33
K	1,69	1,61	1,50	1,68	1,64	1,61	1,61	1,65	1,60	1,63	1,70	1,63	1,53
Sum	14,03	14,02	13,90	14,01	13,97	14,00	13,98	14,05	13,98	14,02	14,02	14,00	14,00
X_{mg}	0,38	0,37	0,39	0,40	0,39	0,45	0,41	0,41	0,43	0,42	0,42	0,45	0,53

Sample:			MOKV			
Position	**incl in Grt**	**incl in Grt**	**matrix**	**matrix**	**matrix**	**matrix**
Mineral	**Bt**	**Chl**	**Cld**	**Cld**	**Cld**	**Cld**
Sample nr	**32 / 1**	**35/1**	**97 / 1**	**101 / 1**	**106 / 1**	**109 / 1**
Wt%						
SiO2	35,53	23,86	24,24	24,41	24,16	23,89
TiO2	2,75	0,04	0,00	0,01		
Al2O3	18,98	21,51	40,02	40,16	40,49	39,66
FeO	20,15	30,83	24,36	24,82	24,57	25,42
MnO	0,00	0,15	0,08	0,09	0,03	0,15
MgO	8,74	10,13	2,19	2,18	2,29	1,76
CaO	0,00	0,01	0,02	0,03	0,02	0,02
Na2O	0,23	0,00	0,00	0,02	0,01	
K2O	9,35	0,01	0,01	0,01	0,01	0,03
Total	95,72	86,53	90,92	91,74	91,58	90,92
No.O	11,00	14,00	12,00	12,00	12,00	12,00
Si	5,54	5,25	2,03	2,03	2,01	2,02
Ti	0,32	0,01	0,00	0,00		0,00
Al	3,49	5,59	3,96	3,94	3,98	3,95
Fe2+	2,63	5,68	1,71	1,73	1,71	1,80
Mn	0,00	0,03	0,01	0,01	0,00	0,01
Mg	2,03	3,33	0,27	0,27	0,28	0,22
Na	0,07	0,00	0,00	0,00	0,00	0,00
K	1,86	0,00	0,00	0,00	0,00	0,00
Sum	15,93	19,88	7,98	7,99	8,00	8,00
X_{mg}	0,44	0,37	0,14	0,14	0,14	0,11

Sample: **MOK II**

Position	**matrix**	in vein	matrix	matrix	**matrix**	**matrix**	**matrix**
Mineral	**Mrg**	Pg	Pg	Pg	**St**	**St**	**St**
Sample nr	**31 / 1 .**	26 / 1 .	32 / 1 .	33 / 1 .	**48 / 1 .**	**49 / 1 .**	**50 / 1 .**
Wt%							
SiO2	45,36	41,54	45,44	45,44	27,01	27,20	27,39
TiO2	0,14	0,03	0,14	0,08	0,73	0,78	0,72
Al2O3	35,92	43,08	41,64	41,26	54,24	53,68	54,08
FeO	1,15	0,50	0,36	0,36	9,91	10,23	9,37
MnO					0,05	0,03	0,03
MgO	0,52		0,01	0,03	0,86	0,87	0,72
CaO	0,00	0,09	0,04	0,05	0,03	0,00	0,02
Na2O	1,14	3,69	1,03	1,21	0,20	0,14	0,16
K2O	9,50	4,77	5,81	5,74	0,00	0,01	
ZnO		1,04	2,09	1,83	4,68	4,35	4,82
Total	84,23	94,74	96,56	95,99	97,71	97,29	97,31
No.O	11,00	11,00	11,00	11,00	24,00	24,00	24,00
Si	6,11	5,40	5,77	5,80	3,95	3,99	4,00
Ti	0,01	0,00	0,01	0,01	0,08	0,09	0,08
Al	5,70	6,61	6,23	6,21	9,34	9,28	9,32
Fe2O3		0,05	0,04	0,04	0,00	0,00	0,00
FeO	0,13	0,00	0,00	0,00	1,21	1,25	1,15
Mn	0,00	0,02	0,01	0,01	0,01	0,00	0,00
Mg	0,10	0,51	0,14	0,17	0,19	0,19	0,16
Ca	0,00	1,20	1,43	1,42	0,00	0,00	0,00
ZnO				0,30	0,50	0,47	0,52
Na	0,30	0,17	0,34		0,06	0,04	0,04
K	1,63				0,00	0,00	0,00
Sum	12,06	13,98	13,98	13,95	15,33	15,31	15,28
X_{mg}					0,13	0,13	0,12

Sample:			MOKV			
Position	**incl in Grt**	**incl in Grt**	**matrix**	**matrix**	**matrix**	**matrix**
Mineral	**Bt**	**Chl**	**Cld**	**Cld**	**Cld**	**Cld**
Sample nr	**32 / 1**	**35/1**	**97 / 1**	**101 / 1**	**106 / 1**	**109 / 1**
Wt%						
SiO2	35,53	23,86	24,24	24,41	24,16	23,89
TiO2	2,75	0,04	0,00	0,01		
Al2O3	18,98	21,51	40,02	40,16	40,49	39,66
FeO	20,15	30,83	24,36	24,82	24,57	25,42
MnO	0,00	0,15	0,08	0,09	0,03	0,15
MgO	8,74	10,13	2,19	2,18	2,29	1,76
CaO	0,00	0,01	0,02	0,03	0,02	0,02
Na2O	0,23	0,00	0,00	0,02	0,01	
K2O	9,35	0,01	0,01	0,01	0,01	0,03
Total	95,72	86,53	90,92	91,74	91,58	90,92
No.O	11,00	14,00	12,00	12,00	12,00	12,00
Si	5,54	5,25	2,03	2,03	2,01	2,02
Ti	0,32	0,01	0,00	0,00		0,00
Al	3,49	5,59	3,96	3,94	3,98	3,95
Fe2+	2,63	5,68	1,71	1,73	1,71	1,80
Mn	0,00	0,03	0,01	0,01	0,00	0,01
Mg	2,03	3,33	0,27	0,27	0,28	0,22
Na	0,07	0,00	0,00	0,00	0,00	0,00
K	1,86	0,00	0,00	0,00	0,00	0,00
Sum	15,93	19,88	7,98	7,99	8,00	8,00
X_{mg}	0,44	0,37	0,14	0,14	0,14	0,11

Mineral	Fsp	Fsp	Fsp	Fsp	Mrg	Mrg	Mrg
Sample nr	39 / 1	40 / 1	41 / 1	42 / 1	95 / 1	96 / 1	99 / 1
Wt%							
SiO2	61,52	62,36	62,95	62,56	29,94	30,61	30,80
TiO2			0,00		0,08	0,28	0,20
Al2O3	24,39	23,63	23,16	23,40	50,07	49,62	48,90
FeO		0,00	0,01	0,02	0,38	0,40	0,67
MnO	0,01		0,01	0,02	0,02	0,01	0,01
MgO			0,01		0,08	0,06	0,07
CaO	6,07	5,29	4,82	4,86	12,76	12,14	11,99
Na2O	7,39	9,08	9,40	8,98	0,87	1,18	1,15
K2O	0,04	0,03	0,04	0,05	0,01	0,02	0,02
Total	99,42	100,39	100,40	99,90	94,18	94,33	93,82
No.O	8,00	8,00	8,00	8,00	11,00	11,00	11,00
Si	2,74	2,76	2,78	2,77	4,03	4,11	4,16
Ti	0,00	0,00	0,00	0,00	0,01	0,03	0,02
Al	1,28	1,23	1,21	1,22	7,94	7,85	7,78
Fe2+	0,00	0,00	0,00	0,00	0,04	0,04	0,08
Mn	0,00	0,00	0,00	0,00	0,00	0,00	0,00
Mg	0,00	0,00	0,00	0,00	0,02	0,01	0,01
Ca	0,29	0,25	0,23	0,23	1,84	1,75	1,73
Na	0,64	0,78	0,80	0,77	0,23	0,31	0,30
K	0,00	0,00	0,00	0,00	0,00	0,00	0,00
Sum	4,94	5,02	5,02	5,00	14,11	14,10	14,09
X_{mg}							
An	31,15	24,33	22,05	22,97			
Ab	68,62	75,52	77,72	76,75			
Or	0,23	0,15	0,23	0,28			

Sample	MOK V					
Position	**inner rim**	**surronding St pseudomorph**	**surrounding Bt**	**surrounding Ms**	**surrounding chl**	
Mineral	**Grt**	**Grt**	**Grt**	**Grt**	**Grt**	**Grt**
Sample nr	**105/1**	**30 / 1**	**33 / 1**	**34 / 1**	**36 / 1**	**37 / 1**
Wt%						
SiO2	36,67	37,11	37,27	37,06	36,87	36,68
TiO2	0,00		0,01	0,02	0,01	0,00
Al2O3	20,52	20,92	20,82	20,99	20,91	21,09
FeO	37,73	36,91	37,24	36,29	35,82	36,62
MnO	0,32	0,16	0,27	0,18	2,68	0,12
MgO	1,98	2,80	2,91	3,18	3,16	3,37
CaO	1,83	1,75	1,85	1,75	0,92	1,74
Na2O	0,03		0,03	0,01	0,01	0,02
K2O	0,01	0,01		0,01		0,01
Total	99,09	99,64	100,40	99,47	100,39	99,65
No.O	12,00	12,00	12,00	12,00	12,00	12,00
Si	3,01	3,00	3,00	3,00	2,97	2,97
Ti	0,00	0,00	0,00	0,00	0,00	0,00
Al	1,98	2,00	1,98	2,00	1,99	2,01
Fe3+	0,01	0,00	0,02	0,00	0,03	0,02
Fe2+	2,58	2,50	2,48	2,45	2,38	2,46
Mn	0,02	0,01	0,02	0,01	0,18	0,01
Mg	0,24	0,34	0,35	0,38	0,38	0,41
Ca	0,16	0,15	0,16	0,15	0,08	0,15
Sum	8,00	8,00	8,01	8,00	8,02	8,02
X_{mg}	0,09	0,12	0,12	0,14	0,14	0,14
Almandine	85,79	83,32	82,42	81,75	78,37	80,95
Andradite	0,50	0,00	1,17	0,02	1,69	0,97
Grossular	4,87	5,05	4,16	5,05	0,99	4,10
Pyrope	8,10	11,27	11,65	12,78	12,79	13,70
Spessartine	0,74	0,36	0,61	0,40	6,16	0,28

Sample:	MOK V				
Position	**matrix**	**incl in Grt**	**pseudomorph in St**	**incl in Grt**	**matrix with Ms**
Mineral	**Ms**	**Ms**	**Ms**	**Ms**	**Pg**
Sample nr	**100 / 1**	**26 / 1 .**	**28 / 1 .**	**31 / 1 .**	**98 / 1**
Wt%					
SiO2	45,45	46,29	45,89	44,95	43,56
TiO2	0,77	0,88	0,13	0,76	0,06
Al2O3	35,31	35,87	38,00	35,08	41,74
FeO	1,64	1,89	0,89	1,76	0,56
MnO	0,00	0,04	0,00		0,00
MgO	0,69	0,63	0,27	0,54	0,01
CaO		0,02		0,01	1,86
Na2O	1,14	1,36	1,42	1,13	5,87
K2O	9,64	8,97	9,12	9,27	1,10
Total	94,65	95,93	95,73	93,51	94,76
No.O	11,00	11,00	11,00	11,00	11,00
Si	6,09	6,10	6,02	6,09	5,64
Ti	0,08	0,09	0,01	0,08	0,01
Al	5,58	5,57	5,88	5,60	6,37
Fe2+	0,18	0,21	0,10	0,20	0,06
Mn	0,00	0,00	0,00	0,00	0,00
Mg	0,14	0,12	0,05	0,11	0,00
Ca		0,00	0,00	0,00	0,26
Na	0,30	0,35	0,36	0,30	1,47
K	1,65	1,51	1,53	1,60	0,18
Sum	14,01	13,95	13,95	13,98	13,99
X_{mg}					

Sample:			**MOK V**		
Position	**matrix**	**matrix**	**matrix**	**matrix**	**incl in Grt pseudomorph Bt + Ms**
Mineral	**St**	**St**	**St**	**St**	**St**
Sample nr	**93 / 1**	**94 / 1**	**107 / 1**	**108 / 1**	**27 / 1**
Wt%					
SiO2	27,22	27,10	27,37	27,07	27,43
TiO2	0,64	0,72	0,75	0,69	0,71
Al2O3	53,57	53,72	53,70	53,63	53,99
FeO	10,00	10,24	9,58	9,02	9,38
MnO	0,06	0,01	0,06	0,03	0,04
MgO	0,78	0,86	0,75	0,70	0,68
CaO	0,02		0,00	0,02	
Na2O	0,14	0,14	0,15	0,20	0,19
K2O	0,01		0,00	0,02	
ZnO	4,30	4,45	4,68	5,20	5,05
Total	96,74	97,23	97,04	96,57	97,46
No.O	48,00	48,00	48,00	48,00	48,00
Si	4,01	3,98	4,02	3,99	4,01
Ti	0,07	0,08	0,08	0,08	0,08
Al	9,30	9,29	9,29	9,33	9,30
Zn	0,47	0,48	0,51	0,57	0,55
Fe2+	1,23	1,26	1,18	1,11	1,15
Mn	0,01	0,00	0,01	0,00	0,00
Mg	0,17	0,19	0,16	0,15	0,15
Ca	0,00	0,00	0,00	0,00	0,00
Na	0,04	0,04	0,04	0,06	0,05
K	0,00	0,00	0,00	0,00	0,00
Sum	15,30	15,32	15,28	15,30	15,28
X_{mg}	0,12	0,13	0,12	0,12	0,11

OS-2

Sample:	OS-2						
Position	matrix Grt rim	Grt crack	inclusion in Grt	matrix	matrix	replacing Grt pseudomorph	matrix
Mineral	Chl	Chl	Chl	Chl	Chl	Chl	Chl
Sample nr	8 / 1	9 / 1	11 / 1	18 / 1	20 / 1	24 / 1	25 / 1
Wt%							
SiO2	24,92	24,19	22,79	24,66	24,62	24,72	24,59
TiO2	0,04	0,05	0,06	0,08	0,04	0,03	0,08
Al2O3	21,18	21,56	20,49	21,21	21,36	21,72	22,01
FeO	26,98	29,88	38,41	25,42	26,21	26,01	26,59
MnO	0,48	0,61	0,79	0,37	0,36	0,44	0,45
MgO	13,06	10,83	4,94	14,42	13,92	13,74	13,32
CaO	0,13	0,09	0,18	0,03	0,05	0,02	
Na2O		0,02		0,01	0,01	0,02	
K2O	0,01	0,01	0,03	0,01	0,02		0,00
Total	86,81	87,25	87,67	86,21	86,57	86,72	87,04
No.O	14,00	14,00	14,00	14,00	14,00	14,00	14,00
Si	5,36	5,27	5,21	5,30	5,29	5,29	5,36
Ti	0,01	0,01	0,01	0,01	0,01	0,01	0,01
Al	5,38	5,54	5,53	5,38	5,41	5,48	5,38
Fe3+	0,06	0,05	0,00	0,01	0,00	0,04	0,06
Fe2+	4,79	5,40	7,36	4,57	4,71	4,61	4,79
Mn	0,09	0,11	0,15	0,07	0,07	0,08	0,09
Mg	4,19	3,51	1,68	4,62	4,46	4,38	4,19
Ca	0,03	0,02	0,04	0,01	0,01	0,00	0,03
Na	0,00	0,02	0,00	0,00	0,01	0,02	0,00
K	0,01	0,00	0,02	0,00	0,01	0,00	0,01
Sum	19,91	19,93	20,00	19,97	19,98	19,92	19,91
X_{mg}	0,47	0,39	0,19	0,50	0,49	0,49	0,47

Sample:							OS-2						
Position	incl in Grt on rim	incl in Grt	incl in Grt on rim	matrix on Grt rim	incl in Grt on rim	incl in Grt on rim	incl in Grt on rim	urrounded b chl, matrix	urrounded b chl, matrix	urrounded b chl, matrix	matrix on Grt rim	in matrix fold	matrix
Mineral	Ep	Ep	Ep	Ep	Ep	Ep	Ep	Ep	Ep	Ep	Ep	Ep	Ep
Sample nı	1 / 1 .	4 / 1 .	6 / 1 .	7 / 1 .	12 / 1 .	14 / 1 .	16 / 1 .	17 / 1 .	19 / 1 .	21 / 1 .	23 / 1 .	28 / 1 .	31 / 1 .
Wt%													
SiO2	37,82	37,49	36,30	37,71	37,78	37,67	37,05	37,45	37,65	37,80	37,29	38,01	37,85
TiO2	0,07	0,02	0,01	0,06	0,10	0,22	0,03	0,09	0,05	0,11	0,07	0,08	0,15
Al2O3	22,91	22,68	22,11	23,19	25,32	23,04	22,76	23,67	24,28	24,11	22,90	24,66	24,99
Fe2O3	15,21	14,47	15,14	14,06	11,73	13,90	13,95	13,68	13,08	12,18	14,01	11,96	10,67
MnO	0,65	0,79	0,92	0,78	0,56	0,76	0,74	0,36	0,28	0,24	0,79	0,29	0,45
MgO	0,00	0,01	0,00	0,00	0,01	0,00	0,03	0,01	0,03	0,03	0,00	0,01	0,02
CaO	22,77	22,62	21,78	22,32	22,78	22,04	21,74	22,67	22,83	23,05	22,56	23,45	22,64
Na2O	0,04	0,03	0,00	0,00	0,00	0,03	0,01			0,00	0,03	0,01	0,01
K2O	0,02	0,02	0,00	0,00	0,02	0,00	0,00			0,02	0,00	0,02	0,06
Total	99,48	98,11	96,27	98,13	98,29	97,67	96,31	97,93	98,20	97,53	97,64	98,49	96,83
No.O	12,50	12,50	12,50	12,50	12,50	12,50	12,50	12,50	12,50	12,50	12,50	12,50	12,50
Si	2,98	3,00	2,97	3,00	2,98	3,01	3,01	2,98	2,98	3,01	2,99	3,00	3,02
Ti	0,00	0,00	0,00	0,00	0,01	0,01	0,00	0,01	0,00	0,01	0,00	0,00	0,01
Al	2,13	2,14	2,13	2,18	2,35	2,17	2,18	2,22	2,27	2,26	2,16	2,29	2,35
Fe3+	0,90	0,87	0,93	0,84	0,70	0,84	0,85	0,82	0,78	0,73	0,85	0,71	0,64
Fe2+													
Mn	0,04	0,05	0,06	0,05	0,04	0,05	0,05	0,02	0,02	0,02	0,05	0,02	0,03
Mg	0,00	0,00	0,00	0,00	0,00	0,00	0,00	0,00	0,00	0,00	0,00	0,00	0,00
Ca	1,92	1,94	1,91	1,90	1,92	1,89	1,89	1,93	1,94	1,97	1,94	1,98	1,93
Na	0,01	0,00		0,00	0,00	0,00	0,00			0,00	0,00	0,00	0,00
K	0,00	0,00	0,00	0,00	0,00	0,00	0,00			0,00	0,00	0,00	0,01
Sum	8,00	8,00	8,00	7,98	7,99	7,98	7,98	7,99	7,99	7,99	8,00	8,00	7,99
X_{mg}													

Sample:	OS-2		
Position	matrix surrounded by	matrix surrounded by	matrix surrounded by
Mineral	Qrz Fsp	Qrz Fsp	Qrz Fsp
Sample:	25 / 1	26 / 1	27 / 1
Wt%			
SiO2	69,51	68,80	68,93
TiO2	0,01		
Al2O3	19,77	19,79	19,76
FeO	0,02	0,03	0,08
MnO		0,03	
MgO	0,00	0,01	0,02
CaO	0,07	0,51	0,20
Na2O	11,78	11,62	11,76
K2O	0,04	0,04	0,03
Total	101,20	100,83	100,78
No.O	8,00	8,00	8,00
An	0,32	2,38	0,94
Ab	99,47	97,40	98,91
Or	0,22	0,22	0,15
Si	3,00	2,98	2,99
Ti	0,00	0,00	0,00
Al	1,01	1,01	1,01
Fe2+	0,00	0,00	0,00
Mn	0,00	0,00	0,00
Mg	0,00	0,00	0,00
Ca	0,00	0,02	0,01
Na	0,99	0,98	0,99
K	0,00	0,00	0,00
Sum	5,00	5,00	5,00
X_{mg}	0,05	0,35	0,34

Sample:				**OS-2**			
Position	**surrounding Ep**	**inner rim**	**inner rim cracked**	**surrounding Ep**	**inner rim**	**Inner rim**	**rim**
Mineral	**Grt**	**Grt**	**Grt**	**Grt**	**Grt**	**Grt**	**Grt**
Sample nr	**2 / 1**	**5 / 1**	**10 / 1**	**13 / 1**	**15 / 1**	**29 / 1**	**30 / 1**
Wt%							
SiO2	37,17	37,11	36,58	36,75	37,20	37,38	37,13
TiO2	0,11	0,12	0,10	0,10	0,23	0,10	0,07
Al2O3	20,57	20,40	20,39	20,53	20,53	21,00	20,80
FeO	33,17	29,97	30,91	32,46	31,32	31,57	30,82
MnO	2,75	5,53	4,66	3,24	4,30	4,20	3,67
MgO	1,80	1,15	1,31	1,61	1,38	1,61	1,67
CaO	4,95	6,04	5,70	5,00	5,52	5,25	5,73
Na2O	0,04		0,01	0,02	0,01	0,04	0,04
K2O		0,00			0,01		0,00
Total	100,54	100,32	99,66	99,71	100,50	101,15	99,93
No.O	12,00	12,00	12,00	12,00	12,00	12,00	12,00
Si	2,99	2,99	2,97	2,98	2,99	2,99	2,99
Ti	0,01	0,01	0,01	0,01	0,01	0,01	0,00
Al	1,95	1,94	1,96	1,97	1,95	1,98	1,98
Fe3+	0,04	0,05	0,05	0,04	0,04	0,02	0,02
Fe2+	2,19	1,98	2,05	2,16	2,07	2,09	2,06
Mn	0,19	0,38	0,32	0,22	0,29	0,28	0,25
Mg	0,22	0,14	0,16	0,19	0,17	0,19	0,20
Ca	0,43	0,52	0,50	0,44	0,48	0,45	0,50
Sum	8,01	8,01	8,02	8,01	8,00	8,01	8,00
X_{mg}	0,09	0,07	0,07	0,08	0,07	0,08	0,09
Almandine	72,28	65,17	67,16	71,42	68,58	69,02	68,38
Andradite	2,22	2,40	2,69	1,93	1,83	1,20	0,98
Grossular	12,03	15,13	14,02	12,65	14,15	13,84	15,57
Pyrope	7,20	4,63	5,34	6,53	5,58	6,42	6,70
Spessartin	6,26	12,68	10,80	7,46	9,85	9,51	8,38

Sample:	OS-2				
Position	**Grt crack**	**matrix**	**matrix**	**matrix**	**matrix**
Mineral	**Ms**	**Ms**	**Ms**	**Ms**	**Ms**
Sample nr	**3 / 1**	**26 / 1**	**27 / 1**	**22 / 1**	**32 / 1**
Wt%					
SiO2	47,53	47,17	46,80	46,24	46,90
TiO2	0,18	0,38	0,35	0,36	0,56
Al2O3	30,04	32,41	31,43	34,04	31,74
FeO	5,06	3,77	4,08	3,73	3,20
MnO	0,18	0,02		0,01	
MgO	1,69	1,54	1,73	1,05	2,01
CaO	0,03				0,01
Na2O	0,34	1,07	1,06	1,15	0,54
K2O	10,37	9,61	9,65	9,61	10,21
Total	95,41	95,96	95,11	96,20	95,18
No.O	11,00	11,00	11,00	11,00	11,00
Si	6,44	6,30	6,32	6,16	6,31
Ti	0,02	0,04	0,04	0,04	0,06
Al	4,80	5,10	5,00	5,35	5,03
Fe2+	0,57	0,42	0,46	0,42	0,36
Mn	0,02	0,00		0,00	
Mg	0,34	0,31	0,35	0,21	0,40
Ca	0,00	0,00	0,00	0,00	0,00
Na	0,09	0,28	0,28	0,30	0,14
K	1,79	1,64	1,66	1,63	1,75
Sum	14,08	14,07	14,11	14,10	14,06
X_{mg}	0,37	0,42	0,43	0,33	0,53

Sample: **BGA2-1**

Position	Matrix				
	occuring together w ith clorite and Bt				
Mineral	**Amph**	**Amph**	**Amph**	**Amph**	**Amph**
Sample nr	**9 / 1 .**	**10 / 1 .**	**11 / 1 .**	**13 / 1 .**	**14 / 1 .**
Wt %					
SiO2	43,76	43,25	43,18	41,80	41,36
TiO2	0,21	0,17	0,20	0,26	0,24
Al2O3	10,78	10,76	11,51	13,73	13,86
FeO	24,08	24,18	23,25	20,86	20,93
MnO	0,82	0,75	0,67	0,38	0,33
MgO	6,96	6,83	7,04	6,71	6,65
CaO	7,63	7,95	8,32	10,46	10,77
Na2O	2,06	2,10	2,21	2,05	1,99
K2O	0,46	0,46	0,50	0,67	0,65
Total	96,77	96,46	96,89	96,91	96,77
No.O	23,00	23,00	23,00	23,00	23,00
Si	6,48	6,45	6,42	6,32	6,28
Ti	0,02	0,02	0,02	0,03	0,03
Al	1,88	1,89	2,02	2,45	2,48
Fe3	2,02	1,92	1,71	0,73	0,68
Fe2	0,96	1,10	1,19	1,91	1,98
Mn	0,10	0,10	0,08	0,05	0,04
Mg	1,53	1,52	1,56	1,51	1,51
Ca	1,21	1,27	1,33	1,69	1,75
Na	0,59	0,61	0,64	0,60	0,59
K	0,09	0,09	0,10	0,13	0,13
Sum	14,89	14,97	15,06	15,43	15,46
X_{mg}	0,32	0,36	0,41	0,72	0,75

Sample: **BGA 2-1**

Position	rim of Grt part of band	part of band	rim of Grt part of band	rim of Grt part of band	rim of Grt part of band	wrapping around Grt	wrapping around Grt	wrapping around Grt	Bt propagating into Grt rim	Matrix	Matrix large cryStal
Mineral	**Bt**	**Bt**	**Bt**	**Bt**	**Bt**	**Bt**	**Bt**	**Bt**	**Bt**	**Bt**	**Bt**
Sample nr	**34 / 1 .**	**35 / 1 .**	**37 / 1 .**	**38 / 1 .**	**43 / 1 .**	**46 / 1 .**	**51 / 1 .**	**54 / 1 .**	**56 / 1 .**	**61 / 1 .**	**64 / 1 .**
wt%											
SiO2	34,94	35,93	36,17	35,83	35,68	35,72	36,25	35,94	36,03	35,88	36,56
TiO2	1,64	1,71	2,03	1,84	2,04	2,21	1,78	1,77	1,75	2,15	1,16
Al2O3	16,43	16,09	16,66	16,73	16,58	16,37	16,39	16,40	16,49	16,16	16,78
FeO	22,85	20,86	19,98	20,16	20,90	21,41	20,49	20,54	20,34	20,77	20,78
MnO	0,64	0,30	0,33	0,27	0,23	0,24	0,30	0,29	0,21	0,24	0,19
MgO	8,90	9,52	8,81	9,03	9,34	8,95	9,71	9,40	9,67	9,30	9,92
CaO	0,07	0,07	0,00								
Na2O	0,04	0,07	0,09	0,10	0,04	0,06	0,14	0,10	0,10	0,09	0,08
K2O	9,04	9,62	9,27	9,55	9,68	9,75	9,49	9,54	9,52	9,63	9,74
Total	94,55	94,17	93,34	93,50	94,49	94,73	94,54	93,97	94,13	94,22	95,21
No.O	22,00	22,00	22,00	22,00	22,00	22,00	22,00	22,00	22,00	22,00	22,00
Si	5,53	5,71	5,79	5,73	5,65	5,67	5,72	5,72	5,71	5,71	5,72
Ti	0,20	0,20	0,24	0,22	0,24	0,26	0,21	0,21	0,21	0,26	0,14
Al	3,06	3,02	3,14	3,16	3,10	3,07	3,05	3,07	3,08	3,03	3,09
Fe2	3,02	2,77	2,67	2,70	2,77	2,84	2,70	2,73	2,69	2,76	2,72
Mn	0,09	0,04	0,05	0,04	0,03	0,03	0,04	0,04	0,03	0,03	0,03
Mg	2,10	2,26	2,10	2,15	2,21	2,12	2,28	2,23	2,28	2,21	2,31
Ca	0,01	0,01	0,00	0,00	0,00	0,00	0,00	0,00	0,00	0,00	0,00
Ba											
Na	0,01	0,02	0,03	0,03	0,01	0,02	0,04	0,03	0,03	0,03	0,02
K	1,82	1,95	1,89	1,95	1,96	1,98	1,91	1,94	1,92	1,95	1,94
Sum	15,85	15,98	15,92	15,98	15,97	16,00	15,95	15,97	15,96	15,98	15,97
X_{mg}	0,41	0,45	0,44	0,44	0,44	0,43	0,46	0,45	0,46	0,44	0,46

Sample: **BGA2-1**

Position	replacing Bt	replacing Bt	replacing Bt contact with Ep		replacing Bt	within Bt
Mineral	**Chl**	**Chl**	**Chl**	**Chl**	**Chl**	**Chl**
Sample nr	**59 / 1 .**	**60 / 1 .**	**63 / 1 .**	**75 / 1 .**	**76 / 1 .**	**15 / 1 .**
Wt%						
SiO2	24,76	24,89	25,18	24,88	25,15	25,65
TiO2	0,08	0,07	0,06	0,06	0,08	0,07
Al2O3	20,29	20,78	20,10	20,96	20,60	19,99
FeO	26,50	26,06	25,94	26,70	25,72	26,30
MnO	0,42	0,46	0,40	0,47	0,49	0,46
MgO	14,19	14,00	14,06	13,82	14,09	14,03
CaO	0,02	0,01	0,03			0,03
Na2O			0,00	0,01	0,03	0,02
K2O	0,00	0,01	0,02	0,01	0,01	0,16
Total	86,25	86,29	85,80	86,92	86,18	86,71
No.O	14,00	14,00	14,00	14,00	14,00	14,00
Si	5,37	5,37	5,46	5,35	5,43	5,52
Ti	0,01	0,01	0,01	0,01	0,01	0,01
Al	5,18	5,29	5,14	5,31	5,24	5,07
Fe2	4,80	4,71	4,71	4,80	4,64	4,73
Mn	0,08	0,08	0,07	0,09	0,09	0,08
Mg	4,58	4,51	4,55	4,43	4,53	4,50
Ca	0,00	0,00	0,01	0,00	0,00	0,01
Ba						
Na	0,00	0,00	0,00	0,00	0,01	0,01
K	0,00	0,00	0,01	0,00	0,00	0,04
Sum	20,03	19,97	19,96	19,99	19,95	19,97
X_{mg}	0,49	0,49	0,49	0,48	0,49	0,49

Sample:		BGA2-1		
Position	**close to Grt rim in band**	**close to Grt rim in band**	**appearing with Bt in band**	**in Bt band**
Mineral	**Ep**	**Ep**	**Ep**	**Ep**
Sample nr	**36 / 1**	**44 / 1 .**	**45 / 1 .**	**48 / 1 .**
Wt%				
SiO2	37,78	37,39	37,61	37,94
TiO2	0,06	0,05	0,07	0,10
Al2O3	25,07	24,05	24,32	24,48
Fe2O3	10,66	11,56	11,47	11,41
MnO	0,19	0,20	0,27	0,31
MgO		0,00	0,01	0,00
CaO	23,20	22,35	22,72	22,80
Na2O	0,02	0,00	0,00	0,01
K2O	0,02	0,02	0,03	0,06
Total	96,99	95,63	96,50	97,11
No.O	12,50	12,50	12,50	12,50
Si	3,01	3,02	3,01	3,02
Ti	0,00	0,00	0,00	0,01
Al	2,35	2,29	2,30	2,30
Fe3	0,64	0,70	0,69	0,68
Mn	0,01	0,01	0,02	0,02
Mg	0,00	0,00	0,00	0,00
Ca	1,98	1,94	1,95	1,95
Na	0,00	0,00	0,00	0,00
K	0,00	0,00	0,01	0,01
Sum	8,00	7,98	7,99	7,99
X_{mg}	0,00	0,00	0,00	0,00

Sample:			BGA2-1			
Position	**in Ms within bands**	**in Ms within bands**	**in Ms within bands**	**in Ms within bands**	**in Ms within bands**	**in Ms within bands**
Mineral	**Fsp (Ab)**	**Fsp (Ab)**	**Fsp (Ab)**	**Fsp (Ab)**	**Fsp (Ab)**	**Fsp (Ab)**
Sample nr	**67 / 1 .**	**68 / 1 .**	**69 / 1 .**	**72 / 1 .**	**73 / 1 .**	**74 / 1 .**
Wt%						
SiO2	69,74	68,85	68,60	67,55	69,45	68,75
TiO2	0,01		0,01	0,00	0,00	0,01
Al2O3	20,01	19,59	19,44	20,00	19,54	20,04
FeO	0,00	0,06	0,08	0,19	0,01	0,15
MnO	0,02		0,01		0,04	
MgO	0,01		0,01	0,01		0,00
CaO	0,00	0,07	0,42	0,63	0,14	0,44
Na2O	12,06	12,20	11,93	11,79	12,24	11,90
K2O	0,04	0,04	0,05	0,07	0,05	0,06
Total	101,89	100,81	100,56	100,24	101,46	101,35
No.O	8,00	8,00	8,00	8,00	8,00	8,00
Si	2,99	2,99	2,99	2,96	2,99	2,97
Ti	0,00	0,00	0,00	0,00	0,00	0,00
Al	1,01	1,00	1,00	1,03	0,99	1,02
Fe2	0,00	0,00	0,00	0,01	0,00	0,01
Mn	0,00	0,00	0,00	0,00	0,00	0,00
Mg	0,00	0,00	0,00	0,00	0,00	0,00
Ca	0,00	0,00	0,02	0,03	0,01	0,02
Na	1,00	1,03	1,01	1,00	1,02	1,00
K	0,00	0,00	0,00	0,00	0,00	0,00
Sum	5,01	5,02	5,02	5,03	5,02	5,02

Sample:	BGA2-1			
Position	**rim**	**close to rim**	**rim**	**dissolved in matrix**
Mineral	**Grt**	**Grt**	**Grt**	**Grt**
Sample nr	**50 / 1 .**	**53 / 1 .**	**57 / 1 .**	**65 / 1 .**
Wt%				
SiO2	37,52	37,33	36,99	37,09
TiO2	0,16	0,15	0,08	0,10
Al2O3	20,37	20,17	20,52	20,07
Fe2O3	0,67	1,27	0,97	1,17
FeO	22,45	21,40	24,58	20,58
MnO	10,86	12,52	9,14	13,06
MgO	0,86	0,77	1,12	0,53
CaO	7,57	7,52	7,13	7,78
Total	100,46	101,12	100,54	100,38
No.O	12,00	12,00	12,00	12,00
Si	3,01	2,99	2,98	3,00
Ti	0,01	0,01	0,00	0,01
Al	1,93	1,91	1,95	1,92
Fe3	0,04	0,08	0,06	0,07
Fe2	1,51	1,44	1,65	1,39
Mn	0,74	0,85	0,62	0,89
Mg	0,10	0,09	0,13	0,06
Ca	0,65	0,65	0,62	0,67
Sum	8,00	8,01	8,02	8,01
X_{mg}	0,06	0,06	0,08	0,04
Almandine	49,44	46,60	53,90	45,17
Andradite	2,05	3,85	2,96	3,59
Grossular	20,02	17,87	17,70	19,06
Pyrope	3,49	3,08	4,51	2,13
Spessartine	25,00	28,60	20,93	30,05

Sample:	BGA2-1				
Position	**in band on Bt rim**	**in band**	**inside Bt in rim**	**matrix**	**matrix**
Mineral	**Ms**	**Ms**	**Ms**	**Ms**	**Ms**
Sample nr	**39 / 1 .**	**42 / 1 .**	**49 / 1 .**	**58 / 1 .**	**66 / 1 .**
Wt%					
SiO2	46,43	46,05	46,73	49,06	48,51
TiO2	0,38	0,51	0,43	0,36	0,26
Al2O3	31,77	30,78	32,60	28,56	29,13
FeO	3,96	3,95	3,75	3,67	4,11
MnO	0,05	0,01	0,04	0,06	0,06
MgO	1,80	1,68	1,56	2,44	2,77
CaO		0,07			0,01
Na2O	0,39	0,41	0,61	0,64	0,41
K2O	10,20	9,60	9,76	9,94	10,22
Total	94,98	93,07	95,48	94,75	95,47
No.O	11,00	11,00	11,00	11,00	11,00
Si	6,28	6,34	6,27	6,63	6,53
Ti	0,04	0,05	0,04	0,04	0,03
Al	5,07	5,00	5,15	4,55	4,62
Fe2	0,45	0,45	0,42	0,41	0,46
Mn	0,01	0,00	0,01	0,01	0,01
Mg	0,36	0,35	0,31	0,49	0,56
Ca	0,00	0,01	0,00	0,00	0,00
Na	0,10	0,11	0,16	0,17	0,11
K	1,76	1,69	1,67	1,71	1,75
Sum	14,07	14,00	14,03	14,00	14,06
X_{mg}	0,45	0,43	0,43	0,54	0,55

BGA2-2

Sample:	BGA 2-2						
Position	**matrix band**	**matrix band**	**matrix band**	**matrix**	**matrix**	**matrix**	**matrix**
Mineral	**Bt**	**Bt**	**Bt**	**Bt**	**Bt**	**Bt**	**Bt**
Sample nr	**45 / 1 .**	**49 / 1 .**	**55 / 1 .**	**60 / 1 .**	**68 / 1 .**	**72 / 1 .**	**63 / 1 .**
Wt%							
SiO2	37,08	36,86	36,95	37,19	36,49	36,89	34,18
TiO2	1,95	1,87	1,84	1,75	1,77	1,92	1,80
Al2O3	16,17	16,35	16,56	16,46	16,46	16,59	15,08
FeO	17,89	17,82	17,79	17,49	17,55	17,63	23,98
MnO	0,25	0,26	0,23	0,27	0,20	0,24	0,19
MgO	11,71	11,85	11,92	11,91	11,81	11,71	10,65
CaO							0,02
Na2O	0,12	0,14	0,10	0,06	0,02	0,09	0,03
K2O	9,53	9,50	9,60	9,92	9,75	9,56	7,87
Total	94,71	94,65	95,00	95,04	94,04	94,64	93,81
No.O	11,00	11,00	11,00	11,00	11,00	11,00	11,00
Si	5,75	5,71	5,70	5,75	5,70	5,72	5,41
Ti	0,23	0,22	0,21	0,20	0,21	0,22	0,21
Al	2,96	2,99	3,01	3,00	3,03	3,03	2,82
Fe3	0,00	0,00	0,00	0,00	0,00	0,00	0,00
Fe2	2,32	2,31	2,30	2,26	2,29	2,29	3,18
Mn	0,03	0,03	0,03	0,04	0,03	0,03	0,03
Mg	2,71	2,74	2,74	2,75	2,75	2,71	2,51
Ca	0,00	0,00	0,00	0,00	0,00	0,00	0,00
Na	0,04	0,04	0,03	0,02	0,01	0,03	0,01
K	1,89	1,88	1,89	1,96	1,94	1,89	1,59
Sum	15,92	15,92	15,92	15,97	15,95	15,92	15,76
X_{mg}	0,54	0,54	0,54	0,55	0,55	0,54	0,44

Sample: **BGA 2-2**

Position	within/rim of Bt	within/rim of Bt	matrix within/rim of Bt	matrix within/rim of Bt	matrix within/rim of Bt
Mineral	**Chl**	**Chl**	**Chl**	**Chl**	**Chl**
Sample nr:	**1/1.**	**2/1.**	**3/1.**	**5/1.**	**7/1.**
Wt%					
SiO2	25,85	26,05	26,07	26,23	26,03
TiO2	0,07	0,07	0,08	0,06	0,07
Al2O3	21,22	21,05	20,55	21,12	21,24
FeO	21,76	22,11	21,03	21,15	21,22
MnO	0,41	0,37	0,41	0,41	0,43
MgO	17,64	17,13	17,91	17,94	17,52
CaO			0,01		0,02
Na2O	0,00				
K2O	0,02	0,01	0,03	0,00	0,01
Total	86,96	86,79	86,08	86,91	86,54
No.O	28,00	28,00	28,00	28,00	28,00
Si	5,39	5,45	5,48	5,45	5,44
Ti	0,01	0,01	0,01	0,01	0,01
Al	5,22	5,19	5,09	5,18	5,23
Fe2	3,80	3,87	3,70	3,68	3,71
Mn	0,07	0,07	0,07	0,07	0,08
Mg	5,49	5,35	5,61	5,56	5,46
Ca		0,00	0,00	0,00	0,00
Na	0,00	0,00	0,00	0,00	0,00
K	0,00	0,00	0,01	0,00	0,00
Sum	19,99	19,94	19,97	19,95	19,93
X_{mg}	0,59	0,58	0,60	0,60	0,60

Sample:	BGA 2-2			
Position	**matrix**	**matrix**	**matrix**	**matrix**
Mineral	**Ep**	**Ep**	**Ep**	**Ep**
Sample nr	**52 / 1 .**	**56 / 1 .**	**65 / 1 .**	**78 / 1 .**
Wt%				
SiO2	38,00	37,63	37,69	37,96
TiO2	0,08	0,07	0,14	0,14
Al2O3	24,94	25,04	25,70	25,44
Fe2O3	10,71	10,56	10,15	10,26
MnO	0,41	0,30	0,35	0,37
MgO	0,02	0,03	0,02	0,01
CaO	22,63	22,70	22,84	22,95
Na2O	0,03	0,00	0,02	0,02
K2O	0,00	0,06	0,04	0,02
Total	98,76	98,30	98,87	99,10
No.O	12,50	12,50	12,50	12,50
Si	3,03	3,01	2,99	3,01
Ti	0,01	0,00	0,01	0,01
Al	2,34	2,36	2,41	2,38
Fe3	0,64	0,64	0,61	0,61
Mn	0,03	0,02	0,02	0,02
Mg	0,00	0,00	0,00	0,00
Ca	1,93	1,95	1,94	1,95
Na	0,00	0,00	0,00	0,00
K	0,00	0,01	0,00	0,00
Sum	7,98	7,99	7,99	7,99

Sample:			BGA 2-2			
Position	**matrix**	**matrix**	**matrix**	**matrix**	**matrix**	**matrix**
Mineral	**Fsp**	**Fsp**	**Fsp**	**Fsp**	**Fsp**	**Fsp**
Sample nr	**48 / 1 .**	**50 / 1 .**	**54 / 1 .**	**64 / 1 .**	**67 / 1 .**	**69 / 1 .**
Wt%						
SiO2	67,40	68,50	67,33	67,82	67,77	68,75
TiO2	0,01	0,01				0,00
Al2O3	20,18	19,95	20,26	19,05	20,25	19,52
FeO	0,13	0,29	0,15	0,12	0,05	0,18
MnO			0,00			
MgO	0,01	0,00	0,02	0,01	0,02	0,03
CaO	1,18	0,56	0,87	0,33	0,84	0,30
Na2O	11,34	11,81	11,32	11,91	11,55	11,99
K2O	0,08	0,10	0,12	0,06	0,09	0,08
Total	100,33	101,22	100,07	99,28	100,58	100,85
No.O	8,00	8,00	8,00	8,00	8,00	8,00
Or	0,46	0,55	0,67	0,35	0,49	0,44
Si	2,94	2,95	2,94	2,98	2,94	2,97
Ti	0,00	0,00	0,00	0,00	0,00	0,00
Al	1,04	1,01	1,04	0,99	1,04	0,99
Fe2	0,00	0,01	0,01	0,00	0,00	0,01
Mn	0,00	0,00	0,00	0,00	0,00	0,00
Mg	0,00	0,00	0,00	0,00	0,00	0,00
Ca	0,06	0,03	0,04	0,02	0,04	0,01
Na	0,96	0,99	0,96	1,01	0,97	1,01
K	0,00	0,01	0,01	0,00	0,00	0,00
Sum	5,00	5,00	5,00	5,00	5,00	5,00
An	5,42	2,54	4,04	1,48	3,85	1,34
Ab	94,12	96,90	95,29	98,17	95,66	98,22

Sample:			BGA 2-2					
Position	**matrix**	**matrix**	**matrix**	**matrix**	**matrix**	**matrix**	**matrix**	**matrix**
Mineral	**Ms**	**Ms**	**Ms**	**Ms**	**Ms**	**Ms**	**Ms**	**Ms**
Sample nr	**57 / 1 .**	**44 / 1 .**	**53 / 1 .**	**61 / 1 .**	**66 / 1 .**	**70 / 1 .**	**74 / 1 .**	**51 / 1 .**
Wt%								
SiO2	46,71	48,41	46,98	46,92	47,80	46,19	45,93	49,10
TiO2	0,54	0,54	0,54	0,45	0,42	0,61	0,61	0,39
Al2O3	31,79	30,04	29,81	29,93	30,08	30,01	30,74	29,58
FeO	3,24	3,15	3,71	3,28	3,16	4,60	3,12	3,17
MnO	0,00	0,05	0,01		0,03	0,03		0,04
MgO	2,17	2,67	2,43	2,11	2,54	2,76	1,87	3,07
CaO			0,02			0,01		
Na2O	0,33	0,22	0,36	0,53	0,35	0,23	0,32	0,27
K2O	10,17	10,73	10,06	9,70	10,34	10,10	10,28	10,06
Total	94,96	95,80	93,92	92,91	94,70	94,54	92,87	95,69
No.O	11,00	11,00	11,00	11,00	11,00	11,00	11,00	11,00
Si	6,30	6,48	6,42	6,45	6,46	6,31	6,34	6,55
Ti	0,05	0,05	0,06	0,05	0,04	0,06	0,06	0,04
Al	5,05	4,74	4,80	4,85	4,79	4,83	5,00	4,65
Fe2	0,37	0,35	0,42	0,38	0,36	0,53	0,36	0,35
Mn	0,00	0,01	0,00	0,00	0,00	0,00	0,00	0,00
Mg	0,44	0,53	0,50	0,43	0,51	0,56	0,38	0,61
Ba	0,00	0,00	0,00	0,00	0,00	0,00	0,00	0,00
Na	0,09	0,06	0,10	0,14	0,09	0,06	0,08	0,07
K	1,75	1,83	1,75	1,70	1,78	1,76	1,81	1,71
Sum	14,04	14,04	14,05	14,00	14,04	14,12	14,04	13,98

Garnet profile MOK

MOK garnet profile Steps 15 µm										
	130 / 1 . Grt	131 / 1 . Grt	132 / 1 . Grt	133 / 1 . Grt	134 / 1 . Grt	135 / 1 . Grt	136 / 1 . Grt	137 / 1 . Grt	138 / 1 . Grt	139 / 1 . Grt
SiO2	37,77	37,28	37,47	37,54	37,47	37,00	37,38	37,43	37,02	37,30
TiO2	0,00	0,02	0,02	0,01	0,01	0,00	0,01	0,02	0,03	0,02
Al2O3	21,19	21,38	21,21	21,04	21,03	21,15	20,99	20,85	20,93	20,76
FeO	36,09	35,98	36,09	36,49	36,21	36,41	36,36	36,59	36,35	36,72
MnO	0,06	0,09	0,09	0,15	0,12	0,13	0,12	0,15	0,12	0,14
MgO	3,40	3,26	3,28	3,31	3,17	3,20	3,05	3,15	3,00	2,97
CaO	1,70	1,91	1,86	1,91	2,25	1,74	1,79	1,75	1,93	1,93
Na2O	0,01	0,01	0,02	0,01	0,01	0,05	0,04	0,02	0,01	0,03
K2O	0,00	0,00	0,00	0,00	0,02	0,00	0,00	0,01	0,00	0,00
Total	100,23	99,93	100,02	100,44	100,28	99,69	99,73	99,96	99,39	99,87
No. O	12,00	12,00	12,00	12,00	12,00	12,00	12,00	12,00	12,00	12,00
Si	3,01	2,99	3,00	3,00	3,00	2,99	3,01	3,01	3,00	3,01
Al	2,00	2,01	2,01	1,99	1,99	2,00	1,99	1,98	2,00	1,98
Fe2+	2,42	2,43	2,43	2,43	2,42	2,46	2,46	2,46	2,46	2,47
Mn	0,00	0,01	0,01	0,01	0,01	0,01	0,01	0,01	0,01	0,01
Mg	0,40	0,39	0,39	0,39	0,38	0,39	0,37	0,38	0,36	0,36
Ca	0,15	0,16	0,16	0,16	0,19	0,15	0,15	0,15	0,17	0,17
Total	7,99	8,00	8,00	8,00	8,00	8,01	7,99	7,99	8,00	8,00
Almandine	81,39	81,30	81,37	81,01	80,63	81,76	82,31	81,88	82,05	82,10
Grossular	4,88	5,49	5,33	5,00	6,11	5,04	5,19	4,73	5,53	4,96
Pyrope	13,59	13,02	13,10	13,20	12,65	12,90	12,24	12,69	12,09	12,00
Spessartine	0,14	0,19	0,20	0,33	0,27	0,30	0,27	0,35	0,28	0,31

MOK garnet profile

Steps 15 µm

	140 / 1 . Grt	141 / 1 . Grt	142 / 1 . Grt	143 / 1 . Grt	144 / 1 . Grt	145 / 1 . Grt	146 / 1 . Grt	147 / 1 . Grt	148 / 1 . Grt	149 / 1 . Grt
SiO2	37,12	37,23	37,15	37,06	36,99	37,01	37,12	36,95	37,17	36,97
TiO2	0,01	0,01	0,01	0,01	0,03	0,01	0,03	0,02	0,00	0,03
Al2O3	21,03	20,93	21,16	20,86	20,88	21,05	20,93	20,91	21,07	20,96
FeO	36,59	36,71	36,38	36,67	36,31	36,48	36,73	36,55	36,59	36,47
MnO	0,12	0,17	0,19	0,21	0,19	0,19	0,16	0,22	0,24	0,26
MgO	2,89	2,91	2,88	2,89	2,87	2,96	2,90	2,82	2,84	2,85
CaO	1,92	1,85	1,91	1,86	2,01	1,85	1,93	1,90	1,89	1,91
Na2O	0,02	0,01	0,01	0,01	0,04	0,04	0,01	0,02	0,03	0,03
K2O	0,01	0,00	0,00	0,00	0,01	0,01	0,01	0,00	0,00	0,01
Total	99,70	99,81	99,70	99,58	99,33	99,61	99,82	99,38	99,83	99,47
No. O	12,00	12,00	12,00	12,00	12,00	12,00	12,00	12,00	12,00	12,00
Si	3,00	3,01	3,00	3,00	3,00	2,99	3,00	3,00	3,00	3,00
Al	2,00	1,99	2,01	1,99	2,00	2,00	1,99	2,00	2,00	2,00
Fe2+	2,48	2,48	2,47	2,48	2,46	2,47	2,47	2,48	2,47	2,47
Mn	0,01	0,01	0,01	0,01	0,01	0,01	0,01	0,01	0,02	0,02
Mg	0,35	0,35	0,35	0,35	0,35	0,36	0,35	0,34	0,34	0,34
Ca	0,17	0,16	0,17	0,16	0,17	0,16	0,17	0,17	0,16	0,17
Total	8,00	8,00	8,00	8,00	8,00	8,00	8,00	8,00	8,00	8,00
Almandine	82,59	82,57	82,46	82,49	82,16	82,29	82,41	82,63	82,59	82,38
Grossular	5,53	5,25	5,52	5,06	5,83	5,35	5,26	5,49	5,46	5,55
Pyrope	11,61	11,69	11,58	11,64	11,58	11,94	11,65	11,37	11,39	11,47
Spessartine	0,27	0,38	0,44	0,48	0,43	0,42	0,37	0,50	0,55	0,60

MOK garnet profile

Steps 15 µm

	150 / 1 . Grt	151 / 1 . Grt	152 / 1 . Grt	153 / 1 . Grt	154 / 1 . Grt	155 / 1 . Grt	156 / 1 . Grt	157 / 1 . Grt	158 / 1 . Grt	159 / 1 . Grt
SiO2	37,20	36,70	37,19	36,92	36,69	36,71	36,99	36,75	36,85	36,66
TiO2	0,01	0,03	0,00	0,01	0,01	0,03	0,01	0,00	0,00	0,02
Al2O3	20,87	20,92	20,98	20,64	20,67	21,00	21,11	20,71	20,96	20,88
FeO	36,68	36,63	36,96	36,61	36,70	36,75	36,85	36,34	36,76	36,55
MnO	0,29	0,29	0,19	0,29	0,30	0,31	0,34	0,38	0,32	0,36
MgO	2,75	2,83	2,92	2,89	2,89	2,87	2,92	2,71	2,81	2,73
CaO	1,89	1,87	1,83	1,92	1,87	1,92	1,83	1,82	1,84	1,89
Na2O	0,00	0,01	0,02	0,00	0,00	0,03	0,00	0,02	0,03	0,04
K2O	0,00	0,01	0,00	0,00	0,01	0,00	0,01	0,00	0,00	0,00
Total	99,69	99,28	100,09	99,29	99,15	99,61	100,06	98,73	99,57	99,13
No. O	12,00	12,00	12,00	12,00	12,00	12,00	12,00	12,00	12,00	12,00
Si	3,01	2,98	3,00	3,00	2,99	2,98	2,98	3,00	2,99	2,99
Al	1,99	1,99	1,99	1,98	1,97	1,98	1,99	2,00	1,99	1,99
Fe2+	2,48	2,48	2,48	2,47	2,48	2,48	2,48	2,48	2,49	2,49
Mn	0,02	0,02	0,01	0,02	0,02	0,02	0,02	0,03	0,02	0,02
Mg	0,33	0,34	0,35	0,35	0,35	0,35	0,35	0,33	0,34	0,33
Ca	0,16	0,16	0,16	0,17	0,16	0,17	0,16	0,16	0,16	0,17
Total	8,00	8,01	8,00	8,00	8,01	8,01	8,01	8,00	8,01	8,01
Almandine	82,74	82,38	82,59	82,06	82,11	82,04	82,17	82,76	82,53	82,53
Grossular	5,43	5,09	4,86	4,61	4,35	4,98	4,93	5,26	5,01	5,27
Pyrope	11,12	11,50	11,69	11,70	11,75	11,65	11,77	11,03	11,38	11,12
Spessartine	0,66	0,66	0,44	0,67	0,69	0,71	0,77	0,88	0,73	0,82

MOK garnet profile

Steps 15 µm

	160 / 1 . Grt	161 / 1 . Grt	162 / 1 . Grt	163 / 1 . Grt	164 / 1 . Grt	165 / 1 . Grt	166 / 1 . Grt	167 / 1 . Grt	168 / 1 . Grt	169 / 1 . Grt
SiO2	36,42	36,75	36,84	36,40	36,74	36,73	37,02	36,95	36,88	36,99
TiO2	0,00	0,00	0,02	0,04	0,02	0,01	0,01	0,02	0,02	0,01
Al2O3	20,83	20,71	20,82	20,66	20,93	20,62	21,00	20,81	21,06	20,93
FeO	36,86	36,55	36,57	36,33	36,22	36,55	36,42	36,21	36,65	36,46
MnO	0,38	0,39	0,40	0,46	0,45	0,43	0,46	0,46	0,54	0,52
MgO	2,88	2,83	2,80	2,78	2,76	2,81	2,74	2,74	2,79	2,73
CaO	1,82	1,94	1,91	1,96	1,94	1,96	1,95	1,89	1,92	1,86
Na2O	0,00	0,01	0,00	0,02	0,04	0,03	0,03	0,01	0,01	0,03
K2O	0,00	0,00	0,00	0,00	0,00	0,00	0,00	0,00	0,00	0,01
Total	99,18	99,17	99,36	98,64	99,11	99,14	99,62	99,09	99,86	99,54
No. O	12,00	12,00	12,00	12,00	12,00	12,00	12,00	12,00	12,00	12,00
Si	2,97	2,99	2,99	2,98	2,99	2,99	3,00	3,01	2,98	3,00
Al	1,97	1,98	1,99	1,98	2,00	1,97	2,00	2,00	1,99	2,00
Fe2+	2,49	2,47	2,47	2,47	2,47	2,47	2,47	2,47	2,47	2,47
Mn	0,03	0,03	0,03	0,03	0,03	0,03	0,03	0,03	0,04	0,04
Mg	0,35	0,34	0,34	0,34	0,33	0,34	0,33	0,33	0,34	0,33
Ca	0,16	0,17	0,17	0,17	0,17	0,17	0,17	0,16	0,17	0,16
Total	8,02	8,01	8,01	8,01	8,00	8,01	8,00	8,00	8,01	8,00
Almandine	81,98	81,99	82,18	81,80	82,09	81,88	82,27	82,35	81,93	82,43
Grossular	4,12	4,76	5,02	4,86	5,67	4,59	5,64	5,50	5,21	5,40
Pyrope	11,78	11,47	11,33	11,37	11,20	11,40	11,04	11,10	11,27	10,99
Spessartine	0,87	0,89	0,92	1,07	1,04	1,00	1,05	1,05	1,23	1,19

MOK garnet profile

Steps 15 µm

	170 / 1 . Grt	171 / 1 . Grt	172 / 1 . Grt	173 / 1 . Grt	174 / 1 . Grt	175 / 1 . Grt	176 / 1 . Grt	177 / 1 . Grt	178 / 1 . Grt	179 / 1 . Grt
SiO2	37,00	36,99	36,72	36,99	37,09	37,11	36,80	37,05	37,11	36,99
TiO2	0,00	0,00	0,02	0,02	0,01	0,01	0,02	0,02	0,01	0,04
Al2O3	20,88	20,83	20,97	20,89	20,97	21,06	20,95	21,07	21,03	20,97
FeO	36,76	36,82	36,75	36,97	36,71	36,55	36,49	36,77	37,04	36,53
MnO	0,53	0,48	0,52	0,48	0,49	0,47	0,41	0,44	0,52	0,42
MgO	2,68	2,81	2,80	2,73	2,67	2,70	2,76	2,76	2,78	2,76
CaO	1,90	1,92	1,89	1,91	1,91	1,86	1,95	1,93	1,94	2,03
Na2O	0,01	0,07	0,02	0,04	0,02	0,06	0,03	0,04	0,01	0,01
K2O	0,00	0,01	0,01	0,00	0,00	0,01	0,00	0,01	0,00	0,00
Total	99,76	99,92	99,69	100,02	99,86	99,83	99,42	100,08	100,42	99,77
No. O	12,00	12,00	12,00	12,00	12,00	12,00	12,00	12,00	12,00	12,00
Si	3,00	2,99	2,98	2,99	3,00	3,00	2,99	2,99	2,99	2,99
Al	1,99	1,98	1,98	1,98	2,00	2,00	1,99	1,99	1,98	1,99
Fe2+	2,48	2,47	2,48	2,48	2,48	2,48	2,47	2,48	2,48	2,47
Mn	0,04	0,03	0,04	0,03	0,03	0,03	0,03	0,03	0,04	0,03
Mg	0,32	0,34	0,34	0,33	0,32	0,32	0,33	0,33	0,33	0,33
Ca	0,16	0,17	0,16	0,17	0,17	0,16	0,17	0,17	0,17	0,18
Total	8,00	8,01	8,01	8,01	8,00	8,00	8,01	8,01	8,01	8,00
Almandine	82,49	82,04	81,91	82,35	82,66	82,71	82,18	82,32	82,07	82,03
Grossular	5,04	4,65	4,77	4,71	5,41	5,37	5,48	5,36	4,80	5,65
Pyrope	10,79	11,31	11,37	11,00	10,73	10,85	11,20	11,09	11,15	11,13
Spessartine	1,21	1,09	1,19	1,11	1,11	1,07	0,95	1,01	1,18	0,95

MOK garnet profile Steps 15 µm										
	180 / 1 . Grt	181 / 1 . Grt	182 / 1 . Grt	183 / 1 . Grt	184 / 1 . Grt	185 / 1 . Grt	186 / 1 . Grt	187 / 1 . Grt	188 / 1 . Grt	189 / 1 . Grt
SiO2	37,06	36,94	36,92	36,76	37,08	37,29	37,15	37,29	37,02	37,11
TiO2	0,01	0,00	0,01	0,00	0,02	0,03	0,04	0,03	0,04	0,03
Al2O3	20,90	20,89	20,94	21,02	21,02	20,88	21,20	20,99	21,20	20,90
FeO	36,92	36,76	36,86	36,84	36,85	36,83	37,08	36,53	36,81	36,60
MnO	0,41	0,45	0,38	0,48	0,50	0,42	0,47	0,43	0,42	0,35
MgO	2,77	2,78	2,82	2,80	2,83	2,80	2,78	2,79	2,80	2,98
CaO	1,91	1,88	1,91	1,91	1,98	1,94	1,91	1,98	2,02	2,02
Na2O	0,03	0,03	0,01	0,02	0,03	0,00	0,01	0,00	0,03	0,04
K2O	0,00	0,01	0,00	0,00	0,02	0,00	0,01	0,00	0,00	0,00
Total	100,00	99,74	99,85	99,83	100,33	100,18	100,64	100,04	100,34	100,04
No. O	12,00	12,00	12,00	12,00	12,00	12,00	12,00	12,00	12,00	12,00
Si	2,99	2,99	2,99	2,98	2,99	3,00	2,98	3,00	2,98	2,99
Al	1,98	1,99	1,98	1,98	1,98	1,98	1,99	1,99	1,99	1,98
Fe2+	2,48	2,48	2,48	2,48	2,47	2,47	2,48	2,46	2,47	2,45
Mn	0,03	0,03	0,03	0,03	0,03	0,03	0,03	0,03	0,03	0,02
Mg	0,33	0,34	0,34	0,34	0,34	0,34	0,33	0,33	0,34	0,36
Ca	0,16	0,16	0,17	0,17	0,17	0,17	0,16	0,17	0,17	0,17
Total	8,01	8,01	8,01	8,01	8,01	8,00	8,01	8,00	8,01	8,01
Almandine	82,40	82,27	82,21	82,00	81,76	82,21	82,27	82,10	81,92	81,38
Grossular	4,82	4,86	4,85	4,83	4,96	5,04	5,10	5,71	5,55	5,00
Pyrope	11,14	11,22	11,39	11,35	11,38	11,23	11,16	11,19	11,29	11,99
Spessartine	0,95	1,04	0,86	1,10	1,15	0,96	1,06	0,99	0,95	0,79

MOK garnet profile Steps 15 µm										
	190 / 1 . Grt	191 / 1 . Grt	192 / 1 . Grt	193 / 1 . Grt	194 / 1 . Grt	195 / 1 . Grt	196 / 1 . Grt	197 / 1 . Grt	198 / 1 . Grt	199 / 1 . Grt
SiO2	36,90	36,82	37,16	37,04	36,68	37,23	37,11	36,80	37,05	36,63
TiO2	0,04	0,02	0,01	0,01	0,03	0,01	0,01	0,01	0,02	0,01
Al2O3	21,09	20,96	20,71	21,21	20,82	20,85	20,86	20,93	20,83	20,94
FeO	36,60	36,63	36,36	36,71	36,49	36,54	36,84	36,90	36,77	37,04
MnO	0,31	0,22	0,27	0,30	0,36	0,35	0,33	0,35	0,32	0,27
MgO	3,10	2,95	3,03	3,06	2,97	2,86	2,86	2,94	2,80	2,85
CaO	1,97	1,98	1,90	1,81	1,88	1,88	1,85	1,87	1,87	1,89
Na2O	0,02	0,03	0,05	0,06	0,03	0,04	0,04	0,02	0,04	0,04
K2O	0,00	0,01	0,00	0,02	0,00	0,01	0,02	0,01	0,01	0,01
Total	100,02	99,61	99,49	100,20	99,26	99,75	99,92	99,83	99,71	99,66
No. O	12,00	12,00	12,00	12,00	12,00	12,00	12,00	12,00	12,00	12,00
Si	2,98	2,98	3,01	2,98	2,98	3,01	3,00	2,98	3,00	2,97
Al	1,98	1,98	1,98	1,99	1,98	1,99	1,99	1,98	1,99	1,98
Fe2+	2,45	2,47	2,45	2,47	2,47	2,47	2,48	2,48	2,48	2,49
Mn	0,02	0,02	0,02	0,02	0,02	0,02	0,02	0,02	0,02	0,02
Mg	0,37	0,36	0,37	0,37	0,36	0,34	0,34	0,36	0,34	0,34
Ca	0,17	0,17	0,17	0,16	0,16	0,16	0,16	0,16	0,16	0,16
Total	8,01	8,01	8,00	8,01	8,01	8,00	8,00	8,01	8,00	8,02
Almandine	81,05	81,78	81,58	81,77	81,63	82,22	82,42	81,82	82,58	82,28
Grossular	4,94	5,12	4,93	5,02	4,66	5,25	4,73	4,38	4,95	4,50
Pyrope	12,53	11,96	12,26	12,31	12,06	11,54	11,49	11,92	11,28	11,58
Spessartine	0,70	0,51	0,62	0,68	0,83	0,80	0,75	0,81	0,73	0,62

MOK garnet profile

Steps 15 µm

	200 / 1 . Grt	201 / 1 . Grt	202 / 1 . Grt	203 / 1 . Grt	204 / 1 . Grt	205 / 1 . Grt	206 / 1 . Grt	207 / 1 . Grt	208 / 1 . Grt	209 / 1 . Grt
SiO2	37,04	36,95	36,82	36,92	36,77	36,84	36,55	36,77	36,78	36,80
TiO2	0,01	0,00	0,01	0,01	0,00	0,02	0,02	0,02	0,01	0,00
Al2O3	20,82	20,81	21,02	20,94	21,06	20,72	20,85	20,68	21,05	20,98
FeO	36,83	36,65	37,11	36,87	36,48	36,74	36,78	36,80	36,71	36,75
MnO	0,35	0,25	0,28	0,26	0,23	0,24	0,22	0,25	0,15	0,17
MgO	2,90	2,83	2,84	2,89	2,90	2,87	2,89	2,96	3,00	2,94
CaO	1,89	1,87	1,87	1,90	1,89	1,93	1,90	1,90	1,96	1,84
Na2O	0,02	0,02	0,03	0,05	0,05	0,04	0,04	0,03	0,02	0,04
K2O	0,01	0,01	0,01	0,02	0,01	0,01	0,01	0,02	0,02	0,00
Total	99,88	99,39	100,00	99,85	99,39	99,41	99,27	99,42	99,69	99,52
No. O	12,00	12,00	12,00	12,00	12,00	12,00	12,00	12,00	12,00	12,00
Si	2,99	3,00	2,98	2,99	2,98	2,99	2,98	2,99	2,98	2,98
Al	1,98	1,99	1,98	1,98	2,00	1,98	1,98	1,97	1,99	1,99
Fe2+	2,47	2,48	2,49	2,48	2,48	2,48	2,49	2,47	2,47	2,48
Mn	0,02	0,02	0,02	0,02	0,02	0,02	0,02	0,02	0,01	0,01
Mg	0,35	0,34	0,34	0,35	0,35	0,35	0,35	0,36	0,36	0,36
Ca	0,16	0,16	0,16	0,16	0,16	0,17	0,17	0,17	0,17	0,16
Total	8,01	8,00	8,01	8,01	8,01	8,01	8,02	8,01	8,01	8,01
Almandine	82,04	82,56	82,39	82,24	82,21	82,21	82,12	81,89	81,81	82,36
Grossular	4,55	5,02	4,62	4,81	5,50	4,69	4,63	4,20	5,12	4,92
Pyrope	11,69	11,44	11,51	11,65	11,74	11,61	11,80	12,00	12,14	11,91
Spessartine	0,80	0,58	0,65	0,61	0,54	0,55	0,51	0,57	0,35	0,38

MOK garnet profile

Steps 15 µm

	210 / 1 . Grt	211 / 1 . Grt	212 / 1 . Grt	213 / 1 . Grt	214 / 1 . Grt	215 / 1 . Grt	216 / 1 . Grt	217 / 1 . Grt	218 / 1 . Grt	219 / 1 . Grt
SiO2	36,84	37,12	36,87	37,35	37,36	36,93	37,05	37,30	37,08	37,38
TiO2	0,03	0,04	0,00	0,02	0,02	0,04	0,03	0,02	0,01	0,02
Al2O3	20,92	21,00	20,91	21,16	21,02	20,96	20,96	21,13	20,92	21,16
FeO	36,79	36,46	36,53	36,36	35,79	36,26	36,21	36,32	36,12	36,11
MnO	0,16	0,14	0,14	0,11	0,07	0,05	0,05	0,06	0,05	0,06
MgO	2,90	3,11	3,17	3,19	3,13	3,35	3,45	3,44	3,52	3,50
CaO	1,87	1,85	1,85	2,05	2,31	2,02	1,91	1,79	1,81	1,85
Na2O	0,04	0,04	0,02	0,04	0,00	0,03	0,02	0,03	0,00	0,03
K2O	0,00	0,00	0,01	0,00	0,00	0,01	0,01	0,00	0,01	0,00
Total	99,54	99,76	99,49	100,27	99,70	99,64	99,69	100,08	99,49	100,12
No. O	12,00	12,00	12,00	12,00	12,00	12,00	12,00	12,00	12,00	12,00
Si	2,99	3,00	2,99	3,00	3,01	2,98	2,99	2,99	2,99	3,00
Al	1,99	1,99	1,98	2,00	1,99	1,98	1,98	1,99	1,98	2,00
Fe2+	2,48	2,46	2,46	2,44	2,41	2,43	2,43	2,43	2,42	2,42
Mn	0,01	0,01	0,01	0,01	0,00	0,00	0,00	0,00	0,00	0,00
Mg	0,35	0,37	0,38	0,38	0,38	0,40	0,42	0,41	0,42	0,42
Ca	0,16	0,16	0,16	0,18	0,20	0,17	0,16	0,15	0,16	0,16
Total	8,01	8,00	8,01	8,00	8,00	8,01	8,01	8,00	8,01	8,00
Almandine	82,46	81,84	81,52	81,13	80,63	80,50	80,47	80,98	80,53	80,60
Grossular	4,94	5,18	4,63	5,78	6,66	4,99	4,75	4,92	4,55	5,22
Pyrope	11,74	12,51	12,80	12,72	12,56	13,53	13,90	13,74	14,14	13,96
Spessartine	0,37	0,31	0,31	0,26	0,15	0,12	0,12	0,13	0,11	0,14

Garnet profile OS-2

OS-2 garnet profile Steps 8 µm										
here	Grt 1 / 1 .	Grt 1 / 2 .	Grt 1 / 3 .	Grt 1 / 4 .	Grt 1 / 5 .	Grt 1 / 6 .	Grt 1 / 7 .	Grt 1 / 8 .	Grt 1 / 9 .	Grt 1 / 10 .
SiO2	37,31	36,87	37,12	37,10	37,15	36,97	36,85	36,89	37,12	39,14
TiO2	0,10	0,07	0,08	0,10	0,07	0,09	0,06	0,11	0,11	0,06
Al2O3	21,01	20,66	20,88	20,55	20,75	20,76	20,72	20,67	20,59	20,88
FeO	32,65	33,29	33,25	33,21	33,52	33,28	33,49	33,22	33,21	32,80
MnO	1,86	1,90	2,05	2,02	2,03	2,23	2,36	2,37	2,37	2,41
MgO	2,02	2,05	2,06	2,02	2,02	1,96	1,97	1,88	1,90	2,05
CaO	4,95	5,03	4,92	5,10	4,96	4,97	4,66	5,14	5,10	4,59
Total	99,90	99,92	100,41	100,17	100,56	100,31	100,18	100,37	100,47	101,93
No. O	12,00	12,00	12,00	12,00	12,00	12,00	12,00	12,00	12,00	12,00
Si	3,00	2,98	2,98	2,99	2,98	2,98	2,98	2,97	2,99	3,07
Al	1,99	1,97	1,98	1,96	1,97	1,97	1,98	1,97	1,96	1,93
Ti	0,01	0,00	0,00	0,01	0,00	0,01	0,00	0,01	0,01	0,00
Fe3+	0,00	0,04	0,03	0,04	0,04	0,04	0,04	0,05	0,05	0,00
Fe2+	2,20	2,21	2,21	2,19	2,21	2,20	2,22	2,19	2,19	2,17
Mn	0,13	0,13	0,14	0,14	0,14	0,15	0,16	0,16	0,16	0,16
Mg	0,24	0,25	0,25	0,24	0,24	0,23	0,24	0,23	0,23	0,24
Ca	0,43	0,44	0,42	0,44	0,43	0,43	0,40	0,44	0,44	0,39
Total	8,00	8,02	8,01	8,01	8,01	8,02	8,02	8,02	8,01	7,96
Almandine	73,39	72,76	72,83	72,54	72,94	72,60	73,07	72,02	72,24	72,88
Andradite	0,00	2,02	1,47	2,18	2,01	1,91	2,03	2,35	2,28	0,00
Grossular	14,28	12,59	12,73	12,54	12,29	12,50	11,52	12,57	12,45	13,33
Pyrope	8,10	8,27	8,29	8,13	8,12	7,88	7,96	7,61	7,62	8,27
Spessartine	4,24	4,36	4,69	4,60	4,64	5,10	5,42	5,45	5,42	5,52
Uvarovite	0,00	0,00	0,00	0,00	0,00	0,00	0,00	0,00	0,00	0,00
Total	99,69	99,15	99,30	99,58	99,33	99,11	99,01	98,92	99,43	97,09

OS-2 garnet profile Steps 8 µm										
here	Grt 1 / 11 .	Grt 1 / 12 .	Grt 1 / 13 .	Grt 1 / 14 .	Grt 1 / 15 .	Grt 1 / 16 .	Grt 1 / 17 .	Grt 1 / 18 .	Grt 1 / 19 .	Grt 1 / 20 .
SiO2	37,13	36,88	36,94	36,77	38,58	36,77	36,75	36,63	36,84	36,69
TiO2	0,11	0,11	0,08	0,09	0,08	0,10	0,12	0,09	0,07	0,06
Al2O3	20,63	20,58	20,55	20,32	21,01	20,44	20,84	20,52	20,50	20,37
FeO	32,67	33,16	33,06	33,07	32,63	32,79	32,37	32,69	32,45	32,73
MnO	2,61	2,73	2,63	2,92	2,80	2,97	3,00	2,99	3,16	3,29
MgO	1,90	1,86	1,83	1,79	1,91	1,78	1,79	1,72	1,66	1,68
CaO	5,17	4,83	4,84	5,04	5,23	5,18	5,53	5,39	5,37	5,15
Total	100,28	100,23	100,00	100,11	102,26	100,14	100,47	100,12	100,14	100,09
No. O	12,00	12,00	12,00	12,00	12,00	12,00	12,00	12,00	12,00	12,00
Si	2,99	2,98	2,99	2,98	3,03	2,97	2,96	2,96	2,98	2,97
Al	1,96	1,96	1,96	1,94	1,95	1,95	1,98	1,96	1,96	1,95
Ti	0,01	0,01	0,01	0,01	0,00	0,01	0,01	0,01	0,00	0,00
Fe3+	0,04	0,05	0,04	0,07	0,01	0,06	0,05	0,06	0,05	0,06
Fe2+	2,16	2,19	2,20	2,17	2,13	2,16	2,13	2,15	2,14	2,15
Mn	0,18	0,19	0,18	0,20	0,19	0,20	0,20	0,21	0,22	0,23
Mg	0,23	0,22	0,22	0,22	0,22	0,22	0,22	0,21	0,20	0,20
Ca	0,45	0,42	0,42	0,44	0,44	0,45	0,48	0,47	0,47	0,45
Total	8,01	8,02	8,01	8,02	7,98	8,02	8,03	8,03	8,02	8,02
Almandine	71,52	72,17	72,52	71,30	71,05	70,83	69,70	70,33	70,38	70,53
Andradite	1,90	2,34	2,02	3,28	0,62	2,93	2,32	3,00	2,62	3,20
Grossular	13,02	11,68	12,03	11,42	14,39	12,17	13,79	12,76	13,00	11,82
Pyrope	7,62	7,53	7,40	7,28	7,60	7,23	7,27	6,98	6,73	6,84
Spessartine	5,95	6,28	6,02	6,73	6,34	6,83	6,91	6,92	7,26	7,60
Uvarovite	0,00	0,00	0,00	0,00	0,00	0,00	0,00	0,00	0,00	0,00
Total	99,58	99,12	99,48	99,05	98,18	98,95	98,38	98,58	99,13	98,90

OS-2 garnet profile Steps 8 µm										
here	Grt 1 / 21 .	Grt 1 / 22 .	Grt 1 / 23 .	Grt 1 / 24 .	Grt 1 / 25 .	Grt 1 / 26 .	Grt 1 / 27 .	Grt 1 / 28 .	Grt 1 / 29 .	Grt 1 / 30 .
SiO2	36,71	36,30	36,67	36,60	36,50	36,46	36,87	36,75	36,60	36,84
TiO2	0,09	0,12	0,08	0,08	0,08	0,11	0,07	0,07	0,08	0,09
Al2O3	20,46	20,56	20,45	20,58	20,44	20,53	20,41	20,23	20,37	20,63
FeO	32,26	32,35	32,50	32,48	32,19	32,66	31,18	31,96	32,02	32,06
MnO	3,31	3,40	3,40	3,49	3,46	3,66	3,51	3,66	3,80	3,94
MgO	1,66	1,70	1,70	1,66	1,67	1,69	1,50	1,56	1,58	1,48
CaO	5,21	5,14	5,24	4,90	5,46	4,60	5,96	5,34	5,13	5,43
Total	99,77	99,64	100,13	99,85	99,90	99,79	99,58	99,65	99,66	100,56
No. O	12,00	12,00	12,00	12,00	12,00	12,00	12,00	12,00	12,00	12,00
Si	2,98	2,95	2,97	2,97	2,96	2,97	2,99	2,99	2,98	2,97
Al	1,96	1,98	1,96	1,97	1,96	1,97	1,96	1,94	1,96	1,97
Ti	0,01	0,01	0,01	0,00	0,00	0,01	0,00	0,00	0,00	0,01
Fe3+	0,05	0,05	0,06	0,04	0,06	0,05	0,04	0,06	0,05	0,05
Fe2+	2,14	2,15	2,14	2,16	2,12	2,17	2,07	2,12	2,13	2,11
Mn	0,23	0,23	0,23	0,24	0,24	0,25	0,24	0,25	0,26	0,27
Mg	0,20	0,21	0,20	0,20	0,20	0,20	0,18	0,19	0,19	0,18
Ca	0,45	0,45	0,45	0,43	0,47	0,40	0,52	0,46	0,45	0,47
Total	8,02	8,03	8,02	8,02	8,03	8,02	8,01	8,01	8,02	8,02
Almandine	70,42	69,92	69,94	70,86	69,14	71,08	68,54	69,68	69,77	69,19
Andradite	2,43	2,77	3,10	2,27	3,22	2,50	2,13	2,89	2,68	2,56
Grossular	12,78	12,40	12,21	12,06	12,80	11,01	15,19	12,67	12,32	13,22
Pyrope	6,72	6,98	6,90	6,74	6,81	6,90	6,08	6,32	6,43	5,98
Spessartine	7,64	7,94	7,85	8,07	8,03	8,51	8,06	8,44	8,80	9,05
Uvarovite	0,00	0,00	0,00	0,00	0,00	0,00	0,00	0,00	0,00	0,00
Total	99,16	98,18	98,73	98,83	98,47	98,61	99,65	99,48	99,08	98,84

OS-2 garnet profile Steps 8 µm										
here	Grt 1 / 31 .	Grt 1 / 32 .	Grt 1 / 33 .	Grt 1 / 34 .	Grt 1 / 35 .	Grt 1 / 36 .	Grt 1 / 37 .	Grt 1 / 38 .	Grt 1 / 39 .	Grt 1 / 40 .
SiO2	36,76	36,75	36,78	36,49	35,64	36,54	36,97	36,88	36,67	36,82
TiO2	0,12	0,10	0,11	0,09	0,08	0,10	0,14	0,11	0,10	0,09
Al2O3	20,34	20,49	20,44	20,54	17,29	20,34	20,59	20,47	20,19	20,20
FeO	31,48	31,51	31,92	31,41	28,71	31,05	31,09	31,04	31,25	30,60
MnO	3,89	3,89	4,10	4,29	3,49	4,20	4,44	4,64	4,68	4,58
MgO	1,47	1,42	1,52	1,48	2,52	1,37	1,35	1,32	1,32	1,31
CaO	5,82	5,63	5,56	5,69	4,57	5,91	6,14	6,09	5,80	6,29
Total	99,98	99,85	100,54	100,10	92,45	99,61	100,82	100,65	100,13	100,00
No. O	12,00	12,00	12,00	12,00	12,00	12,00	12,00	12,00	12,00	12,00
Si	2,98	2,98	2,97	2,96	3,09	2,97	2,97	2,97	2,97	2,98
Al	1,95	1,96	1,95	1,97	1,78	1,96	1,96	1,95	1,94	1,94
Ti	0,01	0,01	0,01	0,01	0,01	0,01	0,01	0,01	0,01	0,01
Fe3+	0,06	0,04	0,07	0,06	0,11	0,06	0,06	0,06	0,07	0,07
Fe2+	2,08	2,09	2,09	2,07	1,98	2,06	2,03	2,03	2,05	2,01
Mn	0,27	0,27	0,28	0,29	0,26	0,29	0,30	0,32	0,32	0,31
Mg	0,18	0,17	0,18	0,18	0,33	0,17	0,16	0,16	0,16	0,16
Ca	0,51	0,49	0,48	0,49	0,42	0,52	0,53	0,53	0,50	0,55
Total	8,02	8,01	8,02	8,03	7,97	8,02	8,02	8,02	8,02	8,02
Almandine	68,12	68,87	68,19	67,28	64,25	67,33	66,59	66,32	66,85	65,87
Andradite	2,95	2,26	3,35	3,08	5,75	2,87	2,84	3,20	3,71	3,35
Grossular	14,01	14,15	12,85	13,63	9,33	14,47	14,96	14,49	13,25	14,94
Pyrope	5,95	5,76	6,17	6,05	11,56	5,58	5,43	5,34	5,38	5,30
Spessartine	8,97	8,96	9,44	9,96	9,10	9,74	10,18	10,65	10,81	10,54
Uvarovite	0,00	0,00	0,00	0,00	0,00	0,00	0,00	0,00	0,00	0,00
Total	99,15	99,22	98,73	98,30	94,34	98,92	98,89	98,87	98,95	99,32

OS-2 garnet profile Steps 8 µm										
here	Grt 1 / 41 .	Grt 1 / 42 .	Grt 1 / 43 .	Grt 1 / 44 .	Grt 1 / 45 .	Grt 1 / 46 .	Grt 1 / 47 .	Grt 1 / 48 .	Grt 1 / 49 .	Grt 1 / 50 .
SiO2	36,83	36,50	36,51	36,72	36,68	36,52	36,74	36,68	36,80	36,47
TiO2	0,11	0,14	0,10	0,14	0,10	0,12	0,10	0,09	0,08	0,09
Al2O3	20,51	20,64	20,55	20,36	20,39	20,24	20,22	20,42	20,43	20,03
FeO	30,45	30,67	30,80	30,77	31,11	30,14	30,80	30,22	29,94	29,76
MnO	4,87	4,91	5,07	5,21	5,31	5,25	5,41	5,45	5,61	5,64
MgO	1,27	1,29	1,27	1,28	1,25	1,23	1,17	1,26	1,24	1,21
CaO	6,24	6,34	5,55	6,22	5,52	6,52	5,83	5,70	6,02	6,00
Total	100,38	100,58	99,94	100,84	100,47	100,15	100,40	99,91	100,21	99,31
No. O	12,00	12,00	12,00	12,00	12,00	12,00	12,00	12,00	12,00	12,00
Si	2,97	2,95	2,97	2,96	2,97	2,96	2,98	2,98	2,98	2,98
Al	1,96	1,97	1,97	1,94	1,95	1,94	1,94	1,96	1,95	1,94
Ti	0,01	0,01	0,01	0,01	0,01	0,01	0,01	0,01	0,00	0,01
Fe3+	0,06	0,07	0,05	0,08	0,07	0,08	0,07	0,05	0,06	0,07
Fe2+	2,00	2,00	2,04	1,99	2,04	1,96	2,01	2,00	1,97	1,97
Mn	0,33	0,34	0,35	0,36	0,36	0,36	0,37	0,37	0,38	0,39
Mg	0,15	0,15	0,15	0,15	0,15	0,15	0,14	0,15	0,15	0,15
Ca	0,54	0,55	0,48	0,54	0,48	0,57	0,51	0,50	0,52	0,53
Total	8,02	8,03	8,02	8,03	8,02	8,03	8,02	8,02	8,02	8,02
Almandine	65,51	64,74	66,75	64,62	66,52	63,66	65,76	65,65	64,55	64,34
Andradite	2,81	3,40	2,52	4,08	3,35	4,06	3,68	2,57	2,84	3,48
Grossular	15,34	15,21	13,79	14,08	12,78	15,08	13,31	14,07	14,69	14,14
Pyrope	5,14	5,25	5,18	5,20	5,07	5,01	4,76	5,12	5,01	4,94
Spessartine	11,21	11,39	11,76	12,02	12,27	12,19	12,48	12,59	12,91	13,10
Uvarovite	0,00	0,00	0,00	0,00	0,00	0,00	0,00	0,00	0,00	0,00
Total	98,95	97,87	98,64	98,36	98,73	98,43	98,97	99,10	99,09	99,19

OS-2 garnet profile Steps 8 µm										
here	Grt 1 / 51 .	Grt 1 / 52 .	Grt 1 / 53 .	Grt 1 / 54 .	Grt 1 / 55 .	Grt 1 / 56 .	Grt 1 / 57 .	Grt 1 / 58 .	Grt 1 / 59 .	Grt 1 / 60 .
SiO2	36,96	37,16	36,71	36,82	36,56	36,57	36,73	36,97	36,88	36,37
TiO2	0,09	0,11	0,14	0,15	0,16	0,16	0,14	0,14	0,14	0,12
Al2O3	20,27	20,27	20,15	20,47	20,60	20,26	20,38	20,13	20,31	20,18
FeO	30,33	29,45	30,11	29,41	29,84	29,40	28,90	29,34	29,58	29,01
MnO	5,63	5,60	5,60	5,80	6,01	5,90	6,07	6,38	6,20	6,42
MgO	1,22	1,14	1,25	1,15	1,14	1,19	1,12	1,13	1,16	1,19
CaO	5,97	6,43	6,36	6,65	6,15	6,50	6,42	6,30	6,30	5,93
Total	100,58	100,25	100,47	100,54	100,56	100,10	99,85	100,52	100,70	99,32
No. O	12,00	12,00	12,00	12,00	12,00	12,00	12,00	12,00	12,00	12,00
Si	2,98	3,00	2,97	2,97	2,95	2,97	2,98	2,99	2,97	2,97
Al	1,93	1,93	1,93	1,95	1,97	1,94	1,95	1,92	1,94	1,95
Ti	0,01	0,01	0,01	0,01	0,01	0,01	0,01	0,01	0,01	0,01
Fe3+	0,07	0,05	0,08	0,06	0,06	0,07	0,05	0,07	0,07	0,06
Fe2+	1,98	1,94	1,95	1,92	1,96	1,92	1,91	1,91	1,92	1,92
Mn	0,38	0,38	0,38	0,40	0,41	0,41	0,42	0,44	0,42	0,44
Mg	0,15	0,14	0,15	0,14	0,14	0,14	0,13	0,14	0,14	0,14
Ca	0,52	0,56	0,55	0,57	0,53	0,56	0,56	0,55	0,54	0,52
Total	8,02	8,01	8,03	8,02	8,03	8,03	8,01	8,02	8,02	8,02
Almandine	64,88	63,78	63,43	62,67	63,42	62,42	62,73	62,56	62,76	62,73
Andradite	3,45	2,66	4,26	3,15	3,09	3,68	2,56	3,69	3,61	3,15
Grossular	13,87	16,07	14,30	16,19	14,94	15,37	16,18	14,57	14,70	14,32
Pyrope	4,90	4,61	5,08	4,65	4,63	4,87	4,53	4,55	4,69	4,86
Spessartine	12,90	12,89	12,93	13,33	13,92	13,66	14,01	14,62	14,24	14,95
Uvarovite	0,00	0,00	0,00	0,00	0,00	0,00	0,00	0,00	0,00	0,00
Total	99,29	99,07	98,71	98,78	98,18	98,60	99,23	99,37	98,94	98,89

OS-2 garnet profile Steps 8 µm										
here	Grt 1 / 61 .	Grt 1 / 62 .	Grt 1 / 63 .	Grt 1 / 64 .	Grt 1 / 65 .	Grt 1 / 66 .	Grt 1 / 67 .	Grt 1 / 68 .	Grt 1 / 69 .	Grt 1 / 70 .
SiO2	36,54	36,68	36,85	36,57	36,66	36,38	36,73	36,67	37,16	37,03
TiO2	0,16	0,08	0,11	0,13	0,11	0,12	0,11	0,13	0,15	0,18
Al2O3	20,30	20,18	20,35	20,36	20,35	20,31	20,16	20,23	20,22	20,28
FeO	29,34	29,29	29,73	29,29	29,47	29,21	28,66	28,40	28,66	28,48
MnO	6,36	6,75	6,78	6,76	6,94	6,79	7,00	7,00	6,87	7,07
MgO	1,12	1,10	1,18	1,14	1,19	1,19	1,11	1,08	1,10	1,07
CaO	6,20	5,68	5,79	5,80	5,72	5,99	6,31	6,49	6,40	6,38
Total	100,13	99,87	100,91	100,15	100,55	100,12	100,22	100,10	100,67	100,60
No. O	12,00	12,00	12,00	12,00	12,00	12,00	12,00	12,00	12,00	12,00
Si	2,97	2,98	2,97	2,97	2,97	2,96	2,98	2,97	2,99	2,99
Al	1,95	1,94	1,94	1,95	1,95	1,95	1,93	1,94	1,93	1,93
Ti	0,01	0,00	0,01	0,01	0,01	0,01	0,01	0,01	0,01	0,01
Fe3+	0,07	0,06	0,07	0,06	0,07	0,08	0,07	0,07	0,06	0,06
Fe2+	1,92	1,93	1,93	1,92	1,92	1,91	1,87	1,86	1,87	1,86
Mn	0,44	0,47	0,46	0,47	0,48	0,47	0,48	0,48	0,47	0,48
Mg	0,14	0,13	0,14	0,14	0,14	0,14	0,13	0,13	0,13	0,13
Ca	0,54	0,50	0,50	0,50	0,50	0,52	0,55	0,56	0,55	0,55
Total	8,03	8,02	8,03	8,02	8,03	8,03	8,02	8,02	8,01	8,01
Almandine	62,50	63,36	62,81	62,70	62,42	61,65	60,93	60,49	61,26	61,02
Andradite	3,49	3,11	3,75	3,20	3,64	3,87	3,76	3,52	3,24	3,16
Grossular	14,70	13,49	13,08	13,80	13,06	13,77	14,65	15,43	15,30	15,31
Pyrope	4,57	4,45	4,77	4,64	4,82	4,89	4,51	4,39	4,46	4,32
Spessartine	14,75	15,59	15,60	15,67	16,04	15,81	16,15	16,16	15,74	16,19
Uvarovite	0,00	0,00	0,00	0,00	0,00	0,00	0,00	0,00	0,00	0,00
Total	98,60	99,34	98,77	98,70	98,61	98,20	99,04	98,92	99,14	99,40

OS-2 garnet profile Steps 8 µm										
here	Grt 1 / 71 .	Grt 1 / 72 .	Grt 1 / 73 .	Grt 1 / 74 .	Grt 1 / 75 .	Grt 1 / 76 .	Grt 1 / 77 .	Grt 1 / 78 .	Grt 1 / 79 .	Grt 1 / 80 .
SiO2	37,14	37,05	33,85	35,97	36,60	29,87	36,87	37,14	36,83	36,74
TiO2	0,16	0,15	0,11	0,13	0,13	0,08	0,11	0,15	0,18	0,21
Al2O3	20,29	20,38	20,82	20,30	20,12	20,03	20,41	20,28	20,41	20,30
FeO	28,37	28,27	30,34	28,23	28,11	31,13	28,53	28,27	28,53	28,08
MnO	7,00	7,24	5,73	6,94	7,15	4,70	6,91	6,98	7,04	6,96
MgO	1,09	1,11	1,98	1,21	1,08	3,09	1,10	1,09	1,14	1,09
CaO	6,26	6,51	5,01	6,41	6,61	3,70	6,28	6,39	6,71	6,18
Total	100,40	100,81	98,00	99,32	99,93	92,91	100,31	100,39	100,98	99,63
No. O	12,00	12,00	12,00	12,00	12,00	12,00	12,00	12,00	12,00	12,00
Si	3,00	2,98	2,82	2,94	2,97	2,66	2,98	3,00	2,96	2,99
Al	1,93	1,94	2,06	1,96	1,93	2,12	1,95	1,93	1,94	1,95
Ti	0,01	0,01	0,01	0,01	0,01	0,01	0,01	0,01	0,01	0,01
Fe3+	0,05	0,06	0,10	0,07	0,08	0,20	0,06	0,05	0,08	0,05
Fe2+	1,86	1,84	2,02	1,86	1,83	2,12	1,87	1,85	1,84	1,86
Mn	0,48	0,49	0,40	0,48	0,49	0,35	0,47	0,48	0,48	0,48
Mg	0,13	0,13	0,25	0,15	0,13	0,41	0,13	0,13	0,14	0,13
Ca	0,54	0,56	0,45	0,56	0,58	0,35	0,54	0,55	0,58	0,54
Total	8,01	8,02	8,10	8,04	8,02	8,21	8,02	8,01	8,03	8,01
Almandine	61,30	60,12	61,09	59,56	59,72	57,94	61,43	60,99	59,64	61,51
Andradite	2,62	3,26	5,32	3,80	3,80	11,25	2,79	2,71	3,88	2,26
Grossular	15,58	15,58	10,52	15,29	15,54	2,03	15,46	15,87	15,66	15,76
Pyrope	4,41	4,49	8,72	4,99	4,40	15,44	4,43	4,39	4,63	4,42
Spessartine	16,08	16,55	14,34	16,35	16,54	13,34	15,88	16,04	16,20	16,05
Uvarovite	0,00	0,00	0,00	0,00	0,00	0,00	0,00	0,00	0,00	0,00
Total	99,09	99,20	93,04	97,73	98,92	86,45	99,23	99,11	98,46	99,47

Garnet profile BGA2-1

Steps 8 µm	1	2	3	4	5	6	7	8	9	10
SiO2	36,72	36,62	36,32	36,71	36,47	36,59	36,22	36,56	36,64	36,71
TiO2	0,21	0,26	0,30	0,25	0,22	0,25	0,27	0,30	0,21	0,33
Al2O3	19,61	19,54	19,57	19,64	19,66	19,53	19,83	19,83	19,82	19,71
FeO	16,24	16,16	16,10	16,07	16,10	16,19	16,12	15,99	16,13	16,25
MnO	19,75	19,50	19,91	19,94	20,11	19,83	20,09	19,79	20,02	19,75
MgO	0,61	0,54	0,55	0,46	0,51	0,50	0,54	0,50	0,54	0,54
CaO	6,59	6,56	6,73	6,66	6,25	6,34	6,30	6,72	6,49	6,50
Na2O		0,05	0,16	0,04	0,04	0,03	0,05	0,02	0,03	0,02
K2O		0,01	0,11				0,00	0,00		
Total	98,71	98,40	98,87	98,64	98,99	98,44	98,70	99,13	99,16	98,62
No.O	12,00	12,00	12,00	12,00	12,00	12,00	12,00	12,00	12,00	12,00
Si	2,99	3,00	2,97	2,99	2,99	3,00	2,97	2,98	2,98	2,99
Al	1,89	1,89	1,90	1,89	1,90	1,89	1,92	1,91	1,91	1,90
Ti	0,01	0,02	0,02	0,02	0,01	0,02	0,02	0,02	0,01	0,02
Fe3+	0,09	0,08	0,10	0,09	0,08	0,08	0,08	0,08	0,08	0,08
Fe2+	1,01	1,02	1,00	1,01	1,02	1,03	1,02	1,01	1,01	1,03
Mn	1,36	1,35	1,38	1,38	1,40	1,38	1,39	1,37	1,38	1,36
Mg	0,07	0,07	0,07	0,06	0,06	0,06	0,07	0,06	0,07	0,07
Ca	0,58	0,58	0,59	0,58	0,55	0,56	0,55	0,59	0,57	0,57
Total	8,01	8,01	8,02	8,01	8,01	8,01	8,02	8,02	8,02	8,01
Almandine	32,11	32,45	31,48	31,98	32,51	32,50	32,17	32,33	32,43	32,61
Andradite	4,67	4,19	5,12	4,38	4,22	4,24	4,22	3,99	4,20	4,12
Grossular	14,75	15,32	14,74	15,27	14,22	14,60	14,41	15,73	14,80	15,03
Pyrope	2,49	2,23	2,24	1,87	2,11	2,08	2,22	2,04	2,21	2,20
Spessartine	45,98	45,81	46,43	46,51	46,94	46,58	46,98	45,91	46,36	46,03

BGA2-1 garnet profile

Steps 8 µm	11	12	13	14	15	16	17	18	19	20
SiO2	36,65	36,80	36,69	36,67	37,06	36,72	36,55	36,36	36,78	36,60
TiO2	0,17	0,21	0,30	0,28	0,26	0,31	0,19	0,12	0,07	0,09
Al2O3	20,01	19,82	19,95	19,56	20,42	19,50	19,53	19,48	19,42	19,55
FeO	16,21	16,10	16,57	16,60	16,14	16,47	16,59	17,04	17,25	16,99
MnO	19,92	20,22	19,62	19,75	17,78	19,82	19,60	19,68	19,57	19,92
MgO	0,49	0,49	0,47	0,49	0,46	0,51	0,44	0,47	0,47	0,43
CaO	6,34	6,37	6,71	6,87	8,17	6,42	7,34	6,86	6,47	6,39
Na2O	0,03	0,02	0,04	0,03	0,02	0,00	0,04			0,03
K2O				0,01	0,00	0,00	0,02			
Total	99,38	98,88	99,03	98,89	99,35	98,33	98,73	98,56	98,67	99,14
No.O	12,00	12,00	12,00	12,00	12,00	12,00	12,00	12,00	12,00	12,00
Si	2,99	2,99	2,98	2,98	2,99	2,99	2,97	2,97	3,00	2,99
Al	1,93	1,91	1,91	1,88	1,94	1,88	1,88	1,88	1,87	1,89
Ti	0,01	0,01	0,02	0,02	0,02	0,02	0,01	0,01	0,00	0,01
Fe3+	0,07	0,08	0,08	0,11	0,05	0,09	0,12	0,13	0,11	0,11
Fe2+	1,04	1,02	1,04	1,02	1,04	1,03	1,01	1,04	1,06	1,05
Mn	1,37	1,39	1,35	1,36	1,21	1,37	1,35	1,36	1,35	1,38
Mg	0,06	0,06	0,06	0,06	0,06	0,06	0,05	0,06	0,06	0,05
Ca	0,55	0,55	0,58	0,60	0,71	0,56	0,64	0,60	0,56	0,56
Total	8,01	8,01	8,02	8,02	8,01	8,01	8,03	8,04	8,02	8,02
Almandine	33,41	32,37	33,21	32,14	33,80	32,51	31,24	32,01	33,49	33,31
Andradite	3,45	4,02	4,15	5,48	2,42	4,71	6,16	6,39	5,66	5,42
Grossular	15,11	14,68	15,44	14,64	21,24	14,31	15,37	13,83	13,37	13,32
Pyrope	2,00	2,02	1,91	1,99	1,85	2,08	1,79	1,92	1,93	1,76
Spessartine	46,04	46,91	45,29	45,74	40,69	46,39	45,43	45,84	45,54	46,18

BGA2-1 garnet profile

Steps 8 µm	21	22	23	24	25	26	27	28	29	30
SiO2	36,76	36,77	36,71	36,53	36,53	36,70	36,68	36,65	36,57	36,75
TiO2	0,08	0,07	0,17	0,21	0,28	0,22	0,28	0,30	0,29	0,30
Al2O3	19,35	19,47	19,36	20,02	19,45	20,12	19,67	19,80	19,63	19,75
FeO	17,35	17,22	16,97	16,60	16,54	16,68	16,62	16,74	16,76	16,89
MnO	19,65	19,57	19,05	19,79	19,53	19,66	19,49	19,13	19,13	18,99
MgO	0,44	0,49	0,47	0,53	0,49	0,50	0,50	0,50	0,51	0,47
CaO	6,65	6,67	7,18	6,55	6,86	6,26	6,48	6,94	6,94	7,23
Na2O	0,02			0,02		0,04	0,02	0,04	0,02	0,01
K2O						0,00				
Total	98,79	98,95	98,63	98,66	98,77	99,22	98,67	99,12	98,99	99,06
No.O	12,00	12,00	12,00	12,00	12,00	12,00	12,00	12,00	12,00	12,00
Si	2,99	2,99	2,99	2,97	2,98	2,98	2,99	2,98	2,98	2,98
Al	1,86	1,87	1,87	1,92	1,88	1,93	1,90	1,90	1,89	1,89
Ti	0,00	0,00	0,01	0,01	0,02	0,01	0,02	0,02	0,02	0,02
Fe3+	0,12	0,12	0,12	0,09	0,11	0,07	0,08	0,09	0,10	0,10
Fe2+	1,06	1,05	1,04	1,04	1,02	1,07	1,05	1,05	1,04	1,05
Mn	1,35	1,35	1,31	1,36	1,35	1,35	1,35	1,32	1,32	1,30
Mg	0,05	0,06	0,06	0,06	0,06	0,06	0,06	0,06	0,06	0,06
Ca	0,58	0,58	0,63	0,57	0,60	0,54	0,57	0,60	0,61	0,63
Total	8,03	8,03	8,02	8,03	8,02	8,02	8,01	8,02	8,02	8,02
Almandine	33,10	33,17	32,58	32,72	32,25	34,32	33,41	33,46	33,16	33,21
Andradite	6,29	5,93	5,93	4,37	5,38	3,35	4,24	4,49	4,92	4,98
Grossular	13,23	13,61	15,21	14,85	14,83	14,92	14,88	15,81	15,44	16,12
Pyrope	1,80	1,99	1,94	2,18	2,02	2,04	2,03	2,04	2,09	1,91
Spessartine	45,58	45,30	44,34	45,89	45,51	45,37	45,44	44,21	44,39	43,78

BGA2-1 garnet profile

Steps 8 µm	31	32	33	34	35	36	37	38	39	40
SiO2	36,65	36,74	36,70	36,53	36,89	36,75	36,58	36,59	37,04	36,70
TiO2	0,20	0,19	0,33	0,29	0,17	0,29	0,30	0,23	0,23	0,24
Al2O3	20,01	20,09	19,71	19,85	19,83	19,56	19,75	19,79	20,11	19,70
FeO	16,61	16,81	16,83	17,21	16,86	17,09	17,27	17,12	17,25	17,37
MnO	19,42	19,50	19,45	19,20	19,43	19,08	18,72	19,01	19,12	18,96
MgO	0,50	0,53	0,48	0,49	0,50	0,54	0,53	0,54	0,53	0,52
CaO	6,30	6,16	6,58	6,99	6,71	6,73	6,96	6,61	6,39	6,46
Na2O	0,01	0,02	0,01	0,02	0,03	0,01	0,05		0,01	0,02
K2O			0,01			0,00		0,00	0,00	
Total	99,25	99,34	98,80	98,37	99,02	98,60	98,90	99,16	99,02	98,89
No.O	12,00	12,00	12,00	12,00	12,00	12,00	12,00	12,00	12,00	12,00
Si	2,99	2,99	2,98	2,96	2,99	2,99	2,97	2,98	2,99	2,99
Al	1,93	1,93	1,90	1,90	1,90	1,88	1,90	1,91	1,92	1,90
Ti	0,01	0,01	0,02	0,02	0,01	0,02	0,02	0,01	0,01	0,01
Fe3+	0,06	0,06	0,09	0,11	0,09	0,10	0,10	0,09	0,07	0,09
Fe2+	1,07	1,08	1,05	1,06	1,05	1,06	1,08	1,08	1,10	1,09
Mn	1,34	1,34	1,34	1,32	1,33	1,31	1,29	1,31	1,31	1,31
Mg	0,06	0,06	0,06	0,06	0,06	0,06	0,06	0,07	0,06	0,06
Ca	0,55	0,54	0,57	0,61	0,58	0,59	0,61	0,58	0,55	0,56
Total	8,01	8,01	8,01	8,03	8,02	8,02	8,02	8,02	8,01	8,02
Almandine	34,48	34,87	33,56	32,98	33,55	33,64	34,12	34,43	35,29	34,86
Andradite	3,24	3,23	4,51	5,34	4,51	5,00	4,91	4,46	3,47	4,52
Grossular	15,23	14,76	14,82	15,15	15,08	14,79	15,47	14,89	15,11	14,46
Pyrope	2,04	2,14	1,97	2,02	2,03	2,19	2,15	2,21	2,15	2,14
Spessartine	45,00	45,00	45,14	44,51	44,82	44,38	43,35	44,00	43,98	44,02

BGA2-1 garnet profile

Steps 8 µm	41	42	43	44	45	46	47	48	49	50
SiO2	36,80	36,53	36,86	36,29	36,91	36,31	36,97	36,78	36,80	36,97
TiO2	0,25	0,20	0,18	0,28	0,33	0,27	0,14	0,23	0,18	0,23
Al2O3	19,56	19,62	19,74	19,68	19,57	19,55	19,70	19,67	19,69	19,75
FeO	17,46	17,52	17,60	17,26	17,59	17,62	17,93	18,18	18,18	18,33
MnO	18,41	18,84	18,43	18,28	18,50	18,12	18,47	17,87	17,44	17,42
MgO	0,54	0,52	0,48	0,51	0,56	0,54	0,51	0,52	0,55	0,55
CaO	6,84	7,25	7,25	7,27	7,21	7,23	6,95	6,99	7,55	7,38
Na2O	0,02	0,01	0,03	0,13	0,02	0,04	0,00	0,03	0,02	0,00
K2O			0,01	0,07						
Total	98,46	98,45	99,11	98,59	98,60	98,62	98,93	98,91	99,09	98,89
No.O	12,00	12,00	12,00	12,00	12,00	12,00	12,00	12,00	12,00	12,00
Si	2,99	2,96	2,98	2,96	2,98	2,97	2,99	2,98	2,98	2,98
Al	1,88	1,89	1,89	1,90	1,87	1,89	1,89	1,89	1,89	1,89
Ti	0,02	0,01	0,01	0,02	0,02	0,02	0,01	0,01	0,01	0,01
Fe3+	0,09	0,12	0,10	0,10	0,11	0,11	0,10	0,10	0,11	0,10
Fe2+	1,09	1,06	1,09	1,08	1,08	1,09	1,11	1,13	1,12	1,14
Mn	1,27	1,29	1,26	1,26	1,27	1,25	1,26	1,23	1,20	1,19
Mg	0,07	0,06	0,06	0,06	0,07	0,07	0,06	0,06	0,07	0,07
Ca	0,60	0,63	0,63	0,64	0,62	0,63	0,60	0,61	0,65	0,64
Total	8,01	8,04	8,02	8,03	8,02	8,03	8,02	8,02	8,03	8,02
Almandine	34,68	32,95	34,55	33,78	33,93	34,18	35,15	36,11	35,65	36,18
Andradite	4,78	6,26	5,23	5,15	5,64	5,67	5,30	5,06	5,47	5,11
Grossular	15,39	15,01	15,88	16,32	15,43	15,68	14,96	15,40	16,52	16,36
Pyrope	2,21	2,11	1,96	2,09	2,26	2,21	2,06	2,11	2,22	2,24
Spessartine	42,93	43,67	42,39	42,66	42,74	42,27	42,54	41,33	40,14	40,10

BGA2-1 garnet profile

Steps 8 µr	51	52	53	54	55	56	57	58	59	60	61
SiO2	36,93	37,18	36,89	36,58	36,78	36,60	36,74	36,71	36,78	37,09	36,60
TiO2	0,25	0,23	0,24	0,12	0,19	0,25	0,16	0,13	0,12	0,21	0,18
Al2O3	19,73	19,41	19,56	19,98	19,95	19,88	19,77	19,86	19,87	19,78	20,08
FeO	18,26	18,30	18,27	18,78	18,41	18,65	19,43	19,68	20,10	19,82	20,05
MnO	17,22	17,12	17,38	17,51	17,21	16,69	16,66	16,20	16,17	15,84	15,60
MgO	0,54	0,54	0,55	0,50	0,58	0,59	0,57	0,60	0,56	0,59	0,62
CaO	7,40	7,05	7,16	6,88	6,88	6,96	6,90	6,76	6,80	7,15	7,21
Na2O		0,01	0,01	0,01	0,03	0,01	0,02	0,01		0,02	0,02
K2O			0,01		0,00	0,01	0,00			0,02	0,02
Total	98,72	97,47	98,45	98,66	99,22	99,20	99,20	99,31	99,15	98,57	98,54
No.O	12,00	12,00	12,00	12,00	12,00	12,00	12,00	12,00	12,00	12,00	12,00
Si	2,99	3,02	2,99	2,97	2,99	2,98	2,98	2,98	2,98	3,00	2,96
Al	1,89	1,87	1,88	1,92	1,92	1,92	1,90	1,91	1,91	1,89	1,92
Ti	0,02	0,01	0,01	0,01	0,01	0,02	0,01	0,01	0,01	0,01	0,01
Fe3+	0,09	0,09	0,10	0,09	0,08	0,08	0,10	0,09	0,09	0,09	0,09
Fe2+	1,14	1,15	1,14	1,18	1,17	1,19	1,22	1,25	1,27	1,25	1,27
Mn	1,18	1,18	1,20	1,20	1,18	1,15	1,15	1,12	1,11	1,08	1,07
Mg	0,06	0,06	0,07	0,06	0,07	0,07	0,07	0,07	0,07	0,07	0,08
Ca	0,64	0,61	0,62	0,60	0,60	0,61	0,60	0,59	0,59	0,62	0,63
Total	8,02	8,00	8,01	8,03	8,02	8,02	8,02	8,02	8,02	8,01	8,03
Almandin	36,38	36,45	36,22	37,27	37,83	38,55	39,15	40,43	40,67	40,06	40,24
Andradite	4,79	4,58	5,02	4,77	3,89	3,87	4,92	4,31	4,78	4,54	4,52
Grossular	16,85	16,42	16,04	15,39	16,19	16,52	15,20	15,42	15,02	16,37	16,59
Pyrope	2,18	2,22	2,27	2,02	2,37	2,40	2,33	2,45	2,27	2,41	2,55
Spessartir	39,81	40,33	40,45	40,54	39,72	38,65	38,41	37,38	37,25	36,63	36,10